# Reactivity Studies of a Donor Stabilized Borylnitrene Using Matrix Isolation and Computational Tools

**Dissertation**

der Mathematisch-Naturwissenschaftlichen Fakultät

der Eberhard Karls Universität Tübingen

zur Erlangung des Grades eines

Doktors der Naturwissenschaften

(Dr. rer. nat.)

vorgelegt von

Virinder Bhagat

aus Kathua, Indien

Tübingen

2024

Gedruckt mit Genehmigung der Mathematisch-Naturwissenschaftlichen Fakultät der Eberhard Karls Universität Tübingen.

| | |
|---|---|
| Tag der mündlichen Qualifikation: | 02.08.2024 |
| Dekan: | Prof. Dr. Thilo Stehle |
| 1. Berichterstatter/-in: | Prof. Dr. Holger F. Bettinger |
| 2. Berichterstatter/-in: | Prof. Dr. Reinhold Fink |
| 3. Berichterstatter/-in: | Prof. Dr. Wolfram Sander |

*“By believing passionately in something that still does not exist, we create it. The nonexistent is whatever we have not sufficiently desired.”*

*— Franz Kafka*

# Table of Contents

# Abbreviations and Symbols

| | |
|---|---|
| **UV/Vis** | Ultravoilet/visible |
| **IR** | Infrared |
| **Ar** | Argon |
| **Ne** | Neon |
| **Kr** | Krypton |
| **Xe** | Xenon |
| **FVP** | Flash vacuum pyrolysis |
| **EPR** | Electron paramagnetic resonance |
| **ISC** | Intersystem crossing |
| **PES** | Potential energy surface |
| **PAL** | Photoaffinity labeling. |
| **cat** | catecholato |
| **pin** | pinacholato |
| **NIPES** | Negative ion photoelectron spectroscopy |
| **OG** | Orange glass |
| **sccm** | Standard cubic centimeters per minute |
| **CASSCF** | Complete active space self-consistent field |
| **HF** | Hartree-Fock |
| **MRPT** | Multireference perturbation |
| **NEVPT2** | N-electron valence state perturbation |
| **CC** | Coupled cluster |
| **MECP** | Minimum energy crossing point |
| **CI** | Conical intersection |
| **FIC** | Full internally contracted |
| **TS** | Transition state |

# Abstract

Matrix isolation studies of the reactivity of a donor stabilized borylnitrene, 2-nitreno-1,3,2-benzodioxaborole (catBN; cat = catecholato), with reactants such as dioxygen ($O_2$), carbon dioxide ($CO_2$), ethene ($C_2H_4$), etc. were carried out which comprised of exploring the mechanistic aspects and product identification. The computational data obtained using density functional theory (DFT) and *ab-initio* methods corroborated the experimental results.

The matrix isolation studies of the thermal reaction of catBN with $O_2$ resulted in the formation of two products: an *anti*-nitroso-*O*-oxide and a nitritoborane catBONO at temperatures as low as 7 K. In the next step, the irradiation with $\lambda$ = 254 nm resulted in the conversion of previously formed *anti*-nitroso-*O*-oxide to catBONO. Computational studies were performed at a high level of theory to explain the experimental observation.

On the other hand, the photoreaction ($\lambda$ > 550 nm) of matrix isolated catBN with $CO_2$ resulted in a 1,2-oxaziridin-3-one derivative, catBN$CO_2$. The computational and heavy isotope studies using the heavy isotopologues of $CO_2$ showed that the CO vibrational mode is unusually shifted in $^{18}O$ and $^{13}C$ isotopologues of catB$NO_2$ due to its involvement in Fermi resonance with ring deformation vibrational mode.

In a separate computational study, the high photoreactivity of catBN with closed-shell molecules upon $\lambda$ > 550 nm irradiation was explained. The study showed that upon photoirradiation with $\lambda$ > 550 nm, catBN relaxes to the lowest singlet electronic state. The lowest singlet electronic state is highly electrophilic, and therefore, evidence is provided by this study that explains the high photoreactivity of catBN. Furthermore, the reaction of

borylnitrene catBN with ethene $C_2H_4$ was investigated under matrix isolation conditions both thermally and photochemically. In the thermal reaction (T = 35 K), the products of the reaction were assigned as aziridine and *syn* isomers of imine. Meanwhile, both the *syn* and *anti* isomers of imine were identified in the photoreaction in addition to aziridine.

# Zusammenfassung

Es wurden Studien zur Reaktivität eines donorstabilisierten Borylnitrens, 2-Nitreno-1,3,2-benzodioxaborol (catBN; cat = catecholato), mittels Matrixisolation mit Reaktanten wie molekularem Sauerstoff ($O_2$), Kohlendioxid ($CO_2$), Ethen ($C_2H_4$) usw. durchgeführt, die die Erforschung mechanistischer Aspekte sowie die Produktidentifizierung umfassten. Computerchemische Berechnungen mit Dichtefunktionaltheorie- (DFT) und *ab-initio*-Methoden wurden zum besseren Verständnis der experimentellen Ergebnisse zu Hilfe genommen.

Die Untersuchungen der Reaktion von catBN mit $O_2$ unter den Bedingungen der Matrixisolation ergaben die Bildung von zwei Produkten: ein *anti*-Nitroso-*O*-oxid und ein Nitritoboran, catBONO, bei Temperaturen von nur 7 K in Neon. Im nächsten Schritt führte die Bestrahlung mit $\lambda$ = 254 nm zur Umwandlung des zuvor gebildeten *anti*-Nitroso-*O*-oxids in catBONO. Um die experimentellen Beobachtungen weiter zu erklären, wurden computerchemische Untersuchungen auf hohem theoretischen Niveau durchgeführt.

Die Photoreaktion ($\lambda$ > 550 nm) von matrixisoliertem catBN mit $CO_2$ führte zu einem 1,2-Oxaziridin-3-on-Derivat, $catBNCO_2$. Die computerchemischen und Isotopensubstitutionsstudien unter Verwendung der schweren $CO_2$-Isotopologe zeigten, dass die CO-Schwingungsfrequenz in den $^{18}O$- und $^{13}C$-Isotopologen von $catBNO_2$ aufgrund von Fermi-Resonanz mit einer Ringdeformationsschwingung ungewöhnlich verschoben ist.

In einer separaten Computerchemiestudie wurde die hohe Photoreaktivität von catBN mit geschlossenschaligen Molekülen bei einer Bestrahlung mit $\lambda$ > 550 nm aufgeklärt. Die Studie zeigte, dass catBN bei einer Bestrahlung mit $\lambda$ > 550 nm in den niedrigsten

elektronischen Singulett-Zustand relaxiert. Die Zusatnd ist hoch elektrophil, was die hohe Photoreaktivität von catBN letztlich erklären kann. Außerdem wurde die Reaktion von Borylnitren catBN mit Ethen $C_2H_4$ unter Bedingungen der Matrixisolierung sowohl thermisch als auch photochemisch untersucht. Bei der thermischen Reaktion ($T$ = 35 K) wurden die Reaktionsprodukte als Aziridin und *syn*-Isomere eines Imins identifiziert. Bei der photochemischen Reaktion wurden neben dem Aziridin auch die *syn*- und *anti*-Isomere des Imins identifiziert.

# List of Publications

## Publications Included in the Thesis

### Publication I

*Unusual Nitrene Oxidation Product Formation by Metathesis Involving the Dioxygen O−O and Borylnitrene B−N Bonds*
V. Bhagat, J. Schumann, H. F. Bettinger, *Chem. Eur. J.* **2020**, *26*, 12654-12663.

### Publication II

*The Reaction of CO2 with a Borylnitrene: Formation of an 3-Oxaziridinone*
V. Bhagat, J. Schumann, H. F. Bettinger, *Angew. Chem. Int. Ed.* **2021**, *60*, 23112-23116.

### Publication III

*Computational Exploration of the Intersystem Crossing from the $\tilde{X}^3A_2$ to the $\tilde{a}^1A_1$ State in Boryl Nitrenes upon Photoexcitation*
V. Bhagat, H. F. Bettinger, *J. Phys. Chem. A* **2022**, *126*, 7660-7666.

## Other Publications

*A Metastable Ketenyl Radical–Water Complex from UV Photolysis of the Carboxymethyl Radical*
J. P. Wagner, V. Bhagat, *J. Phys. Chem. A* **2023**, *127*, 3171-3178.

*Direct Spectroscopic Identification of BN-Arynes and Subtle Steric Effects on Nitrogen Fixation*
D. Gupta, C. Keck, C. Tönshoff, V. Bhagat, R. Strobel, M. Eder, P. Baylère, S. Labat, A. Chrostowska, H. F. Bettinger, *Chem. Eur. J.* **2023**, *n/a*, e202302444.

# Personal Contributions

**Publication I**

*Unusual Nitrene Oxidation Product Formation by Metathesis Involving the Dioxygen O−O and Borylnitrene B−N Bonds*
V. Bhagat, J. Schumann, H. F. Bettinger, *Chem. Eur. J.* **2020**, *26*, 12654-12663.

V. Bhagat: Experimental data generation using matrix isolation setup related to the reaction of catBN (**6**) with $O_2$. In addition, computational data generation using different quantum chemistry software. Also, the generated data was interpreted along with writing the publication.

J. Schumann: Did the preliminary matrix isolation experiments on the reaction of catBN (**6**) with $O_2$, which led to open questions regarding the mechanism of the reaction.

H. F. Bettinger: Provided the scientific ideas regarding the study. In addition, did the CR-CCSD(T) computations and cooperated in carrying out the other computational studies. Also, provided his suggestions and corrections while writing the publication.

**Publication II**

*The Reaction of CO2 with a Borylnitrene: Formation of an 3-Oxaziridinone*
V. Bhagat, J. Schumann, H. F. Bettinger, *Angew. Chem. Int. Ed.* **2021**, *60*, 23112-23116.

V. Bhagat: Synthesized the azide precursor $catBN_3$ for catBN **3**. Experimental data generation using matrix isolation setup related to the photochemical reaction of **3** with $CO_2$. In addition, computational data generation using different quantum chemistry software. Also, the interpretation of the generated data was done along with writing the publication.

J. Schumann: Did the preliminary experimental work on the reaction of catBN **3** with $CO_2$, which opened unsolved problems, such as the unusual isotopic IR shifts of $^{18}O$ and $^{13}C$ isotopologues of 3-Oxaziridinone **5**.

H. F. Bettinger: Provided the scientific ideas regarding the study. In addition, cooperated in carrying out the computational and provided his suggestions/corrections while writing the publication.

**Publication III**

*Computational Exploration of the Intersystem Crossing from the $\tilde{X}^3A_2$ to the $\tilde{a}^1A_1$ State in Boryl Nitrenes upon Photoexcitation*
V. Bhagat, H. F. Bettinger, *J. Phys. Chem. A* **2022**, *126*, 7660-7666.

V. Bhagat: Computational data generation using ORCA 5.0.1 and Molpro 2021.3 quantum chemistry software. In addition, the interpretation of the generated data was done along with writing the publication.

H. F. Bettinger: Provided the scientific ideas regarding the study. In addition, provided his suggestions/corrections while writing the publication.

* *The chemical species are numbered as they appear in the respective publications.*

# 1 Introduction

## 1.1 Nitrenes: A General Overview

Reactive intermediates are short-lived chemical species whose involvement in many chemical reactions is well understood. In a multistep chemical reaction, reactive intermediates are formed and converted to other reactive intermediates or the final product.[1] Examples of some of the well-studied reactive intermediates are radicals, ions, arynes, carbenes, nitrenes, etc.[1-6] Out of these reactive intermediates, nitrenes are highly important for introducing a nitrogen atom into a chemical moiety. A nitrene is a monovalent and *sp* hybridized nitrogen atom containing a reactive intermediate as it exhibits only a sextet of electrons on the nitrogen atom and not a full octet.[1, 7] The nitrogen center displays three non-bonding orbitals: two unhybridized orbitals, $p_y$ and $p_x$, and one *sp* hybridized orbital represented as $n_{LP}$ (Figure 1a).[1] The chemical behavior of nitrenes can be understood in terms of the distribution of four electrons over the three non-bonding orbitals. The orbital $p_x$ is usually referred to as $\pi_p$ because it is perpendicular to the plane of the nitrene, and the in-plane $p_y$ is referred to as $\sigma_p$. The four electrons are then filled in different ways into these non-bonding orbitals, which leads to four different types of electronic configurations (Figure 1c) exhibiting overall triplet or singlet spin multiplicities.[8] Due to the high *s* character of *sp* hybridized orbital $n_{LP}$, it is lower in energy than $\pi_p$ and $\sigma_p$ and remains doubly occupied in these electronic configurations.[8] These electronic configurations account for the chemically relevant lower electronic states in nitrenes. Depending on the electronic configuration of a specific state, the reactivity of nitrene changes.[8]

In the simplest case of a nitrene, called imidogen **1** (HN), the high molecular symmetry leads to degenerate, unhybridized $p_y$ and $p_x$ orbitals.[1]

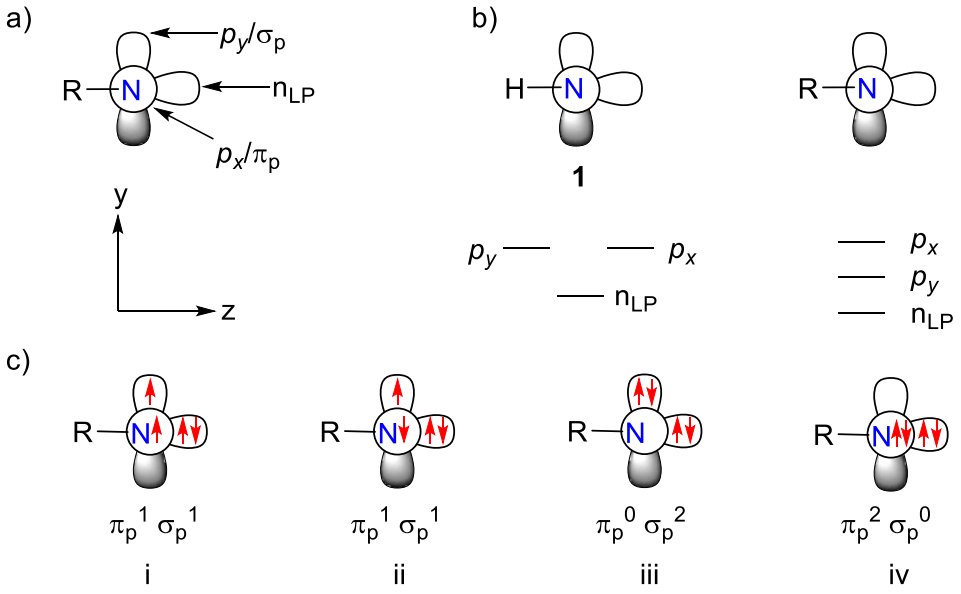


Figure 1. a) Frontier non-bonding orbitals in a nitrene. b) Lifting of degeneracy between the *p* orbitals because of substituting the H atom with other substituents. c) Different electronic configurations of nitrene that are responsible for lower electronic states.

This degeneracy is lifted once the H atom gets replaced with electron donating substituents like -$CH_3$, -$NH_2$, -$OCH_3$, etc., by stabilizing or destabilizing the $p_x$ orbital through the interaction with electron-filled donor orbitals (Figure 1b). The degeneracy can also be affected by the discriminatory interactions with in-plane $p_y$ orbitals, e.g., in acylnitrenes.[9] The magnitude of the energy gap $\Delta E_{px\text{-}py}$ between the $p_x$ and $p_y$ orbitals in a nitrene is a function of the electron-donating power of the substituent (-R group) attached to the nitrogen atom as indicated in Figure 2 ($R_1 < R_2 < R_3$). $\Delta E_{px\text{-}py}$, in turn, affects the singlet-triplet energy splitting $\Delta E_{S\text{-}T}$ ($E_S$ -$E_T$) and, hence, the reactivity of a nitrene. Another determining factor for the relative energy ordering of singlet and triplet states is the magnitude of exchange energy $E_{ex}$ in the triplet state. A higher $E_{ex}$ than the $\Delta E_{px\text{-}py}$ leads to a triplet ground state and a positive $\Delta E_{S\text{-}T}$, and a lower $E_{ex}$ than the $\Delta E_{px\text{-}py}$ leads to the singlet being the ground state and a negative $\Delta E_{S\text{-}T}$ (Figure 2).[8] Similarly, the lifting of degeneracy between $p_x$ and $p_y$ by different substituents

can explain the relative energetic ordering within different types of singlet states (Figure 1b). In the case of small energy splitting between $p_x$ and $p_y$, the pair of electrons prefer to minimize the Coulomb repulsion between each other with a slight energetic penalty by promoting one of the electrons into the higher energy *p* orbital. This results in the singlet state having the lowest energy with an electronic configuration of type ii (Figure 1c). In the high energy splitting case, the energetic penalty of promoting one of the electrons into a higher energy *p* orbital is prohibitively high compared to the energetic stabilization gained by reducing the Coulomb repulsion. In this case, electronic configurations of type iii or iv (Figure 1c) are preferred and, therefore, present in the lowest singlet state in a nitrene.[8]

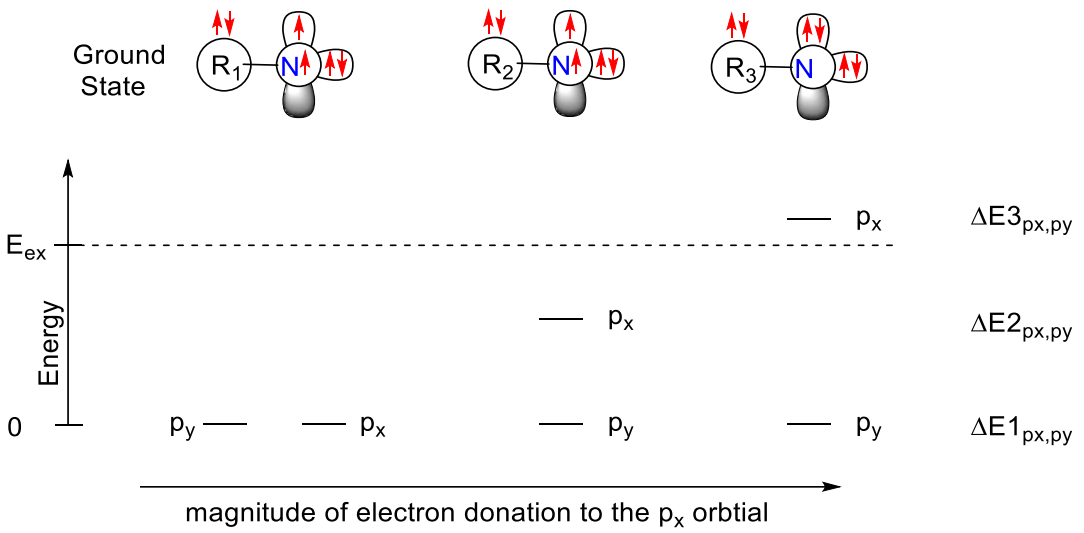


Figure 2. The interplay between energy splitting, $\Delta E_{px\text{-}py}$, between $p_x$ and $p_y$ orbitals, and exchange energy $E_{ex}$ determining the ground state multiplicity of a nitrene.[8]

The history of nitrenes dates back to 1891 when Tiemann first proposed them as a reactive intermediate in the Lossen rearrangement reaction.[10] One of the earliest and simplest studied nitrenes, HN **1**, was first proposed as a reactive intermediate by Beckman and Dickinson. In their study, they used the hydrazoic acid $HN_3$ **2** as a precursor that would release **1** upon high energy UV light irradiation (Scheme 1, eq. 1). They concluded that 27 %

of the photodecomposition products of **2** correspond to dihydrogen $H_2$ and dinitrogen $N_2$, while ammonia ($NH_3$) accounts for the remainder.[11] Until this point, there was no experimental evidence for the direct detection of nitrene **1,** which was observed for the first time in 1936 using UV-VIS spectroscopy targeting a strong absorption at 336 nm.[12] HN **1** was also formed during ammonia pyrolysis at very high temperatures exceeding 2000 °C (Scheme 1, eq. 2). Later, in 1960, under very low temperature conditions (4.2 K), Keyser isolated **2** in frozen xenon and krypton and formed **1** photochemically, which could be analyzed using UV-VIS spectroscopy (Scheme 1, eq. 3). Furthermore, their experimental finding also concluded the formation of $NH_2$ radical **4** as a minor product in the photoreaction.[13]

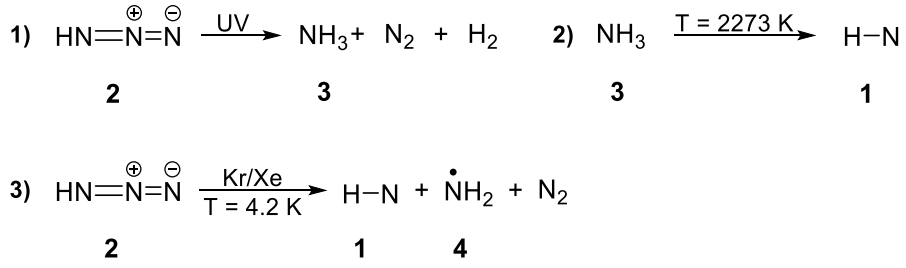


Scheme 1. Early studies of imidogen **1** (HN) under different reaction conditions and using different precursors.

### 1.2 Typical Reactions of Nitrenes and Different Methods of Generation

The neutral monovalent nitrogen-centered reactive intermediates, namely nitrenes, are frequently used species to introduce nitrogen containing functional groups into a stable molecule. Because of high electron deficiency, nitrenes react ferociously by intermolecular insertion, even into very strong bonds (Scheme 2). One of the well-known reactions of nitrenes correspond to the addition to the unsaturated bonds to form aziridine **5**[14-16] and the insertion into the stable $C_{(sp3)}$−H bond of a molecule that results in amine **6**.[16-20] Furthermore, the insertion reactions into the strong O−H bond of alcohol and the N−H bond of an amine to

the form products **7** and **8**, respectively, were also reported. In the case of O−H bond insertions, nitrenes such as alkoxycarbonylnitrene **14** and sulfonylnitrene **17**, when generated photochemically or thermally from the corresponding azides **13** and **16,** respectively, have shown considerable reactivity.[21] *p*-Cyanophenylazide **19** photochemically forms a nitrene **20** that inserts into the N−H bond of dimethylamine to form **21**; this reaction pathway is preferred only for a particular wavelength of light used to generate the nitrene.[22]

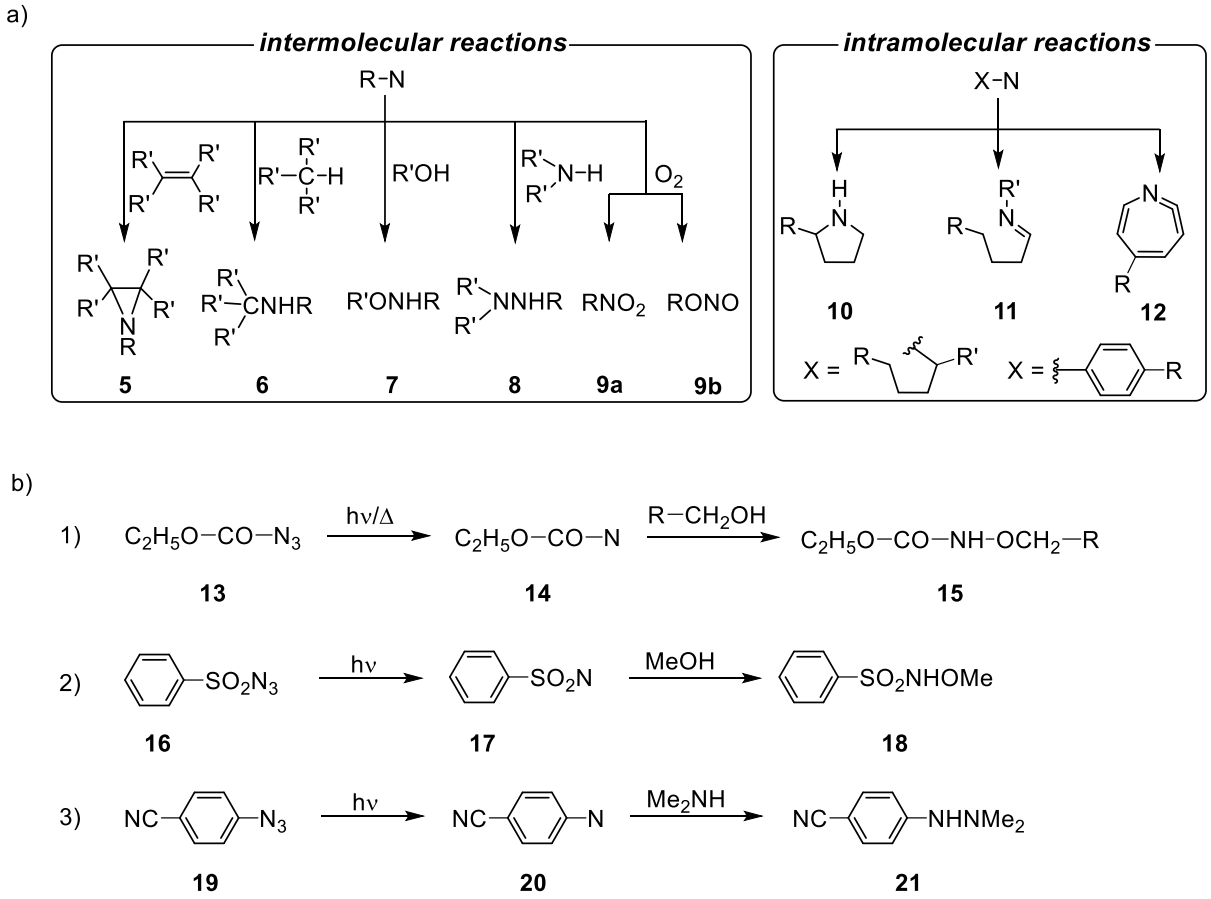


Scheme 2. a) General reactions of nitrenes. b) Examples of nitrene insertion into the O−H bond of alcohol and the N−H bond of amine.

Regarding the triplet state reactivity of nitrenes, the reaction with dioxygen ($O_2$) is widely studied with different nitrenes. The nature of the final product (**9a** or **9b**) formed in this reaction strongly depends on the type of nitrene employed. For instance, phenylnitrenes

give the nitro product as the thermodynamic product, and borylnitrenes are known to form the nitrito product (Section 1.7.1 for details).[23-26] Also, depending on the substituent attached to the nitrene, intramolecular rearrangements can be highly competitive with the often-desired intermolecular reactivity. In this regard, some of the well-known reactions are: 1) Intramolecular C−H bond insertion to form cyclic amines **10**;[27] 2) 1,2-shift of an alkyl group or H atom that forms imines **11**; and [27, 28] 3) Ring expansion reactions in phenylnitrenes that result in the formation of ketenimine products **12**.[29] Moreover, there are several methods to characterize and study the reactivity of nitrenes using different precursors used to produce them.

Studies related to nitrenes mainly constitute: 1) Kinetically trapping nitrenes under cryogenic conditions using inert gas matrices and their characterization using spectroscopic methods, e.g., the matrix isolation technique; 2) time-resolved spectroscopy; and 3) the trapping of nitrenes with a suitable scavenger in the solution. Several precursors to nitrenes have been used to characterize and study their reactivity using these techniques. Scheme 3 illustrates some of these precursors, such as azides,[9, 29-32] isocyanates,[33, 34] alkanamidates,[35, 36] and sulfinilimines.[37] Organic azides are primarily used as precursors for the generation of nitrenes. In matrix isolation studies, these precursors are co-deposited with the inert matrix host (e.g., Ar, $N_2$, etc.) on a cold window, and the deposited mixture is photolyzed to give the corresponding nitrenes.[9, 23, 38, 39] These precursors are known to yield nitrene upon flash vacuum pyrolysis (FVP), which can then be trapped by co-deposition with the matrix host on the cold window.[26] The nitrenes produced in these ways are characterized by different spectroscopic methods, e.g., UV-VIS, infrared (IR), electron paramagnetic resonance (EPR) spectroscopies, etc. In addition, time-resolved spectroscopy combined with

UV-VIS detection plays an instrumental role in deciphering the reactivity of nitrenes and their characterization. In this technique, the precursor of the nitrene is photoexcited, and then, a change in the absorption wavelength is monitored using a pulsed laser as time evolves. Different absorption patterns at different points indicate the precursor's temporal evolution in different excited states and, eventually, the formation of nitrene and other products.[9, 30, 32, 40]

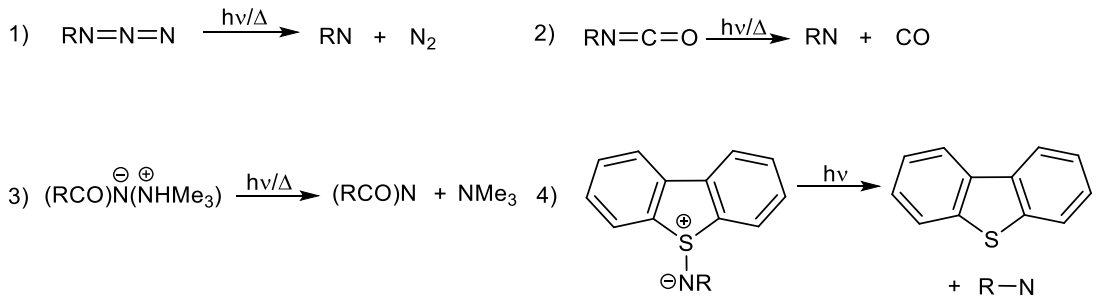


Scheme 3. Various known precursors for the generation of nitrenes.

In the solution phase, nitrenes are generated by photolyzing a suitable azide precursor dissolved in a hydrocarbon solvent (e.g., cyclohexane, cyclohexene, etc.). These nitrenes are then trapped by reaction with the hydrocarbon solvents, resulting in C−H insertion products or aziridines in the case of unsaturated hydrocarbon solvents.[14, 17, 20, 41, 42] Depending on the substituent attached to the nitrene center, there are alternative reaction channels that compete with the intermolecular trapping reactions. For example, the photodecomposition of phenylazide in solution results in the formation of polymeric tars despite the presence of trapping reagents.[29] In contrast, fluorinated phenylazide results in an efficient C−H insertion in the presence of a scavenger.[18, 43] Also, sulfonylazides,[44] carbonylazides,[45] and phosphorylazides[46] show similar reactivity and are known for their intermolecular trapping reactions.

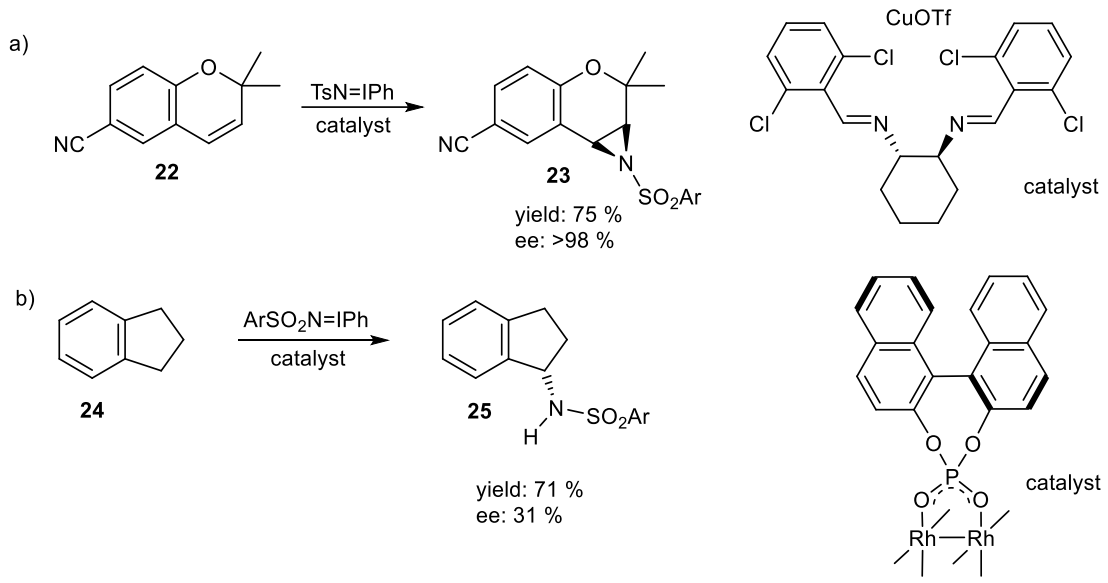


Scheme 4. Transition metal mediated enantioselective nitene transfer reactions.

Using transition metal complexes as nitrene surrogates and utilizing them for C−H bond amination and unsaturated C=C bond aziridination is also one of the critical aspects of nitrene from a synthetic chemist's point of view.[47] This kind of nitrene transfer reaction dates back to the work of Groves and Takahashi, where they used a manganese-nitrene complex for the aziridination of an olefin.[48] Later on, a similar idea was used for C−H bond amination as well by Breslow, where he used a different nitrene precursor [N-(p-toluenesulfonyl)imino]phenyliodinane (TsN=IPh) together with iron and manganese TPP (tetraphenylporphyrin) complexes.[49] Furthermore, Jacobsen *et al.* demonstrated the high tendency of these transition metal nitrene complexes to react enantioselectively when a chiral ligand is employed.[50] They reported an enantioselective aziridination of several alkenes using a copper-based catalyst and TsN=IPh as a nitrene source. In the case of 6-cyano-2,2-dimethylchromene, the enantioselective aziridination of **22** with a high enantiomeric excess of >98 % was obtained (Scheme 4a). Similarly, enantioselective C−H bond amination was also attempted using a transition metal-based surrogate. The first of such reactions was

reported by Müller using a combination of $ArSO_2N$=IPh and a di-rhodium(II) complex.[51] The C−H insertion of indan **24** resulted in enantioselective amination with an enantiomeric excess of 31 % (Scheme 4b). Efforts to improve the enantioselectivity were made after that by using different types of coordinating groups to the rhodium(II) metal center, e.g., $Rh_2(TCPTAD)_4$ [TCPTAD =N-tetrachlorophthaloyl-(1-adamantyl)glycinate] was able to give an excellent enantioselectivity for the C−H amination reaction.[52]

### 1.3 Comparison Between the Reactivity of Carbenes and Nitrenes

Nitrenes are usually considered as the nitrogen analogs of carbenes due to their comparable electronic properties.[53] Consequently, a comparison between the two types of reactive intermediates is often provided in the literature.[53-57] In the case of reactivity, carbenes and nitrenes differ significantly even though they differ only in terms of replacing a lone pair with a C−R bond (such as in HN and $H_2C$ or comparably substituted carbenes and nitrenes ). [55, 58] As an example, the reaction rate of triplet phenylnitrene with dioxygen is much lower than that of triplet phenylcarbene. The initial interaction of carbenes and nitrenes with $O_2$ gives carbonyl *O*-oxides **27** and nitroso-*O*-oxide **29**, respectively, as shown in Scheme 5a.[59] A study by Sander has shown that, even under cryogenic conditions, the rate of the reaction of phenylcarbenes with $O_2$ can approach the limit of diffusion control.[59] In contrast, the rate for the reaction of *p*-substituted phenylnitrenes and $O_2$ amounts to only $10^{-6}$ L $mol^{-1}$ $s^{-1}$ in solvents such as toluene and hexane.[60] A detailed computational study by Borden *et al.* has explained the lower reactivity of triplet nitrenes compared to that of carbenes using the thermodynamical argument.[57] For comparison, the study was carried out on isoelectronic carbene **31** and nitrene **31**. According to the study, the enthalpy of triplet **32** is lower than that of triplet **31** by 25−26 kcal $mol^{-1}$, which reflects the relatively lower bond dissociation

energies (BDE) of **30** than **33**. Separately calculated difference of BDEs of N–H and C–H bonds for **30** and **33**, repectrively(Scheme 5b) came out to be around 20 kcal $mol^{-1}$, which qualitatively matches their relative enthalpies. The enthalpy calculations and BDE calculations point towards a higher thermodynamical stability of triplet **32** compared to triplet **31** and, therefore, an opposite trend in the triplet state reactivity.

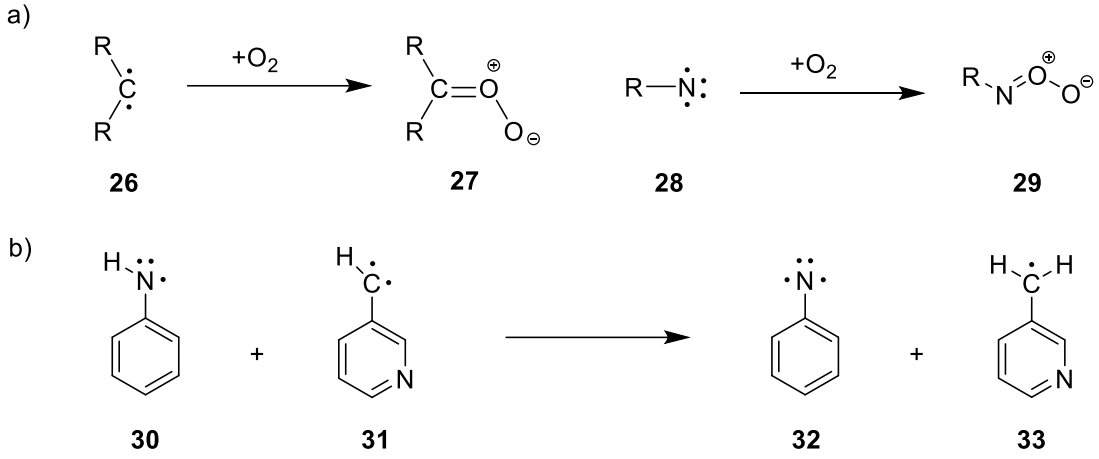


Scheme 5. a) Comparison of triplet state reactivity of carbenes and nitrenes. b) Equation to calculate the relative BDEs of **30** and **33**.

Another point of contrast between phenylcarbenes and phenylnitrenes is their singlet state reactivity. In solution, both phenylcarbenes and phenylnitrenes are produced photochemically from their precursors, which usually correspond to diazo derivatives and azides, respectively (Scheme 6). This photochemical extrusion of dinitrogen from the precursors **34** and **39** results in the lowest singlet state of phenylcarbene ($\tilde{a}^1A'$) **35** and phenylnitrene ($\tilde{a}^1A_2$) **32**, respectively. So formed phenylcarbene **35** and its derivatives are known to be efficiently trapped by various trapping agents, such as alcohols, alkanes, etc., and hence, relevant from an organic synthesis point of view.[61, 62] A high kinetic barrier for the ring expansion of **35** in the $\tilde{a}^1A'$ electronic state to form 1,2,4,6-cycloheptatetraene **37**

makes this step possible only in the gas phase, which results from the inability of phenylcarbene to dissipate its vibrational excess energy.[56] On the contrary, the singlet state ($\tilde{a}^1A_2$) of phenylnitrene **32** yields polymeric tars in solution, which result from the polymerization of an intramolecularly rearranged ketenimine 1-aza-1,2,4,6-cycloheptatetraene **41.**[29, 63] In the presence of trapping reagents, such as diethylamine, **41** can be trapped, forming an azepine derivative **42** (Scheme 6).[64] At low temperatures, rearrangement reactions are frozen out, and the intersystem crossing (ISC) step becomes favorable, resulting in the formation of triplet phenylnitrene $\tilde{X}^3A_2$-**32**.[29]

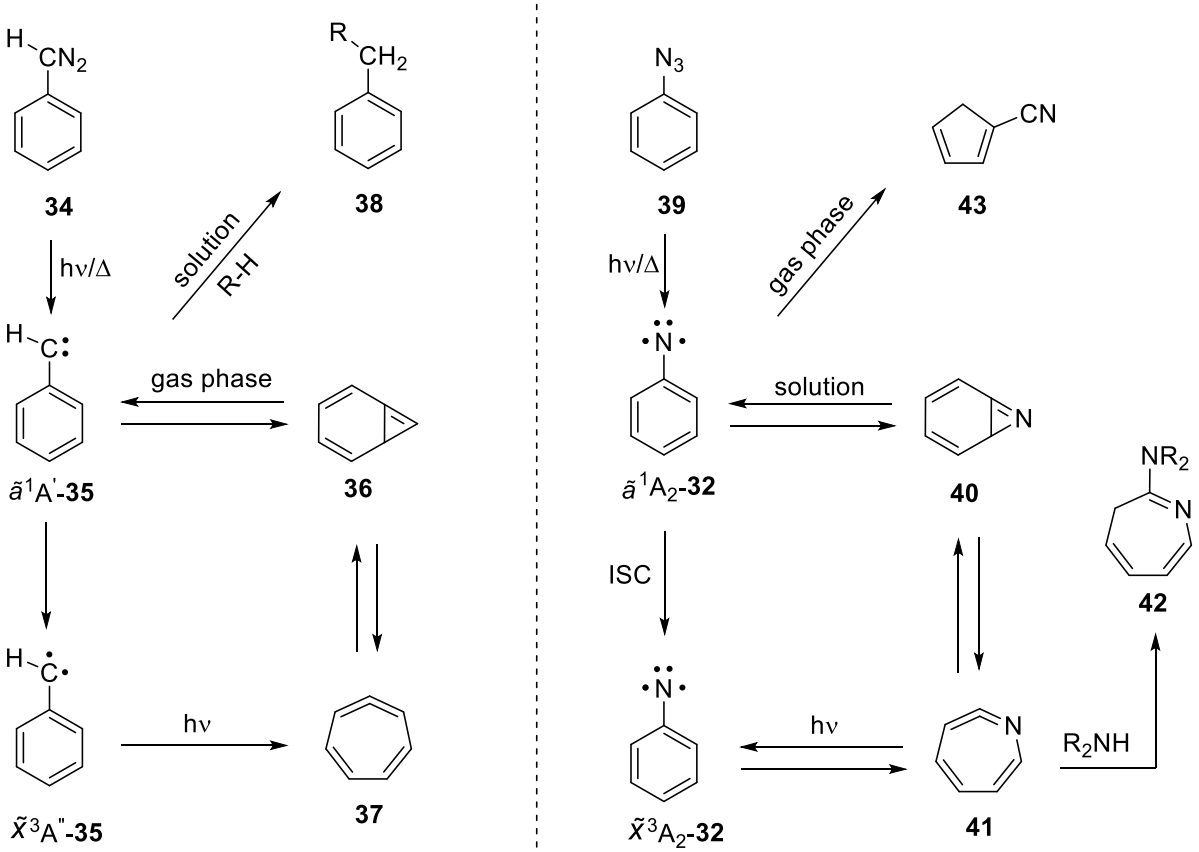


Scheme 6. A comparison of the reactivity of phenylcarbenes **35** and phenylnitrene **32**.

## 1.4 Applications of Nitrenes

Regarding the application of nitrenes, these highly reactive species have been exploited in diverse fields of chemistry in different ways and for different purposes. Physical organic chemists tend to explore the structure-property relationship of these species, which is further used in synthetic organic chemistry to introduce the nitrogen atom into a stable molecule.[65] On the other hand, nitrenes find their application in chemical biology and drug discovery, where they are used as photoprobes for photoaffinity labeling (PAL). In this technique, the photoprobe containing an azide moiety (e.g., polyfluorinated arylazides) is prone to bind covalently to the target biomolecule (a protein molecule, usually) upon photoirradiation *via* nitrene formation. In this way, the technique can help in identifying a new binding site for proteins, providing structural information, identifying conformational changes, and others.[66, 67] Azides, precursors to nitrenes, are used as photoresists in the fabrication of semiconductor circuits in photolithography processes.[68] Furthermore, nitrenes (oxycarbonyl nitrenes) are also used to functionalize carbon nanotubes and fullerenes.[69, 70] In recent times, the potential of nitrenes as magnetic materials has been recognized. High-spin nitrenes have been employed as model systems to create metal-free magnetic materials.[71-73] These high-spin nitrenes, which have strong ferromagnetic coupling, are produced from aromatic molecules containing multiple azide moieties.[73-75]

## 1.5 Borylnitrenes

Vinylidenes are a type of carbene known for their high reactivity.[2, 76-83] Such high reactivity arises from the high electrophilicity of these species. They are known to activate very stable C−H bonds by inserting into them (e.g., the C−H bond of the methane molecule, Scheme

7a).[80] Also, the insertion into the H−H bond is well known for these carbenes.[80] On the contrary, a typical singlet ground state carbene containing an electronegative substituent displays a reduced electrophilicity and, hence, faces high enough barriers to impede the insertion reactions at low-temperature conditions.[84] The reason for such a high electrophilicity and reactivity of vinylidenes is understood by visualizing the electronic structure of these species (Scheme 7a). Vinylidenes exhibit a singlet ground state ($\tilde{X}^1A_1$), unlike typical carbenes such as $H_2C$, PhHC, etc., which have triplet ground states ($\tilde{X}^3A_2$/($\tilde{X}^3A''$).[2, 85, 86] Due to the higher *s*-character of the doubly occupied *sp* hybridized orbital in vinylidenes as compared to the lower *s*-character of the doubly occupied $sp^2$ hybridized orbital in a typical carbene, the singlet state is more stable than the triplet state in vinylidenes. This can also be understood by the relationship between the bond angle R−C−R of a carbene with regard to the singlet-triplet gap. The lowest singlet state of a carbene gets stabilized upon a decrease in the bond angle; vinylidenes can be viewed as displaying a zero degree bond angle.[81] To use the high reactivity of vinylidenes, they must display a long enough lifetime. In the prototype of a vinylidene **44**, the barrier for intramolecular [1,2] H-shift was calculated to be only 1.3 kcal $mol^{-1}$. Hence, it prefers to convert into acetylene **45** rather than react intermolecularly with stable C−H bonds.[87] In contrast, replacing the two H substituents with two F atoms results in metastable vinylidene **46**, with a calculated barrier of around 36 kcal $mol^{-1}$ to undergo the [1,2] F-shift.[76] The origin of the barrier was shown to be the antiaromatic nature of the transition state (TS) involved, where the migrating F atom is unbound in the TS.[88] Therefore, **46** shows high bimolecular reactivity towards stable chemical systems (e.g., Xe, $CH_4$, $H_2$, etc.) under cryogenic conditions.[77-80]

In addition to this, borylnitrenes (Scheme 7b) display a BN unit that is isoelectronic to the CC unit of vinylidenes. Therefore, similar properties of borylnitrenes and vinylidenes can be expected.[31] Additionally, a compound like borazine is isoelectronic to benzene, where three CC units are replaced by three BN units. It has been established that borazine has comparable properties to benzene and is often referred to as "inorganic" benzene.[89-92] Using a similar analogy, iminoborane **49** can be related to acetylene **45,** as shown in Scheme 7a.

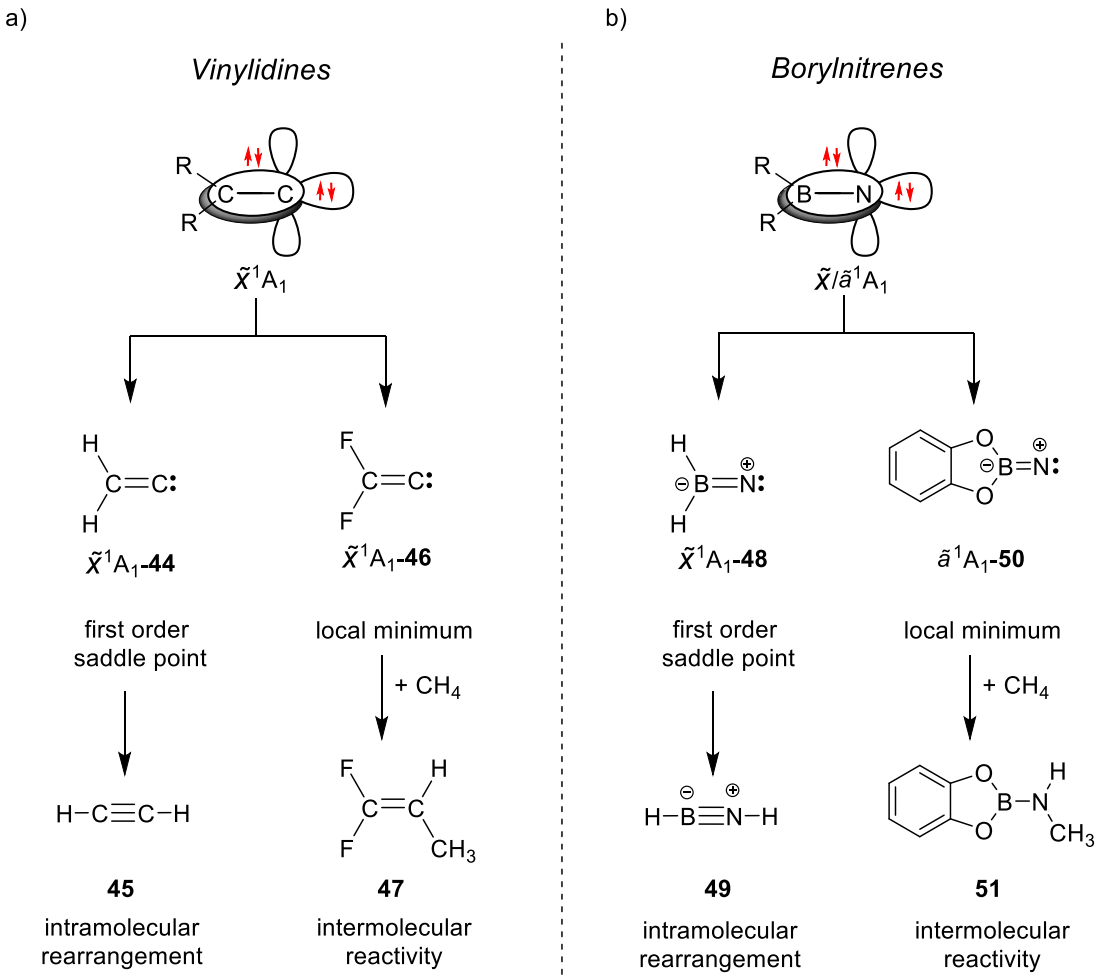


Scheme 7. The isoelectronic relationship between vinylidenes and borylnitrenes leading to a similar reactivity.

Further, in borylnitrenes, the similarity in the chemical behavior compared to vinylidenes is reflected by the similarity in the electronic structure of their lowest $^1A_1$ state. The prototype

of borylnitrene **48** has a singlet ground electronic state $\tilde{X}^1A_1$, which closely resembles the ground electronic state of **44**. The resemblance is due to the empty in-plane *p* orbital electronic states on both species, which results in their high electrophilicity.[31, 93, 94] Computationally, it was found that borylnitrene **48** is a first-order saddle point within the $C_{2v}$ point group, which relaxes iminoborane **49** upon removing the symmetry constraint.[95] The computational findings were supported by the experimental data, which showed that the thermolysis of dialkyl and diaryl azidoborane forms iminoboranes without the observation of trapping products resulting from potentially forming borylnitrene intermediates.[96] This kind of chemical behavior of borylnitrenes is reminiscent of the reactivity of vinylidene **44**. Nevertheless, the diamino derivatives of **48** with bulky substituents were successfully trapped in a photolysis experiment of precursors $(R_2N)_2BN_3$.[97] Compared to **48**, the stronger B–N bonds between the amino substituents and the boron atom, along with the reduced electrophilicity, helped evade the intramolecular rearrangements. Another similar type of borylnitrenes with two oxygen donor atoms attached to the boron atom could also show similar chemical behavior, such as the 2-nitreno-1,3,2-benzodioxaborole **50** (catBN; cat = catecholato) and the 2-nitreno-4,4,5,5-tetramethyl-1,3,2-dioxaborolane **93** (pinBN: pin = pinacholato).[19, 20, 31, 94, 98-100] Matrix isolation studies have shown that **50** in its $\tilde{X}^3A_2$ state gives insertion reaction photochemically with $CH_4$ to form **51**.[19] In solution, nitrene **93** was observed to be trapped by hydrocarbons such as cyclopentane and cyclohexane.[19, 99] In this way, there is a distinct category of borylnitrenes where the intramolecular rearrangement can be effectively suppressed by the addition of an electron donor, leading to what is known as donor stabilized borylnitrenes.

## 1.6 Donor Stabilized Borylnitrenes *vs*. Other Nitrenes: Comparison of the Electronic Structure

The electronic state of a nitrene is characterized by its spin multiplicity (triplet and singlet) and constituent electronic configurations. The reactivity of a nitrene is influenced by the type of electronic state of the nitrene that is participating in the reactivity.[8] Therefore, it becomes very important to know the characteristics and relative energy ordering of the lower energy electronic states that are important from a practical point of view.

In imidogen **1** (HN), the lowest electronic state, $\tilde{X}^3\Sigma^-$ has triplet spin multiplicity and is characterized by one configuration of electrons, where two unpaired electrons occupy the unhybridized *p* orbitals, as shown in Figure 3.[1] The triplet ground state is possible due to the low Coulomb repulsion between the electrons when they are present in the two separate orbitals ($p_x$ and $p_y$) and the high exchange energy between the unpaired electrons. This electronic state is followed by a singlet state, $\tilde{a}^1\Delta$, which is relatively higher in energy by 36 kcal $mol^{-1}$ determined experimentally and encompasses four different electronic configurations.[1, 7, 8, 101] This situation arises from the high symmetry of **1** that leads to the degeneracy of the non-bonding $p_y$ and $p_x$ orbitals, as discussed in Section 1.1. The third electronic state, $\tilde{b}^1\Sigma^+$, is of singlet multiplicity and made up of two closed-shell configurations,[1, 7] as determined by the computational studies, which is higher in energy by 61 kcal $mol^{-1}$ according to the experimental data. In the case of phenylnitrene **32**, which has been subject to many experimental and computational investigations, the ground state, $\tilde{X}^3A_2$, is of triplet spin multiplicity. Following that, there is a singlet state, $\tilde{a}^1A_2$, with a leading configuration similar to the ground triplet state but with unpaired electrons arranged in opposite spins. According to negative ion photoelectron spectroscopy (NIPES) data, this state

is higher in energy by 15.1 kcal mol$^{-1}$ compared to the ground triplet state.[102] Next in the energetic order is another singlet state, $\tilde{b}^1A_1$, in which the leading electronic configurations exhibit a doubly occupied $p_y$ orbital and an empty $p_x$ orbital. Energetically, the state is approximately 30 kcal mol$^{-1}$ above the ground state, according to the NIPES data.[29, 58, 102]

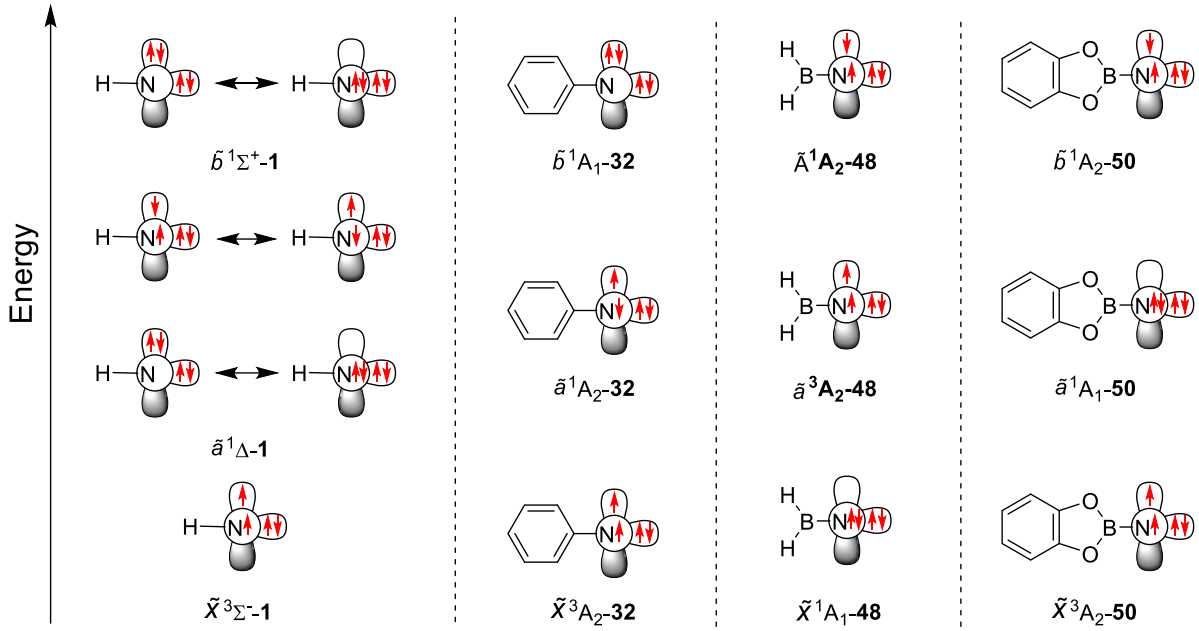


Figure 3. Major electronic configurations of the lowest three electronic states in nitrenes **1**, **32**, **48**, and **50**.

The energy ordering in borylnitrene **48** is unusual among the nitrenes discussed so far. As mentioned in Section 1.5, **48** being a first-order saddle point in the ground singlet state, there is only computational data available related to the relative energy ordering of its electronic states. The lowest state, $\tilde{X}^1A_1$, is a singlet with a doubly occupied $p_x$ orbital, resulting from a Lewis acidic boron atom attached next to the nitrogen center.[31] The empty $p$ orbital of the boron atom results in the electron-withdrawing effect from the nitrogen center that moves the $p_x$ and $p_y$ orbitals far in terms of energy. The energy difference is high enough that nitrene **48** is more stabilized by having two electrons paired in the low-energy $p_x$

orbital despite the associated Coulomb repulsion. $\tilde{a}^3A_2$ is the next electronic energy level in the energetic order, which is similar in terms of electron occupation as the ground state triplets of **1** and **32**. The electronic state $\tilde{a}^3A_2$ lies 7-9 kcal mol$^{-1}$ higher in energy than the ground electronic state $\tilde{X}^1A_1$. The next energy level, $\tilde{A}^1A_2$, lies 28 kcal mol$^{-1}$ higher in energy with both the opposite spin electrons unpaired in the $p_x$ and $p_y$ orbitals.[31] However, in borylnitrene **50**, due to the presence of two electron donor oxygen atoms, the energy order alters compared to **48**. The reduced Lewis acidity of the boron atom due to the two electron donor oxygen atoms destabilizes the $\tilde{a}^1A_1$ state as compared to that of $\tilde{X}^1A_1$ in **48.** Due to this reason, **50** favors the triplet state $\tilde{X}^3A_2$ as the ground state.[31, 103] The relative energy order for **50** is $\tilde{X}^3A_2$ < $\tilde{a}^1A_1$ < $\tilde{b}^1A_2$ where $\tilde{a}^1A_1$ and $\tilde{b}^1A_2$ lie 33 kcal mol$^{-1}$ and 34 kcal mol$^{-1}$ above the ground state, respectively.[31, 103]

As mentioned above, the reactivity of nitrene is strongly affected by the nature of the electronic state participating in the reaction. Access to a particular electronic state for a reaction depends on various factors, such as temperature, medium of reaction, and concentration of the precursor used. Wirz and Platz, using transient absorption spectroscopy, observed that the solution phase photoirradiation of phenylazide **39** resulted in phenylnitrene **32**, whose preferred singlet state reactivity on the $\tilde{a}^1A_2$ surface finally results in the formation of ketenimine **41** in the presence of a trapping reagent (Scheme 6).[104, 105] Whereas, if the reaction is executed at lower temperatures (<170 K), ISC is favored, leading to the formation of the nitrene dimer, an azo compound.[106] In a glass matrix at 77 K, one of the earliest detections of triplet **32** was accomplished by photodecomposition of precursor **39**. It was observed that the presence of the EPR signal was dependent on the temperature at which **39** was photolyzed.[107] The rate constants for ISC ($\tilde{a}^1A_2$ to $\tilde{X}^3A_2$) for **32** at 170 K and

77 K were found to be 3.2 ± 0.3 × $10^{-6}$ $s^{-1}$ and 3.8 ± 0.3 ×$10^{-6}$ $s^{-1}$, respectively.[108] The concentration also plays a significant role in terms of the reactivity of **32** as it was found that photolysis of highly diluted solutions of **39** led to the formation of azobenzene, which again was the result of the dimerization of triplet phenylnitrene **32**. Also, photolysis gave azobenzene in a highly concentrated solution of **39**, which could be traced back to a reaction of triplet **32** and phenylazide **39**.[109] Regarding the reactivity of **32** in the gas phase, it undergoes rearrangements on the singlet surface $\tilde{a}^1A_2$ but with a different final product, namely cyanocyclopentadiene **43**.[110] The difference in final product formation occurs due to the excess energy in the nascent hot vibrational states of $\tilde{a}^1A_2$ electronic state of **32**. The hot vibrational states allow the molecule to fully explore the potential energy surface (PES) and even surmount high energy reaction barriers. Product **43** is the global minimum of the PES of $C_6H_5N$, which has a > 30 kcal $mol^{-1}$ kinetic barrier of formation from the singlet state $\tilde{a}^1A_2$ of **32**.[55]

### 1.7 Donor Stabilized Borylnitrenes *vs.* Other Nitrenes: Comparison of Reactivity

#### 1.7.1 Reactivity in the Triplet State

The reactivity of the triplet state of nitrenes is mainly observed under low-temperature conditions (matrix isolation). As mentioned in Section 1.3, the low temperature favors the ISC for phenylnitrene **32**; and hence, the yield of the triplet becomes higher.[106] A substantial yield of triplet **32** is possible if the precursor azide **39** is irradiated in the presence of a triplet photosensitizer.[111] Similarly, borylnitrene is known to show similar chemical behavior. On the one hand, in the solution phase, the reactivity of **93**, which is a pinacholato analog of borylnitrene **50**, is produced from the corresponding azide **92** and is known to be trapped by

the cycloalkane solvents as discussed later in Section 1.7.2 (Scheme 17). This room-temperature photoreactivity gives amino-boranes, the C-H insertion products of the singlet borylnitrene, into the C-H bond of cycloalkane.[19, 20, 31, 94, 98-100] However, in the low-temperature matrices, triplet state $\tilde{X}^3A_2$ of borylnitrene **50** was obtained in high yields, as confirmed by the UV-VIS, IR, and EPR spectroscopy.[31, 39, 98, 99]

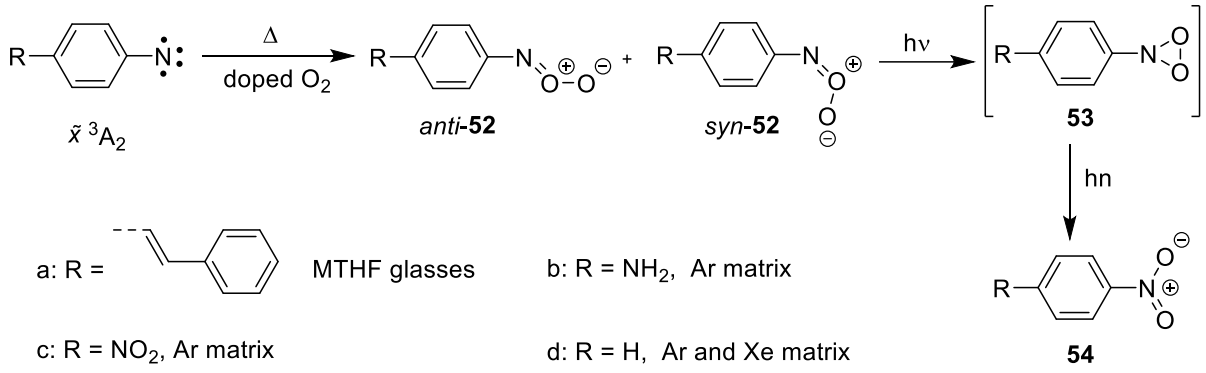


Scheme 8. The reactivity of *p*-substituted phenylnitrenes with dioxygen $O_2$ in their respective triplet ground state.

The reactivity of nitrenes and carbenes with $O_2$ is also a qualitative indication of the spin state of the involved species. The reaction of dioxygen with phenylnitrene **32** and its substituted variants has been studied thoroughly under low temperatures and with different frozen media (Scheme 8). The reaction of a stilbene derivative of arylnitrene (*p*-nitrenostilbene) with $O_2$ was thermally carried out in frozen methyltetrahydrofuran (MTHF). [23] The triplet nitrene was photochemically produced from the azidostilbene precursor at 77 K, and after that, the frozen solution was heated up to 95 K to induce a thermal reaction. The heating resulted in the formation of singlet nitroso-*O*-oxide **52a**, which, upon photoirradiation, gave nitro compound **54a**, assumed to be forming *via* dioxaziridine intermediate **53**. A much more detailed study of such a reaction was done with *p*-aminophenylnitrene using matrix isolation and argon as the host material.[24] The thermal

reaction between the nitrene and $O_2$ at 30 K leads to the formation of *syn*- and *anti*-*p*-aminophenylnitroso-*O*-oxide (*syn*-**52**b and *anti*-**52**b) as the kinetic products. The two isomers of *p*-aminophenylnitroso-*O*-oxide oxide were interconvertible at different wavelengths of light. Eventually, they could photoreact to give the thermodynamic product *p*-nitroaniline **54b**. The case of *p*-nitrophenylnitrene was also similar, whose reaction with $O_2$ was studied with Xe as the host material, and hence, the reaction could have access to higher temperatures.[25] The reaction resulted in nitroso-*O*-oxide products *syn*-**52c** and *anti*-**52c**, detected for the first time with IR spectroscopy, finally giving the 4,4'-dinitroazobenzene **54c**. Notwithstanding the results discussed so far, phenylnitrene **32** does not undergo a thermal oxygen addition reaction even in solid $O_2$.[26] Considering the higher barrier for the addition, the reaction was performed in an Xe matrix at 50 K, but still, only 40 % conversion was achieved even after 12 h. The reaction gave nitroso-*O*-oxide product *syn*-**52d**, which was converted photochemically to nitro product **54d**. The experimentally determined activation barriers for the reaction of phenylnitrene **32** with $O_2$ were found to be 4.3 ± 0.5 kcal $mol^{-1}$ using flash photolysis experiments, which supports the experimental findings where a slow reaction of phenylnitrene with $O_2$ was observed.[112] In the case of solution phase studies of the reactivity (in solvents such as toluene and hexane), Gritsan and Pritchina reported that *p*-substituted phenylnitrene reacts much slower than the phenylcarbenes.[113]

In contrast, some nitrenes are as reactive as carbenes in their triplet state, as reflected by their reactivity studies with $O_2$. In the gas phase, HN **1** is known to react with $O_2$ to form NO and OH as the major products, which hints at the involvement of one or more intermediates during the reaction.[114] Computational studies have explored the potential energy surface for this reaction (HN + $O_2$) and found several possible minima, as shown in

Scheme 9a.[115, 116] Furthermore, the thermal reaction of triplet HN **1** with $O_2$ was carried out in Ar and Xe matrices.[117] It was found that in the Xe matrix, the reaction between $\tilde{X}^3\Sigma^-$-**1** and $O_2$ began at 20 K and continued until all the NH was consumed at 50 K, forming a new product. The formation of nitrous acid **55** and hydrogen nitryl **56** was ruled out based on their already-known IR spectra.

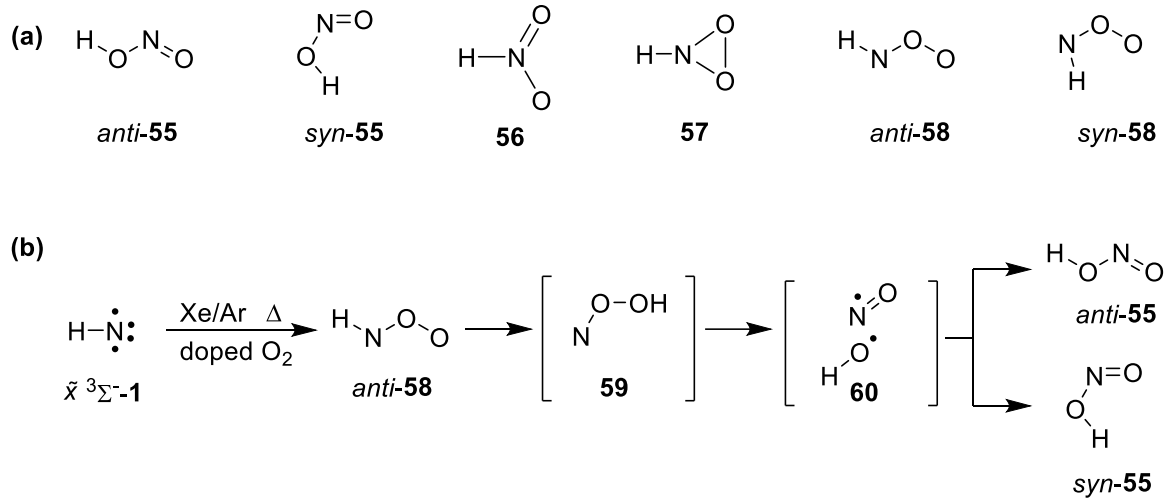


Scheme 9. a) Possible minima in the reaction of **1** in $\tilde{X}^3\Sigma^-$ electronic state with $O_2$. b). The ground state reactivity of **1** with $O_2$. c) The ground state reactivity of triplet **50** with $O_2$.

Also, due to high energy barriers of reaction to form dioxaziridine **57**,[116] it could not be the possible product forming at such low temperature conditions. Moreover, the computed IR stretches and their respective intensities of nitroso-*O*-oxide *anti*-**58** were in good agreement with that of newly observed stretches in the reaction, and therefore, it was assigned as the product of the reaction between $\tilde{X}^3\Sigma^-$-**1** and $O_2$ upon annealing.[117] Computational results

have shown that the reaction resulting in *anti*-**58** should take place without any energy barrier.[116, 117] In the Ar matrix, the formation of *anti*-**58** started at 12 K and continued until 33 K, after which the matrix started losing its rigidity.[117] According to the thermodynamical argument given in the study, the observation of only *anti*-**58** is due to the equilibrium distribution between *anti*-**58** and *syn*-**58**, with *anti*-**58** being lower in energy by 3 kJ $mol^{-1}$. On the other hand, in another computational study by Talipov et al., it was argued that the preference for the formation of *anti*-**58** has a lower energy barrier of formation than *syn*-**58**.[115] Also, the potential energy scans were performed in both singlet and triplet multiplicities with N-O bond distance as the parameter, and singlet *anti*-**58** was shown to have the lowest energy barrier of formation. [115, 117] The resulting *anti*-**58** was photolabile and, upon photoirradiation with UV or visible light, converted to two geometric isomers of nitrous acid *anti*-**55** and *syn*-**55**.[117] Based on the calculated ground state (PES), the photoconversion to *anti*-**55** was proposed to happen *via* intermediates **59** and **60**, but there was no experimental evidence to prove their formation. Therefore, **1** showed higher reactivity with $O_2$ compared to arylnitrenes in their triplet state. It resulted in a different final thermodynamic product, *anti*-**55**, instead of nitro product **56**, as in the case of arylnitrenes.

Later on, it was found that borylnitrene **50** was one of the arylnitrenes that showed high reactivity in their ground state, $\tilde{X}^3A_2$, towards $O_2$ in matrix isolation (Scheme 9c).[31] The reactivity of **50** with $O_2$ in its ground state is reminiscent of that of **1** with $O_2$. In the thermal reaction of **50** with $O_2$, there was the formation of nitroso-*O*-oxide *anti*-**61** and nitritoborane *anti*-**62,** in contrast to the case of **1,** where nitroso-*O*-oxide was the sole product.[31] After that, the photoreactivity of the product formed was explored, and 254-nm-irradiation of the

matrix resulted in the conversion of *anti*-**61** into *anti*-**62**. The mechanistic aspects of this reaction were covered in a separate study discussed in Section 4.1.

### 1.7.2 Reactivity in the Singlet State

Nitrenes in the lowest singlet state are prone to intramolecular rearrangements. Depending on the substituents attached to an azide precursor, there can be a competing concerted thermal or photochemical pathway leading to intramolecular rearrangements without the involvement of a nitrene (Scheme 10a).[45, 118] In the case of photochemical or thermal pathways, resulting in the corresponding nitrene from the azide, the lowest energy singlet state is populated.[40, 104, 105, 107] On the lowest singlet state PES, nitrenes usually undergo intramolecular rearrangements that compete with the relaxation (ISC) to the lower ground triplet state (Scheme 10a).[29, 63, 119] The intramolecular rearrangements occur on a faster time scale compared to that of ISC, and this trend can be reversed in some special cases, e.g., in phenylnitrene **32** at lower temperatures.[106]

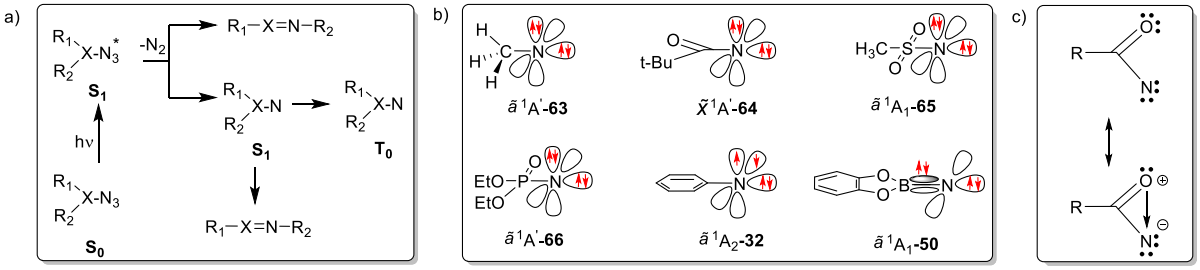


Scheme 10. a) Different reaction channels of a photochemically generated nitrene. b) electronic configurations of the lowest energy singlet state of different types of nitrenes. c) Donor-acceptor type intramolecular interaction in the ground singlet state of a carbonylnitrene.

The electronic configuration of the lowest singlet state is also a significant factor influencing the rate of ISC. Phenylnitrenes, unlike the rest of the nitrenes shown in Scheme 10b, have

unpaired electrons in the unhybridized *p* orbitals.[29, 102] This makes the ISC crossing from $\tilde{a}^1A_2$ to the ground triplet state $\tilde{X}^3A_2$ El-Sayed disallowed and hence leads to slower ISC. Moreover, the intramolecular rearrangements can also be suppressed by including some adequate chemical moieties in the nitrene.[17, 44, 120] Also, the singlet state of the nitrene can be shifted to the lowest energy in cases of very strong intramolecular interactions.[9, 121] For instance, in carbonylnitrenes, donor-acceptor interactions between the in-plane lone pair of the carbonyl oxygen atom and the unhybridized *p* orbital of nitrogen enforce an overall singlet ground state (Scheme 10c). An unusually short N-O bond in the carbonylnitrenes is another evidence of such an interaction, which leads to a singlet ground state, as in the case of benzoylnitrene.[9, 121]

One of the earliest reports on intramolecular rearrangements in the lowest singlet electronic state was presented by Milligan for alkylnitrenes, which were prepared from the photolysis of methylaizde **67i** isolated in Ar and $CO_2$ in separate experiments (Scheme 11a).[119] The photochemistry of the **67i** at 4.2 K and 50 K for Ar and $CO_2$ matrices, respectively, was analyzed using IR spectroscopy, and methyleneimine **68i** was found to be the photochemical product.[119] To some extent, computational studies could explain the experimental findings. Whereas the earlier experimental studies suggested that the $\tilde{a}^1A'$-**63i** is a saddle point on the PES,[122] recent studies have shown the $\tilde{a}^1A'$-**63i** is a minimum on the PES that has a very low barrier of a few kcal $mol^{-1}$ for the [1,2]-H shift.[123] This also explains the absence of bimolecular reactivity of singlet **63i** and being undetectable in femtosecond spectroscopy.[124] In an attempt to suppress the intramolecular rearrangements, different substituents were attached to the carbon atom of **63i**.[124] In the case of *tert*-butylazide **67ii**, photolysis in matrix isolation led to the formation of trimethylimine **68ii**, which indicates

similar photochemistry as in the case of **67i**.[28] The case of trifluoromethyl azide **67iii** gave different results, and the product was identified as a triplet ($\tilde{X}^3A''$) trifluoromethylnitrene **63iii** in an argon matrix.[120] A higher kinetic barrier for the 1,2-fluorine shift led to a slower rearrangement on the $S_1$ PES compared to the ISC.

In the early studies on intramolecular rearrangements of carbonylnitrene, called Curtius rearrangement (Scheme 11b), the reaction mechanism remained unclear.

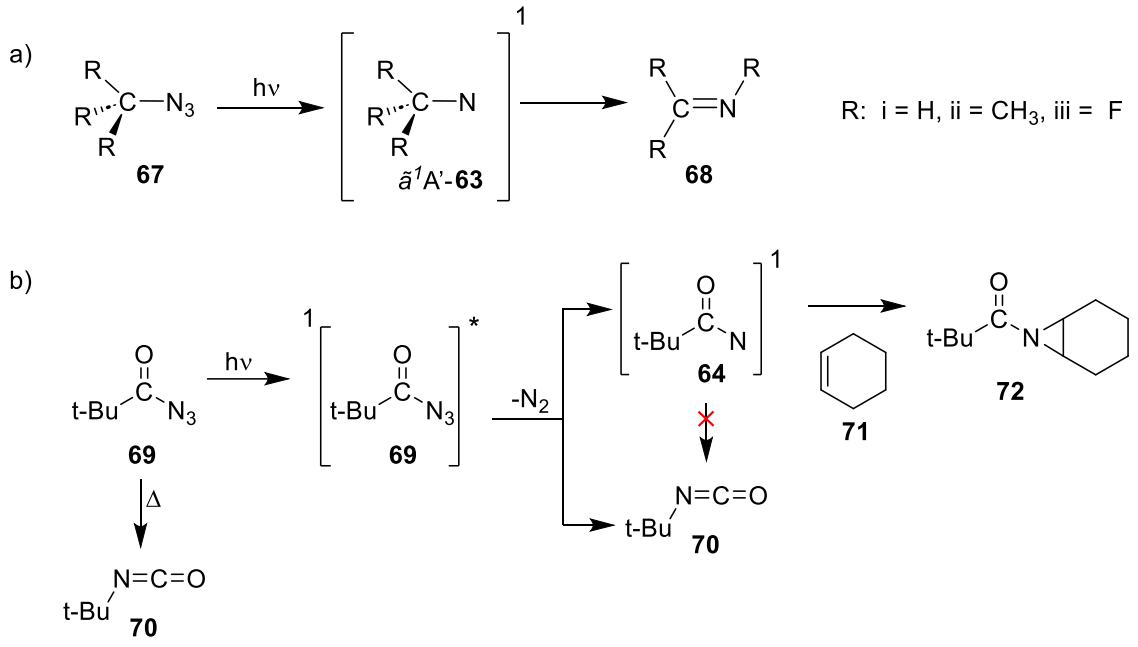


Scheme 11. Singlet state reactivity of alkylnitrenes (a) and carbonylnitrenes (b).

Both the possibility of a concerted mechanism and a step-wise mechanism with the involvement of acylnitrene **64** were considered. Thermolysis experiments by Lwowski on the pivaloylazide **69** in cyclohexane, cyclohexene, and 2-methylbutane led to the observation of the corresponding isocyanate **70** only, and no trapping product was observed.[118] Later, in more advanced experimental studies by Lwowski on the photolysis of **69**, it was found that nitrene **64** could be trapped by solvents such as cyclohexene, resulting in an aziridine **72**

(Scheme 11b). Another important observation was that the yield of isocyanate **70** was not affected by the amount of trapping reagent in the photolysis experiments.[45] Hence, it was concluded that the Curtius rearrangement occurs in a concerted way without the involvement of nitrene **64**. This also reflected the relatively higher potential of carbonylnitrenes for bimolecular reactivity than their alkyl counterparts. Further, trapping of β-naphthoylnitrene in the presence and absence of a triplet sensitizer resulted in the same products, which is an experimental evidence for the singlet ground state of carbonylnitrenes. The absence of EPR signals for the nitrene at 77 K supports this conclusion.[125]

Sulfonylnitrenes are another class of nitrenes that have been widely explored. EPR studies on **65** have shown a triplet ground state, but they are known to be generated in their lowest singlet state, $\tilde{a}^1A_1$, from methanesulfonylazide precursors **73** upon photolysis or thermolysis.[126, 127] The singlet state $\tilde{a}^1A_1$ of sulfonylnitrene **65** was found to insert into the C−H bonds of 2,4-dimethylpentane, resulting in three different products **74**, **74'**, and **74''** (Scheme 12a).[44] Moreover, the intramolecular rearrangement pathways are very slow on the lowest singlet PES compared to the previously discussed nitrenes.[21] There was no conclusive evidence for a Curtius-type rearrangement in sulfonylnitrenes unless the traces of $FN{=}SO_2$ were detected after photolysis of thermally generated nitrene $FSO_2N$.[32, 128] Additionally, trifluoromethylsulfonylnitrene ($CF_3SO_2N$) **76** was studied using matrix isolation and was shown to be isolated in the triplet ground state.[38] The further photoirradiation of this nitrene leads to the formation of $CF_3N{=}SO_2$ **77** and $CF_3S(O)NO$ **78** through a Curtius-type rearrangement.[38]

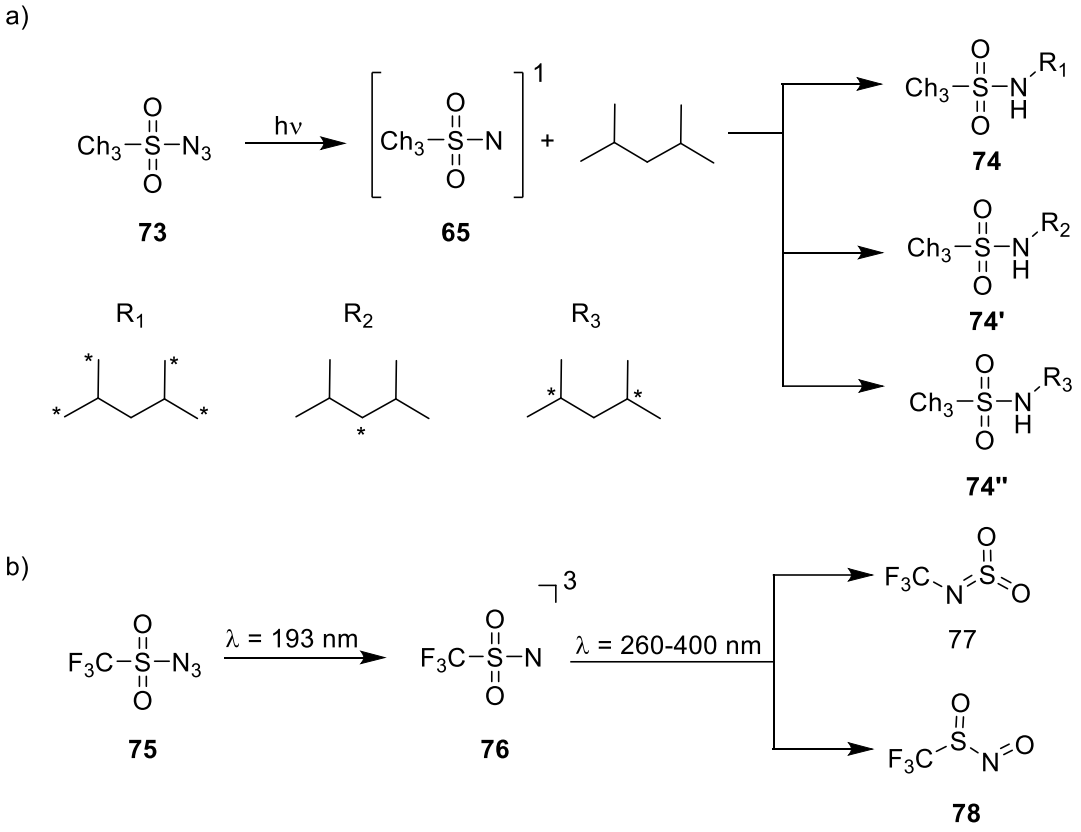


Scheme 12. a) Singlet state reactivity of sulfonylnitrenes **65**. b) Curtius-type rearrangement in sulfonylnitrenes **76**.

Another type of nitrenes is the phosphorylnitrenes, known for eluding intramolecular rearrangements and showing significant bimolecular reactivity. According to the results from ultrafast spectroscopy, when photochemically produced from the (diethoxyphosphoryl)azide **79**, the lowest singlet electronic state, $\tilde{a}^1A_1$, of (diethoxyphosphoryl)nitrene **66** is initially formed. The singlet state (Scheme 13) then bifurcates into two channels: 1) bimolecular reactivity with the trapping agents on the $\tilde{a}^1A_1$ PES, and 2) ISC to the ground triplet state $\tilde{X}^3A_2$.[40] For **66**, an efficient insertion by the $\tilde{a}^1A_1$ singlet state into the C−H bonds of 2,3-dimethylbutane, giving amines **80** and **80'**, with a yield of almost 60% (Scheme 13).[46] The minor product was identified as an amide **81**, which resulted from the triplet state reactivity ($\tilde{X}^3A_2$) of **66** by radical pair formation and recombination.[46]

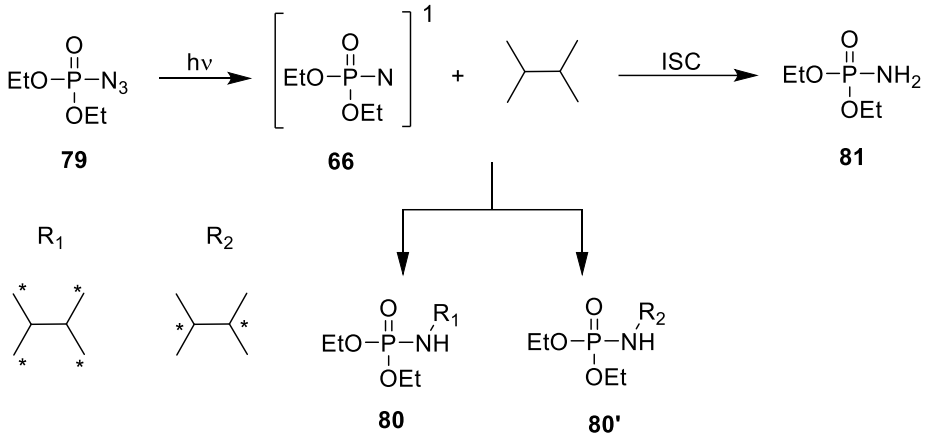


Scheme 13. Singlet state reactivity of (diethoxyphosphoryl) nitrene **66**.

Phenylnitrene **32**, also referred to as the prototype of aromatic nitrene,[26] is one reactive intermediate that has been the subject of research for many decades.[29, 58] In Sections 1.3 and 1.6, reactivity aspects of the singlet state, $\tilde{a}^1A_2$, have already been discussed. In these sections, It has been shown that there is a preference for forming a ring expansion product, ketenimine **41**, which could form an insertion product **42** or a polymeric tar, depending on the availability of the trapping reagent (Scheme 14a).[29, 63] Therefore, $\tilde{a}^1A_2$ electronic state of phenylnitrene **32** is known to have poor bimolecular reactivity and is prone to high intramolecular reactivity. The explanation for such a poor bimolecular reactivity of $\tilde{a}^1A_2$ in **32** lies in its electronic configuration. Whereas for other nitrenes, the electrons in the lowest singlet state are paired, leaving one of the orbitals vacant, phenylnitrene exhibits unpaired electrons in the unhybridized *p* orbitals (Scheme 10b).[102] The empty orbitals on nitrenes make them highly electrophilic and hence reactive towards, e.g., intermolecular C−H bond insertions, which is not possible in the case of phenylnitrene **32** due to a lack of empty *p* orbitals. Also, the ISC from $\tilde{a}^1A_2$ to the ground triplet state $\tilde{X}^3A_2$ is slower due to ISC being El-Sayed disallowed (Scheme 14b),[58] and hence, no pathway can compete with the intramolecular reactivity on the $\tilde{a}^1A_2$ PES. Computational studies have successfully added to

the knowledge explaining the reactivity of $\tilde{a}^1A_2$. According to the computational study by Karny and Borden, starting from **32**, the formation of benzazirine intermediate **40** precedes the formation of trappable ketenimine **41**, with an activation barrier of 9 kcal mol$^{-1}$ (Scheme 14a).[56] The barrier obtained for further reaction to form **41** was calculated to amount to around 3 kcal mol$^{-1}$.[56]

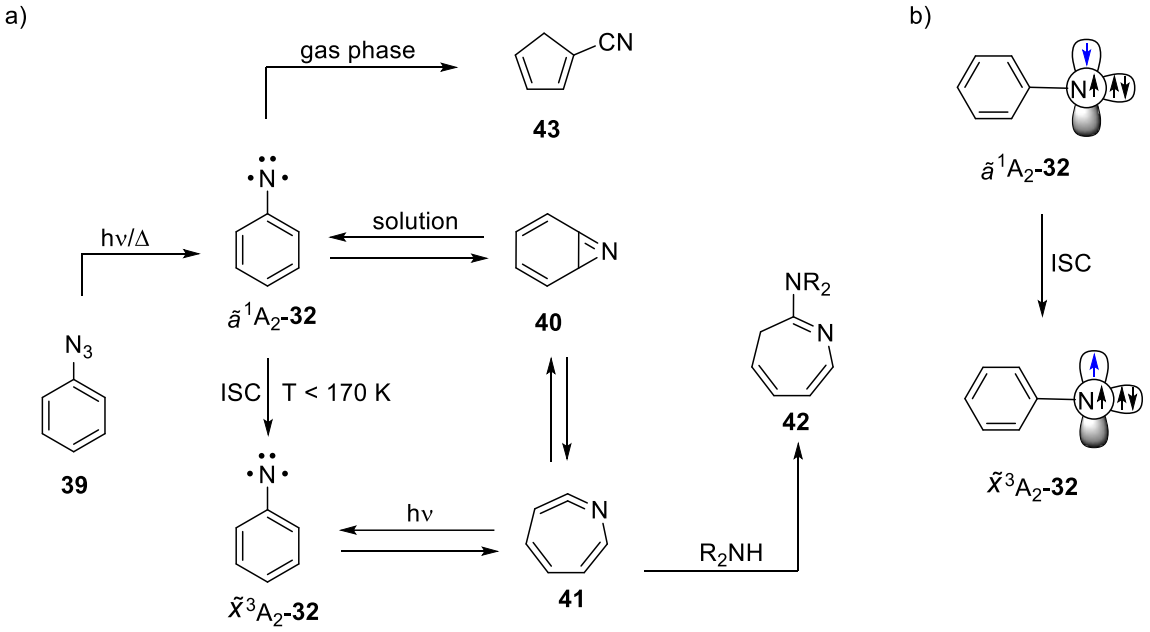


Scheme 14. a) Singlet state reactivity of phenylnitrenes **32**. b) El-Sayed disallowed intersystem crossing between the lowest energy singlet ($\tilde{a}^1A_2$) and triplet ($\tilde{X}^3A_2$) electronic state of phenylnitrenes **32**.

Hence, due to the lower kinetic barrier for the conversion of **40** to **41**, only **41** is trappable. Also, under low temperatures, such activation barriers are too high to be surpassed, and, therefore, ISC to the $\tilde{X}^3A_2$ state becomes the favorable pathway.

Borylnitrenes, as discussed in Section 1.5, are BN analogs of highly reactive vinylidenes. In the singlet state, borylnitrenes have an electronic structure like that of the highly reactive ground state of vinylidenes. Therefore, similar reactivity in borylnitrenes in the

singlet state is expected and, in fact, also observed. However, the high electrophilicity in the borylnitrenes can lead to intramolecular rearrangements and, hence, can suppress the bimolecular reactivity of borylnitrenes. In addition to the already discussed borylnitrene **48** in Section 1.5, which tends to undergo [1,2] H-shits, there are other examples of borylnitrenes that prefer such intramolecular rearrangements. The dibenzo derivative of borylazide (9-azido-9-borafluorene) **82**, when irradiated in benzene solvent at room temperature, gave the dibenzo derivative of 1,2-azaborinine **83**, which is a BN analog of 9,10-phenanthryne (Scheme 15). This reactive intermediate, in the absence of trapping reagents, undergoes cyclo-oligomerization but can be trapped by the large excess of trapping reagents, as shown in Scheme 15.[129-132] Based on computational studies of the ground state potential energy surface, the ring enlargement was proposed to happen via concerted pathways without the involvement of nitrene upon photolysis of **82**.

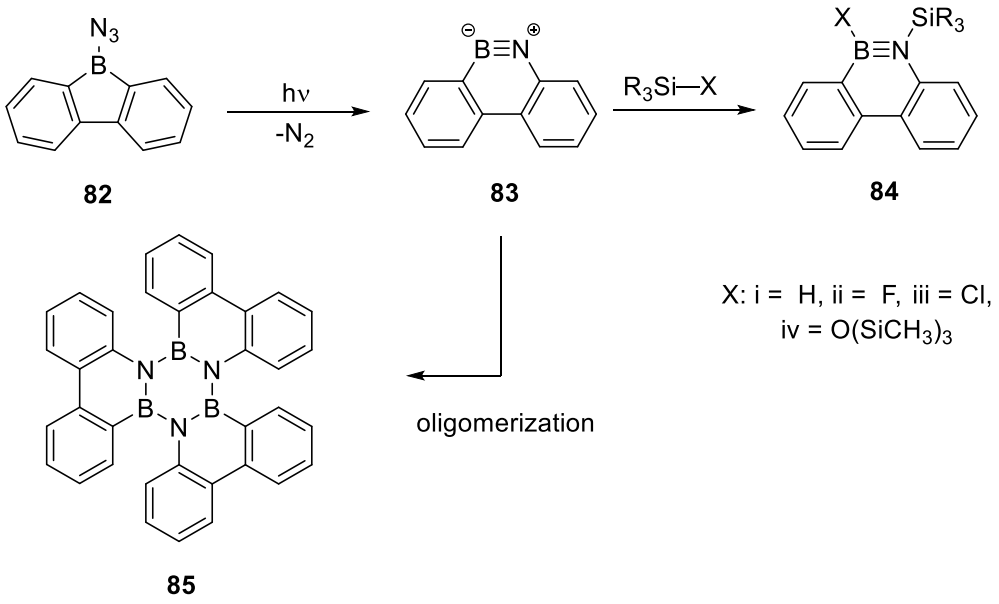


Scheme 15. Photochemical reactivity of 9-azido-9-borafluorene **82**.

On the other hand, as discussed in Section 1.5, the reduced electrophilicity by adding electron donor (oxygen, nitrogen, etc.) atoms with their strong bonding to the boron atom

promotes the bimolecular molecular reactivity of the lowest singlet state $\tilde{a}^1A_1$ of borylnitrenes (Scheme 16).[19, 31, 39, 94, 98] For this reason, these borylnitrenes are also called donor stabilized borylnitrenes.[19, 20, 31, 39, 94, 98-100, 103] Also, in the relative energy ordering of various electronic states in borylnitrene **50**, the lowest singlet electronic state $\tilde{a}^1A_1$ moves higher in energy as compared to the lowest electronic triplet state $\tilde{X}^3A_2$.[31] This type of energy ordering is another consequence of the reduced electrophilicity of the boron atom.

Similar to other nitrenes, the reactivity and characterization of donor stabilized borylnitrenes have been studied under low temperatures, using matrix isolation, and in the solution phase under ambient conditions.[19, 31, 39, 94, 98] The characterization and extensive reactivity studies of donor stabilized borylnitrene **50** have been done using matrix isolation.

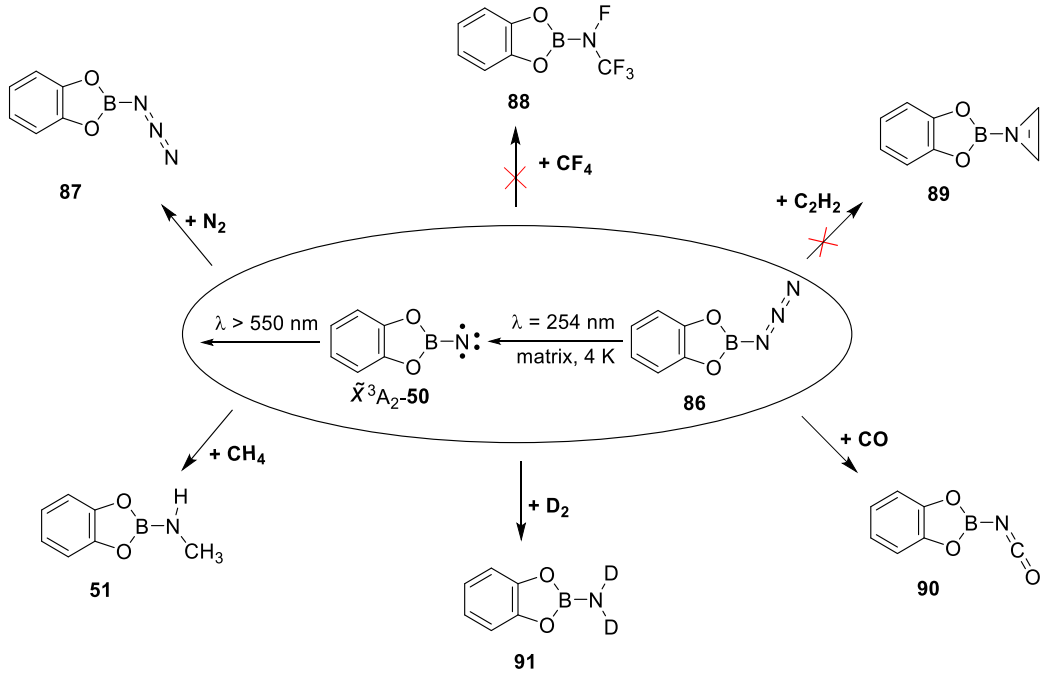


Scheme 16. Matrix isolation study of the singlet state reactivity of borylnitrene **50** with stable compounds.

EPR spectroscopy confirmed the triplet ground state $\tilde{X}^3A_2$ of **50** with | $D / hc$ | = 1.492 $cm^{-1}$ and | $E / hc$ | = 0.004 $cm^{-1}$.[31, 39] Further characterization of the triplet ground state has been done using UV-VIS and IR spectroscopy. Regarding the reactions of **50**, no transformations were observed with closed-shell species, such as $N_2$, $D_2$, CO, $CH_4$, etc., in the triplet ground state, which was induced by heating the matrix to a certain temperature depending on the material of the host matrix.[19, 31, 98] The reaction of $N_2$ with **50** in the Ar matrix, for example, could not proceed even after evaporating most of the Ar host at 55 K. However, UV-VIS and IR spectroscopy gave some indication in favor of forming a dimer or an oligomer of **50** at such a temperature.[99] Nevertheless, from the low-temperature UV-VIS spectrum of **50**, it could be seen that it absorbs an extended region of visible light from 400 nm < λ < 600 nm.[31] With this in mind, **50** was made to react photochemically with closed-shell molecules by irradiating the matrix with a wavelength λ > 550 nm.

One of the first photochemical reactions observed was the photoreaction of **50** with $N_2$, which is present from the borylazide 2-azido-1,3,2benzodioxaborole **86**.[31] The size of $N_2$ does not allow it to diffuse away from its production site in most of the matrices. Hence, the initially cleaved $N_2$ from azide **86** (using λ = 254 nm) is present in the vicinity of **50** and photochemically reacts to undergo a reverse reaction to form **83** (Scheme 16). The trapping of **50** with other closed-shell molecules (CO, $D_2$, $CH_4$, $C_2H_2$, and $CF_4$) was attempted photochemically by using them as dopants in the matrix host. The dopant CO (1.5%) reacted with **50** isolated in an Ar matrix upon irradiation with λ > 550 nm, resulting in the formation of isocyanate **90**. The product was identified using IR spectroscopy with its signature N=C=O stretch at 2301 $cm^{-1}$.[31] Similarly, borylnitrene **50** isolated in $D_2$ or neon matrices doped with deuterium ($D_2$) or $H_2$ reacted photochemically, forming borylamine **91**.[31]

A computational investigation to explain such a high photochemical reactivity of **50** with $D_2$ was carried out, and it was found that the reaction of **50** in its $\tilde{a}^1A_1$ electronic state has a very small activation barrier of 1.3 kcal $mol^{-1}$, which could be easily surpassed under the experimental conditions provided during the reaction.[98] Hence, a presumption was made that **50 (**with $\lambda > 550$ nm), when photoexcited from the ground, the electronic state $\tilde{X}^3A_2$ eventually relaxes to the highly reactive $\tilde{a}^1A_1$. The resemblance of $\tilde{a}^1A_1$-**50** with the highly reactive vinylidenes has been discussed in detail in Section 1.5. Further, nitrene **50** has the potential to activate the $sp^3$ hybridized C–H bonds in $CH_4$. The reaction was performed at 10 K by doping the Ar matrix with 1-2% of $CH_4$ and photoactivating the isolated nitrene **50**. The N−H stretch of the resulting amine **51** has a characteristic N−H vibration at 3480 $cm^{-1}$, which was red-shifted to 2572 $cm^{-1}$ for the heavy isotopically labeled amine **51**-$d_4$ which was formed in the photoreaction of **50** with $CD_4$.[19] In contrast, the photoactivated nitrene **50** was not reactive enough to activate $CF_4$ and $C_2H_2$, as the concentration of nitrene was unchanged during the experiment.[99] In this way, borylnitrene **50** was found to be highly reactive once it was irradiated with $\lambda > 550$ nm, and it was presumed that the reaction was happening at the PES of the $\tilde{a}^1A_1$ state, which is getting populated during the irradiation.

Considering the feasible photoreactions of borylnitrene **50** in matrix isolation,[31, 98] the reactivity studies of borylnitrenes were also investigated in solution. Attempts were made to react borylnitrene **50** with cyclohexane, also used as the solvent.[99] It was observed that the photolysis of azide **86** resulted in uncharacterized polymeric tars.[99] The polymeric tars were supposedly the result of the oligomerization of the expected primary product (catBNHR), as catBNHR is known to tend to oligomerize.[133] Later on, borylnitrene **93** was investigated for its reactivity in different hydrocarbon solvents.[19, 20, 99] The azide **92**, when

irradiated in hydrocarbon solvents, resulted in aminoboranes **94**(i-iv) formed by the insertion of nitrene **93** into the C−H bonds of the hydrocarbon solvents (Scheme 17).

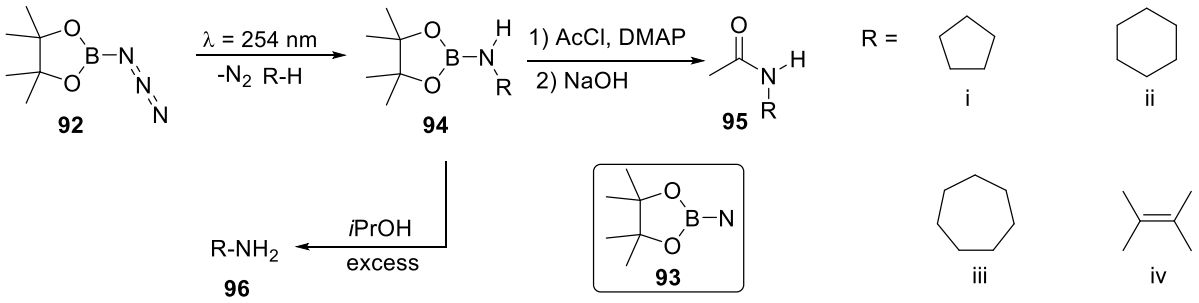


Scheme 17. Solution phase study of the borylnitrene **93** with different hydrocarbons.

The yield for the formation of aminoboranes **94**(i-iv) was reported to be as high as 85%. Furthermore, aminoboranes **94**(i-iv) displayed a high propensity to undergo alcoholysis and acylation to form amides **95**(i-iv) and primary amines **96**(i-iv).

# 2 Objective and Expected Outcomes

Reactive intermediates are short-lived species, and therefore, their study demands a special technique such as matrix isolation. Matrix isolation provides very low temperature and pressure conditions that increase their stability and allow their spectroscopic detection. In addition, computational chemistry has proved to be an integral part of matrix isolation studies that supplement the identification of isolated reactive intermediates.

This thesis contributes to the existing knowledge regarding the reactivity of donor stabilized borylnitrenes. The reactivity studies focused on product identification and elucidating the reaction mechanism involved in product formation. Aromatic nitrenes are known to have slow thermal reactivity with dioxygen, so the thermal reaction between borylnitrene and dioxygen was studied in detail under matrix isolation. Additionally, computational studies were conducted to understand the formation of the final product, nitritoborane, which differs from the nitro products formed in the case of aromatic nitrenes. Constrained geometry and unconstrained optimization were performed to comprehend the initial interaction between the borylnitrene and dioxygen and the final product formation. On the other hand, considering the ability of catBN to photochemically activate stable molecules such as methane, the reactivity of catBN was tested against another stable and closed-shell species, carbon dioxide $CO_2$. Although $CO_2$ can be a potential candidate for a C1 building block in organic synthesis, its high stability makes it difficult to activate. Further, catBN presumably attains a highly electrophilic electronic state upon irradiation with $\lambda > 550$ nm. Therefore, catBN was assumed to be a good candidate to activate $CO_2$ photochemically. The matrix isolation experiments and computational studies proved that catBN could react

photochemically with $CO_2$ to form cycloaddition product 3-oxaziridinone. Furthermore, attempts were made to understand the reactivity of catBN with unsaturated hydrocarbons, and for simplicity, ethene, $C_2H_4$, was chosen as the suitable candidate. Preliminary data showed that catBN could thermally react with $C_2H_4$ to form an aziridine and a *syn*-imine. On the other hand, the photochemical reaction between catBN and $C_2H_4$ resulted in the formation of the aziridine and the two geometric isomers of imine, *syn* and *anti*.

In past studies on the reactivity of catBN with closed-shell species such as $CO_2$, $CH_4$, $H_2$, etc., its lowest singlet state was assumed to be taking part in the photoreaction. Therefore, efforts were made to find evidence regarding the relaxation of catBN to the lowest singlet state upon photoexcitation ($\lambda$ > 550 nm). Electronically, the lowest singlet state of catBN is found to be in close resemblance with a highly electrophilic species called vinylidines. In the study, using a model borylnitrene, it was found that there is an energy-favorable pathway in catBN that could relax it to its lowest singlet upon photoexcitation so that it can take part in the reactivity.

# 3 Methodology

## 3.1 Matrix Isolation Setup

The involvement of reactive intermediates like radicals, ions, carbenes, nitrenes, etc., in chemical reactions has led to the invention of many sophisticated techniques that enable us to study them. The short lifetime of the reactive intermediates is one of the factors that make it difficult for the analytical tools to characterize the reactive intermediate. Therefore, there are special analytical tools, which are required to study the reactive intermediates. Matrix isolation is a technique developed by George C. Pimentel to study reactive intermediates.[134-136] This technique works on the principle of kinetically trapping the reactive intermediate by isolating it in a huge excess of an unreactive host gas under very low temperature and pressure conditions, increasing its lifetime. The kinetically trapped reactive intermediates can then be analyzed using different spectroscopic methods, such as UV-VIS, infrared (IR), and electron paramagnetic resonance spectroscopy (EPR).[135, 136]

In matrix isolation, the reactive intermediates are produced by two different methods. The first is the photochemical in-situ generation of reactive intermediates from their precursors using a UV-VIS light source. The second method is called flash vacuum pyrolysis (FVP), in which precursors are passed through a hot oven maintained at a high enough temperature to produce the reactive intermediates prior to their deposition on the cold spectroscopic window. Depending on the method of generation of a reactive intermediate, the percussor, or reactive intermediate (in FVP), and the host gas are co-deposited on the cold spectroscopic window (approximately in the ratio of 1:2000). [135, 136] The excess of host

gas ensures that the reactive intermediates are well separated from each other (Figure 4a) and do not have intermolecular interactions.

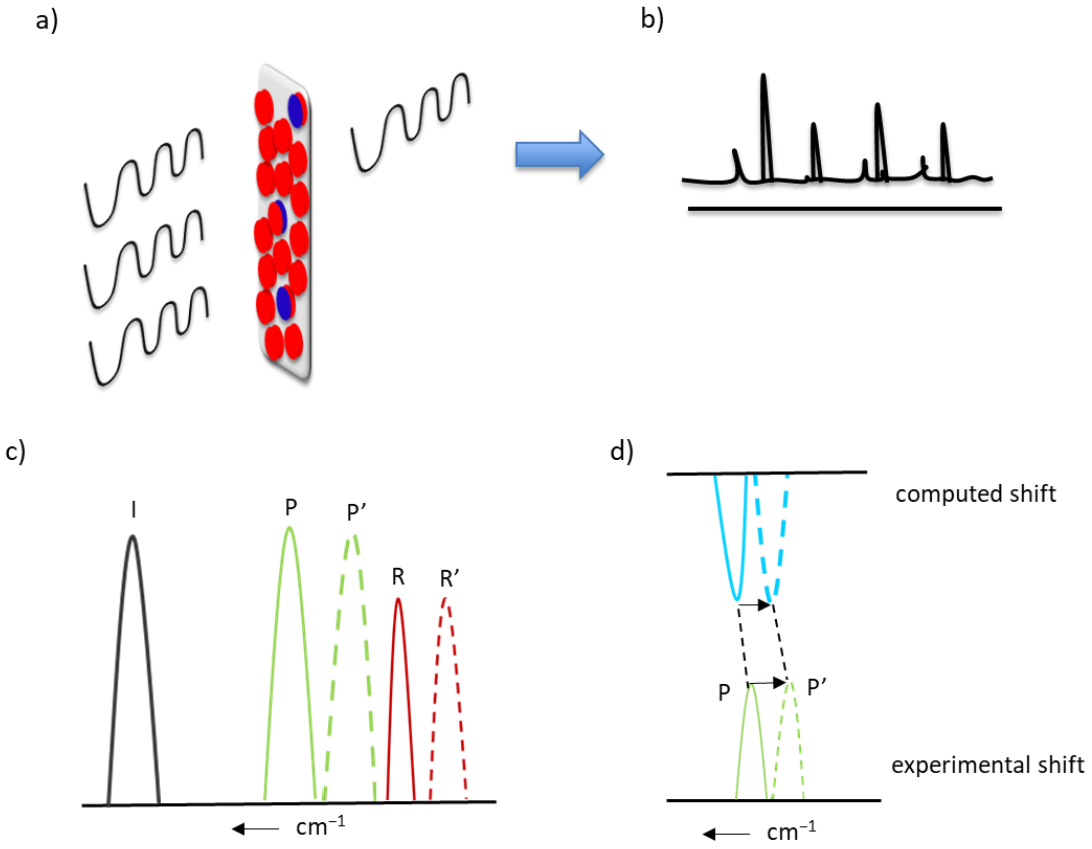


Figure 4. a) Reactive intermediate Isolated in the matrix host at the cold spectroscopic window. b) Output of a spectroscopic method applied on the cold window. c) Redshift in the IR stretch of heavier isotopologues (R' and P') of reactant, R, and product, P. d) Comparison of the experimental and computed IR shifts of the heavier isotopologue, P', with respect to the product, P.

Low temperatures (as low as 4 K) are maintained using a closed-cycle cryostat, which maintains the rigidity of the matrix and prevents any diffusion of the isolated molecules. The reactive intermediates are then analyzed using different spectroscopic methods. The choice of matrix host gases (Ar, Ne, Xe, $N_2$, etc.) is made in such a way that it should be transparent to the spectroscopic method used and also be unreactive towards the reactive

intermediate.[135, 136] In addition, matrix isolation is also used to study the reaction of a reactive intermediate with another reactant. In this case, the matrix host is doped with a certain amount (2-5%) of reactant, and this mixture is then co-deposited with the precursor or the reactive intermediate. The reaction is then induced, thermally or photochemically, between the reactant and the reactive intermediate present in close proximity to each other. The thermal reaction is induced by warming the matrix up to a certain temperature (depending on the matrix host), within which the rigidity of the matrix is maintained. However, the photochemical reaction is triggered by photoirradiation of the matrix in the region of UV-VIS light absorbed by one of the two reacting species. Regarding the identification of products formed in the reactions, computational chemistry plays an important role. The experimental spectra obtained from the spectroscopic methods are compared to the simulated spectra of the potential products, which is evidence to support the product assignment. Product assignment is further strengthened by using isotopically labeled reactants. In these studies, the heavier isotopologue (R') of a reactant, R, reacts with the reactive intermediate, I, as shown in Figure 4c. The resulting heavier isotopologue (P') of a reactant, P, gives a redshifted IR spectrum, which is then compared with the corresponding shift of the computed spectra (Figure 4d). A good match in experimental and computed IR shifts is an additional indication for the formation of product P in the reaction.

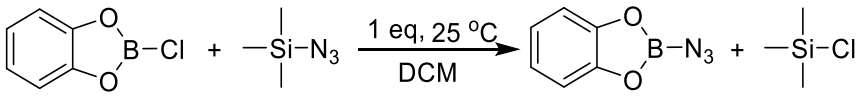


Scheme 18. Synthetic procedure for the synthesis of 2-azido-1,3,2-benzodioxaborole.

In the matrix isolation studies described in this thesis, a Sumitomo SH-1 closed-cycle helium cryostat was used to obtain a temperature as low as 4 K. The species were analyzed

with IR spectroscopy and Brucker's Vertex 70 FTIR spectrometer, in the range 400-4000 $cm^{-1}$, with a standard resolution of 0.5 $cm^{-1}$. The precursor compound **86**, for borylnitrene **50,** was synthesized using the procedure described in the literature (Scheme 18).[137] The reactive intermediate, borylnitrene **50**, was generated from its percussor **86** using a low-pressure mercury lamp ($\lambda = 254$ nm, PenRay). The photochemical reactions of borylnitrene **50** with different reactants were carried out using a high-pressure mercury lamp (USHIO, USH-508S) along with a Schott cutoff filter (550 OG). Different matrix host gases of very high purity were used, including Ar, $N_2$, and Ne (Messer-Griesheim, 99.9999% purity), and reactants such as $O_2$ (Westfalen, 99.999% purity), $CO_2$ (Westfalen, 99.999% purity), and cyclopropane (abcr, 99% purity) were used. To maintain the constant flow (usually 2.0 sccm) of matrix host gases during the deposition, an MKS mass flow PR400B controller was used.

### 3.2 Computational Methods

Computational chemistry tools were used to get more insights into the experimental results obtained from the matrix isolation studies. These computational tools were employed using various quantum chemistry packages, including Gaussian 16,[138] ORCA (4.2 and 5.0),[139-141] Molpro 2021.3,[142] Gamess-US,[143, 144] and CFOUR v2.00beta.[145] The visualization of the computational results from these packages was done using different graphical user interfaces (GUIs): GaussView 6,[146] Chemcraft,[147] and MacMolplt.[148]

Two different types of approaches were used to calculate different molecular properties. One of them is wavefunction based theories (post-Hartree-Fock), also called *ab-initio* methods, that solve the Schrödinger equation with a molecular Hamiltonian operator (to calculate energy) without any experimental parameters and contain only fundamental

physical constants. In *ab-initio* methods, the complete active space self-consistent field (CASSCF) method is one of the methods that has been widely used to describe the electronic structure of a molecule that has a multireference wavefunction or to study the reaction mechanisms that involve bond breaking and formation. The CASSCF method can be considered an extension of the Hartree-Fock (HF) method, which takes care of a particular kind of correlation effect called static correlation, which is not taken care of by the HF method.[149-151] The lack of dynamic correlation effects in CASSCF calculations makes this method only qualitatively relevant. The dynamic correlation on top of CASSCF as a zeroth order wavefunction can be included using multireference perturbation methods (MRPT). Two of the widely used MRPT methods are complete active space second-order perturbation theory (CASPT2)[152, 153] and N-electron valence state perturbation theory (NEVPT2).[154] Another post-Hartree-Fock ab-initio method is the coupled cluster method, which takes the HF wavefunction as the reference wavefunction and includes the dynamic correlation effect in describing the electronic structure of a chemical system.[155-157] In addition to this, for the molecules that do not show a multireference character, *ab-initio* methods employing coupled-cluster theory were used. Coupled-cluster methods are known for providing a highly correlated wavefunction and, hence, predicting molecular properties very accurately, such as energy.[158, 159] In this method, the exponential of a cluster operator, T, acts on a reference wavefunction, which is usually obtained from the HF method (eq. 1).[158, 159] The cluster operator T, when acting on the reference wavefunction $\Phi_{HF}$, gives a linear combination of excited determinants containing single, double, triple, etc., excitations from the reference determinants.[158, 159]

$$|\psi\rangle = e^{T}\phi_{HF} \qquad (1)$$

In addition to the *ab-initio* methods, density functional theory (DFT) is widely used to calculate different molecular properties.[160-162] DFT is a type of method that uses the electron density of a molecule instead of its wavefunction to calculate molecular properties. [160-162] The ground state electron density ρ is used to predict the ground state wavefunction $\Psi[\rho]$ and, hence, used to predict the ground state properties (such as energy $E[\rho]$) of a molecule, as shown in eq.2. [160-162]

$$E[\rho] = \langle \Psi[\rho] | T + V + U | \Psi[\rho] \rangle \quad (2)$$

T, V, and U in eq.2 refer to the quantum mechanical operators for kinetic energy, nuclear potential energy, and electron-electron repulsion energy, respectively.

Detailed information on different computational tools used throughout the work can be found in the published data.[39, 94, 103]

# 4 Results and Discussion

## 4.1 Mechanism for the reaction of Dioxygen with Triplet Borylnitrene

As mentioned in Section 1.7.1, borylnitrene **50,** in its triplet ground state, shows reactivity towards $O_2$, which is similar to that of **1**.[31, 39] Further computational and matrix isolation studies explained the contrastingly high reactivity and formation of different thermodynamic products *anti*-**62** in this reaction compared to arylnitrenes.[39] In matrix isolation studies, the reaction was carried out using Ar, Ne, and $N_2$ as matrix host material.

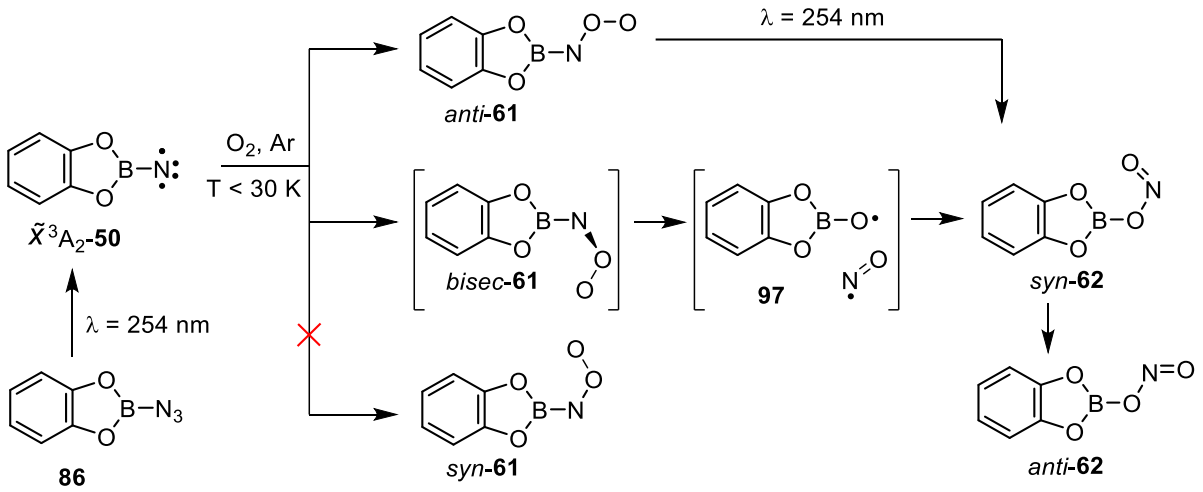


Scheme 19. Mechanism for the reaction of triplet borylnitrene **50** with $O_2$ in matrix isolation.

In the first step, the borylazide **86** was photolyzed, resulting in new photoproducts. Using computed IR spectra at a high level of theory (CCSD(T)/DZP), the photoproducts were identified as triplet borylnitrene **50** and nitritoborane *anti*-**62**. The triplet ground state $\tilde{X}^3A_2$ of **50** is well described by the EPR, US-VIS, and IR spectroscopy.[31] In the next step, the thermal reaction was carried out between the so-formed triplet **50** and $O_2$. The matrices were annealed to specific temperatures for the thermal reaction depending on the matrix host. The

reaction resulted in the consumption of **50** and the concomitant formation of new products, as reflected by the new IR bands that appeared during the reaction. Remarkably, the reaction could happen at temperatures as low as 7 K in the Ne matrix. The new IR bands were assigned to products *anti*-**61** and *anti*-**62.** In the final step, the product formed in the previous step was photoirradiated with $\lambda$ = 254 nm, which led to further reaction of *anti*-**61**. The photoproduct was identified as *anti*-**62** as the new IR bands matched the previously formed *anti*-**62**. In order to support the assignment of products in every step discussed so far, a similar step was repeated with a heavy isotope containing dioxygen $^{18}O_2$.

To support the experimental findings, a detailed computational study was carried out. Firstly, to explain the high reactivity of triplet **50** and $O_2$, relaxed potential energy scans were carried out using the distance between the nitrogen atom of **50** and one of the oxygen atoms of $O_2$ as the scan parameter. The complex electronic structure of different PES points was handled by the multireference method NEVPT2. Although three geometric isomers of **61** were identified as minima on the PES (Scheme 19), potential energy scans resulted in the formation of *anti*-**61** and *bisec*-**61**. The potential energy scan for the formation of *anti*-**61** suggested a shallow energy barrier of formation that could easily be surpassed in the cryogenic conditions, as presented in the matrix isolation experiments. This explains the observation of *anti*-**61** as the result of thermal reaction but does not explain the formation of *anti*-**62**. The ground state potential energy surfaces were investigated for the reactivity of three geometrical isomers of **61** to find a low energy pathway for the formation of *anti*-**62**. The PES showed that *bisec*-**61** is a starting point for a very low energy demanding reaction resulting in the formation of the final product *ant*i-**62**. According to the PES, *bisect*-**61** undergoes the breaking of B-N and O-O bonds in a single step, resulting in the formation of complex **97,** which recombines to form

*syn*-**62,** finally isomerizing to *anti*-**62,** as shown in Scheme 19. In addition, despite being similar in energy, the ground state PES showed a high energy barrier for the interconversion of *anti*-**61** and *bisec*-**61**. Due to the high energy barrier, the *anti*-**61** was kinetically trapped in thermal reaction and could react further using photoirradiation with $\lambda$ = 254 nm, which finally converted it into *anti*-**62**.

### 4.2 Reaction of Singlet Borylnitrene with Carbon Dioxide

Borylnitrene **50**, in past studies, has shown photochemical reactivity with closed-shell molecules ($N_2$, CO, $D_2$, and $CH_4$).[19, 31, 98] Similarly, the reactivity of borylnitrene **50** with another closed-shell singlet molecule, carbon dioxide ($CO_2$), was also tested in a different study.[94] The borylnitrene **50** was produced from the azide precursor **86** in matrix isolation conditions using different matrix host materials (Ne, $N_2$, and Ar) doped with 5 % $CO_2$. Initially, an attempt was made to react **50** with $CO_2$ in its ground state $\tilde{X}^3A_2$-**50** by annealing the matrix, but no reaction was observed as the measure IR spectrum indicated. Similar observations were made while reacting **50** in the $\tilde{X}^3A_2$-**50** electronic state with closed-shell species ($CH_4$, $D_2$, $N_2$, and CO). [19, 31, 98] However, a similar reaction became feasible upon photoirradiation of the matrix with $\lambda$ > 550 nm (Scheme 20).[94] The photoreaction resulted in the formation of a 1,2-oxaziridin-3-one derivative **98**, the first report for isolating the smallest possible cyclic carbamate.

In order to further support the formation of cyclic carbamate **98**, a similar reaction was carried out with the two other isotopologues of $^{12}C(^{16}O)_2$, $^{13}C(^{16}O)_2$, and $^{12}C(^{18}O)_2$. According to the experimental results, only carbonyl stretch $\nu_5$ (Scheme 20b) showed an isotopic shift for $^{18}O$ and $^{13}C$ isotopologues of **98** with a shift of 35 $cm^{-1}$ and 34 $cm^{-1}$,

respectively. On the other hand, harmonic frequency calculations at the B3LYP/6-311++G(2d,p) level of theory suggested an isotopic shift of 33 $cm^{-1}$ and 53 $cm^{-1}$ for $^{18}O$ and $^{13}C$ isotopologues, respectively.

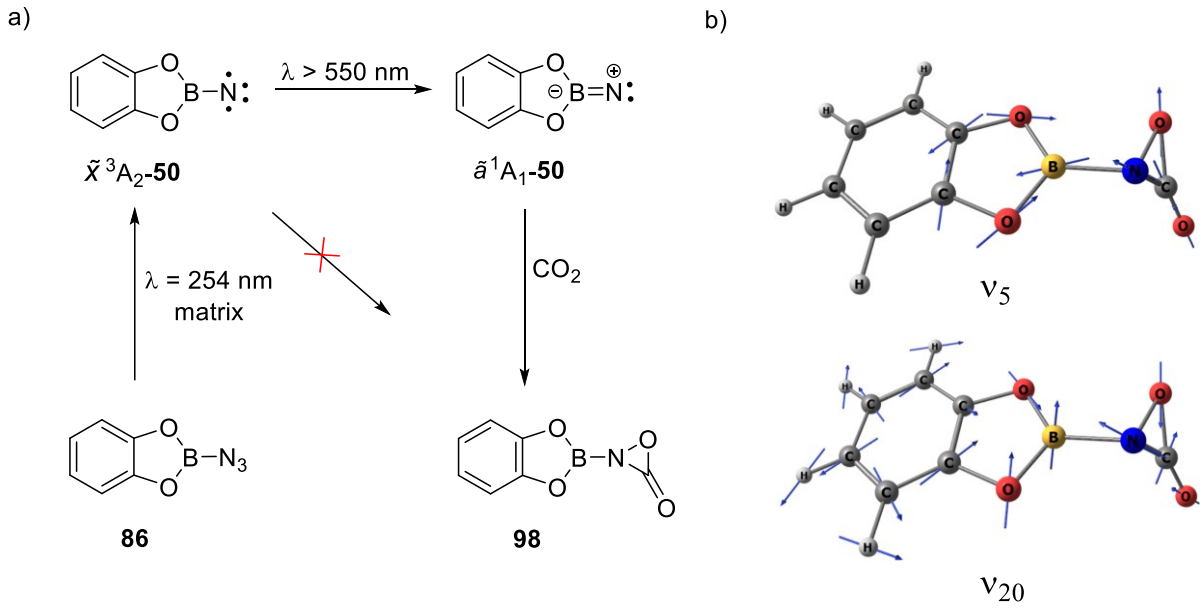


Scheme 20. a) Reaction of borylnitrene **50** with $CO_2$. b) IR stretching modes involved in Fermi resonance in **98**.

To get insights into the unusually shifted stretching mode of $\nu_5$, anharmonic IR stretching modes were calculated at MP2/6-311 ++ G(2d,p) level of theory. According to these calculations, unexpected isotopic shifts for $^{13}C$ and $^{18}O$ isotopologues of **98** were observed due to Fermi resonance between the $\nu_5$ stretching mode and overtones of ring deformation mode $\nu_{20}$.

Computationally, efforts were made to understand the photoreactivity of **50** with $CO_2$. It was again presumed, as previously (during photochemical reaction), [19, 31, 98] that **50** upon λ > 550 nm irradiation attains the highly electrophilic state $\tilde{a}^1A_1$-**50** (Scheme 20a). Having this in mind, a relaxed energy scan was calculated at the B3LYP/6-311++G(2d,p) level of theory with the distance between the nitrogen atom of **50** in $\tilde{a}^1A_1$-**50** electronic state and one of the

oxygen atoms of $CO_2$ as the scan parameter. The relaxed energy scan came out to be downhill right from when the two reacting moieties were at a large distance and gave the minimum **98**. Moreover, similar calculations at NEVPT2//CASSCF/def2-SVP level of theory were in unison with the DFT results. Therefore, computational results provided another piece of evidence in favor of photochemical reactivity, resulting in the formation of **98**. In addition, strain energy was also calculated for **98,** which was 36.7 kcal/mol, less than that of a $\alpha$-lactone and $\alpha$-lactam.

### 4.3 Photoexcitation of Borylnitrene to $\tilde{a}^1A_1$ electronic state

High photochemical reactivity of borylnitrene **50** upon irradiation with $\lambda$ > 550 nm was presumed to occur on $\tilde{a}^1A_1$-**50** PES. An assumption was made that **50** upon irradiation with $\lambda$ > 550 from its ground electronic state $\tilde{X}^3A_2$-**50** was excited to a highly electrophilic state $\tilde{a}^1A_1$-**50** (Scheme 21a).[19, 20, 31, 94, 98] Moreover, the energy barrier for the reaction of $\tilde{a}^1A_1$-**50** with closed-shell molecules such as $CO_2$ and $D_2$ was accessible under cryogenic conditions.[94, 98] Experimental studies in the solution phase, as discussed in Section 1.7.2, show efficient C–H insertion by borylnitrene **93** with a small measured kinetic isotope effect.[20] This experimental observation, in turn, points towards the insertion reaction and, hence, participation of a closed-shell electronic state in the reactivity.

The main goal of this study was to provide supporting evidence for the involvement of $\tilde{a}^1A_1$-**50** electronic state in the photochemical reactivity of **50**. Such evidence could be a low-energy photophysical pathway connected via various critical points that could relax $\tilde{X}^3A_2$-**50** to $\tilde{a}^1A_1$-**50** electronic state. To properly characterize the pathway involving the electronically excited pathways, having a multiconfigurational character of their

wavefunction, complete active space self-consistent field (CASSCF) theory was used in the study.[103]

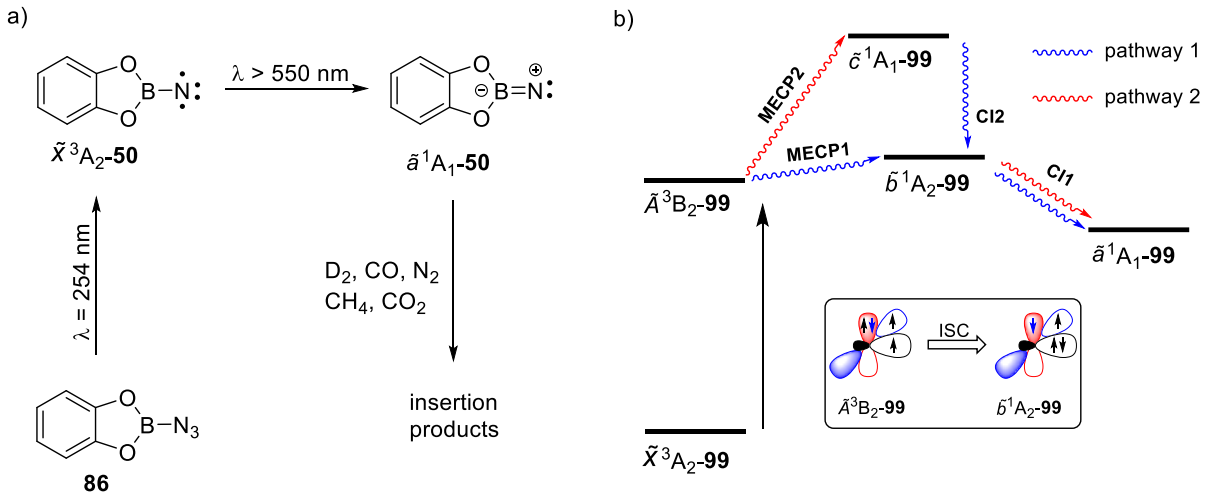


Scheme 21. a) Photochemical reactivity of borylnitrene **50**. b) Relaxation of model borylnitrene **99** to the minimum of $\tilde{a}^1A_1$ upon irradiation.

Considering the high computational cost of doing CASSCF calculations on borylnitrene **50,** a similar but smaller borylnitrene **99** was used as a model system. In the first part of the study, the choice of model borylnitrene **99** was tested by comparing the relative energy and character of the five lowest electronic states with that of **50**. In this comparison, relative energies and the character of the electronic states considered were similar, which substantiates the choice of model borylnitrene **99** for the study. The next part of the study was to search for a low-energy photophysical pathway. The first step in any possible pathway was believed to be the Franck–Condon (FC) excitation to $\tilde{A}^3B_2$-**99** electronic state based on the non-negligible oscillator strength calculated for this excitation for **50** and **99** (Scheme 21b). Based on the following steps, two different pathways were obtained connecting different critical points (Scheme 21b, designated by curly blue and red arrows for pathway 1 and pathway 2, respectively).

In pathway 1, the FC excitation to the $\tilde{A}^3B_2$-**99** electronic state is followed by ISC to the $\tilde{b}^1A_2$-**99** electronic state via optimized minimum energy crossing point (MECP) named MECP1. Qualitatively, the ISC step was feasible as it follows El-Sayed's rules.[163, 164] According to these rules, ISC between a singlet and a triplet is feasible, which involves flipping the electron spin and moving it to a perpendicular orbital.[163, 164] Also, a calculated spin-orbit coupling of 34.5 $cm^{-1}$ at MECP1 between the states involved in the ISC further supports the feasibility of this step. The potential energy surfaces for $\tilde{A}^3B_2$-**99** and $\tilde{b}^1A_2$-**99** near MECP1 showed a slopped topology, which indicates a high probability of relaxation from the triplet to the singlet state. After that, the next step was the relaxation of the $\tilde{b}^1A_2$-**99** electronic state to minimum of $\tilde{a}^1A_1$-**99** electronic state, which was happening at the conical intersection CI1. Regarding the energy demand of pathway 1, from FC to MECP1, there was a barrier of 7-8 kcal $mol^{-1}$ involved in the process, and the next steps were downhill in energy till the minimum of $\tilde{a}^1A_1$-**99**. In pathway 2, steps that followed FC to $\tilde{A}^3B_2$-**99** were: 1) relaxation to $\tilde{c}^1A_1$-**99** at MECP2. 2) relaxation to $\tilde{b}^1A_2$-**99** via CI2. 3) finally, relaxation to $\tilde{a}^1A_1$-**99** at CI1 and eventually to its minimum. Comparatively, the calculated energy demand in the first step was almost double that of pathway 1, and the calculated spin-orbit coupling at MECP2 was only 21.5 $cm^{-1,}$ which is also less than the spin-orbit coupling at MECP1. Therefore, pathway 1, obtained using model borylnitrene **99**, was assigned as the probable pathway that could relax ground state $\tilde{X}^3A_2$-**50** to $\tilde{a}^1A_1$-**50** electronic state upon irradiation with $\lambda > 550$ nm.

### 4.4 The reaction of Borylnitrene with Ethene

Matrix isolation experiments were carried out to study the reactivity of borylnitrene **50** with ethene, $C_2H_4$. The reactivity of borylnitrene **50** was studied in both the ground electronic state $\tilde{X}^3A_2$ and the lowest singlet electronic state $\tilde{a}^1A_1$, as shown in Scheme 22. In both cases, the

generation of borylnitrene **50** from the azide precursor **86,** isolated in the argon matrix doped with 2-3 % of $C_2H_4$, is the common step. This step is also common to the previous reactivity studies of **50**.[19, 31, 39, 94, 98, 103]

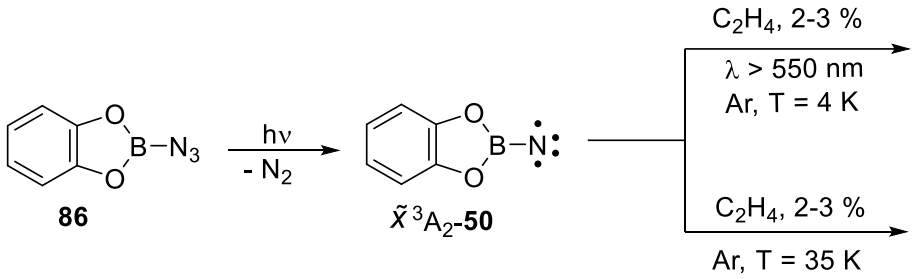


Scheme 22. Photochemical generation and thermal and photochemical reaction of borylnitrene **50** with ethene.

The reaction of **50** in the ground electronic state $\tilde{X}^3A_2$ was carried out by annealing the matrix at 35 K for 30 min. The annealing of the matrix resulted in the consumption of borylnitrene **50** and $C_2H_4$, as indicated by IR bands pointing downward in the difference IR spectrum (Figure 5a). Along with the IR bands pointing downward, there are IR bands pointing upward in the difference spectrum, corresponding to one or more products. For the product identification, a comparison was made between the computed anharmonic IR spectra of the possible products, as shown in Figure 6. Based on the comparison, the formation of enamines, *anti*-**102**, and *syn*-**102** could be ruled out as the candidates for the obtained products in the thermal reaction. Aziridine **100** was assigned as one of the products based on the comparison between the computed and the experimental difference IR spectra. In the experimental spectrum (Figure 5a), IR bands at 1504 and 1521 $cm^{-1}$ were identified as the signature IR modes involving both the B-N bond and aziridine ring, according to the computed IR modes.

Similarly, the ring breathing IR mode of **100**, mostly localized at the three-membered ring, was identified at 1215 $cm^{-1}$.

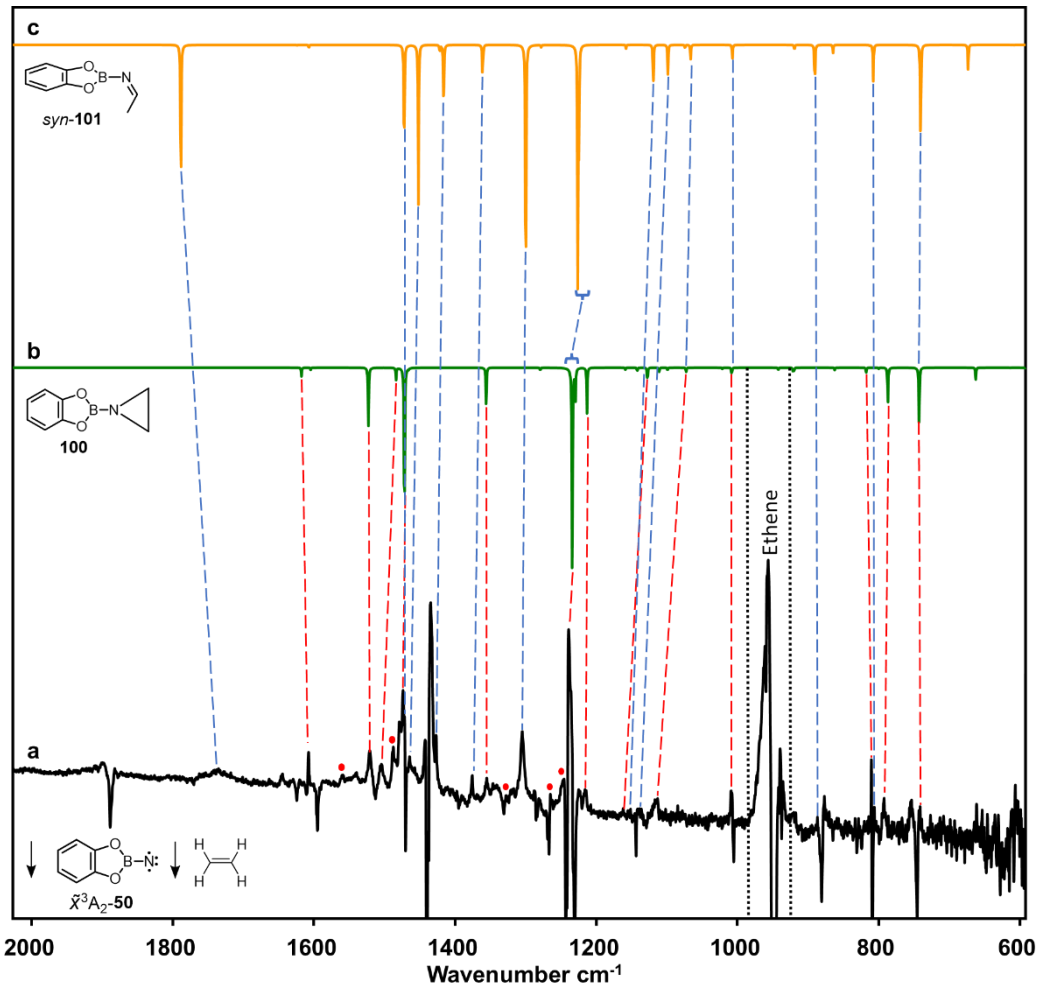


Figure 5. (a) Difference experimental spectrum after annealing the Ar matrix doped with 2-3 % of $C_2H_4$ at 35 K for 30 min. (b) and (c) Calculated anharmonic spectrum (fundamental bands) for $^{11}B$ isotopologue of **100** and *syn*-**101**, respectively, at (U)B3LYP/6311+G(d,p) level of theory. ● IR bands present in $^{10}B$ isotopologues as the result of large shift compared to similar IR bands in $^{11}B$ isotopologues.

In addition, the presence of IR bands at 1305 $cm^{-1}$ and in the region from 1730 to 1800 $cm^{-1}$ in the experimental spectra indicates the presence of isomeric imine *syn*-**101** and *anti*-**101**. Based on computed spectra, the IR band at 1305 $cm^{-1}$ corresponds to N-C-H angle bending,

and those between 1730 and 1800 $cm^{-1}$ correspond to N=C bond stretching, combination, and overtone bands. Due to the overlapping IR bands of *syn*-**101** and *anti*-**101** an assignment is difficult.

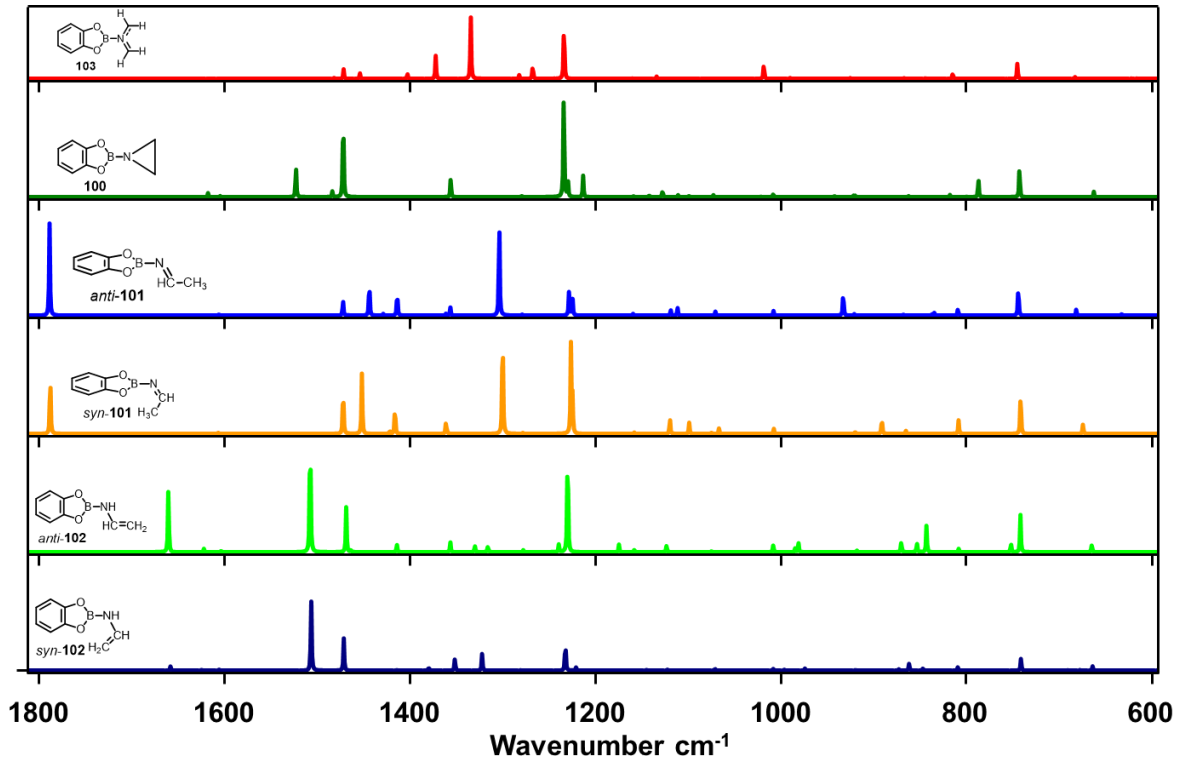


Figure 6. Calculated anharmonic spectra (fundamental bands) for $^{11}B$ isotopologues of the probable products for the thermal and photochemical reaction of triplet borylnitrene **50** and ethene at (U)B3LYP/6311+G(d,p) level of theory.

Multireference calculations for imine formation pathways were performed to find the most likely imine product forming in the experiment. The multireference calculations were performed on model system **99**, considering the high computational cost for borylnitrene **50** and the previous identification of **99** as a good model system for **50**.[103] Four different potential energy surface scans were considered for the reaction steps in the computational studies, as shown in Figure 7. The first step corresponds to the initial reaction of **99** in the

$\tilde{X}^3A_2$ electronic state with ethene, resulting in the formation of triplet 1,3-diradical species *syn*-**104'** (Figure 7a). The initial reaction has an energy barrier of 4 kcal mol$^{-1}$ obtained from the PES scan, which is likely an upper bound for the barrier. Such a low barrier reflects the feasibility of a similar reaction for catBN **50** in the matrix isolation conditions.

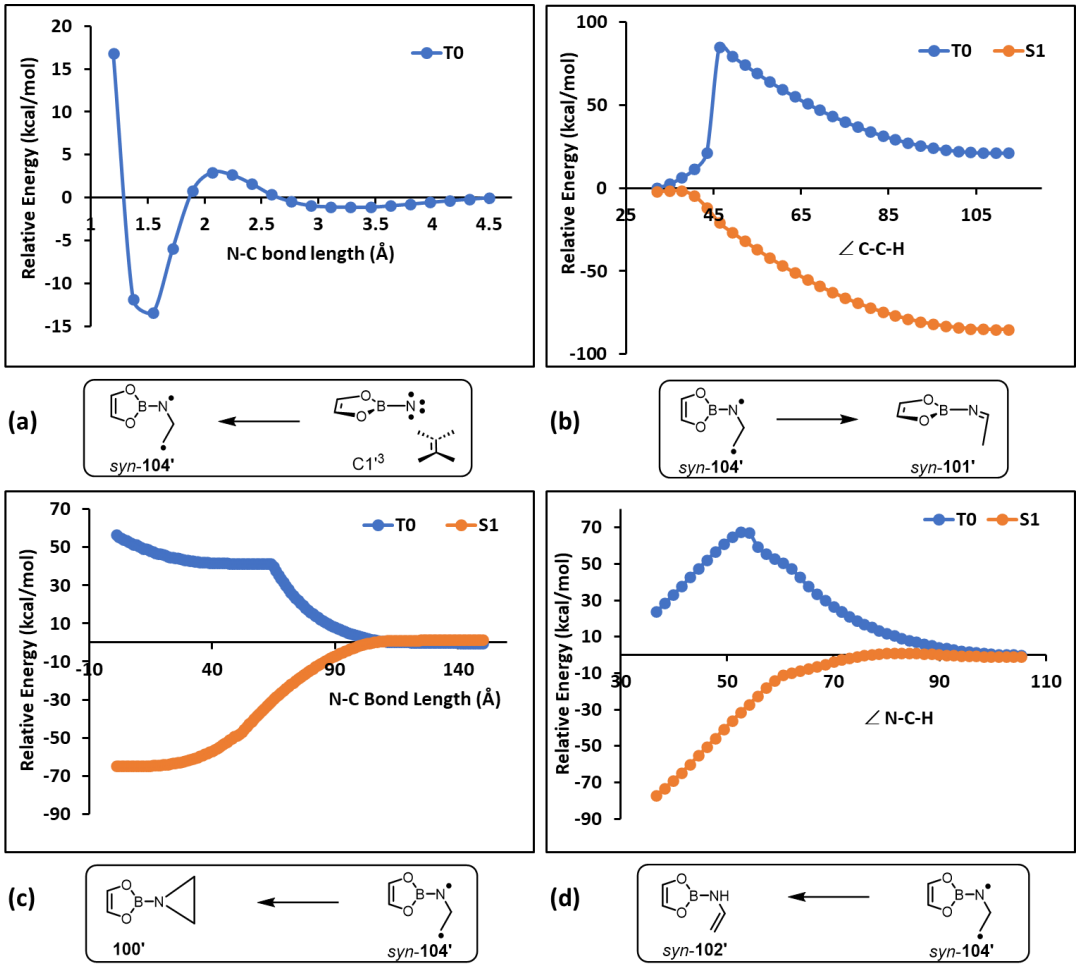


Figure 7. Potential energy surface corresponding to the reactivity of the triplet borylnitrene **50** with ethene calculated at FIC-NEVPT2/def2-TZVPP//SA-(1S,1T)-CAS(n,m)/def2-SV(P) level of theory. (a) The initial reaction of triplet borylnitrene **99** and ethene. (b), (c), and (d) Reaction of triplet biradical *syn*-**104'** leading to the formation of *syn*-**101'**, **100**, and *syn*-**102'**, respectively. The (n,m), where n stands for the number of electrons and m stands for the number of orbitals, is (10,10) except for the potential energy surface in (c), for which the value is (8,9).

Thereafter, there are three different PES scans (Figure 7b, 7c, and 7d) with *syn*-**104'** as the starting geometry showing the conversion of triplet spin *syn*-**104'** into stable singlet spin species *syn*-**101'**, **100**, and *syn*-**102'**. A similar approach was used in computational studies studying the reaction of triplet HN and $C_2H_4$, and it was found that the cyclization of 1,3-diradical **105**$^{3}$ into the more stable singlet species **106** happens via an MECP without an energy barrier (Scheme 23a).[165, 166] Furthermore, the PESs Figure 7b, 7c, and 7d were obtained by calculating the single points at the FIC-NEVPT2/def2-TZVPP level of theory with SA-CASSCF wavefunctions averaged over the lowest singlet ($S_1$) and the lowest triplet ($T_0$) electronic state. The geometries for the single points in the three PES scans correspond to the one obtained by performing relaxed scans of the $S_1$ PES at the CASSCF/def2-SV(P) level of theory. The relaxed PES scans were calculated with one geometry constraint, which is used as the scan parameter as mentioned on the x axis in Figure 7b, 7c, and 7d. In each of the three cases, there is the possibility of energy-favorable population transfer from the triplet *syn*-**104'** to singlet *syn*-**101'**, **100'**, and *syn*-**102'** via MECPs as $S_1$ and $T_0$ are very close in energy near the geometry of *syn*-**104'** (Figure 7b, 7c, and 7d). Energy barriers for the formation of **100'** and *syn*-**101**' are less than one kcal mol$^{-1}$ (0.04 kcal mol$^{-1}$ and 0.66 kcal mol$^{-1}$, respectively), and that of *syn*-**102'** is only 1.8 kcal mol$^{-1}$. In addition, efforts were made to calculate the PESs for the formation of *anti*-**104'**, but during the early steps of the scan calculation, the system adopted the geometries that resulted in *syn*-**104'**. On the other hand, DFT studies at (U)B3LYP/6-311+G(d,p) level of theory gave an energy barrier of 13.9 kcal mol$^{-1}$ for the direct H abstraction from ethene which makes this reaction unfeasible under matrix isolation conditions. Hence, a computational argument is provided that favors the formation of **100** and *syn*-**101** and disfavors the formation of other possible products as shown in Figure 6 in the experiment.

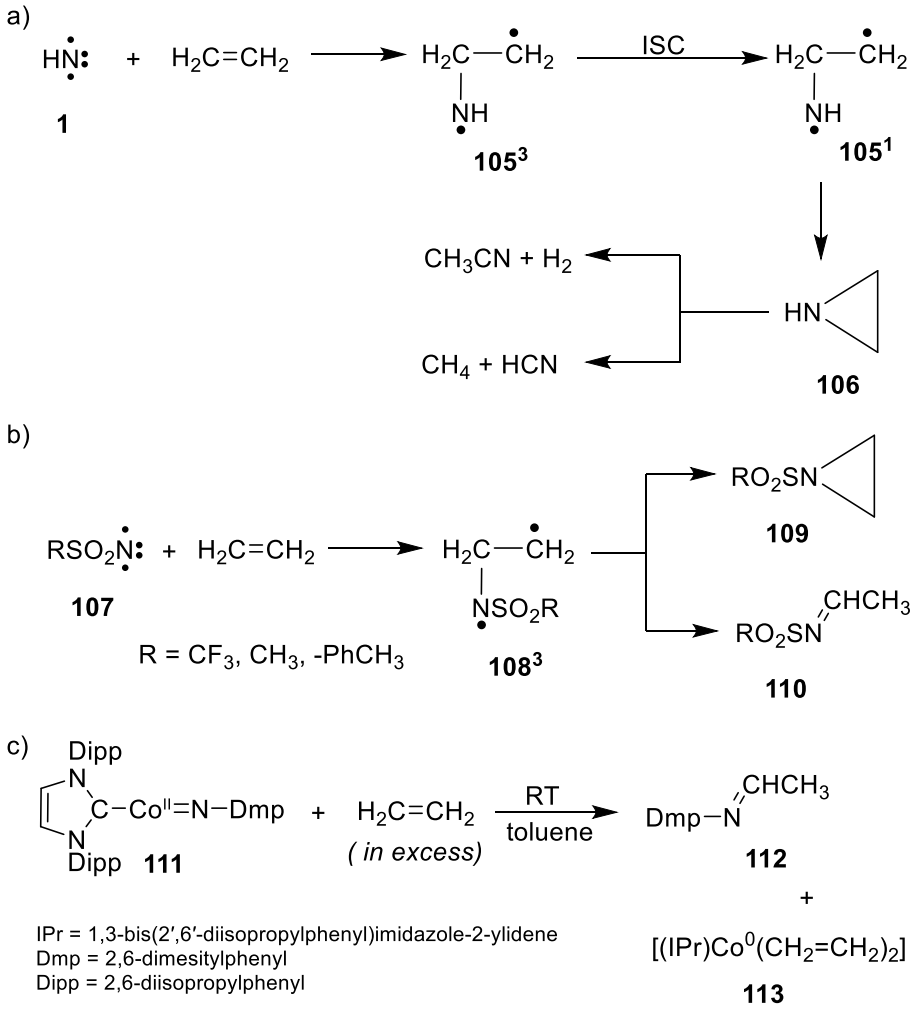


Scheme 23. Reaction of triplet nitrene **1** with ethene.

The formation of aziridine **100** from the reaction of triplet **50** with ethane follows known triplet nitrene reactivity patterns and is further supported by computational investigations of the HN + $C_2H_4$ system by Fueno and Zhang.[165, 166] The barrier for the formation of the diradical **105³** is higher (8-11 kcal $mol^{-1}$) for NH + $C_2H_4$, but, as observed by Cornell *et al.* using flash kinetic absorption spectroscopy, the reaction is feasible at 1000-1500 K and at room temperature.[167] Diradical **105³**, in this case, eventually converts to $CH_3CN$ and HCN. According to Fueno and Zhang's study, $CH_3CN$ and HCN are the secondary product of the reaction between triplet NH and $C_2H_4$. They are formed via aziridine **106** (Scheme 23a)

with a high energy barrier that can be surmounted under the conditions of Cornell's experimental study but cannot be passed under the matrix isolation conditions.[165]

Imine formation is unexpected. Sulfonylimine **110** was suggested in a computational study of the reaction of sulfonylnitrenes with $C_2H_4$ as a viable product from 1,3-diradical **108³** that in turn can from without barrier (Scheme 23b).[168] An alternative fate of **108³** is formation of aziridine **109**. The only experimental observation of imine formation is the reaction of the cobalt complex **111** with excess ethylene to give **112** (Scheme 23c). [169] Moreover, there are reports on forming imine products as the secondary products in thermal 1,3-dipolar cycloaddition reaction of aziridines with olefins, where 1,2,3-triazolines form as the primary products.[170-172]

The reaction of borylnitrene **50** in the lowest singlet $\tilde{a}^1A_1$ state with ethene was carried out by photoexcitation ($\lambda$ > 550 nm) of its $\tilde{X}^3A_2$ electronic state, as discussed above. The photoirradiation resulted in new IR peaks and a decrease in the intensity of the IR bands corresponding to borylnitrene **50**, as shown in the difference spectrum in Figure 8a. Two sets of peaks were similar to the one that appeared after the annealing step, indicating the formation of **100** and *syn*-**101** in the photoreaction of **50** with ethene. Also, the two sets of peaks were in good agreement with the computed spectra of **100** and *syn*-**101** (Figure 8b and Figure 8c). The formation of aziridine **100** is supported by a study from Jacox *et al.*, who showed that the photolysis of $HN_3$ isolated in an Ar matrix doped with $C_2H_4$ resulted in the formation of aziridine by reaction of the lowest singlet state of HN, which was produced initially, with $C_2H_4$.[173] In addition to the two sets of peaks, there was another set of peaks that shifted slightly compared to *syn*-**101** and closely matched with the computed IR spectrum of *anti*-**101** (Figure 8d).

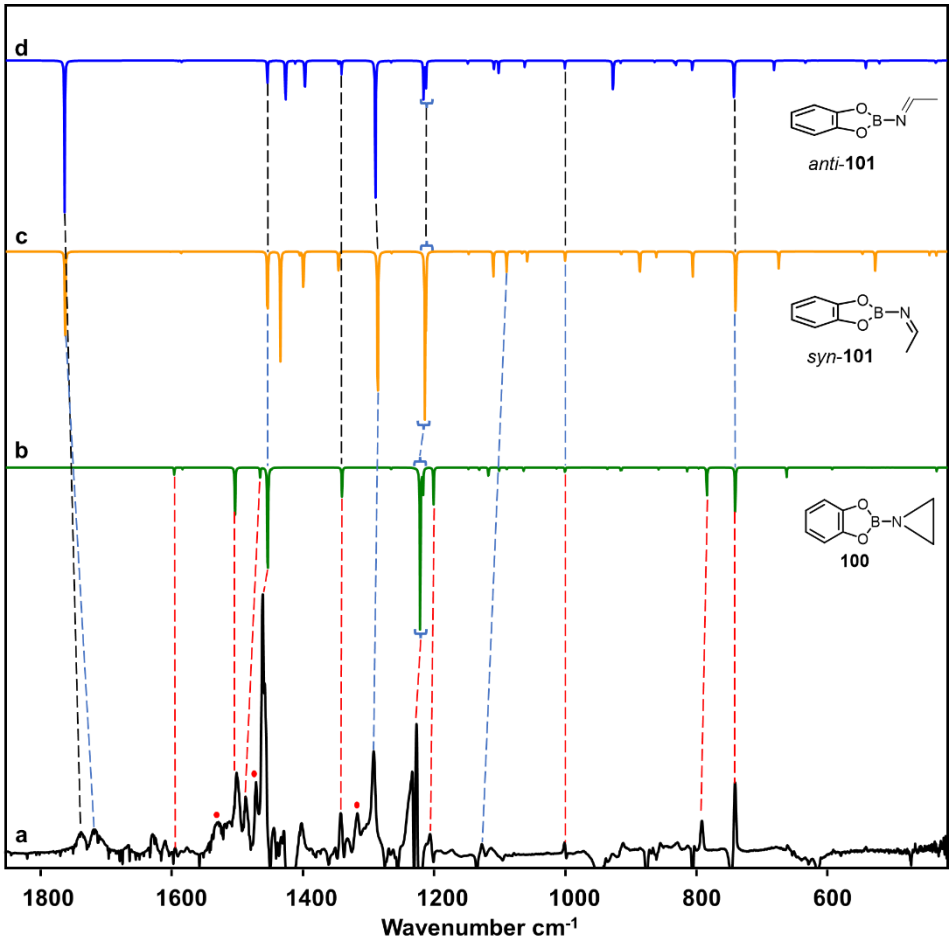


Figure 8. (a) Difference experimental spectrum after photoirradiating the Ar matrix doped with 2-3 % of $C_2H_4$ with $\lambda$ > 550 nm for 180 min. (b), (c), and (d) Calculated anharmonic spectrum (fundamental bands) for $^{11}B$ isotopologue of **100**, *syn*-**101**, and *anti*-**101** at (U)B3LYP/6311+G(d,p) level of theory. ● IR bands present in $^{10}B$ isotopologues as the result of large shift compared to similar IR bands in $^{11}B$ isotopologues.

Computational investigations were performed using density functional theory to understand the experimental findings in the photochemical reaction of the lowest singlet state of **50** with ethene (Figure 9). The PES shows a very low energy barrier of 1.3 kcal $mol^{-1}$ for the formation of **100**. This is so low that the reaction can proceed under matrix isolation conditions. In contrast, no low energy barriers for the formation of the two isomers of **101**

were found. Indirect pathways, via aziridine **100**, to *syn*-**101** and *anti*-**101** were obtained with very high energy barriers but lower than the energy of reagents.

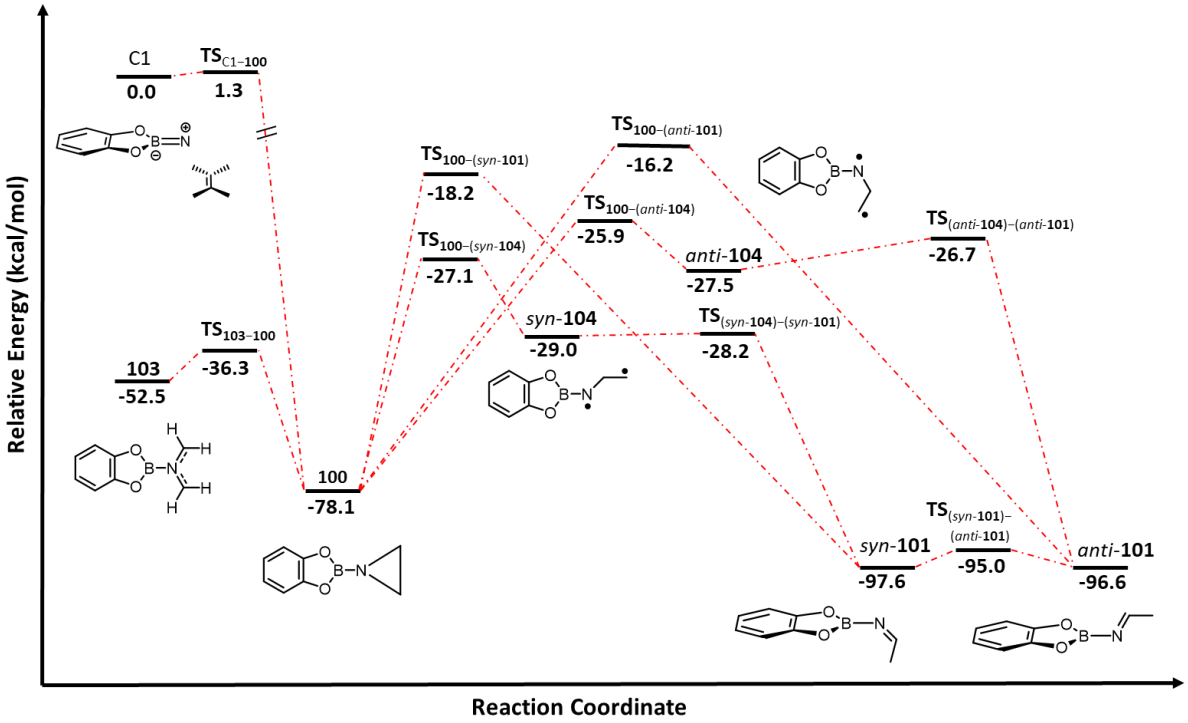


Figure 9. Potential energy surface corresponding to the reactivity of the singlet borylnitrene **50** with ethene calculated at B3LYP/6-311+G(d,p) level of theory.

According to the UV-VIS spectrum calculated at CAM-B3LYP/6-311+G(d,p) level of theory, aziridine **100** does not absorb light at $\lambda > 550$ nm. Therefore, the *syn* and *anti* isomers of **101** cannot be assigned as the photodissociation products of **100**. On the other hand, the photochemical reaction ($\lambda > 550$ nm) could lead to the formation of vibrationally hot aziridine molecules, a portion of which could break into the imine products while the matrix environment vibrationally cooled the rest of them. Hence, the utilization of vibrational hot states by **100** can be used as an argument to support the formation of isomeric imines *syn*-**100** and *anti*-**100** in the photoreaction. Furthermore, matrix isolation experiments were performed with borylnitrene **50**, and heavy isotopologue of ethene doped in the Ar matrix

($C_2D_4$). Due to the appearance of broad bands in the IR spectra, the heavy isotope experiments were repeated with the Ne matrix. In these experiments, sharper IR bands of the products were obtained, which helped assign the shifted IR bands in the case of $d_4$ labeled products, as shown in Figure 10.

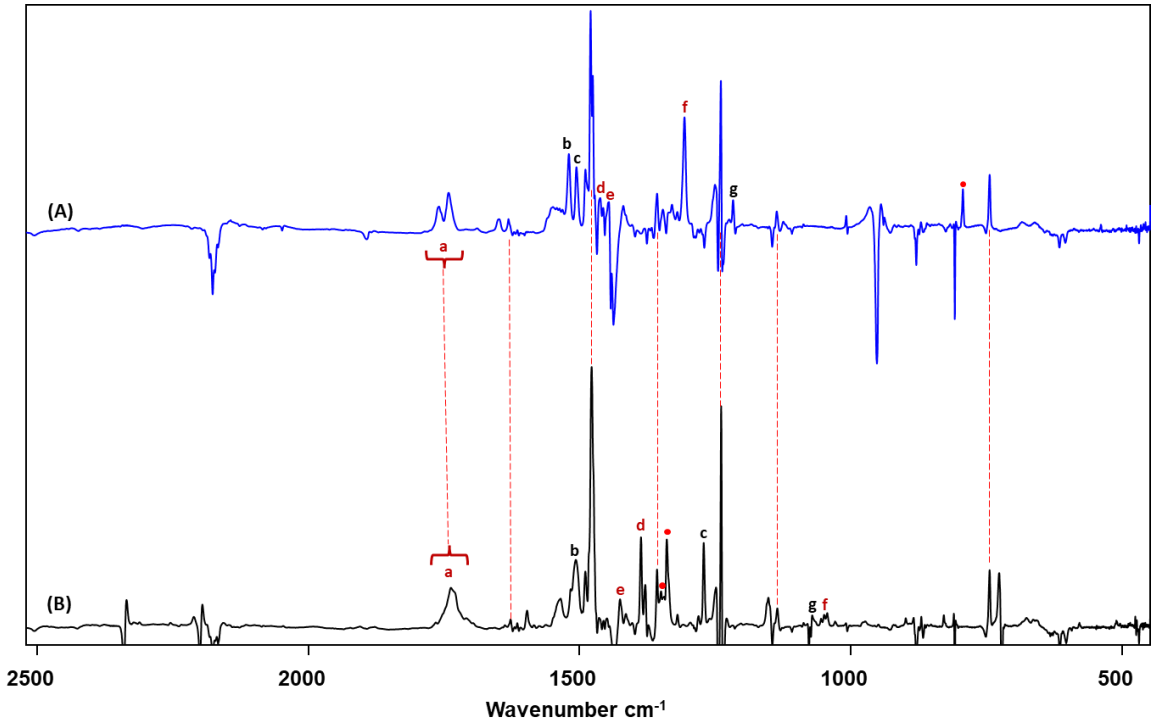


Figure 10. Isotopic shifts of the IR bands of $d_4$ isotopomer of **100**, *syn*-**101**, and *anti*-**101**. Difference IR spectra A and B showing the IR bands of the products formed upon photoreaction ($\lambda$ > 550 nm) of borylnitrene **50** with $C_2H_4$ and $C_2D_4$ respectively. Shifted IR bands are named from a-f (black: correspond to **100**, red: correspond to both the isomers of **101**). ● IR bands observed only in one of the isotopomers.

The band shifts in $cm^{-1}$ for the bands a-f was observed as 4 $cm^{-1}$, 13 $cm^{-1}$, 235 $cm^{-1}$, 70 $cm^{-1}$, 22 $cm^{-1}$, 259 $cm^{-1}$, and 146 $cm^{-1}$, which, within a certain degree of error, match with the computed shifts (10 $cm^{-1}$, 6 $cm^{-1}$, 220 $cm^{-1}$, 76 $cm^{-1}$, 22 $cm^{-1}$, 255 $cm^{-1}$, and 164 $cm^{-1}$). Hence, isotopic studies support the assignments of the products formed in the matrix experiments.

The results for the reaction of borylnitrene **50** with $C_2H_4$ are summarized in Scheme 24. Matrix isolation studies related to the reactivity of **50** in the triplet state with ethene provide evidence for the formation of aziridine **100** and imine *syn*-**101**. The experimental observations have been supported by multi-reference computational studies. Similar studies for the singlet state reactivity of the borylnitrene **100** with ethene hint towards the formation of aziridine **100** and two geometrical isomers of imine *syn*-**101** and *anti*-**101**. Computational studies could explain the formation of aziridine **100** in the singlet electronic state reaction of **50** but remained unconvincing in explaining the formation of the isomeric imines.

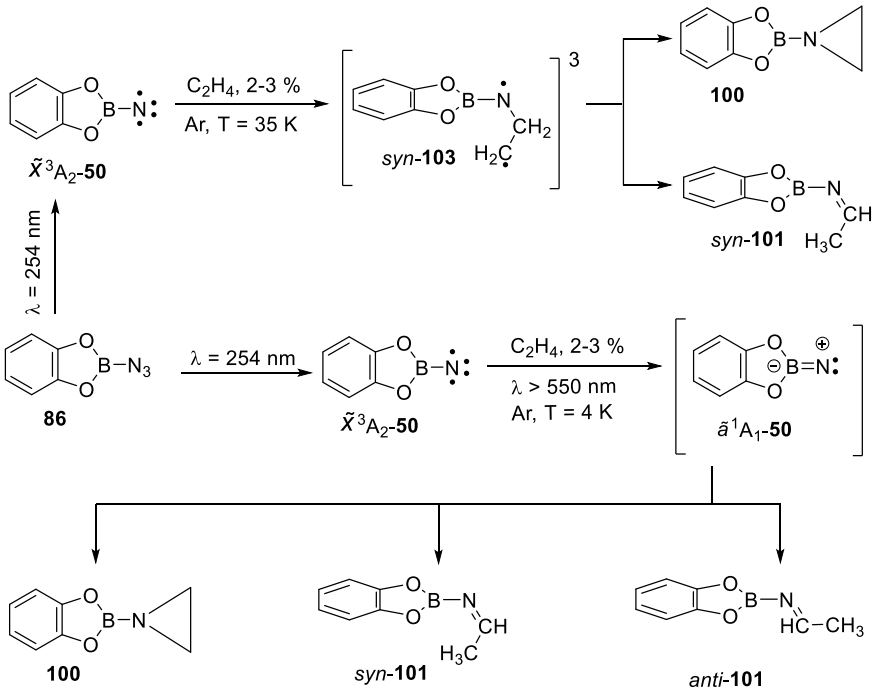


Scheme 24. Reaction of Borylnitrene **50** with ethene in singlet and triplet electronic state.

# 5 References


[1] M. S. Platz, in *Reactive Intermediate Chemistry* (Eds.: R. A. Moss, M. S. Platz, M. Jones), Wiley-Interscience, **2003**, pp. 501-559.

[2] W. Sander, G. Bucher, S. Wierlacher, *Chem. Rev.* **1993**, *93*, 1583-1621.

[3] S. Kumar, Y. Kumar, S. K. Keshri, P. Mukhopadhyay, *Magnetochemistry* **2016**, *2*, 42.

[4] H. Pellissier, M. Santelli, *Tetrahedron* **2003**, *59*, 701-730.

[5] D. H. Aue, *WIREs Comput. Mol. Sci.* **2011**, *1*, 487-508.

[6] J. C. Stowell, *Carbanions in Organic Synthesis*, Wiley, **1979**.

[7] N. P. Gritsan, M. S. Platz, W. T. Borden, in *Mol. Supramol. Photochem.* (Ed.: A. G. Kutateladze), CRC Press, **2005**, pp. 235-340.

[8] S. Vyas, A. H. Winter, C. M. Hadad, in *Nitrenes and nitrenium ions* (Eds.: D. E. Falvey, A. D. Gudmundsdottir), Wiley New York, **2013**, pp. 33-76.

[9] E. A. Pritchina, N. P. Gritsan, A. Maltsev, T. Bally, T. Autrey, Y. Liu, Y. Wang, J. P. Toscano, *Physical Chemistry Chemical Physics* **2003**, *5*, 1010-1018.

[10] F. Tiemann, *Ber. Dtsch. Chem. Ges.* **1891**, *24*, 4162-4167.

[11] A. O. Beckman, R. G. Dickinson, *J. Am. Chem. Soc.* **1928**, *50*, 1870-1875.

[12] H. H. Franck, H. Reichardt, *Naturwissenschaften* **1936**, *24*, 171-171.

[13] L. F. Keyser, G. W. Robinson, *J. Am. Chem. Soc.* **1960**, *82*, 5245-5246.

[14] T. Autrey, G. B. Schuster, *J. Am. Chem. Soc.* **1987**, *109*, 5814-5820.

[15] G. R. Felt, W. Lwowski, *J. Org. Chem.* **1976**, *41*, 96-101.

[16] W. Lwowski, T. W. Mattingly Jr, *J. Am. Chem. Soc.* **1965**, *87*, 1947-1958.

[17] G. T. Tisue, S. Linke, W. Lwowski, *J. Am. Chem. Soc.* **1967**, *89*, 6303-6307.

[18] R. Poe, K. Schnapp, M. J. T. Young, J. Grayzar, M. S. Platz, *J. Am. Chem. Soc.* **1992**, *114*, 5054-5067.

[19] H. F. Bettinger, M. Filthaus, H. Bornemann, I. M. Oppel, *Angew. Chem. Int. Ed.* **2008**, *47*, 4744-4747.

[20] M. Filthaus, L. Schwertmann, P. Neuhaus, R. W. Seidel, I. M. Oppel, H. F. Bettinger, *Organometallics* **2012**, *31*, 3894-3903.

[21] W. Lwowski, in *Azides and Nitrenes* (Ed.: E. F. V. Scriven), Academic Press, **1984**, pp. 205-246.

[22] R. A. Odum, G. Wolf, *J. Chem. Soc., Chem. Commun.* **1973**, 360-361.

[23] T. Harder, P. Wessig, J. Bendig, R. Stösser, *J. Am. Chem. Soc.* **1999**, *121*, 6580-6588.

[24] E. A. Pritchina, N. P. Gritsan, T. Bally, *Phys. Chem. Chem. Phys.* **2006**, *8*, 719-727.

[25] I. Hiroshi, I. Masatoshi, O. Shigero, *Chem. Lett.* **2005**, *34*, 478-479.

[26] J. Mieres-Pérez, E. Mendez-Vega, K. Velappan, W. Sander, *J. Org. Chem.* **2015**, *80*, 11926-11931.

[27] R. Abramovitch, E. Kyba, *J. Am. Chem. Soc.* **1974**, *96*, 480-488.

[28] I. R. Dunkin, P. C. P. Thomson, *Tetrahedron Lett.* **1980**, *21*, 3813-3816.

[29] N. P. Gritsan, M. S. Platz, *Chem. Rev.* **2006**, *106*, 3844-3867.

[30] G. T. Burdzinski, T. L. Gustafson, J. C. Hackett, C. M. Hadad, M. S. Platz, *J. Am. Chem. Soc.* **2005**, *127*, 13764-13765.

[31] H. F. Bettinger, H. Bornemann, *J. Am. Chem. Soc.* **2006**, *128*, 11128-11134.

[32] J. Kubicki, H. L. Luk, Y. Zhang, S. Vyas, H.-L. Peng, C. M. Hadad, M. S. Platz, *J. Am. Chem. Soc.* **2012**, *134*, 7036-7044.

[33] D. A. Bamford, C. H. Bamford, *J. Chem. Soc.* **1941**, 30-34.

[34] J. H. Boyer, W. E. Krueger, G. J. Mikol, *J. Am. Chem. Soc.* **1967**, *89*, 5504-5505.

[35] V. Desikan, Y. Liu, J. P. Toscano, W. S. Jenks, *J. Org. Chem.* **2007**, *72*, 6848-6859.

[36] V. Desikan, Y. Liu, J. P. Toscano, W. S. Jenks, *J. Org. Chem.* **2008**, *73*, 4398-4414.

[37] P. Robson, P. R. H. Speakman, *J. Chem. Soc. B* **1968**, 463-467.

[38] X. Zeng, H. Beckers, H. Willner, P. Neuhaus, D. Grote, W. Sander, *J. Phys. Chem. A* **2015**, *119*, 2281-2288.

[39] V. Bhagat, J. Schumann, H. F. Bettinger, *Chem. Eur. J.* **2020**, *26*, 12654-12663.

[40] S. Vyas, S. Muthukrishnan, J. Kubicki, R. D. McCulla, G. Burdzinski, M. Sliwa, M. S. Platz, C. M. Hadad, *J. Am. Chem. Soc.* **2010**, *132*, 16796-16804.

[41] R. E. Banks, D. Berry, M. J. McGlinchey, G. J. Moore, *J. Chem. Soc. C* **1970**, 1017-1023.

[42] R. Abramovitch, S. Challand, E. Scriven, *J. Am. Chem. Soc.* **1972**, *94*, 1374-1376.

[43] R. E. Banks, I. M. Madany, *J. Fluorine Chem.* **1985**, *30*, 211-226.

[44] D. S. Breslow, E. I. Edwards, E. C. Linsay, H. Omura, *J. Am. Chem. Soc.* **1976**, *98*, 4268-4275.

[45] S. Linke, G. T. Tisue, W. Lwowski, *J. Am. Chem. Soc.* **1967**, *89*, 6308-6310.

[46] P. Maslak, *J. Am. Chem. Soc.* **1989**, *111*, 8201-8207.

[47] T. Uchida, T. Katsuki, *Chem. Rec.* **2014**, *14*, 117-129.

[48] J. T. Groves, T. Takahashi, *J. Am. Chem. Soc.* **1983**, *105*, 2073-2074.

[49] R. Breslow, S. H. Gellman, *J. Am. Chem. Soc.* **1983**, *105*, 6728-6729.

[50] Z. Li, K. R. Conser, E. N. Jacobsen, *J. Am. Chem. Soc.* **1993**, *115*, 5326-5327.

[51] P. Müller, C. Baud, Y. Jacquier, M. Moran, I. Nägeli, *J. Phys. Org. Chem.* **1996**, *9*, 341-347.

[52] R. P. Reddy, H. M. Davies, *Org. Lett.* **2006**, *8*, 5013-5016.

[53] B. A. Shainyan, A. V. Kuzmin, M. Y. Moskalik, *Comput. Theor. Chem.* **2013**, *1006*, 52-61.

[54] C. Wentrup, *Angew. Chem. Int. Ed.* **2018**, *57*, 11508-11521.

[55] M. S. Platz, *Acc. Chem. Res.* **1995**, *28*, 487-492.

[56] W. L. Karney, W. T. Borden, *J. Am. Chem. Soc.* **1997**, *119*, 1378-1387.

[57] C. R. Kemnitz, W. L. Karney, W. T. Borden, *J. Am. Chem. Soc.* **1998**, *120*, 3499-3503.

[58] W. T. Borden, N. P. Gritsan, C. M. Hadad, W. L. Karney, C. R. Kemnitz, M. S. Platz, *Acc. Chem. Res.* **2000**, *33*, 765-771.

[59] W. W. Sander, *J. Org. Chem.* **1989**, *54*, 4265-4267.

[60] N. P. Gritsan, E. A. Pritchina, *Russ. Chem. Rev.* **1992**, *61*, 500-516.

[61] A. Admasu, A. D. Gudmundsdóttir, M. S. Platz, *J. Phys. Chem. A* **1997**, *101*, 3832-3840.

[62] R. A. Moss, U. H. Dolling, *J. Am. Chem. Soc.* **1971**, *93*, 954-960.

[63] E. Meijer, S. Nijhuis, F. Van Vroonhoven, *J. Am. Chem. Soc.* **1988**, *110*, 7209-7210.

[64] W. v. E. Doering, R. A. Odum, *Tetrahedron* **1966**, *22*, 81-93.

[65] T. Shioiri, in *Comprehensive Organic Synthesis* (Eds.: B. M. Trost, I. Fleming), Pergamon, **1991**, pp. 795-828.

[66] N. Soundararajan, S. H. Liu, S. Soundararajan, M. S. Platz, *Bioconjugate Chem.* **1993**, *4*, 256-261.

[67] E. Smith, I. Collins, *Future Med. Chem.* **2015**, *7*, 159-183.

[68] W. Abraham, S. Siegert, *J. Inf. Rec. Mater.* **1989**, *17*, 379.

[69] M. R. Banks, J. I. G. Cadogan, I. Gosney, P. K. G. Hodgson, P. R. R. Langridge-Smith, D. W. H. Rankin, *J. Chem. Soc., Chem. Commun.* **1994**, 1365-1366.

[70] M. Holzinger, J. Abraham, P. Whelan, R. Graupner, L. Ley, F. Hennrich, M. Kappes, A. Hirsch, *J. Am. Chem. Soc.* **2003**, *125*, 8566-8580.

[71] S. Nimura, A. Yabe, in *Magnetic properties of organic materials* (Ed.: P. M. Lahti), Routledge, **2023**, pp. 127-145.

[72] C. Ling, M. Minato, P. M. Lahti, H. Van Willigen, *J. Am. Chem. Soc.* **1992**, *114*, 9959-9969.

[73] S. V. Chapyshev, D. V. Korchagin, M. F. Budyka, T. N. Gavrishova, P. Neuhaus, W. Sander, *ChemPhysChem* **2012**, *13*, 2721-2728.

[74] S. V. Chapyshev, D. Grote, C. Finke, W. Sander, *J. Org. Chem.* **2008**, *73*, 7045-7051.

[75] S. V. Chapyshev, D. V. Korchagin, P. Neuhaus, W. Sander, *Beilstein J. Org. Chem.* **2013**, *9*, 733-742.

[76] J. Breidung, H. Bürger, C. Kötting, R. Kopitzky, W. Sander, M. Senzlober, W. Thiel, H. Willner, *Angew. Chem. Int. Ed. Engl.* **1997**, *36*, 1983-1985.

[77] C. Kötting, W. Sander, J. Breidung, W. Thiel, M. Senzlober, H. Bürger, *J. Am. Chem. Soc.* **1998**, *120*, 219-220.

[78] C. Kötting, W. Sander, M. Senzlober, *Chem. Eur. J.* **1998**, *4*, 2360-2365.

[79] C. Kötting, W. Sander, M. Senzlober, H. Bürger, *Chem. Eur. J.* **1998**, *4*, 1611-1615.

[80] C. Kötting, W. Sander, *J. Am. Chem. Soc.* **1999**, *121*, 8891-8897.

[81] W. Sander, C. Kötting, *Chem. Eur. J.* **1999**, *5*, 24-28.

[82] W. Sander, C. Kötting, R. Hübert, *J. Phys. Org. Chem.* **2000**, *13*, 561-568.

[83] D. P. Fox, P. J. Stang, M. Karni, *J. Am. Chem. Soc.* **1986**, *108*, 750-756.

[84] I. S. Ignatyev, H. F. Schaefer, *J. Am. Chem. Soc.* **1997**, *119*, 12306-12310.

[85] M. Jones Jr., R. A. Moss, in *Reactive Intermediate Chemistry* (Eds.: R. A. Moss, M. S. Platz, M. Jones), Wiley-Interscience, **2003**, pp. 273-328.

[86] H. Tomioka, in *Reactive Intermediate Chemistry* (Eds.: R. A. Moss, M. S. Platz, M. Jones), Wiley-Interscience, **2003**, pp. 375-461.

[87] K. M. Ervin, J. Ho, W. C. Lineberger, *J. Chem. Phys.* **1989**, *91*, 5974-5992.

[88] Z.-H. Loh, R. W. Field, *J. Chem. Phys.* **2003**, *118*, 4037-4044.

[89] E. Wiberg, A. Bolz, *Ber. Dtsch. Chem. Ges. B* **1940**, *73*, 209-232.

[90] E. Wiberg, K. Hertwig, *Z. Anorg. Chem.* **1947**, *255*, 141-184.

[91] E. Wiberg, K. Hertwig, A. Bolz, *Z. Anorg. Chem.* **1948**, *256*, 177-216.

[92] E. Wiberg, K. Hertwig, *Z. Anorg. Chem.* **1948**, *257*, 138-144.

[93] G. Vacek, J. R. Thomas, B. J. DeLeeuw, Y. Yamaguchi, H. F. Schaefer, III, *J. Chem. Phys.* **1993**, *98*, 4766-4776.

[94] V. Bhagat, J. Schumann, H. F. Bettinger, *Angew. Chem. Int. Ed.* **2021**, *60*, 23112-23116.

[95] M. T. Nguyen, *J. Chem. Soc., Chem. Commun.* **1987**, 342-344.

[96] P. Paetzold, in *Adv. Inorg. Chem., Vol. 31* (Eds.: H. J. Emeléus, A. G. Sharpe), Academic Press, **1987**, pp. 123-170.

[97] P. Paetzold, R. Truppat, *Chem. Ber.* **1983**, *116*, 1531-1539.

[98] H. F. Bettinger, M. Filthaus, P. Neuhaus, *Chem. Commun.* **2009**, 2186-2188.

[99] H. F. Bettinger, M. Filthaus, *Org. Biomol. Chem.* **2010**, *8*, 5477-5482.

[100] H. F. Bettinger, H. Bornemann, *Z. Anorg. Allg. Chem.* **2011**, *637*, 2169-2174.

[101] P. W. Fairchild, G. P. Smith, D. R. Crosley, J. B. Jeffries, *Chem. Phys. Lett.* **1984**, *107*, 181-186.

[102] N. Wijeratne, P. G. Wenthold, *Heron Island Conference on ReactiVe Intermediates and Unusual Molecules (Heron 4)* **2007**, July 7-14.

[103] V. Bhagat, H. F. Bettinger, *J. Phys. Chem. A* **2022**, *126*, 7660-7666.

[104] N. P. Gritsan, T. Yuzawa, M. S. Platz, *J. Am. Chem. Soc.* **1997**, *119*, 5059-5060.

[105] R. Born, C. Burda, P. Senn, J. Wirz, *J. Am. Chem. Soc.* **1997**, *119*, 5061-5062.

[106] E. Leyva, M. S. Platz, G. Persy, J. Wirz, *J. Am. Chem. Soc.* **1986**, *108*, 3783-3790.

[107] G. Smolinsky, E. Wasserman, W. Yager, *J. Am. Chem. Soc.* **1962**, *84*, 3220-3221.

[108] M.-L. Tsao, M. S. Platz, *J. Am. Chem. Soc.* **2003**, *125*, 12014-12025.

[109] A. K. Schrock, G. B. Schuster, *J. Am. Chem. Soc.* **1984**, *106*, 5228-5234.

[110] D. Kvaskoff, H. Lüerssen, P. Bednarek, C. Wentrup, *J. Am. Chem. Soc.* **2014**, *136*, 15203-15214.

[111] A. Reiser, L. Leyshon, *J. Am. Chem. Soc.* **1971**, *93*, 4051-4052.

[112] R. L. Safiullin, S. L. Khursan, E. M. Chainikova, V. T. Danilov, *Kinet. Catal.* **2004**, *45*, 640-648.

[113] N. P. Gritsan, E. S. Pritchina, *J. Inf. Rec. Mater.* **1989**, *17*, 391-404.

[114] W. Hack, H. Kurzke, H. G. Wagner, *J. Chem. Soc., Faraday Trans. 2* **1985**, *81*, 949-961.

[115] M. R. Talipov, S. L. Khursan, R. L. Safiullin, *J. Phys. Chem. A* **2009**, *113*, 6468-6476.

[116] T. Fueno, K. Yokoyama, S.-y. Takane, *Theor. Chim. Acta* **1992**, *82*, 299-308.

[117] S. L. Laursen, J. E. Grace, R. L. DeKock, S. A. Spronk, *J. Am. Chem. Soc.* **1998**, *120*, 12583-12594.

[118] W. Lwowski, G. T. Tisue, *J. Am. Chem. Soc.* **1965**, *87*, 4022-4023.

[119] D. E. Milligan, *J. Chem. Phys.* **1961**, *35*, 1491-1497.

[120] N. P. Gritsan, I. Likhotvorik, Z. Zhu, M. S. Platz, *J. Phys. Chem. A* **2001**, *105*, 3039-3041.

[121] N. P. Gritsan, E. A. Pritchina, *Mendeleev Commun.* **2001**, *11*, 94-96.

[122] M. J. Travers, D. C. Cowles, E. P. Clifford, G. B. Ellison, P. C. Engelking, *J. Chem. Phys.* **1999**, *111*, 5349-5360.

[123] C. R. Kemnitz, G. B. Ellison, W. L. Karney, W. T. Borden, *J. Am. Chem. Soc.* **2000**, *122*, 1098-1101.

[124] J. H. Glownia, J. Misewich, P. P. Sorokin, in *The Supercontinuum Laser Source: Fundamentals with Updated References* (Ed.: R. R. Alfano), Springer New York, **2006**, pp. 337-376.

[125] T. Autrey, G. B. Schuster, *J. Am. Chem. Soc.* **1987**, *109*, 5814-5820.

[126] E. Wasserman, *Prog. Phys. Org. Chem* **1971**, *8*, 319-336.

[127] G. Smolinsky, E. Wasserman, W. A. Yager, *J. Am. Chem. Soc.* **1962**, *84*, 3220-3221.

[128] X. Zeng, H. Beckers, H. Willner, *J. Am. Chem. Soc.* **2013**, *135*, 2096-2099.

[129] C. Keck, J. Hahn, D. Gupta, H. F. Bettinger, *Chem. Eur. J.* **2022**, *28*, e202103614.

[130] S. Biswas, M. Müller, C. Tönshoff, K. Eichele, C. Maichle-Mössmer, A. Ruff, B. Speiser, H. F. Bettinger, *Eur. J. Org. Chem.* **2012**, *2012*, 4634-4639.

[131] M. Müller, C. Maichle-Mössmer, P. Sirsch, H. F. Bettinger, *ChemPlusChem* **2013**, *78*, 988-994.

[132] R. Köster, S. Hattori, Y. Morita, *Angew. Chem.* **1965**, *77*, 719-720.

[133] M. F. Lappert, M. K. Majumdar, B. P. Tilley, *J. Chem. Soc. A* **1966**, 1590-1595.

[134] E. Whittle, D. A. Dows, G. C. Pimentel, *J. Chem. Phys.* **2004**, *22*, 1943-1943.

[135] R. N. Perutz, *Annu. Rep. Prog. Chem., Sect. C* **1985**, *82*, 157-191.

[136] I. Dunkin, *Chem. Soc. Rev.* **1980**, *9*, 1-23.

[137] W. Fraenk, T. Habereder, T. M. Klapötke, H. Nöth, K. Polborn, *J. Chem. Soc., Dalton Trans.* **1999**, 4283-4286.

[138] M. J. Frisch, G. W. Trucks, H. B. Schlegel, G. E. Scuseria, M. A. Robb, J. R. Cheeseman, G. Scalmani, V. Barone, G. A. Petersson, H. Nakatsuji, X. Li, M. Caricato, A. V. Marenich, J. Bloino, B. G. Janesko, R. Gomperts, B. Mennucci, H. P. Hratchian, J. V. Ortiz, A. F. Izmaylov, J. L. Sonnenberg, Williams, F. Ding, F. Lipparini, F. Egidi, J. Goings, B. Peng, A. Petrone, T. Henderson, D. Ranasinghe, V. G. Zakrzewski, J. Gao, N. Rega, G. Zheng, W. Liang, M. Hada, M. Ehara, K. Toyota, R. Fukuda, J. Hasegawa, M. Ishida, T. Nakajima, Y. Honda, O. Kitao, H. Nakai, T. Vreven, K. Throssell, J. A. Montgomery Jr., J. E. Peralta, F. Ogliaro, M. J. Bearpark, J. J. Heyd, E. N. Brothers, K. N. Kudin, V. N. Staroverov, T. A. Keith, R. Kobayashi, J. Normand, K. Raghavachari, A. P. Rendell, J. C. Burant, S. S. Iyengar, J. Tomasi, M. Cossi, J. M. Millam, M. Klene, C. Adamo, R. Cammi, J. W. Ochterski, R. L. Martin, K. Morokuma, O. Farkas, J. B. Foresman, D. J. Fox, Wallingford, CT, **2016**.

[139] F. Neese, *WIREs Comput. Mol. Sci.* **2012**, *2*, 73-78.

[140] F. Neese, *WIREs Comput. Mol. Sci.* **2022**, *12*, e1606.

[141] F. Neese, *WIREs Comput. Mol. Sci.* **2018**, *8*, e1327.

[142] H. J. Werner, P. J. Knowles, G. Knizia, F. R. Manby, M. Schütz, *WIREs Comput. Mol. Sci.* **2012**, *2*, 242-253.

[143] M. W. Schmidt, K. K. Baldridge, J. A. Boatz, S. T. Elbert, M. S. Gordon, J. H. Jensen, S. Koseki, N. Matsunaga, K. A. Nguyen, S. Su, T. L. Windus, M. Dupuis, J. A. Montgomery Jr, *J. Comput. Chem.* **1993**, *14*, 1347-1363.

[144] M. S. Gordon, M. W. Schmidt, in *Theory and Applications of Computational Chemistry* (Eds.: C. E. Dykstra, G. Frenking, K. S. Kim, G. E. Scuseria), Elsevier, Amsterdam, **2005**, pp. 1167-1189.

[145] J.F. Stanton, J. Gauss, L. Cheng, M.E. Harding, D.A. Matthews, P. G. Szalay, *CFOUR*, Coupled-Cluster techniques for Computational Chemistry, Version 2.00beta, for the updates, see http://www.cfour.de.

[146] R. Dennington, T. A. Keith, J. M. Millam, *Semichem Inc., Shawnee Mission, KS,* **2016**, GaussView Version 6.1.

[147] Chemcraft - graphical software for visualization of quantum chemistry computations. Version 1.8, build 165.

[148] B. M. Bode, M. S. Gordon, *J. Mol. Graphics Modell.* **1998**, *16*, 133-138.

[149] B. O. Roos, P. R. Taylor, P. E. Sigbahn, *Chem. Phys.* **1980**, *48*, 157-173.

[150] B. O. Roos, K. Lawley, *Adv. Chem. Phys.* **1987**, *69*, 399-446.

[151] P. E. M. Siegbahn, J. Almlöf, A. Heiberg, B. O. Roos, *J. Chem. Phys.* **1981**, *74*, 2384-2396.

[152] K. Andersson, P. A. Malmqvist, B. O. Roos, A. J. Sadlej, K. Wolinski, *J. Phys. Chem.* **1990**, *94*, 5483-5488.

[153] B. O. Roos, P. Linse, P. E. Siegbahn, M. R. Blomberg, *Chem. Phys.* **1982**, *66*, 197-207.

[154] C. Angeli, R. Cimiraglia, S. Evangelisti, T. Leininger, J.-P. Malrieu, *J. Chem. Phys.* **2001**, *114*, 10252-10264.

[155] J. Čížek, *J. Chem. Phys.* **2004**, *45*, 4256-4266.

[156] J. Čižek, J. Paldus, *Int. J. Quantum Chem* **1971**, *5*, 359-379.

[157] R. J. Bartlett, G. D. Purvis, *Int. J. Quantum Chem* **1978**, *14*, 561-581.

[158] R. J. Bartlett, *J. Phys. Chem.* **1989**, *93*, 1697-1708.

[159] R. J. Bartlett, M. Musiał, *Rev. Mod. Phys.* **2007**, *79*, 291-352.

[160] W. Kohn, A. D. Becke, R. G. Parr, *J. Phys. Chem.* **1996**, *100*, 12974-12980.

[161] F. Neese, *Coord. Chem. Rev.* **2009**, *253*, 526-563.

[162] C. M. Marian, N. Gilka, *J. Chem. Theory Comput.* **2008**, *4*, 1501-1515.

[163] M. A. El-Sayed, *J. Chem. Phys.* **2004**, *38*, 2834-2838.

[164] M. A. El-Sayed, *Acc. Chem. Res.* **1968**, *1*, 8-16.

[165] B. Du, W. Zhang, L. Mu, C. Feng, *J. Mol. Struct.* **2007**, *816*, 21-29.

[166] T. Fueno, V. Bonacic-Koutecky, J. Koutecky, *J. Am. Chem. Soc.* **1983**, *105*, 5547-5557.

[167] D. W. Cornell, R. S. Berry, W. Lwowski, *J. Am. Chem. Soc.* **1966**, *88*, 544-550.

[168] A. V. Kuzmin, B. A. Shainyan, *J. Phys. Org. Chem.* **2014**, *27*, 794-802.

[169] J. Du, L. Wang, M. Xie, L. Deng, *Angew. Chem. Int. Ed.* **2015**, *54*, 12640-12644.

[170] R. A. Abramovitch, S. R. Challand, Y. Yamada, *J. Org. Chem.* **1975**, *40*, 1541-1547.

[171] R. Banks, G. Sparkes, *J. Chem. Soc., Perkin Trans. 1* **1972**, 2964-2970.

[172] P. Scheiner, *J. Org. Chem.* **1967**, *32*, 2022-2023.

[173] E. Jacox, D. E. Milligan, *J. Am. Chem. Soc.* **1963**, *85*, 278-282.

Chemistry–A European Journal | Full Paper doi.org/10.1002/chem.202002445 | Chemistry Europe European Chemical Societies Publishing

Reaction Mechanisms

# Unusual Nitrene Oxidation Product Formation by Metathesis Involving the Dioxygen O—O and Borylnitrene B—N Bonds

Virinder Bhagat, Julia Schumann, and Holger F. Bettinger*[a]

**Abstract:** The reaction of dioxygen with nitrenes can have significant energy barriers, although both reactants are triplet diradicals and the formation of nitroso-*O*-oxides is spin-allowed. By means of matrix-isolation infrared spectroscopy in solid argon, nitrogen, and neon, and through high-level computational quantum chemistry, it is shown herein that a 3-nitreno-1,3,2-benzodioxaborole CatBN (Cat = catecholato) reacts with dioxygen under cryogenic conditions thermally at temperatures as low as 7 K to produce two distinct products, an *anti*-nitroso-*O*-oxide and a nitritoborane CatBONO. The computed barriers for the formation of nitroso-*O*-oxide isomers are very low. Whereas *anti*-nitroso-*O*-oxide is kinetically trapped, its bisected isomer has a very low barrier for metathesis, yielding the CatBO + NO radicals in a strongly exothermic reaction; these radicals can combine under matrix-isolation conditions to give nitritoborane CatBONO. The trapped isomer, *anti*-nitroso-*O*-oxide, can form the nitritoborane CatBONO only after photoexcitation, possibly involving isomerization to the bisected isomer of *anti*-nitroso-*O*-oxide.

## Introduction

Dioxygen is a very unusual molecule because it is an open-shell triplet diradical, but enjoys extraordinary persistence, which means it forms a substantial fraction of the earth's atmosphere. Almost all of its reactions, oxidations, are very exothermic due to the weak O–O σ bond, but often barriers are sufficiently high to preclude them.[1] This arises from the substantial 100 kcal mol$^{-1}$ resonance energy of two three-electron, two-center π bonds.[1] Dioxygen, however, undergoes very fast reactions with other open-shell species, such as radicals and diradicals. Thus, the suppression of a reaction in the presence of oxygen is a qualitative test for the involvement of radicals. Likewise, the fast reaction of triplet carbenes with dioxygen, even at very low temperatures, as provided by matrix-isolation conditions, can serve as a qualitative test for the carbene spin state.[2]

It is well established that triplet aromatic nitrenes react much slower with oxygen than triplet aromatic carbenes.[3,4] According to the reports of Gritsan and Pritchina,[5] the rate of the reaction of *para*-substituted phenylnitrene and oxygen in solvents such as toluene and hexane is in the order of $10^{-6}$ L mol$^{-1}$ s$^{-1}$. On the other hand, the reaction rate in the case of phenylcarbenes can reach the limit of diffusion control, even at low temperatures.[6] *p*-Aminophenylnitrene reacts to both the *syn*- and *anti*-*p*-aminophenylnitroso oxide (**2a** and **2b**, respectively) upon annealing of an argon matrix doped with 4% oxygen (Scheme 1a).[7] The isomers of *p*-aminophenylnitroso oxide were found to be photochemically interconvertible and, upon irradiation with $\lambda > 365$ nm, ultimately reacted to form *para*-nitroaniline.[7]

Remarkably, phenylnitrene undergoes no reaction, even in a solid $O_2$ matrix at 20 K, as shown by Sander et al.[8] Annealing in $O_2$-doped Xe matrix only consumed 40% of phenylnitrene, even after 12 h at 50 K, resulting mainly in the formation of *syn*-nitroso-*O*-oxide **2b** and finally nitrobenzene **4** after irradiating with visible light of wavelength 450 nm (Scheme 1a).[8] This indicates a high barrier for the reaction of molecular oxygen and phenylnitrene under matrix-isolation conditions. A computational study by Platz et al. explained the lower reactivity of phenylnitrene compared with that of phenylcarbene towards oxygen by thermodynamic arguments.[9]

However, not all nitrenes react reluctantly with molecular oxygen. For example, the parent nitrene, imidogen NH, is known to react in Xe matrix with $O_2$,[10] and a computational investigation agrees with the experimental results related to this reaction.[11] A particularly reactive nitrene is borylnitrene **6** CatBN (Cat = catecholato) formed in situ by irradiating matrix-isolated boryl azide **5**.[12] Nitrene **6** prefers a triplet electronic ground state, according to ESR spectroscopy and high-level computations.[12,13] Nitrene **6** and closely related borylnitrenes are very reactive towards sigma bonds (e.g., C(sp$^3$)–H, H–H) after *photoexcitation*, most likely due to the formation of the highly electrophilic singlet nitrene.[14–18] Borylnitrene **6**, however, also shows very high *thermal* reactivity towards $O_2$ in an

[a] V. Bhagat, Dr. J. Schumann, Prof. Dr. H. F. Bettinger
Institut für Organische Chemie, Universität Tübingen
Auf der Morgenstelle 18, 72076 Tübingen (Germany)
E-mail: holger.bettinger@uni-tuebingen.de
Supporting information and the ORCID identification number(s) for the author(s) of this article can be found under:
https://doi.org/10.1002/chem.202002445.

Chemistry–A European Journal | Full Paper doi.org/10.1002/chem.202002445 | Chemistry Europe European Chemical Societies Publishing

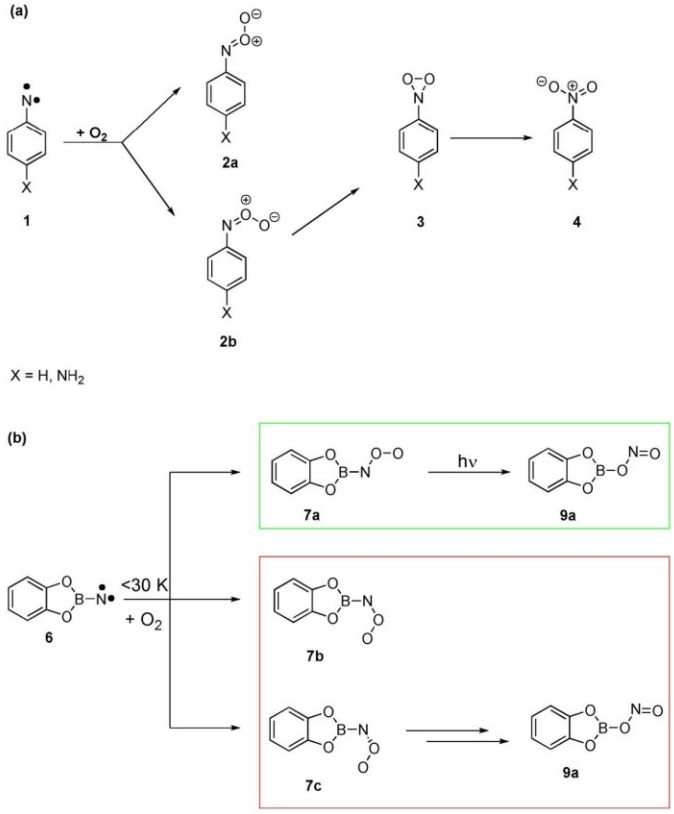


**Scheme 1.** a) Reaction of aromatic nitrenes **1** and the formation of nitroarenes **4** via intermediates **2a**, **2b**, and **3**. b) The reaction of borylnitrene **6** with oxygen and the formation of *anti*-nitritoborane **9a**. The portion enclosed in the green box corresponds to already explored aspects,[12] regarding the interaction of **6** with $O_2$, and that enclosed within the red box is unexplored and the subject of the present work.

argon matrix because annealing in the presence of $O_2$ quickly results in the formation of nitroso oxide **7a** (Scheme 1b).[12] The latter was shown to undergo, upon photoexcitation ($\lambda =$ 254 nm), a formal dyotropic rearrangement[19–21] to nitritoborane **9a**. Not only is the thermal reactivity of **6** towards $O_2$ higher than that of aryl nitrenes, but also the final oxidation product differs because not the nitro- ($CatBNO_2$) but the nitritoborane (CatBONO) is formed.[12] In addition, three isomers of nitroso oxide **7** could be identified computationally (UB3LYP/6-311+G**), but only conformation **7a** (*anti*) could be observed experimentally.[12] Neither the reason for the high reactivity of **6** towards oxygen upon annealing, nor the preference for the formation of **7a**, or even the mechanism of nitritoborane formation from nitroso oxide are currently known.

Herein, we show by combining matrix-isolation experiments and high-level computations that the thermal reaction of borylnitrene **6** with $O_2$ results in multiple products. Besides **7a**, which is kinetically locked under matrix-isolation conditions and only reacts upon subsequent photoexcitation, a low-barrier pathway via the bisected nitroso oxide isomer (**7c**) exists that allows the formation of a radical pair (**8**: CatBO + NO) by metathesis of the B–N and O–O bonds. The radical pair within the matrix cage eventually collapses to final product **9a**. Hence, it is possible for the system $CatBN + O_2$ to undergo simultaneous insertions into the B–N and O–O bonds to form CatBONO at temperatures as low as 30 K in argon and 7 K in Ne.

## Experimental Section

### Experiments

$CatBN_3$ was synthesized according to a published procedure.[22] Matrix-isolation experiments were performed by standard techniques on a Sumitomo SH-1 closed-cycle helium cryostat.[23] Matrices were produced by deposition of different materials, such as argon, nitrogen, and neon (Messer-Griesheim, 99.9999%), on top of a CsI (IR) window at 15, 10, and 4 K, respectively, with oxygen as a dopant (2–3%, 99.999% purity). IR spectra were recorded with a Bruker Vertex 70 FTIR spectrometer with a standard resolution of 0.5 $cm^{-1}$ in the range of 400–4000 $cm^{-1}$. Irradiations were carried out by using a low-pressure mercury lamp ($\lambda = 254$ nm, PenRay).

### Computations

Geometries of stationary points were optimized at the B3LYP level,[24,25] as implemented in Gaussian 16,[26] in conjunction with the 6-311+G** basis set. The stability of the spin-restricted B3LYP solution was probed, and spin-unrestricted UB3LYP was employed if a triplet instability was detected. Harmonic vibrational frequencies confirmed that the structures corresponded to minima or first-order saddle points. The obtained zero-point vibrational energies were used for correcting the electronic energies of isomers. Intrinsic reaction coordinate calculations were performed to confirm that transition states indeed connected the expected reactive intermediates. Natural bond orbital (NBO)[27,28] analyses were performed for some species at the (U)B3LYP/6-311+G(d,p) level of theory by using the NBO 3.1[29] program.

Energies were refined by coupled-cluster theory involving single, double, and a perturbative estimate of triple excitations (CCSD(T)).[30,31] The coupled-cluster computations used Dunning's[32] correlation consistent triple-ζ basis set (cc-pVTZ) and were performed with the Molpro program.[33] Because the $T_1$ diagnostic values were larger than those recommended for a number of stationary points ($T_1 < 0.02$),[34] completely renormalized coupled cluster theory, CR-CCSD(T), was employed for some stationary points.[35–37] $T_1$ diagnostic values greater than a certain limit ($T_1 >$ 0.02) obtained in a coupled cluster calculation could signal an inadequacy of the single-reference-based coupled cluster method,[34] and showed the demand for a multiconfigurational treatment of the reference wavefunction. One way to describe the nondynamic electron correlation in diradicaloid species by using "black box" single-reference methods is the application of CR-CCSD(T), which has been shown to be able to describe diradicaloid and bond-breaking situations as reliably as CCSD(T) for closed-shell species.[35–37] The CR-CCSD(T) computations were performed with Dunning's[38] triple-ζ basis set with two sets of polarization functions on the hydrogen and heavy atoms with orbital exponents $\alpha_d(C) =$ 1.44, 0.36; $\alpha_d(O) = 2.56$, 0.64; $\alpha_d(B) = 1.00$, 0.25; $\alpha_d(N) = 1.96$, 0.49; and $\alpha_d(H) = 2.0$, 0.5, yielding the TZ2P[38] basis set. The renormal-

Chemistry–A European Journal | Full Paper doi.org/10.1002/chem.202002445 | Chemistry Europe European Chemical Societies Publishing

ized coupled cluster computations were performed with the GAMESS program.[39,40]

Because the relative energies of nitroso oxides **7**, computed at the CCSD(T) level, did not differ significantly from the renormalized coupled-cluster results, and because the appropriateness of the CCSD(T) method for the related HNOO molecule was demonstrated previously,[41] geometry optimizations were also performed at the CCSD(T) level of theory by using analytic gradients.[42] Dunning's DZP double-ζ basis set, with one set of polarization functions on the hydrogen and heavy atoms with orbital exponents $\alpha_d(C)=0.654$, $\alpha_d(O)=1.211$, $\alpha_d(B)=0.386$, $\alpha_d(N)=0.902$, and $\alpha_d(H)=0.7$, was employed. Harmonic vibrational frequencies were obtained by finite differences of analytic gradients at the CCSD(T)/DZP level of theory. The CCSD(T) gradient computations were run with the CFOUR program.[43] The CCSD(T) harmonic vibrational frequencies for **7** were in better agreement with experiments than those at the B3LYP/6-311+G** level used previously,[12] whereas for **9** both methods gave very similar spectra.

The reaction of nitrene **6** with $O_2$ was investigated by using complete active space self-consistent field (CASSCF) theory. Relaxed potential-energy scan calculations were performed with the computational chemistry package ORCA[44] by using the valence double-ζ basis set def2-SV(P).[45] Because the CASSCF method considered nondynamic correlation only, the potential-energy curves obtained from the CASSCF relaxed scans were further refined with fully internally contracted *N*-electron valence state perturbation theory[46] (FIC-NEVPT2) in combination with the def2-SV(P) basis set, which also took into account dynamic correlation. The advantage of NEVPT2 is that it does not suffer from intruder states that could cause problems for other multireference perturbation theories, such as the more popular CASPT2 method.[47] Studies have shown that NEVPT2 performs similarly to CASPT2 or even better if intruder states caused problems for the latter method.[48,49]

## Results and Discussion

### Matrix-isolation experiments

Matrix-isolation infrared spectroscopic studies of boryl azide **5** were performed with different matrix hosts (Ar, $N_2$, and Ne, but only the Ar data are presented herein in detail; for very similar spectra obtained in $N_2$ and Ne, see Figures S2 and S3 in the Supporting Information) doped with 2–3% $O_2$. Irradiation of matrix-isolated precursor **5** with $\lambda=254$ nm until it was completely bleached, as shown in Figure 1a, resulted in new IR bands. With the help of spectra computed at the CCSD(T)/DZP level of theory, it was confirmed that the species that formed after irradiation with $\lambda=254$ nm were borylnitrene **6** and *anti*-nitritoborane **9a**.[12]

As reported previously,[12] nitrene **6** was consumed during annealing at 30 K for 30 min and new signals were observed, as shown in Figure 1b. One set of signals was the same as that which appeared after irradiation (Figure 1a) and was due to *anti*-nitritoborane **9a**. With the help of the computed spectrum (Figure 2b), the second set of new signals in Figure 1b was assigned to *anti*-nitroso-*O*-oxide **7a**, as done previously.[12] Furthermore, the matrix was irradiated at $\lambda=254$ nm for 30 min and it was observed that **7a** was bleached, as observed in signals pointing downwards in Figure 1c. The set of signals pointing upwards (Figure 1c) is the same as that in both previous steps, and hence, was assigned to **9a**.

To further strengthen the assignments, heavy isotopic molecular oxygen, $^{18}O_2$, was used in one set of experiments with $N_2$ as a host material (Figure 3). The normal modes of calculated **7a** and **7a′** were compared and, as expected, normal modes with a significant contribution from the terminal NOO fragment of *anti*-nitroso-*O*-oxide showed significant shifts in their stretching frequencies. The experimental IR bands that were assigned to these normal modes ($\nu_{29}$, $\nu_{25}$, and $\nu_{23}$, see Figure 4) in the case of experiments with $^{16}O_2$ were shifted if $^{18}O_2$ was employed and were assigned to **7a′**. The above observations further provide evidence in favor of the formation of *anti*-nitroso-*O*-oxide **7a** as one of the species upon annealing. All assignments of experimental IR spectra to their corresponding calculated spectra in Figures 2 and 3 are listed in Tables S3–S6 in the Supporting Information.

As reported earlier, the three isomers of **7** are very similar in energy.[12] However, in contrast to B3LYP, bisected isomer **7c** is the lowest energy isomer at the NEVPT2//CASSCF, CCSD(T)//B3LYP, and the CCSD(T) levels. Since the $T_1$ diagnostics of isomers **7** are higher (0.02 to 0.03) than those recommended (0.02),[34] the completely renormalized coupled-cluster method CR-CCSD(T) was employed as well. These results concurred with the CCSD(T) result that the relative energy of the isomers increased as **7c** < **7a** < **7b**. In addition, *syn*-isomer **7b** is a first-order saddle point at the CCSD(T)/DZP level of theory with a small imaginary vibrational frequency of 12*i* $cm^{-1}$. This explains why we do not detect formation of **7b** in our experiments. A comparison of the computed harmonic vibrational frequencies of **7a** and **7c** suggests that they differ to such an extent that the two isomers should be distinguishable (see Figure S5 in the Supporting Information). This leaves two important questions: 1) Why is the most stable isomer **7c** not detected? 2) How can the nitritoborane be formed thermally, that is, without photoexcitation? To further investigate the properties of **7a** and **7c**, additional computational investigations were performed as discussed in the next section.

### Computational studies

To elucidate the mechanistic aspects for the formation of *anti*-nitritoborane **9a** after the reaction of triplet borylnitrene **6** and oxygen, a computational investigation was performed. This computational study is divided into two parts: 1) the formation of initial nitroso-*O*-oxide products upon annealing, as a result of the reaction between borylnitrene **6** and oxygen; and 2) the further reaction pathway that results in the formation of *anti*-nitritoborane **9a** as the final product.

The first reaction product formed from triplet CatBN **6** and triplet $O_2$, nitroso-*O*-oxide **7a**, has a singlet electronic ground state based on the (U)B3LYP and CCSD(T) computations. The triplet state is 26 and 40 kcal $mol^{-1}$, respectively, higher in energy. The singlet state of **7a** can be formed in a spin-allowed reaction from triplet nitrene **6** and triplet $O_2$ with all four open-shell electrons coupled to a singlet electronic state. It is clear that the electronic structure of the corresponding open-shell singlet state at a large distance is essentially impossible to describe with single-reference-based methods, such as

 

Chemistry–A European Journal
Full Paper
doi.org/10.1002/chem.202002445
Chemistry Europe
European Chemical Societies Publishing

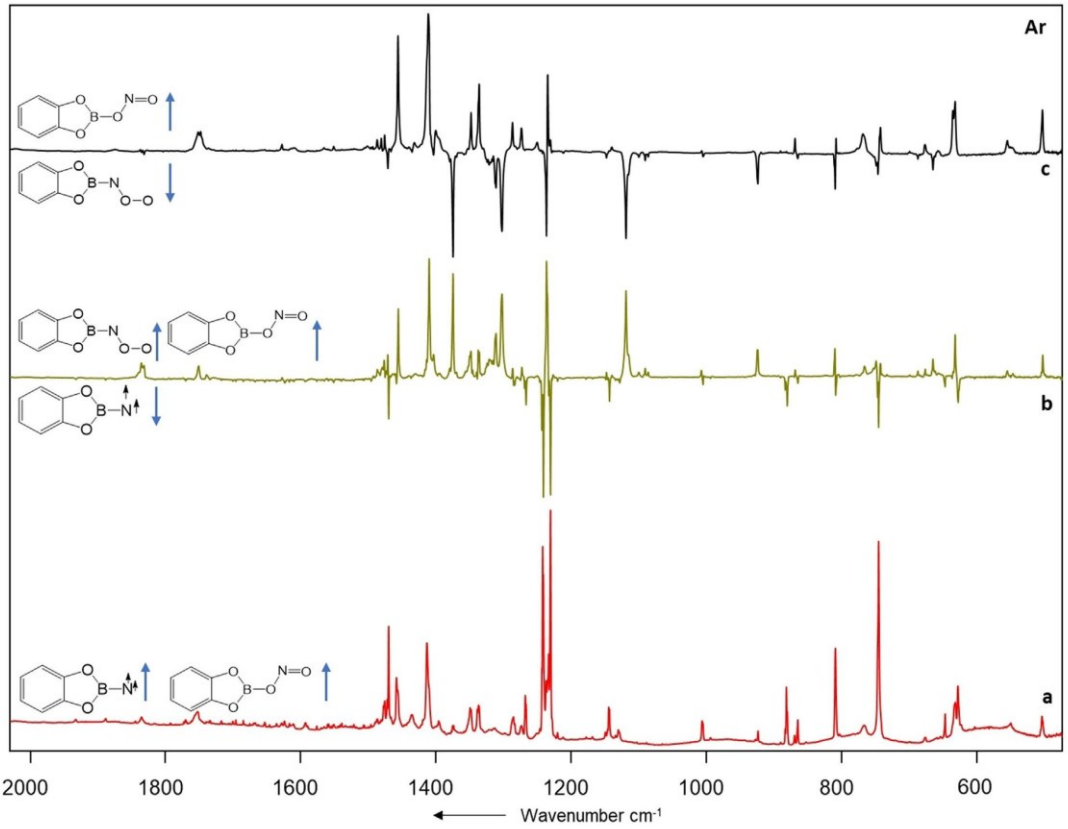


**Figure 1.** Infrared spectra obtained after irradiation of boryl azide **5** in $O_2$ (2–3 %) doped argon matrix. a) After 60 min irradiation with $\lambda = 254$ nm at $T = 10$ K. b) Difference spectrum after annealing for 30 min at 30 K. c) Difference spectrum after irradiation with $\lambda = 254$ nm for 30 min.

Kohn–Sham DFT and Hartree–Fock reference-based coupled cluster methods. Hence, we employed the CASSCF method in conjunction with the def2-SV(P) basis set in CASSCF relaxed scan calculations with the N–O distance as the scan parameter, followed by single-point energy evaluations by using CASSCF-based second-order perturbation theory, NEVPT2. The choice of the proper active space for such a complex reaction with four open shells coupled to a singlet electronic state turned out to be challenging. Hence, we first selected the reaction of NH and $O_2$ as a model system that was previously studied by Talipov et al. using a full-valence active space and second-order perturbation theory (MCQDPT2//CASSCF).[11] Due to the small system size, we also performed the CASSCF and NEVPT2//CASSCF scan calculations with full-valence active space (18,13). The potential-energy curve (Figure 5 a) shows that the barrier for the formation for imine peroxide, as a result of reaction of $NH + O_2$, is 7.1 kcal mol$^{-1}$ at the CASSCF(18,13)/def-SV(P) level of theory. This was reduced to 0.4 kcal mol$^{-1}$ by using NEVPT2/def-SV(P) single points. It has been reported that the formation of imine peroxide from NH and $O_2$ is barrierless under matrix-isolation conditions[10] and in the gas phase.[50] Hence, our refined barrier (0.4 kcal mol$^{-1}$) at the NEVPT2/def-SV(P) level is in agreement with regard to the reported experimental barriers for the formation of imine peroxide. It is also in agreement with closely related multiconfiguration perturbation theory (MCQDPT2; 1.4 kcal mol$^{-1}$) and multireference configuration interaction (MRCI; 0.8 kcal mol$^{-1}$) computations by using the full-valence active space reported by Talipov et al.[11]

A full-valence active space is computationally too demanding for treating the reaction of **6** + $O_2$, but close visual inspection of the relevant active-space orbitals of NH + $O_2$ allowed identification of relevant orbitals for the title reaction. Including the corresponding orbitals (see Figure S4 in the Supporting Information) in the active space of the **6** + $O_2$ system gave barriers for the formation of the *anti*- and bisected isomers of **7** of 7.1 and 13.4 kcal mol$^{-1}$, respectively, at the CASSCF(14,10)/def2-SV(P) level (Figure 5 b,c). These barriers obtained from CASSCF calculations are too high to overcome under matrix-isolation conditions, but similar to the case of the NH + $O_2$ reaction, these barriers were reduced significantly after refinement with NEVPT2 (Figure 5 a). The barriers of 0.4 kcal mol$^{-1}$ for the formation of *anti*-isomer **7 a** and 1.4 kcal mol$^{-1}$ for bisected isomer **7 c** (Figure 5 b,c) are very small, similar to that of the NH + $O_2$ reaction at the same level of theory.

Chemistry–A European Journal | Full Paper doi.org/10.1002/chem.202002445 | Chemistry Europe European Chemical Societies Publishing

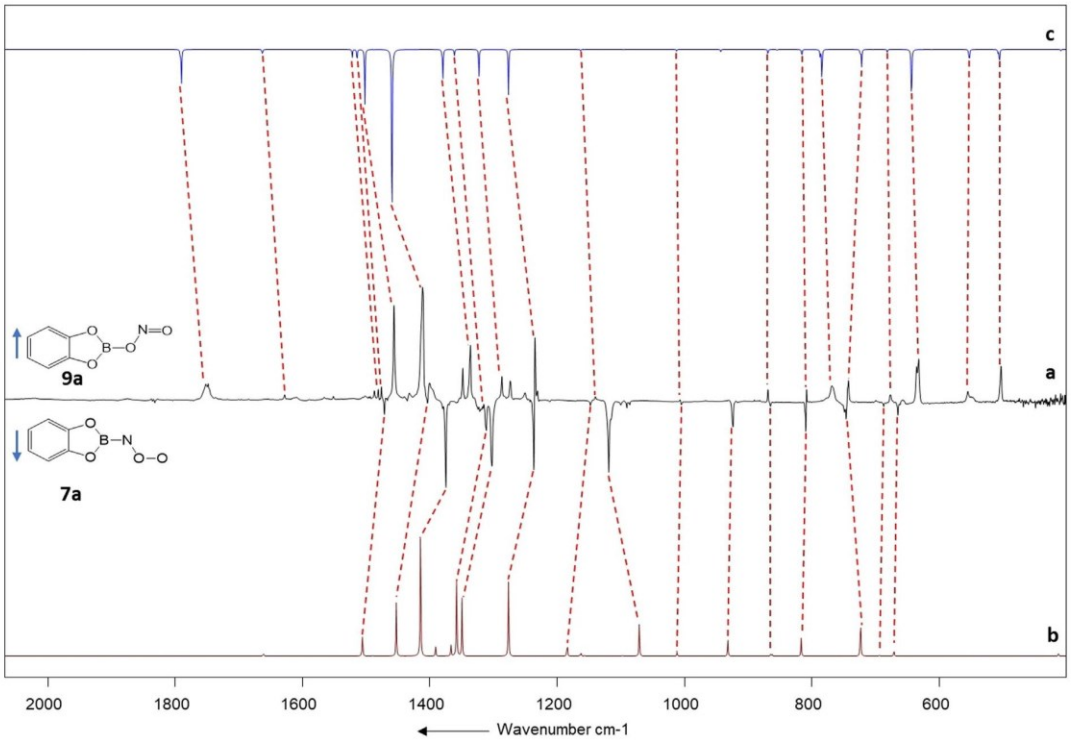


**Figure 2.** a) Difference IR spectrum after irradiation with $\lambda = 254$ nm for 30 min (following the annealing step). b) Calculated spectrum for $^{11}B$ and $^{10}B$ isotopologues (81:19) of *anti*-nitroso-*O*-oxide **7a** at the CCSD(T)/DZP level. c) Calculated spectrum for $^{11}B$ and $^{10}B$ isotopologues (81:19) of *anti*-nitritoborane **9a** at the CCSD(T)/DZP level.

The barriers for the formation of isomers **7a** and **7c** are low, but differ by roughly 1 kcal mol$^{-1}$ at the present level of theory. It can be assumed that the barrier heights are further reduced by a more sophisticated treatment of electron correlation and expansion of the one-electron basis set, as shown by Talipov et al. for the NH + $O_2$ reaction, which does not rule out the absence of an activation barrier altogether.[11] Because both products **7a** and **9** are also formed in Ne matrix upon annealing to 10 K, the experiment suggests that the barriers are very small or may not even exist. That only isomer **7a** can be safely assigned in the experiments could be due to a kinetic preference for its formation, as suggested for the preferred formation of *trans*-HNOO in the case of the related HN + $O_2$ reaction.[10,11] However, we still need a channel for the formation of **9a** that has essentially no barrier. We therefore investigated the ground-state thermal reaction pathway from various geometrical isomers of nitroso-*O*-oxide (**7a**, **7b**, and **7c**) that finally resulted in *anti*-nitritoborane **9a** as the second part of our computational investigation. These calculations were performed at the CCSD(T)/cc-pVTZ//UB3LYP/6-311 + G** level, unless noted otherwise.

Despite their very similar energy contents (within 3 kcal mol$^{-1}$), the interconversions of **7a** to **7b** (a minimum at B3LYP, but a saddle point at CCSD(T)) or to **7c** have high energy demand (> 30 kcal mol$^{-1}$; Figure 6). Similarly, high barriers have been obtained computationally for the isomerization of *cis*- and *trans*-HNOO.[11] These interconversions are thus impossible thermally under cryogenic conditions.

The higher barriers associated with $\mathbf{TS_2}$ and $\mathbf{TS_3}$ are due to rotation about the N–O bonds that have pronounced double-bond character, according to their Wiberg bond indexes of 1.4–1.5 for all isomers **7a–c** (see Table S1 in the Supporting Information). On the other hand, transition-state $\mathbf{TS_4}$ corresponds to rotation about the B–N bond. NBO calculations showed that the Wiberg bond orders of the B–N bonds were in the range of 0.8–1.0 for isomers **7a–c** (see Table S1 in the Supporting Information). Hence, rotation about the B–N bond, as in $\mathbf{TS_4}$, is expected to be a low-energy process, whereas rotation about the N–O bond, as in $\mathbf{TS_2}$ and $\mathbf{TS_3}$, requires much more energy.

The bisected geometry **7c** provides the starting point for the low-barrier breaking of the B–N bond that results in a complex of **8** CatBO with NO (Figure 6). The barrier at the CCSD(T) level is only 0.8 kcal mol$^{-1}$. Because the $T_1$ diagnostic values (0.028 for **7c** and 0.029 for $\mathbf{TS_5}$) are larger than that of the generally accepted threshold of 0.02 suggested by Lee and Taylor,[34] we also performed CR-CCSD(T) computations that were significantly more robust for diradicaloids.[35–37] The classical barrier is < 0.1 kcal mol$^{-1}$ at the CR-CCSD(T)/TZ2P//UB3LYP/6-311 + G** level, which confirms that thermal reaction of **7c** is clearly a low-energy process. The resulting complex **8** of the CatBO + NO radical pair is likely poorly described by CCSD(T)

 

Chemistry–A European Journal | Full Paper doi.org/10.1002/chem.202002445 | Chemistry Europe European Chemical Societies Publishing

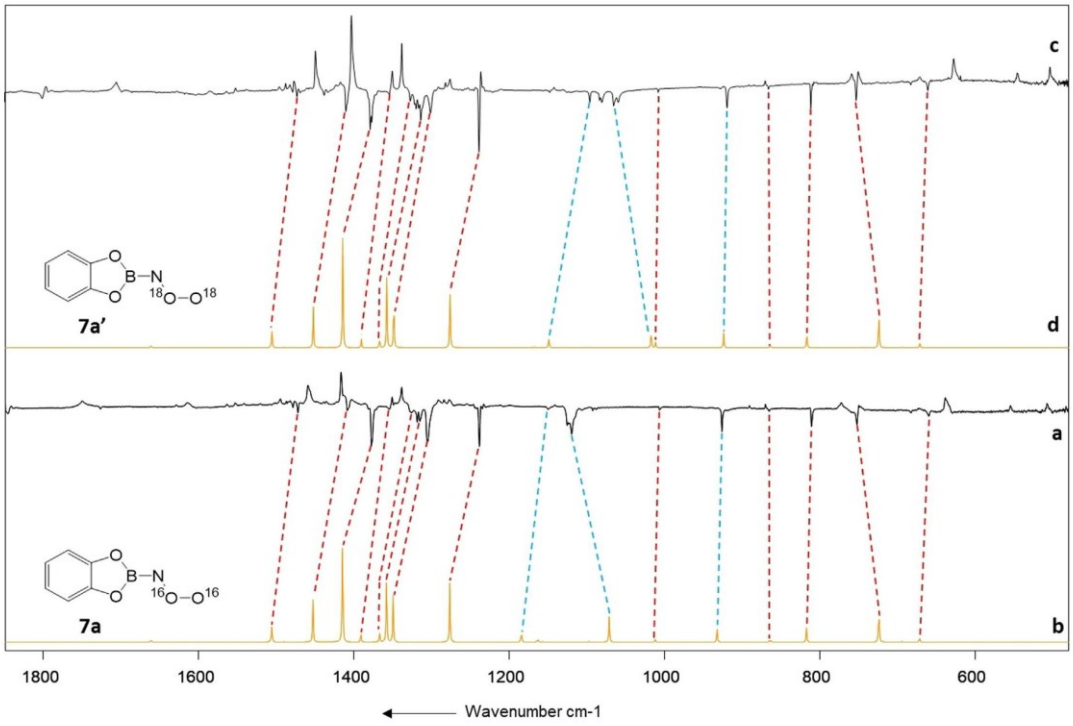


**Figure 3.** a) Difference spectrum after irradiation with $\lambda = 254$ nm for 40 min (following the annealing step). b) Calculated spectrum for $^{11}B$ and $^{10}B$ isotopologues (81:19) of *anti*-nitroso-*O*-oxide **7a** at the CCSD(T)/DZP level (with $^{16}O_2$). c) Difference spectrum after irradiation with $\lambda = 254$ nm for 30 min (following the annealing step). d) Calculated spectrum for $^{11}B$ and $^{10}B$ isotopologues (81:19) of *anti*-nitroso-*O*-oxide **7a'** at CCSD(T)/DZP (with $^{18}O_2$).

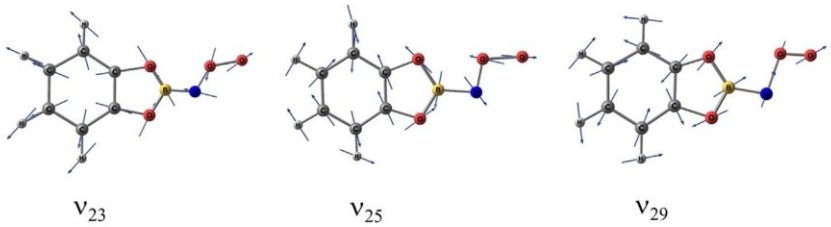


**Figure 4.** Normal modes with a significant contribution from the terminal NOO fragment of *anti*-nitroso-*O*-oxide **7a** (with $^{16}O_2$) calculated at the CCSD(T)/DZP level.

due to the large $T_1$ diagnostic of 0.032, and we consider the UB3LYP data more reliable. Complex **8** is stabilized by 59 kcal mol$^{-1}$ relative to bisected isomer **7c**. Combination of the two radicals to give *syn*-nitritoborane **9b** is strongly exothermic and its barrier can likely be overcome by due to the energy gained by formation and the fixation in a matrix cage.[51] A very low barrier (0.2 kcal mol$^{-1}$) N–O bond rotation finally gives the more stable and experimentally observed *anti*-nitritoborane **9a**.

The formation of CatBO + NO from CatBN + OO can be regarded as a metathesis reaction that proceeds essentially without a barrier. Metal-free bond metathesis reactions involving boron are currently receiving attention.[52–58] For example, Kinjo et al. observed metal-free σ-bond metathesis in the reaction of alkoxyphosphine **10** and pinacolborane **11** that involved breaking of the P–O and B–H bonds, as shown in Scheme 2b.[52] This was explained by the high electrophilicity of boron on Bpin and hence, the formation of a strong B–O bond.[52] We observed similar reactivity for **6** + $O_2$ under matrix-isolation conditions, but in a stepwise manner. The high oxophilicity of the boron center plays an important role in attracting the terminal oxygen in $\mathbf{TS_5}$, eventually leading to nitritoborane **9**, instead of the more often observed nitroborane.[7,8,59]

## Conclusion

Detailed combined experimental and computational investigations reveal that borylnitrene shows high reactivity towards di-

 

Chemistry–A European Journal
Full Paper
doi.org/10.1002/chem.202002445
Chemistry Europe
European Chemical Societies Publishing

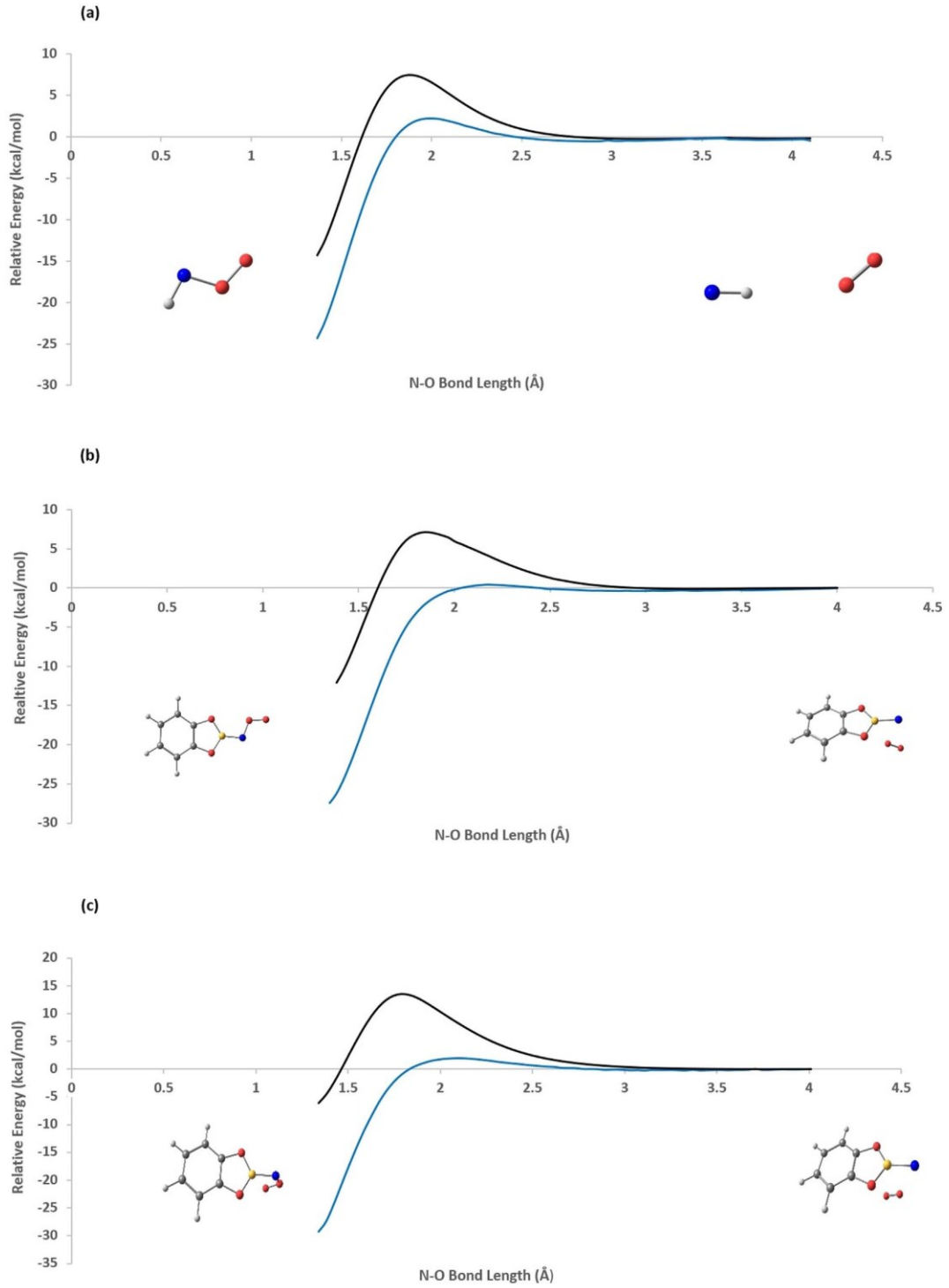


**Figure 5.** Potential-energy curves with the N–O bond as the scan parameter for reactions of nitrenes with $O_2$ computed at the CASSCF(n,m)/def2-SV(P) (black) and NEVPT2/def2-SV(P)// CASSCF(n,m)/def2-SV(P) (blue) levels. a) Formation of HNOO ($n=18$, $m=13$). b) Formation of *anti*-**7a** ($n=14$, $m=10$). c) Formation of bisected **7c** ($n=14$, $m=10$).

Chemistry–A European Journal | Full Paper doi.org/10.1002/chem.202002445 | Chemistry Europe European Chemical Societies Publishing

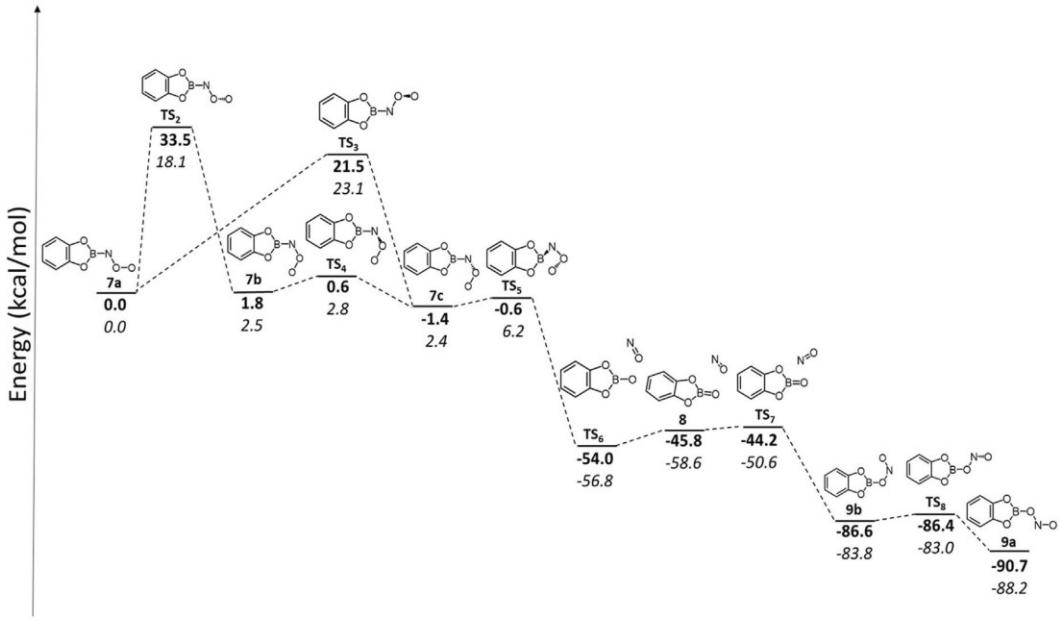


**Figure 6.** Potential-energy diagram showing the stationary points corresponding to various species involved and transition states for the formation of nitritoborane **9** after the reaction of triplet borylnitrene **6** and oxygen. All stationary points were calculated at the (U)B3LYP/6-311 + G(d,p) (italics) and CCSD(T)/cc-pVTZ//(U)B3LYP/6-311 + G(d,p) (bold) levels. Notably, the shape of the B3LYP potential-energy surface in the vicinity of **7b** is incorrect because it corresponds to a saddle point at CCSD(T)/DZP, which explains the unphysically low energy of $TS_4$ at the CCSD(T)//B3LYP level.

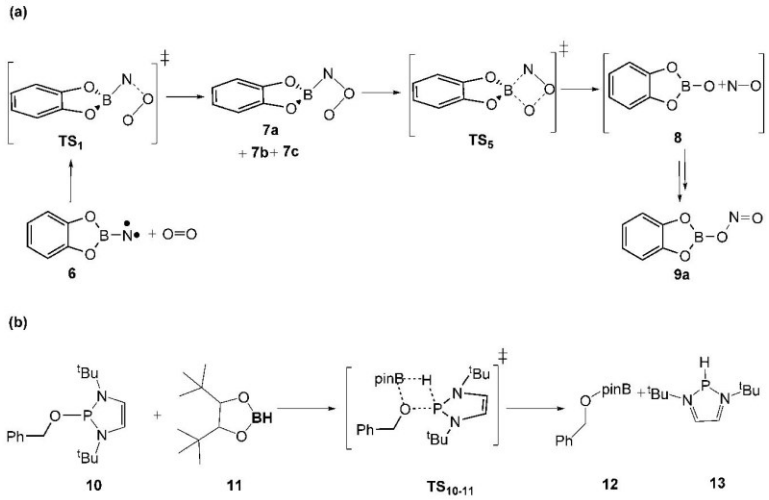


**Scheme 2.** a) Stepwise metathesis involving B–N and O–O bonds in current work driven by two transition states resulting in $O_2$ cleavage. b) The σ-bond metathesis between product **10** and pinacolborane **11**, resulting in breaking of the P–O bond, and hence, formation of **12** and **13**. Bpin = bis(pinacolato)diboron.

oxygen, even at very low temperatures, reminiscent of the behavior of the parent imidogen (NH), resulting in *anti*-nitroso-*O*-oxide **7a**. However, even the reaction of CatBN + $O_2$ → CatBO-NO (nitritoborane **9**) is feasible under very low temperature conditions. This unusual double insertion is stepwise and involves the metathesis reaction CatBN + OO → CatBO$^{\bullet}$ + $^{\bullet}$NO followed by radical combination in the matrix cage. Essential for this unprecedented reaction are the formation of bisected nitroso-*O*-oxide **7c** and the vanishingly low barrier for intramolecular attack of its terminal oxygen atom at the boron center. In contrast, *anti*-isomer **7a** behaves more conventionally. It is kinetically trapped under cryogenic conditions and is accessible to spectroscopy. It can form the more stable product **9** only after photoirradiation. We speculate that this induces iso-

 

Chemistry–A European Journal | Full Paper doi.org/10.1002/chem.202002445 | Chemistry Europe European Chemical Societies Publishing

merization and puts the system on the slippery slope towards the product.

The formation of **9** proceeds by the combination of CatBO and NO radicals in the stiff cryogenic matrix, which precludes separation of these species. It will be interesting to learn if this radical recombination would also be observable under more conventional solution-phase conditions, or if the heat of reaction of roughly $-59$ kcal mol$^{-1}$ would result in radical pair separation by diffusion and allow observation of CatBO reactivity, for example, with solvent molecules.

## Acknowledgements

This work was supported by the Deutsche Forschungsgemeinschaft and the Fonds der Chemischen Industrie. We are sincerely thankful to the state of Baden-Württemberg for bwHPC and to the German Research Foundation (DFG) through grant no. INST 40/467-1 FUGG for computation facilities. We would also like to thank Constanze Keck for her help in the synthesis of boryl azide **5**. Open access funding enabled and organized by Projekt DEAL.

## Conflict of interest

The authors declare no conflict of interest.

**Keywords:** boron · density functional calculations · nitrenes · radicals · reaction mechanisms

[1] W. T. Borden, R. Hoffmann, T. Stuyver, B. Chen, *J. Am. Chem. Soc.* **2017**, *139*, 9010–9018.
[2] W. Sander, G. Bucher, S. Wierlacher, *Chem. Rev.* **1993**, *93*, 1583–1621.
[3] W. T. Borden, N. P. Gritsan, C. M. Hadad, W. L. Karney, C. R. Kemnitz, M. S. Platz, *Acc. Chem. Res.* **2000**, *33*, 765–771.
[4] M. S. Platz, *Acc. Chem. Res.* **1995**, *28*, 487–492.
[5] N. P. Gritsan, E. A. Pritchina, *Russ. Chem. Rev.* **1992**, *61*, 500–516.
[6] W. Sander, *J. Org. Chem.* **1989**, *54*, 333–339.
[7] E. A. Pritchina, N. P. Gritsan, T. Bally, *Phys. Chem. Chem. Phys.* **2006**, *8*, 719–727.
[8] J. Mieres-Pérez, E. Mendez-Vega, K. Velappan, W. Sander, *J. Org. Chem.* **2015**, *80*, 11926–11931.
[9] J. Liu, C. M. Hadad, M. S. Platz, *Org. Lett.* **2005**, *7*, 549–552.
[10] S. L. Laursen, J. E. Grace, R. L. DeKock, S. A. Spronk, *J. Am. Chem. Soc.* **1998**, *120*, 12583–12594.
[11] M. R. Talipov, S. L. Khursan, R. L. Safiullin, *J. Phys. Chem. A* **2009**, *113*, 6468–6476.
[12] H. F. Bettinger, H. Bornemann, *J. Am. Chem. Soc.* **2006**, *128*, 11128–11134.
[13] S. S. Ullah, P. K. Sharma, A. K. Guha, *Comput. Theor. Chem.* **2017**, *1115*, 307–312.
[14] H. F. Bettinger, M. Filthaus, H. Bornemann, I. M. Oppel, *Angew. Chem. Int. Ed.* **2008**, *47*, 4744–4747; *Angew. Chem.* **2008**, *120*, 4822–4825.
[15] H. F. Bettinger, M. Filthaus, P. Neuhaus, *Chem. Commun.* **2009**, 2186–2188.
[16] M. Filthaus, L. Schwertmann, P. Neuhaus, R. W. Seidel, I. M. Oppel, H. F. Bettinger, *Organometallics* **2012**, *31*, 3894–3903.
[17] M. Müller, C. Maichle-Mossmer, H. F. Bettinger, *Chem. Commun.* **2013**, *49*, 11773–11775.
[18] H. F. Bettinger, M. Filthaus, *Org. Biomol. Chem.* **2010**, *8*, 5477–5482.
[19] I. Fernández, F. P. Cossío, M. A. Sierra, *Chem. Rev.* **2009**, *109*, 6687–6711.
[20] M. T. Reetz, *Angew. Chem. Int. Ed. Engl.* **1972**, *11*, 129–130; *Angew. Chem.* **1972**, *84*, 161–162.
[21] M. T. Reetz, *Angew. Chem. Int. Ed. Engl.* **1972**, *11*, 130–131; *Angew. Chem.* **1972**, *84*, 163–163.
[22] W. Fraenk, T. Habereder, T. Klapoetke, H. Nöth, K. Polborn, *J. Chem. Soc. Dalton Trans.* **1999**, 4283–4286.
[23] I. R. Dunkin, *Matrix-isolation techniques: a practical approach*, Oxford University Press, New York, **2002**.
[24] A. D. Becke, *J. Chem. Phys.* **1993**, *98*, 5648–5652.
[25] C. Lee, W. Yang, R. G. Parr, *Phys. Rev. B* **1988**, *37*, 785–789.
[26] Gaussian 16, Revision C.01 M. J. Frisch, G. W. Trucks, H. B. Schlegel, G. E. Scuseria, M. A. Robb, J. R. Cheeseman, G. Scalmani, V. Barone, G. A. Petersson, H. Nakatsuji, X. Li, M. Caricato, A. V. Marenich, J. Bloino, B. G. Janesko, R. Gomperts, B. Mennucci, H. P. Hratchian, J. V. Ortiz, A. F. Izmaylov, J. L. Sonnenberg, Williams, F. Ding, F. Lipparini, F. Egidi, J. Goings, B. Peng, A. Petrone, T. Henderson, D. Ranasinghe, V. G. Zakrzewski, J. Gao, N. Rega, G. Zheng, W. Liang, M. Hada, M. Ehara, K. Toyota, R. Fukuda, J. Hasegawa, M. Ishida, T. Nakajima, Y. Honda, O. Kitao, H. Nakai, T. Vreven, K. Throssell, J. A. Montgomery, Jr., J. E. Peralta, F. Ogliaro, M. J. Bearpark, J. J. Heyd, E. N. Brothers, K. N. Kudin, V. N. Staroverov, T. A. Keith, R. Kobayashi, J. Normand, K. Raghavachari, A. P. Rendell, J. C. Burant, S. S. Iyengar, J. Tomasi, M. Cossi, J. M. Millam, M. Klene, C. Adamo, R. Cammi, J. W. Ochterski, R. L. Martin, K. Morokuma, O. Farkas, J. B. Foresman, D. J. Fox, Wallingford, CT, **2016**.
[27] J. P. Foster, F. Weinhold, *J. Am. Chem. Soc.* **1980**, *102*, 7211–7218.
[28] J. E. Carpenter, F. Weinhold, *THEOCHEM* **1988**, *169*, 41–62.
[29] NBO Version 3.1., E. D. Glendening, A. E. Reed, J. E. Carpenter, F. Weinhold, **2003**, Gaussian Inc., Pittsburgh.
[30] K. Raghavachari, G. W. Trucks, J. A. Pople, M. Head-Gordon, *Chem. Phys. Lett.* **1989**, *157*, 479–483.
[31] R. J. Bartlett, J. D. Watts, S. A. Kucharski, J. Noga, *Chem. Phys. Lett.* **1990**, *165*, 513–522.
[32] T. H. Dunning, Jr., *J. Chem. Phys.* **1989**, *90*, 1007–1023.
[33] H.-J. Werner, P. J. Knowles, G. Knizia, F. R. Manby, M. Schütz, *WIREs Comput. Mol. Sci.* **2012**, *2*, 242–253.
[34] T. J. Lee, P. R. Taylor, *Int. J. Quantum Chem.* **1989**, *36*, 199–207.
[35] P. Piecuch, S. A. Kucharski, K. Kowalski, M. Musiał, *Comput. Phys. Commun.* **2002**, *149*, 71–96.
[36] K. Kowalski, P. Piecuch, *J. Chem. Phys.* **2000**, *113*, 18–35.
[37] K. Kowalski, P. Piecuch, *J. Chem. Phys.* **2000**, *113*, 5644–5652.
[38] T. H. Dunning, *J. Chem. Phys.* **1971**, *55*, 716–723.
[39] M. W. Schmidt, K. K. Baldridge, J. A. Boatz, S. T. Elbert, M. S. Gordon, J. H. Jensen, S. Koseki, N. Matsunaga, K. A. Nguyen, S. Su, T. L. Windus, M. Dupuis, J. A. Montgomery, Jr., *J. Comput. Chem.* **1993**, *14*, 1347–1363.
[40] M. S. Gordon, M. W. Schmidt in *Theory and Applications of Computational Chemistry* (Eds.: C. E. Dykstra, G. Frenking, K. S. Kim, G. E. Scuseria), Elsevier, Amsterdam, **2005**, pp. 1167–1189.
[41] R. L. DeKock, M. J. McGuire, P. Piecuch, W. D. Allen, H. F. Schaefer, K. Kowalski, S. A. Kucharski, M. Musiał, A. R. Bonner, S. A. Spronk, D. B. Lawson, S. L. Laursen, *J. Phys. Chem. A* **2004**, *108*, 2893–2903.
[42] G. E. Scuseria, *J. Chem. Phys.* **1991**, *94*, 442–447.
[43] J. F. Stanton, J. Gauss, L. Cheng, M. E. Harding, D. A. Matthews, P. G. Szalay, CFOUR, Coupled-Cluster techniques for Computational Chemistry, Version 2.00beta, for the updates, see http://www.cfour.de.
[44] F. Neese, *WIREs Comput. Mol. Sci.* **2012**, *2*, 73–78.
[45] F. Weigend, R. Ahlrichs, *Phys. Chem. Chem. Phys.* **2005**, *7*, 3297–3305.
[46] C. Angeli, R. Cimiraglia, J.-P. Malrieu, *J. Chem. Phys.* **2002**, *117*, 9138–9153.
[47] C. Angeli, R. Cimiraglia, S. Evangelisti, T. Leininger, J.-P. Malrieu, *J. Chem. Phys.* **2001**, *114*, 10252–10264.
[48] C. Camacho, R. Cimiraglia, H. A. Witek, *Phys. Chem. Chem. Phys.* **2010**, *12*, 5058–5060.
[49] R. W. A. Havenith, P. R. Taylor, C. Angeli, R. Cimiraglia, K. Ruud, *J. Chem. Phys.* **2004**, *120*, 4619–4625.
[50] T. Fueno, K. Yokoyama, S.-Y. Takane, *Theor. Chim. Acta* **1992**, *82*, 299–308.
[51] Z. Wu, C. Chen, J. Liu, Y. Lu, J. Xu, X. Liu, G. Cui, T. Trabelsi, J. S. Francisco, A. Mardyukov, A. K. Eckhardt, P. R. Schreiner, X. Zeng, *J. Am. Chem. Soc.* **2019**, *141*, 3361-3365.
[52] C. C. Chong, H. Hirao, R. Kinjo, *Angew. Chem. Int. Ed.* **2015**, *54*, 190–194; *Angew. Chem.* **2015**, *127*, 192–196.
[53] Y. Wang, W. Chen, Z. Lu, Z. H. Li, H. Wang, *Angew. Chem. Int. Ed.* **2013**, *52*, 7496–7499; *Angew. Chem.* **2013**, *125*, 7644–7647.

 

Chemistry–A European Journal | Full Paper doi.org/10.1002/chem.202002445 | Chemistry Europe European Chemical Societies Publishing

[54] H. Braunschweig, A. Damme, C. Hoerl, T. Kupfer, J. Wahler, *Organometallics* **2013**, *32*, 6800-6803.
[55] C.-Y. Lee, S.-J. Ahn, C.-H. Cheon, *J. Org. Chem.* **2013**, *78*, 12154-12160.
[56] Q. Yin, S. Kemper, H. F. T. Klare, M. Oestreich, *Chem. - Eur. J.* **2016**, *22*, 13840-13844.
[57] Y. K. Loh, K. Porteous, M. A. Fuentes, D. C. H. Do, J. Hicks, S. Aldridge, *J. Am. Chem. Soc.* **2019**, *141*, 8073–8077.
[58] S. A. Iqbal, J. Pahl, K. Yuan, M. J. Ingleson, *Chem. Soc. Rev.* **2020**, *49*, 4564-4591.
[59] N. Sawwan, A. Greer, *Chem. Rev.* **2007**, *107*, 3247–3285.

Manuscript received: May 18, 2020
Revised manuscript received: June 11, 2020
Version of record online: September 9, 2020

Chemistry—A European Journal

Supporting Information

# Unusual Nitrene Oxidation Product Formation by Metathesis Involving the Dioxygen O—O and Borylnitrene B—N Bonds

Virinder Bhagat, Julia Schumann, and Holger F. Bettinger*[a]

Cartesian Coordinates of all the optimized species calculated at B3LYP/6-311+G(d,p) level of theory.

**7a**

Symmetry: Cs

Method: (U)B3LYP/6-311+G(d,p)

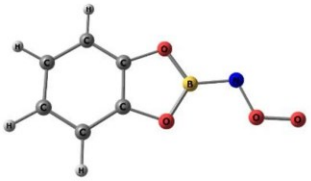

Cartesian Coordinates in Angstroms

| Atomic Number | X | Y | Z |
|---|---|---|---|
| 6 | -0.869853000 | 0.627396000 | 0.000001000 |
| 6 | -1.067794000 | -0.753682000 | 0.000003000 |
| 6 | -2.331295000 | -1.314906000 | 0.000004000 |
| 6 | -3.406116000 | -0.420613000 | 0.000004000 |
| 6 | -3.206911000 | 0.965376000 | 0.000002000 |
| 6 | -1.923589000 | 1.521444000 | 0.000000000 |
| 1 | -2.472713000 | -2.387891000 | 0.000005000 |
| 1 | -4.416726000 | -0.810696000 | 0.000005000 |
| 1 | -4.066750000 | 1.624326000 | 0.000001000 |
| 1 | -1.757967000 | 2.590960000 | -0.000002000 |
| 8 | 0.485400000 | 0.887063000 | -0.000002000 |
| 8 | 0.156921000 | -1.383936000 | 0.000002000 |
| 5 | 1.084234000 | -0.359280000 | 0.000008000 |
| 7 | 2.506857000 | -0.677589000 | 0.000000000 |
| 8 | 3.196095000 | 0.424535000 | -0.000008000 |
| 8 | 4.483877000 | 0.293930000 | -0.000009000 |

**7b**

Symmetry: Cs

Method: (U)B3LYP/6-311+G(d,p)

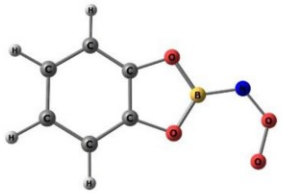

Cartesian Coordinates in Angstroms

| Atomic Number | X | Y | Z |
|---|---|---|---|
| 6 | 0.742375000 | 0.592491000 | 0.000001000 |
| 6 | 0.996989000 | -0.779715000 | 0.000001000 |
| 6 | 2.284331000 | -1.288267000 | 0.000003000 |
| 6 | 3.319051000 | -0.350005000 | 0.000004000 |
| 6 | 3.062394000 | 1.028495000 | 0.000004000 |
| 6 | 1.758931000 | 1.530935000 | 0.000002000 |
| 1 | 2.470877000 | -2.354324000 | 0.000003000 |
| 1 | 4.345433000 | -0.696634000 | 0.000006000 |
| 1 | 3.895045000 | 1.721497000 | 0.000005000 |
| 1 | 1.547791000 | 2.592355000 | 0.000002000 |

| | | | |
|---|---|---|---|
| 8 | -0.618324000 | 0.797148000 | -0.000001000 |
| 8 | -0.196890000 | -1.454256000 | 0.000000000 |
| 5 | -1.174743000 | -0.468004000 | -0.000002000 |
| 7 | -2.556824000 | -0.943597000 | -0.000004000 |
| 8 | -3.536149000 | -0.113904000 | -0.000005000 |
| 8 | -3.332648000 | 1.180850000 | -0.000004000 |

**7c**

Symmetry: Cs

Method: (U)B3LYP/6-311+G(d,p)

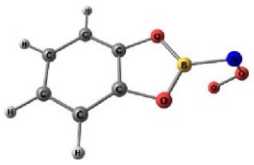

Cartesian Coordinates in Angstroms

| Atomic Number | X | Y | Z |
|---|---|---|---|
| 6 | -0.141751000 | 0.829099000 | 0.695722000 |
| 6 | -0.141751000 | 0.829099000 | -0.695722000 |
| 6 | 0.051627000 | 1.980681000 | -1.431477000 |
| 6 | 0.250264000 | 3.157409000 | -0.698886000 |
| 6 | 0.250264000 | 3.157409000 | 0.698886000 |
| 6 | 0.051627000 | 1.980681000 | 1.431477000 |
| 1 | 0.050395000 | 1.968152000 | -2.513655000 |
| 1 | 0.408226000 | 4.088121000 | -1.230278000 |
| 1 | 0.408226000 | 4.088121000 | 1.230278000 |
| 1 | 0.050395000 | 1.968152000 | 2.513655000 |
| 8 | -0.363973000 | -0.464685000 | 1.147823000 |
| 8 | -0.363973000 | -0.464685000 | -1.147823000 |
| 5 | -0.465126000 | -1.211426000 | 0.000000000 |
| 7 | -0.872570000 | -2.650341000 | 0.000000000 |
| 8 | 0.098189000 | -3.466276000 | 0.000000000 |
| 8 | 1.329095000 | -2.993016000 | 0.000000000 |

**8**

Symmetry: C1

Method: (U)B3LYP/6-311+G(d,p)

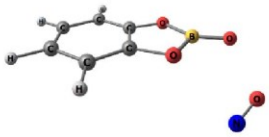

Cartesian Coordinates in Angstroms

| Atomic Number | X | Y | Z |
|---|---|---|---|
| 6 | -0.612215000 | 0.463965000 | -0.305505000 |
| 6 | -1.021310000 | -0.830075000 | 0.100741000 |
| 6 | -2.345883000 | -1.101825000 | 0.428260000 |
| 6 | -3.241394000 | -0.039408000 | 0.356129000 |
| 6 | -2.831253000 | 1.251823000 | -0.038385000 |
| 6 | -1.509249000 | 1.525617000 | -0.373144000 |
| 1 | -2.651299000 | -2.094574000 | 0.732736000 |
| 1 | -4.281588000 | -0.204449000 | 0.610816000 |
| 1 | -3.566958000 | 2.045848000 | -0.084683000 |
| 1 | -1.185487000 | 2.510869000 | -0.683498000 |

| | | | |
|---|---|---|---|
| 8 | 0.693847000 | 0.448781000 | -0.600030000 |
| 8 | 0.028667000 | -1.658316000 | 0.110033000 |
| 5 | 1.181514000 | -0.912738000 | -0.352304000 |
| 7 | 3.045392000 | 1.494011000 | 0.602958000 |
| 8 | 3.614598000 | 0.539528000 | 0.479384000 |
| 8 | 2.391369000 | -1.301576000 | -0.494779000 |

**9a**

Symmetry: $C_S$

Method: B3LYP/6-311+G(d,p)

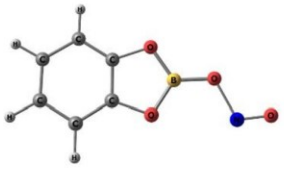

Cartesian Coordinates in Angstroms

| Atomic Number | X | Y | Z |
|---|---|---|---|
| 6 | -0.850701000 | 0.621310000 | 0.000000000 |
| 6 | -1.063219000 | -0.755584000 | 0.000001000 |
| 6 | -2.331337000 | -1.300476000 | 0.000003000 |
| 6 | -3.400969000 | -0.394988000 | 0.000002000 |
| 6 | -3.187398000 | 0.985245000 | 0.000000000 |
| 6 | -1.893769000 | 1.524692000 | -0.000001000 |
| 1 | -2.484840000 | -2.372008000 | 0.000004000 |
| 1 | -4.414909000 | -0.776752000 | 0.000003000 |
| 1 | -4.038321000 | 1.655852000 | 0.000000000 |
| 1 | -1.716181000 | 2.592521000 | -0.000003000 |
| 8 | 0.510961000 | 0.870363000 | -0.000001000 |
| 8 | 0.157593000 | -1.404252000 | 0.000002000 |
| 5 | 1.098433000 | -0.386213000 | 0.000000000 |
| 7 | 3.320284000 | 0.582118000 | -0.000002000 |
| 8 | 4.426322000 | 0.272972000 | -0.000002000 |
| 8 | 2.440681000 | -0.654654000 | 0.000000000 |

**9b**

Symmetry: C1

Method: B3LYP/6-311+G(d,p)

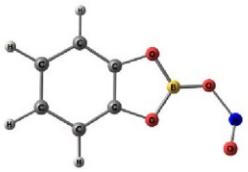

Cartesian Coordinates in Angstroms

| Atomic Number | X | Y | Z |
|---|---|---|---|
| 6 | -0.714876000 | 0.571802000 | -0.078810000 |
| 6 | -1.007780000 | -0.785960000 | 0.028187000 |
| 6 | -2.305672000 | -1.248693000 | 0.117845000 |
| 6 | -3.317739000 | -0.280149000 | 0.096702000 |
| 6 | -3.022685000 | 1.081279000 | -0.010115000 |
| 6 | -1.700902000 | 1.537286000 | -0.100657000 |
| 1 | -2.522918000 | -2.305934000 | 0.200112000 |
| 1 | -4.351708000 | -0.596557000 | 0.164910000 |
| 1 | -3.831469000 | 1.802004000 | -0.023479000 |

| | | | |
|---|---|---|---|
| 1 | -1.459855000 | 2.589306000 | -0.183985000 |
| 8 | 0.657161000 | 0.734440000 | -0.150920000 |
| 8 | 0.169250000 | -1.507111000 | 0.026477000 |
| 5 | 1.172443000 | -0.554077000 | -0.091552000 |
| 7 | 3.635955000 | 0.090525000 | -0.070628000 |
| 8 | 3.343831000 | 1.113659000 | 0.361213000 |
| 8 | 2.488503000 | -0.916674000 | -0.177310000 |

**$TS_2$**
Symmetry: C1
Method: (U)B3LYP/6-311+G(d,p)

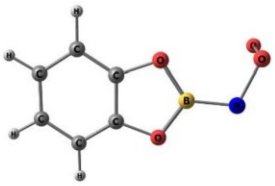

Cartesian Coordinates in Angstroms

| Atomic Number | X | Y | Z |
|---|---|---|---|
| 6 | 0.750280000 | 0.587060000 | -0.108963000 |
| 6 | 1.025842000 | -0.781198000 | 0.026503000 |
| 6 | 2.319183000 | -1.260257000 | 0.164079000 |
| 6 | 3.334263000 | -0.304500000 | 0.160599000 |
| 6 | 3.057517000 | 1.067101000 | 0.025045000 |
| 6 | 1.753667000 | 1.542298000 | -0.113133000 |
| 1 | 2.520209000 | -2.318418000 | 0.268588000 |
| 1 | 4.363255000 | -0.626361000 | 0.265636000 |
| 1 | 3.879129000 | 1.773085000 | 0.028693000 |
| 1 | 1.528928000 | 2.595713000 | -0.217047000 |
| 8 | -0.598920000 | 0.761646000 | -0.226037000 |
| 8 | -0.146164000 | -1.478173000 | -0.002736000 |
| 5 | -1.144439000 | -0.516923000 | -0.155866000 |
| 7 | -2.525491000 | -0.904546000 | -0.231730000 |
| 8 | -3.340790000 | 0.270341000 | -0.395026000 |
| 8 | -3.706050000 | 0.744859000 | 0.765149000 |

**$TS_3$**
Symmetry: C1
Method: (U)B3LYP/6-311+G(d,p)

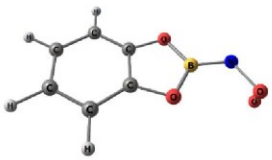

Cartesian Coordinates in Angstroms

| Atomic Number | X | Y | Z |
|---|---|---|---|
| 6 | -1.949274000 | 1.512839000 | -0.044462000 |
| 6 | -0.886733000 | 0.633576000 | -0.070098000 |
| 6 | -1.063411000 | -0.745842000 | 0.008476000 |
| 6 | -2.314267000 | -1.318164000 | 0.114365000 |
| 6 | -3.404669000 | -0.437521000 | 0.140533000 |
| 6 | -3.226563000 | 0.944911000 | 0.062915000 |
| 1 | 0.467921000 | 0.918664000 | -0.171885000 |

| | | | |
|---|---|---|---|
| 1 | 1.075631000 | -0.330133000 | -0.143516000 |
| 1 | 2.466693000 | -0.517756000 | -0.224329000 |
| 1 | 3.538321000 | 0.090698000 | -0.376654000 |
| 8 | 4.217231000 | 0.461915000 | 0.664358000 |
| 8 | 0.171712000 | -1.372479000 | -0.036098000 |
| 5 | -2.440107000 | -2.391520000 | 0.174939000 |
| 7 | -4.406358000 | -0.841750000 | 0.223544000 |
| 8 | -4.092067000 | 1.596102000 | 0.086236000 |
| 8 | -1.798440000 | 2.582945000 | -0.104976000 |

**$TS_4$**
Symmetry: C1
Method: (U)B3LYP/6-311+G(d,p)

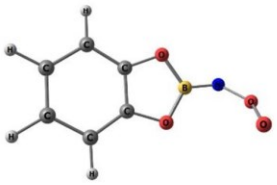

Cartesian Coordinates in Angstroms

| Atomic Number | X | Y | Z |
|---|---|---|---|
| 6 | 0.768951000 | 0.601464000 | -0.182494000 |
| 6 | 0.950458000 | -0.762966000 | 0.033246000 |
| 6 | 2.197731000 | -1.313416000 | 0.256415000 |
| 6 | 3.277367000 | -0.423665000 | 0.245358000 |
| 6 | 3.095670000 | 0.946084000 | 0.023566000 |
| 6 | 1.826183000 | 1.490771000 | -0.197778000 |
| 1 | 2.326105000 | -2.374766000 | 0.424828000 |
| 1 | 4.277190000 | -0.806054000 | 0.411703000 |
| 1 | 3.957511000 | 1.602440000 | 0.025251000 |
| 1 | 1.672926000 | 2.548814000 | -0.365884000 |
| 8 | -0.578483000 | 0.854999000 | -0.354135000 |
| 8 | -0.278134000 | -1.393318000 | -0.023830000 |
| 5 | -1.183693000 | -0.377838000 | -0.248624000 |
| 7 | -2.586555000 | -0.714239000 | -0.562419000 |
| 8 | -3.517829000 | -0.014107000 | -0.041586000 |
| 8 | -3.238998000 | 0.888525000 | 0.871334000 |

**$TS_5$**
Symmetry: Cs
Method: (U)B3LYP/6-311+G(d,p)

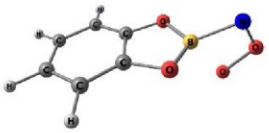

Cartesian Coordinates in Angstroms

| Atomic Number | X | Y | Z |
|---|---|---|---|
| 6 | -0.096505000 | -0.768378000 | -0.696423000 |
| 6 | -0.096505000 | -0.768378000 | 0.696423000 |
| 6 | 0.014569000 | -1.931742000 | 1.429134000 |
| 6 | 0.128093000 | -3.122686000 | 0.697887000 |
| 6 | 0.128093000 | -3.122686000 | -0.697887000 |

| | | | |
|---|---|---|---|
| 6 | 0.014569000 | -1.931742000 | -1.429134000 |
| 1 | 0.014316000 | -1.919043000 | 2.511443000 |
| 1 | 0.218141000 | -4.061498000 | 1.231059000 |
| 1 | 0.218141000 | -4.061498000 | -1.231059000 |
| 1 | 0.014316000 | -1.919043000 | -2.511443000 |
| 8 | -0.229079000 | 0.534440000 | -1.156620000 |
| 8 | -0.229079000 | 0.534440000 | 1.156620000 |
| 5 | -0.228356000 | 1.298120000 | 0.000000000 |
| 7 | -0.931415000 | 2.712022000 | 0.000000000 |
| 8 | 0.093371000 | 3.396890000 | 0.000000000 |
| 8 | 1.195149000 | 2.579230000 | 0.000000000 |

**$TS_6$**
Symmetry: Cs
Method: (U)B3LYP/6-311+G(d,p)

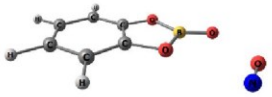

Cartesian Coordinates in Angstroms

| Atomic Number | X | Y | Z |
|---|---|---|---|
| 6 | 0.629961000 | 0.499687000 | 0.000000000 |
| 6 | 1.090156000 | -0.818251000 | 0.000002000 |
| 6 | 2.439655000 | -1.114515000 | 0.000003000 |
| 6 | 3.326933000 | -0.029159000 | 0.000002000 |
| 6 | 2.864739000 | 1.288126000 | 0.000000000 |
| 6 | 1.492705000 | 1.577592000 | -0.000001000 |
| 1 | 2.787795000 | -2.139671000 | 0.000005000 |
| 1 | 4.393693000 | -0.219662000 | 0.000003000 |
| 1 | 3.577257000 | 2.104466000 | -0.000001000 |
| 1 | 1.123487000 | 2.595603000 | -0.000003000 |
| 8 | -0.747714000 | 0.498190000 | -0.000001000 |
| 8 | 0.024325000 | -1.684069000 | 0.000002000 |
| 5 | -1.123780000 | -0.870717000 | 0.000000000 |
| 7 | -3.316097000 | 1.457614000 | -0.000004000 |
| 8 | -3.660512000 | 0.403724000 | -0.000003000 |
| 8 | -2.380544000 | -1.294262000 | 0.000000000 |

**$TS_7$**
Symmetry: C1
Method: (U)B3LYP/6-311+G(d,p)

Cartesian Coordinates in Angstroms

| Atomic Number | X | Y | Z |
|---|---|---|---|
| 6 | -0.564319000 | -0.452014000 | -0.347231000 |
| 6 | -0.922018000 | 0.848312000 | 0.068052000 |
| 6 | -2.221322000 | 1.145042000 | 0.454649000 |

| | | | |
|---|---|---|---|
| 6 | -3.150673000 | 0.103989000 | 0.416330000 |
| 6 | -2.794737000 | -1.189713000 | -0.000868000 |
| 6 | -1.491415000 | -1.487339000 | -0.394671000 |
| 1 | -2.492238000 | 2.144627000 | 0.769965000 |
| 1 | -4.174626000 | 0.299218000 | 0.712879000 |
| 1 | -3.548909000 | -1.967239000 | -0.020999000 |
| 1 | -1.204690000 | -2.477492000 | -0.726839000 |
| 8 | 0.737641000 | -0.470722000 | -0.696969000 |
| 8 | 0.138364000 | 1.674361000 | -0.001266000 |
| 5 | 1.276009000 | 0.904392000 | -0.432299000 |
| 8 | 2.517819000 | 1.168375000 | -0.486962000 |
| 8 | 3.177485000 | -0.704021000 | 1.003018000 |
| 7 | 2.762407000 | -1.382097000 | 0.243764000 |

**$TS_8$**
Symmetry: C1
Method: B3LYP/6-311+G(d,p)

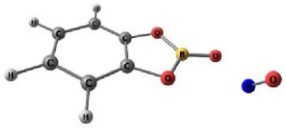

Cartesian Coordinates in Angstroms

| Atomic Number | X | Y | Z |
|---|---|---|---|
| 6 | 0.724821000 | 0.573616000 | -0.094931000 |
| 6 | 1.024899000 | -0.781597000 | 0.030664000 |
| 6 | 2.323877000 | -1.233738000 | 0.144476000 |
| 6 | 3.331446000 | -0.259174000 | 0.127784000 |
| 6 | 3.029705000 | 1.098091000 | 0.001987000 |
| 6 | 1.705407000 | 1.543854000 | -0.113108000 |
| 1 | 2.546421000 | -2.288684000 | 0.241355000 |
| 1 | 4.366026000 | -0.569001000 | 0.214646000 |
| 1 | 3.833496000 | 1.824479000 | -0.007312000 |
| 1 | 1.459555000 | 2.593545000 | -0.211453000 |
| 8 | -0.647524000 | 0.726602000 | -0.190272000 |
| 8 | -0.146523000 | -1.514551000 | 0.018773000 |
| 5 | -1.155878000 | -0.570266000 | -0.118483000 |
| 7 | -3.475297000 | 0.293553000 | -0.344196000 |
| 8 | -3.602558000 | 0.879319000 | 0.626859000 |
| 8 | -2.470890000 | -0.892645000 | -0.182446000 |

Table S1. Wiberg bond order of N-O and B-N bonds in different isomers of nitroso-O-oxide and transition states responsible for the interconversion of these isomers calculated from the NBO calculations at (U)B3LYP/6-311+G(d,p)

| | **Bond Order (N-O)** | **Bond Order (B-N)** |
|---|---|---|
| **7a** | 1.4 | 1.0 |
| **7b** | 1.4 | 1.0 |
| **7c** | 1.5 | 0.9 |
| **$TS_2$** | 1.2 | 1.1 |
| **$TS_3$** | 1.2 | 1.0 |
| **$TS_4$** | 1.5 | 0.9 |

Table S2. Zero point vibrational energy and the total energy of all the species calculated at different levels of theory (in the units of Hartree).

| | **ZPE** | **(U)B3LYP/6-311+G(d,p)** | **CCSD(T)/cc-pVTZ//B3LYP/6-311+G(d,p)** |
|---|---|---|---|
| **7a** | 0.10292 | -611.61426 | -610.48625 |
| **7b** | 0.10302 | -611.61034 | -610.48350 |
| **7c** | 0.10284 | -611.61028 | -610.48839 |
| **8** | 0.10009 | -611.70488 | -610.55638 |
| **9a** | 0.10343 | -611.75528 | -610.63130 |
| **9b** | 0.10319 | -611.74800 | -610.62450 |
| **$TS_2$** | 0.10062 | -611.58314 | -610.43054 |
| **$TS_3$** | 0.10254 | -611.57704 | -610.45165 |
| **$TS_4$** | 0.10281 | -611.60972 | -610.48525 |
| **$TS_5$** | 0.10254 | -611.60403 | -610.48679 |
| **$TS_6$** | 0.10138 | -611.70319 | -610.57069 |
| **$TS_7$** | 0.10114 | -611.69317 | -610.55494 |
| **$TS_8$** | 0.10301 | -611.74664 | -610.62409 |

Table S3. Infrared Spectroscopic Data of *anti*-nitroso-O-oxide **7a** in Argon matrix.

| | Argon matrix, 10 K | | | CCSD(T)/DZP | | | | |
|---|---|---|---|---|---|---|---|---|
| Vibrational Mode No.[a] | $\tilde{\nu}$, $cm^{-1}$ | I[b] | $\tilde{\nu}_i/\tilde{\nu}^c$ | $\tilde{\nu}$, $cm^{-1}$ | I[b] | $\tilde{\nu}_i/\tilde{\nu}^c$ | sym[d] | assignments |
| 42 | - | - | - | 3239 | 1 | 1.000 | A' | C-H str |
| 41 | - | - | - | 3235 | 1 | 1.000 | A' | C-H str |
| 40 | - | - | - | 3220 | 2 | 1.000 | A' | C-H str |
| 38 | - | - | - | 1662 | 1 | 1.000 | A' | ring str |
| 36 | 1471 | 10 | 1.000 | 1506 | 16 | 0.999 | A' | ring str |
| 34 | 1375 | 92 | 0.980 | 1415 | $100_e$ | 0.974 | A' | B-N str, ring str |
| 33 | 1311 | 38 | 0.992 | 1358 | 63 | 0.993 | A' | B-N str, ring str, B-O str |
| 32 | 1302 | 100 | 0.960 | 1350 | 42 | 0.970 | A' | ring str, B-O str |
| 30 | 1237 | 41 | 1.000 | 1277 | 44 | 1.000 | A' | ring str, C-O str |
| 29 | 1148 | 4 | 1.000 | 1184 | 8 | 0.999 | A' | ring str, N-O str |
| 25 | 1119 | 96 | 1.000 | 1071 | 20 | 1.000 | A' | O-O str, B-N-O bending |
| 24 | 1005 | 3 | 1.000 | 1012 | 2 | 1.000 | A' | ring breathing |
| 23 | 924 | 28 | 1.000 | 933 | 10 | 1.000 | A' | N-O-O bending, ring str, B-O str |
| 21 | 865 | 5 | 1.000 | 865 | 1 | 1.000 | A' | skel. Ring, in pl. C-H |
| 20 | - | - | - | 862 | 1 | 1.000 | A'' | asym. C-H wag, skel. wag |
| 19 | 810 | 15 | 1.000 | 817 | 11 | 1.000 | A' | Ring breathing |
| 16 | 746 | 28 | 1.000 | 724 | 24 | 1.000 | A'' | Sym. C-H wag, skel. wag |
| 14 | 665 | 7 | 0.968 | 672 | 5 | 0.989 | A'' | OOBN wag |
| 9 | - | - | - | 413 | 2 | 1.000 | A'' | skel. wag |
| 4 | - | - | - | 204 | 2 | 0.998 | A'' | skel. Wag, BNOO wag |

[a] The numbering of the vibrational modes is according to calculated spectrum. [b] Intensity relative to the strongest band. [c] Ratio of frequencies of the natural 11B vs 10B isotopomers. [d] Symmetry of the vibrations are taken from calculated IR spectrum. [e] Computed absolute intensity: 314.2 km $mol^{-1}$

Table S4. Infrared Spectroscopic Data of *anti*-nitritoborane **9a** in Argon matrix.

| | Argon matrix, 10 K | | | CCSD(T)/DZP | | | | |
|---|---|---|---|---|---|---|---|---|
| Vibrational Mode No.[a] | $\tilde{\upsilon}$, $cm^{-1}$ | I[b] | $\tilde{\upsilon}_i/\tilde{\upsilon}$[c] | $\tilde{\upsilon}$, $cm^{-1}$ | I[b] | $\tilde{\upsilon}_i/\tilde{\upsilon}$[c] | sym[d] | assignments |
| 40 | - | - | - | 3217 | 1 | 1 | A' | C-H str |
| 38 | 1752 | 64 | 1 | 1790 | 16 | 0.999 | A' | N-O str |
| 36 | 1628 | 3 | 1 | 1663 | 1 | 1 | A' | ring str |
| 35 | 1476 | 3 | 0.997 | 1514 | 6 | 0.995 | A' | ring str |
| 33 | 1411 | 100 | 0.969 | 1459 | 100[e] | 0.972 | A' | B-O str |
| 32 | 1336 | 37 | 1 | 1379 | 13 | 0.999 | A' | ring str, B-O str |
| 31 | 1287 | 15 | 0.979 | 1323 | 13 | 0.972 | A' | O-B asym str, skel. ring |
| 29 | 1235 | 23 | 1 | 1276 | 16 | 1 | A' | C-O str, ring str |
| 28 | 1140 | 5 | 1 | 1163 | 1 | 0.996 | A' | C-O str, skel. ring |
| 25 | 1007 | 0 | 1 | 1012 | 1 | 1 | A' | skel. ring, in pl. C-H |
| 22 | 869 | 3 | 1 | 869 | 2 | 1 | A' | skel. ring, C-O str, O-N str |
| 20 | 808 | 2 | 1 | 816 | 3 | 1 | A' | ring breathing |
| 18 | 768 | 37 | 1 | 784 | 15 | 0.996 | A' | O-N-O bending |
| 17 | 742 | 12 | 1 | 722 | 8 | 0.997 | A'' | skel. Wag. sym C-H wag |
| 16 | 676 | 7 | - | 681 | 1 | 0.968 | A'' | OOBO wag |
| 14 | 632 | 50 | 1 | 644 | 23 | 0.999 | A' | skel. ring, O-N str |
| 12 | 555 | 15 | 1 | 553 | 6 | 0.998 | A' | skel. ring, ONO bending |
| 10 | 503 | 22 | 1 | 505 | 7 | 0.996 | A' | skel. ring |
| 8 | - | - | - | 381 | 3 | 0.999 | A' | skel. ring |
| 6 | - | - | - | 281 | 3 | 0.999 | A' | B-O-N bending |

[a] The numbering of the vibrational modes is according to calculated spectrum. [b] Intensity relative to the strongest band. [c] Ratio of frequencies of the natural 11B vs 10B isotopomers. [d] Symmetry of the vibrations are taken from calculated IR spectrum. [e] Computed absolute intensity: 1017.8 km $mol^{-1}$

Table S5. Infrared Spectroscopic Data of *anti*-nitroso-O-oxide **7a** in Nitrogen matrix.

| | Nitrogen matrix, 10 K | | | | CCSD(T)/DZP | | | | | |
|---|---|---|---|---|---|---|---|---|---|---|
| | with $^{16}O_2$ | | with $^{18}O_2$ | | with $^{16}O_2$ | | with $^{18}O_2$ | | | |
| Mode No.[a] | $\tilde{\upsilon}$, cm$^{-1}$ | I[b] | $\tilde{\upsilon}$, cm$^{-1}$ | I[b] | $\tilde{\upsilon}$, cm$^{-1}$ | I[b] | $\tilde{\upsilon}$, cm$^{-1}$ | I[b] | sym[c] | assignments |
| 42 | - | - | - | - | 3239 | 1 | 3239 | 1 | A’ | C-H str |
| 41 | - | - | - | - | 3235 | 1 | 3235 | 1 | A’ | C-H str |
| 40 | - | - | - | - | 3220 | 2 | 3220 | 2 | A’ | C-H str |
| 38 | - | - | - | - | 1662 | 1 | 1662 | 1 | A’ | ring str |
| 36 | 1472 | 8 | 1472 | 7 | 1506 | 16 | 1506 | 16 | A’ | ring str |
| ($^{10}$B)34 | 1408 | 20 | 1408 | 82 | 1453 | 38 | 1453 | 38 | A’ | B-N str, ring str |
| 34 | 1377 | 65 | 1377 | 100 | 1414 | 100[d] | 1414 | 100 | A’ | B-N str, ring str |
| ($^{10}$B )32 | 1318 | 21 | 1318 | 30 | 1367 | 8 | 1367 | 8 | A’ | ring str, B-O str |
| 33 | 1314 | 2 | 1313 | 67 | 1358 | 63 | 1358 | 64 | A’ | B-N str, ring str, B-O str |
| ($^{10}$B )33 | - | - | - | - | 1391 | 8 | 1391 | 8 | A’ | B-N str, ring str, B-O str |
| 32 | 1304 | 82 | 1300 | 58 | 1349 | 42 | 1348 | 44 | A’ | ring str, B-O str |
| 30 | 1238 | 34 | 1238 | 67 | 1276 | 44 | 1276 | 44 | A’ | ring str, C-O str |
| 29 | 1150 | 4 | 1095 | 11 | 1184 | 8 | 1149 | 8 | A’ | ring str, N-O str |
| 25 | 1120 | 100 | 1064 | 48 | 1071 | 20 | 1017 | 13 | A’ | O-O str, B-N-O bending |
| 24 | 1006 | 2 | 1006 | 2 | 1012 | 2 | 1012 | 4 | A’ | ring breathing |
| 23 | 926 | 19 | 918 | 28 | 932 | 10 | 924 | 11 | A’ | N-O-O bending, ring str, B-O str |
| 21 | 865 | 2 | 865 | 3 | 865 | 1 | 865 | 1 | A’ | skel. Ring, in pl. C-H |
| 20 | - | - | - | - | 862 | 1 | 862 | 1 | A’’ | asym. C-H wag, skel. wag |

| | | | | | | | | | | |
|---|---|---|---|---|---|---|---|---|---|---|
| 19 | 810 | 17 | 810 | 21 | 817 | 11 | 817 | 11 | A’ | Ring breathing |
| 16 | 752 | 33 | 752 | 15 | 724 | 24 | 724 | 24 | A’’ | Sym. C-H wag, skel. wag |
| 14 | 660 | 6 | 660 | 12 | 671 | 5 | 671 | 5 | A’’ | OOBN wag |
| 9 | - | - | - | - | 413 | 2 | 413 | 2 | A’’ | skel. wag |
| 4 | - | - | - | - | 204 | 2 | 197 | 1 | A’’ | skel. Wag, BNOO wag |

[a] The numbering of the vibrational modes is according to calculated spectrum. [b] Intensity relative to the strongest band. [c] Symmetry of the vibrations are taken from calculated IR spectrum. [d] Computed absolute intensity: 314.2 km $mol^{-1}$

Table S6. Infrared Spectroscopic Data of *anti*-nitritoborane **9a** in Nitrogen matrix.

| | Nitrogen matrix, 10 K | | | | CCSD(T)/DZP | | | | | |
|---|---|---|---|---|---|---|---|---|---|---|
| | with $^{16}O_2$ | | with $^{18}O_2$ | | with $^{16}O_2$ | | with $^{18}O_2$ | | | |
| Mode No.[a] | $\tilde{\upsilon}$, $cm^{-1}$ | I[b] | $\tilde{\upsilon}$, $cm^{-1}$ | I[b] | $\tilde{\upsilon}$, $cm^{-1}$ | I[b] | $\tilde{\upsilon}$, $cm^{-1}$ | I[b] | sym[c] | assignments |
| 40 | - | - | - | - | 3217 | 1 | 3217 | 1 | A' | C-H str |
| 38 | 1750 | 57 | 1705 | 28 | 1790 | 16 | 1744 | 15 | A' | N-O str |
| 36 | 1629 | 2 | 1629 | 0 | 1663 | 1 | 1663 | 2 | A' | ring str |
| ($^{10}$B)35 | 1482 | 10 | 1481 | 6 | 1522 | 4 | 1517 | 0 | A' | ring str |
| 35 | 1476 | 9 | 1476 | 15 | 1514 | 6 | 1514 | 8 | A' | ring str |
| ($^{10}$B)33 | 1459 | 83 | 1448 | 50 | 1502 | 24 | 1492 | 29 | A' | B-O str |
| 33 | 1416 | 100 | 1402 | 100 | 1459 | 100[d] | 1447 | 100 | A' | B-O str |
| 32 | 1338 | 56 | 1337 | 38 | 1379 | 13 | 1379 | 18 | A' | ring str, B-O str |
| ($^{10}$B)31 | - | - | - | - | 1361 | 3 | 1361 | 3 | A' | O-B asym str, skel. ring |
| 31 | 1291 | 23 | 1291 | 3 | 1323 | 13 | 1323 | 13 | A' | O-B asym str, skel. ring |
| 29 | 1236 | 9 | 1236 | 17 | 1276 | 16 | 1276 | 17 | A' | C-O str, ring str |
| 28 | 1141 | 5 | 1141 | 5 | 1163 | 1 | 1163 | 1 | A' | C-O str, skel. ring |
| 25 | 1008 | 3 | - | - | 1012 | 1 | 1012 | 1 | A' | skel. ring, in pl. C-H |
| 22 | 870 | 5 | 870 | 3 | 869 | 2 | 869 | 2 | A' | skel. ring, C-O str, O-N str |
| 20 | - | - | - | - | 816 | 3 | 816 | 3 | A' | ring breathing |
| 18 | 772 | 34 | 758 | 19 | 784 | 15 | 770 | 16 | A' | O-N-O bending |
| 17 | 749 | 11 | 749 | 21 | 722 | 8 | 722 | 8 | A'' | skel. Wag. sym C-H wag |
| 16 | - | - | - | - | 681 | 1 | 680 | 2 | A'' | OOBO wag |
| 14 | 638 | 68 | 626 | 32 | 644 | 23 | 631 | 21 | A' | skel. ring, O-N str |
| 12 | 555 | 11 | 544 | 13 | 553 | 6 | 544 | 7 | A' | skel. ring, ONO bending |
| 10 | 507 | 23 | 502 | 36 | 505 | 7 | 501 | 8 | A' | skel. ring |

| | | | | | | | | | | |
|---|---|---|---|---|---|---|---|---|---|---|
| 8 | - | - | - | - | 381 | 3 | 370 | 3 | A’ | skel. ring |
| 6 | - | - | - | - | 281 | 3 | 277 | 3 | A’ | B-O-N bending |

[a] The numbering of the vibrational modes is according to calculated spectrum. [b] Intensity relative to the strongest band. [c] Symmetry of the vibrations are taken from calculated IR spectrum. [d] Computed absolute intensity: 1017.8 km mol$^{-1}$

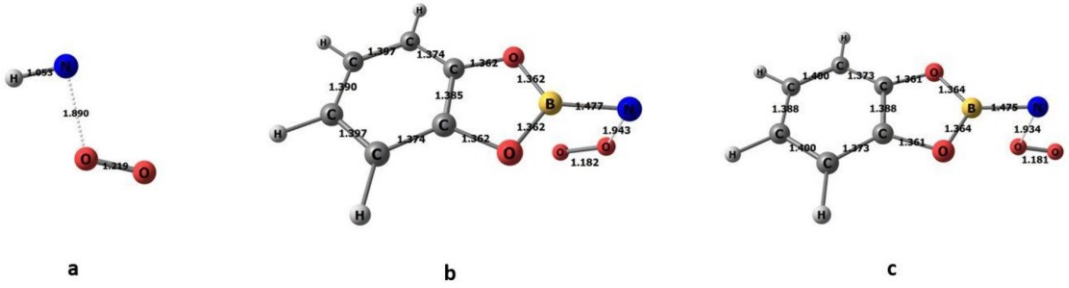


Figure S1. Structural parameters corresponding to the geometries of respective maximum in the scan curve of Fig.5 for (a) Imine Peroxide, (b) *anti*-nitroso-O-oxide **7a** and, (c) bisected nitroso-O-oxide **7c**, calculated at CASSCF(14,10)/def-SV(P).

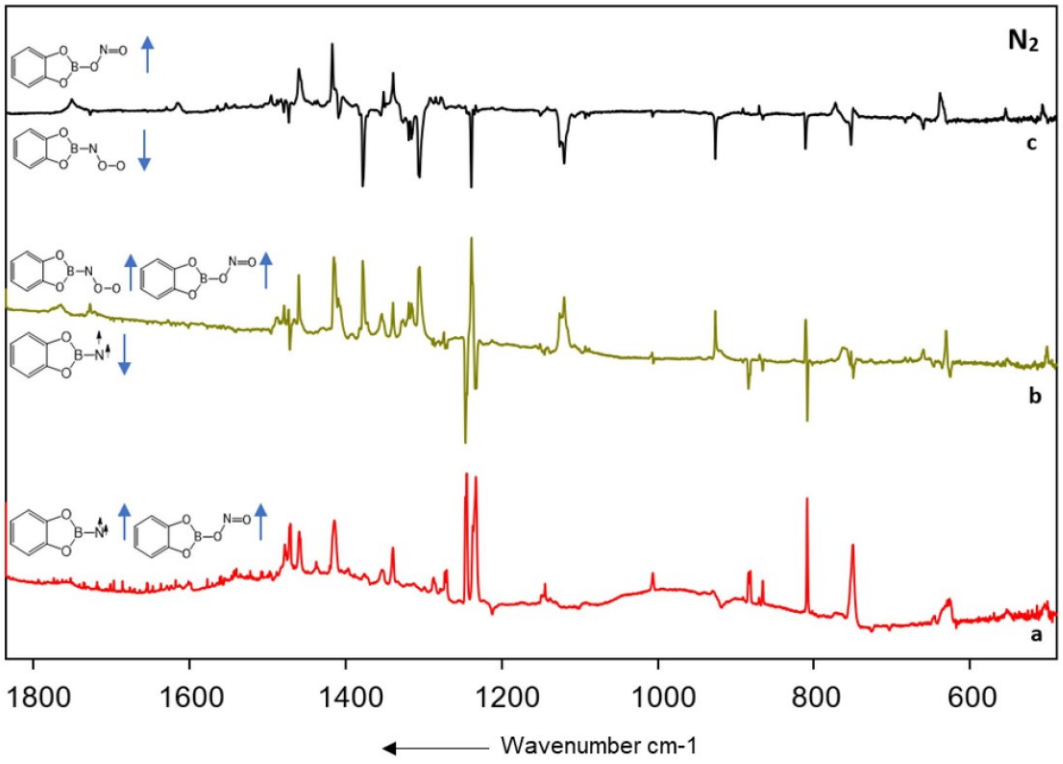

Figure S2. (a) Infrared spectra obtained after irradiation of boryl azide **5** in $O_2$ (2-3 %) doped nitrogen matrix. (a) After 60 min irradiation with λ = 254 nm at T = 10 K. (b) Difference spectrum after annealing for 30 min at 30 K. (c) Difference spectrum after irradiation with λ = 254 nm for 40 min.

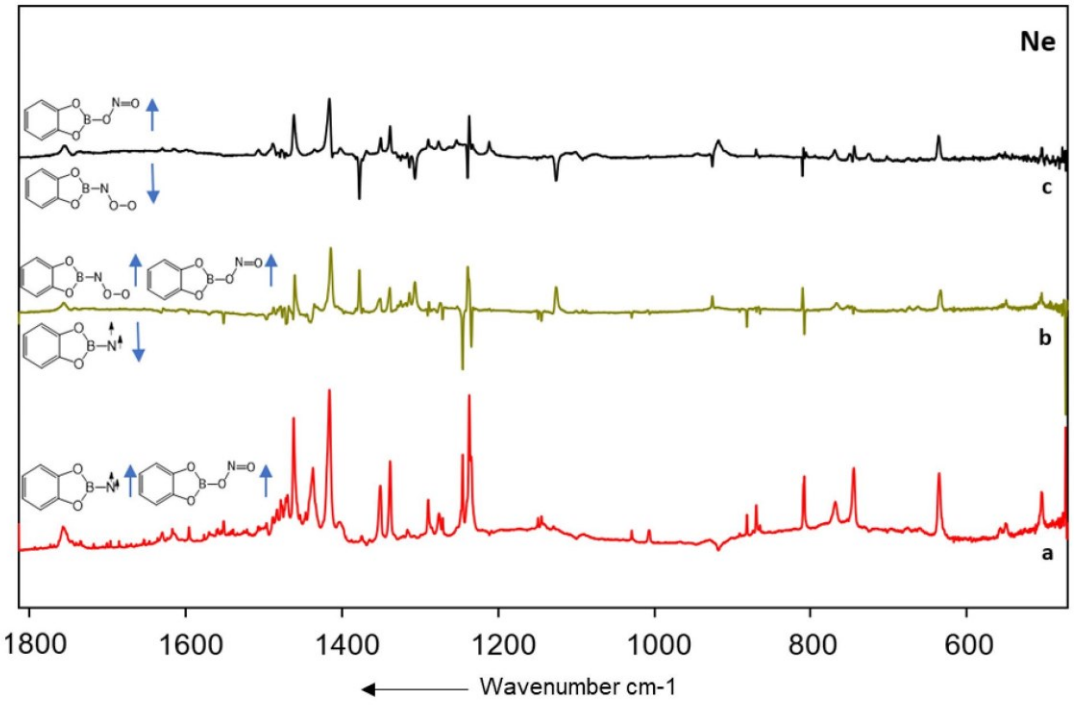


Figure S3. (a) Infrared spectra obtained after irradiation of boryl azide **5** in $O_2$ (2-3 %) doped neon matrix. (a) After 50 min irradiation with λ = 254 nm at T = 4 K. (b) Difference spectrum after annealing for 30 min at 10 K. (c) Difference spectrum after irradiation with λ = 254 nm for 30 min.

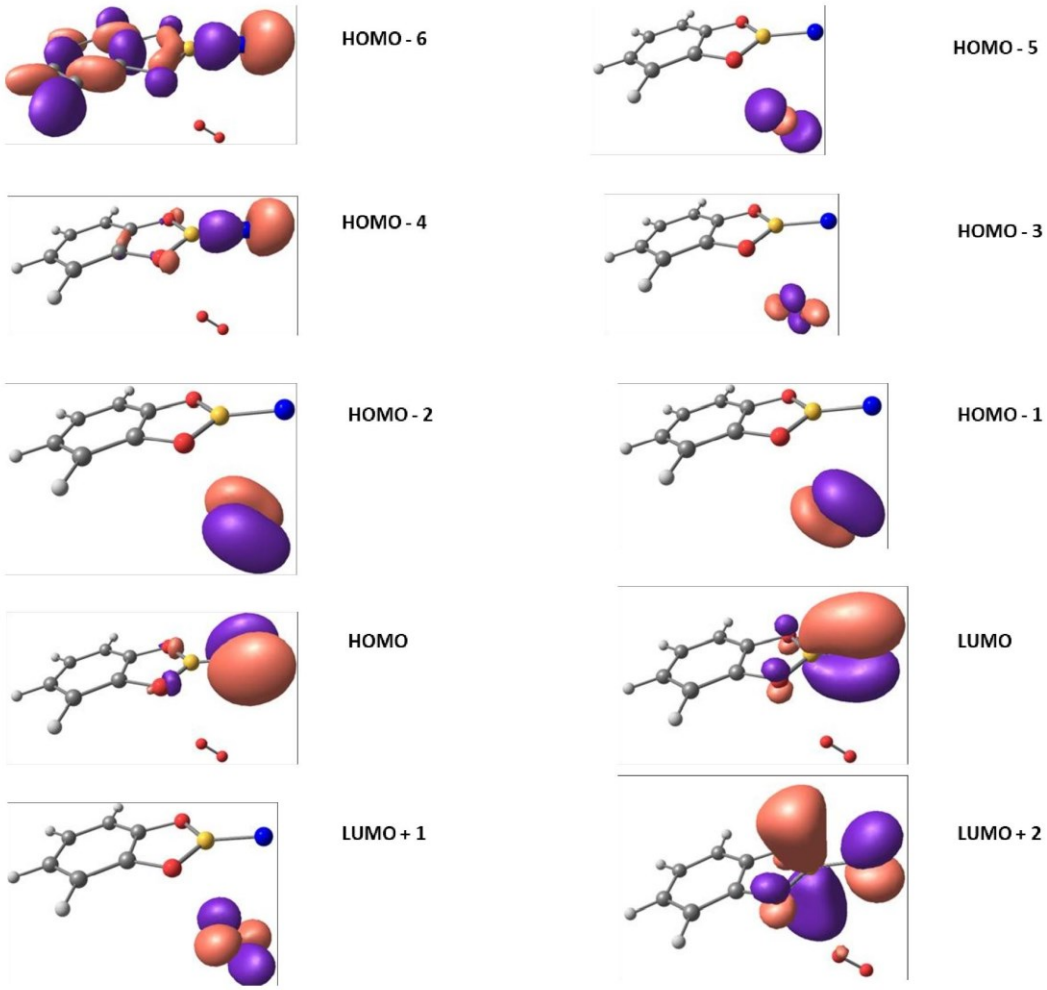


Figure S4. Active space orbital for the system **6** + $O_2$ obtained at HF/def2-SV(P) level of theory followed by necessary orbital rotations and used as the initial guess orbitals in multireference perturbation theory FIC-NEVPT2/def2-SV(P).

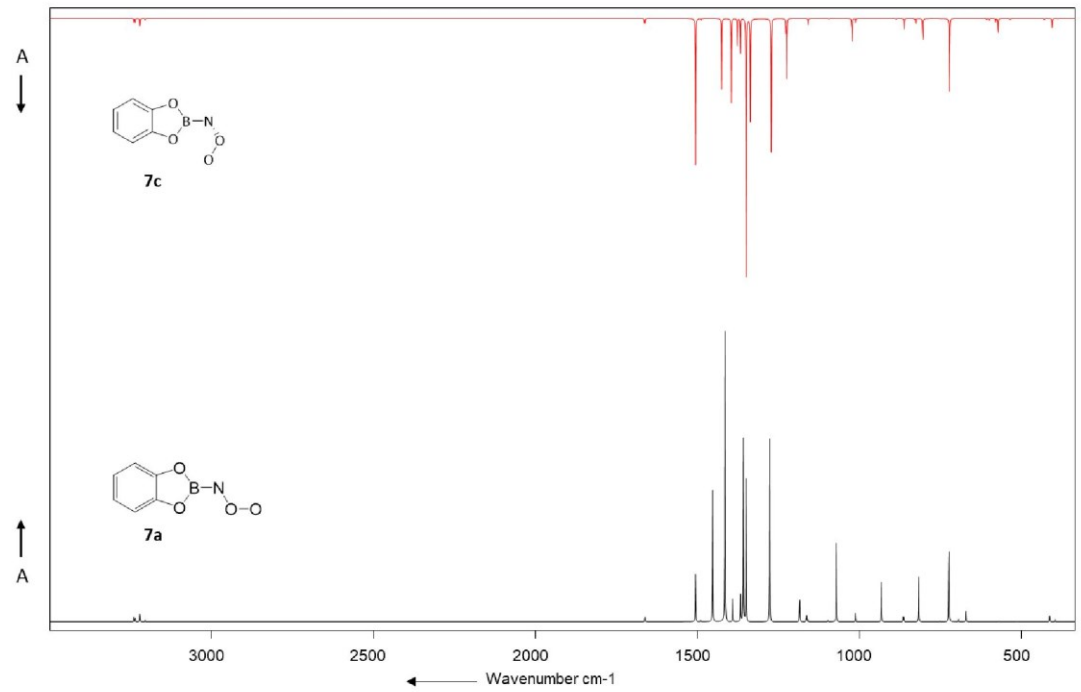


Figure S5. Calculated IR spectrum of anti-nitroso-O-oxide **7a** (bottom) and bisected nitroso-O-oxide **7c** calculated at CCSD(T)/DZP.

GDCh Communications Angewandte International Edition Chemie

Heterocycles Hot Paper

How to cite: *Angew. Chem. Int. Ed.* **2021**, *60*, 23112–23116
International Edition: doi.org/10.1002/anie.202105171
German Edition: doi.org/10.1002/ange.202105171

# The Reaction of $CO_2$ with a Borylnitrene: Formation of an 3-Oxaziridinone

*Virinder Bhagat, Julia Schumann, and Holger F. Bettinger**

***Abstract:*** *The reaction of a borylnitrene with carbon dioxide is studied under cryogenic matrix isolation conditions. Photogenerated CatBN (Cat = catecholato) reacts with $CO_2$ under formation of the cycloaddition product CatBNCO$_2$, a 3-oxaziridinone derivative, after photoexcitation (> 550 nm). The product shows Fermi resonances between the CO stretching and ring deformation modes that cause unusual $^{13}C$ and $^{18}O$ isotopic shifts. A computational analysis of the 3-oxaziridinone shows this cyclic carbamate to be less strained than an α-lactone or an α-lactame.*

Carbon dioxide is one important contributor to the greenhouse effect, and its increasing emission from various sources triggers research of its capture and recycling into chemicals.[1–13] The use of $CO_2$, which is non-toxic and abundantly present in nature, as a C1 building block in chemical reaction systems is still not very common due to its high thermodynamic and kinetic stability.[14] However, despite this, there are systems which are known to show reactivity towards $CO_2$. The reduction of $CO_2$ using many heterogenous and homogenous transition metal catalysts is well documented.[15–22] Furthermore, the use of metal-free $CO_2$ reductants has evolved over the years considering the toxicity and cost of the metal-based reducing/activation agents. These involve frustrated Lewis pairs, N-heterocyclic carbene (NHC), and nitrogen bases (e.g. 1,5,7-triazabicyclo[4.4.0]dec-5-ene and 1,8-diazabicyclo-(5.4.0)undec-7-ene).[23–33]

Electrophilic carbenes can also react with $CO_2$.[34] Sander has shown that the reaction of diphenylcarbene **1** with $CO_2$ yields both thermally and photochemically the corresponding α-lactone, diphenyloxiranone **2**, in cryogenic matrix isolation experiments (Scheme 1a).[34] Nitrenes are analogues of carbenes that generally undergo similar reactions, but for these the related cycloaddition reaction with $CO_2$ was never demonstrated. We have previously identified a class of particularly reactive nitrenes, borylnitrenes, carrying two oxygen atoms at the boron center that preclude isomerization

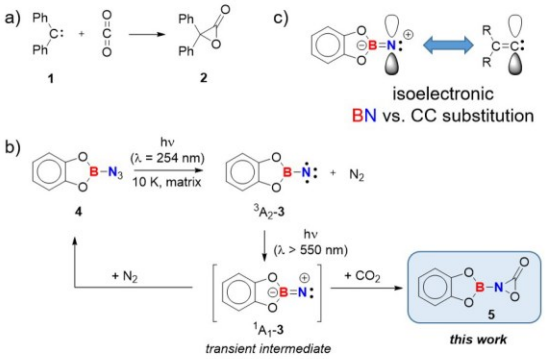


***Scheme 1.*** a) Formation of diphenyloxiranone **2** as the result of the reaction of diphenylcarbene **1** with $CO_2$.[34] b) Photogeneration of borylnitrene $^3A_2$-**3** under matrix isolation conditions and its photoreaction with closed-shell molecules $N_2$ and $CO_2$ (this work) via the transient singlet nitrene $^1A_1$-**3**. c) Isoelectronic relationship between $^1A_1$-**3** and vinylidenes and the in-plane p-type orbital that comprises the LUMO of both.

to iminoboranes.[35–41] The catechol derivative **3** (CatBN, Cat = catecholato), accessible under matrix isolation conditions from azide **4** (Scheme 1b), has a triplet electronic ground state ($^3A_2$-**3**) and shows high reactivity towards small molecules even under matrix isolation conditions ($N_2$, CO, $D_2$, $CH_4$, $O_2$).[35–41] The reaction with closed-shell molecules requires photoactivation ($\lambda > 550$ nm) presumably involving the closed-shell singlet state ($S_1$) $^1A_1$-**3**. The electronic structure of $^1A_1$-**3** is reminiscent of vinylidenes as their reactive centers are related by an isoelectronic substitution of the C=C by the B=N unit (Scheme 1c). The $^1A_1$ state of **3** and vinylidene have both a $\pi^2\sigma^0$ type configuration that causes low-lying vacant orbitals at their monocoordinate carbon or nitrogen atoms and high electrophilicity.[35,42] A particular reactive derivative is super electrophilic difluorovinylidene that inserts into methane and dihydrogen at 20–40 K.[43–49]

We here report for the first time the reaction of a borylnitrene with $CO_2$ and show that this results in an 1,2-oxaziridin-3-one derivative.[50] These are the smallest possible cyclic carbamates, which were suggested as reactive intermediates[51–57] and have been studied computationally before,[58–61] but never could be isolated.

To investigate the reaction of **3** with carbon dioxide, azide **4** was isolated at 10 K in nitrogen doped with carbon dioxide (5 % $CO_2$). Photolysis of **4** using UV irradiation ($\lambda = 254$ nm) resulted in the complete disappearance of **4** and the concomitant formation of nitrene **3**. Annealing of the matrix isolated nitrene in the presence of $CO_2$ to 35 K did not result in new

[*] V. Bhagat, Dr. J. Schumann, Prof. Dr. H. F. Bettinger
Institut für Organische Chemie, Universität Tübingen
Auf der Morgenstelle 18, 72076 Tübingen (Germany)
E-mail: Holger.Bettinger@uni-tuebingen.de
Supporting information and the ORCID identification number(s) for the author(s) of this article can be found under: https://doi.org/10.1002/anie.202105171.

signals. Long-wavelength irradiation ($\lambda > 550$ nm), on the other hand, resulted primarily in the growth of the signals of the azide **4** owing to the efficient reaction of **3** with $N_2$ as reported previously.[40] However, also a set of rather weak new signals at 1934, 1457, 1393, 1332, 1312, 1303, 1237, 1019, 919, 803, and 748 $cm^{-1}$ (see Figure 1, Table S1) was observed. A similar new set of bands is also observed in solid argon, but also in this matrix the photo generation of azide **4** dominates (see Figure S3).

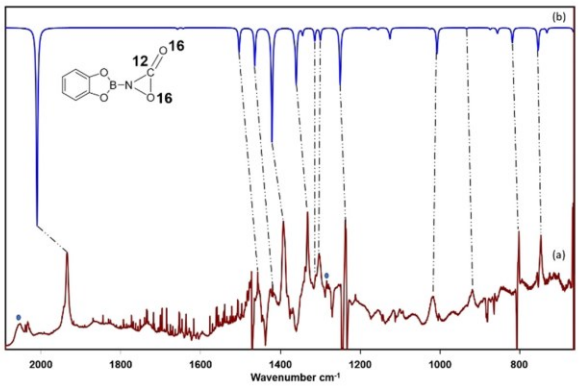


***Figure 1.*** a) Difference spectrum obtained after irradiation of $N_2$ matrix with $\lambda > 550$ nm (following the irradiation with $\lambda = 254$ nm) in the presence of $CO_2$. b) Calculated spectrum for $^{11}B$ and $^{10}B$ isotopologues (81:19) of 3-oxaziridinone **5** at the B3LYP/6–311++G(2d,p) level (with $^{16}O_2$). ● correspond to the signals for overtones/combination bands of the resulting product.

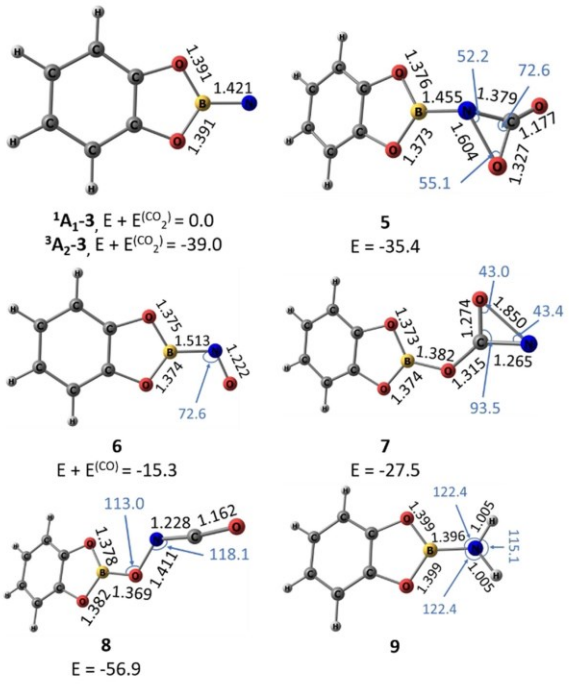


***Figure 2.*** Geometrical parameters (black font: bond lengths in Å; blue font: bond angles in degrees) and relative energies (in kcal $mol^{-1}$) of $^1A_1$-**3** and various possible photoproducts that can be formed as the result of the reaction between **3** and $CO_2$.

The strong signal at 1934 $cm^{-1}$ excludes nitroso borane **6**, acyl nitrene **7**, and isocyanatoxy borane **8** (Figure 2) as the carrier of these bands based on their computed (B3LYP/6–311++G(2d,p) level of theory, see Figure S1 for details) harmonic vibrational spectra. Note the short N–O distance in **7** of 1.850 Å, which is similar to that computed earlier for singlet formylnitrene, indicates a structure in between acylnitrene and oxazirine.[62]

3-Oxaziridinones are not known to date, and hence no experimental data is available for their ν(CO) stretching vibrations. For the α-lactone **2**, a very strong vibration at 1890 $cm^{-1}$ was observed by Sander.[34] The computational study by Liebman et al. showed the presence of harmonic C=O stretch of 1,2-oxaziridine-3-one at 1974 $cm^{-1}$ at MP2/6–311++G(2d,2p) which is very close (1969 $cm^{-1}$) to the C=O stretch that we calculated for **5** at the MP2/6–311++G(2d,p) level.[58] The computed harmonic value of the C=O stretching vibration in the 3-oxaziridinone derivative **5** is 2009 $cm^{-1}$ at B3LYP/6–311++G(2d,p), in support of an assignment to **5**. Additional strong bands are computed for **5** in the 1500–700 $cm^{-1}$ range, in agreement with the experiment (see Figure 1).

To further support the assignment to **5**, we investigated the reactions with $^{13}C(^{16}O)_2$ and $^{12}C(^{18}O)_2$ that produce two additional isotopologues of **5**. The $^{18}O$ isotopic shift of 35 $cm^{-1}$ for the strong band at 1934 is similar to that observed for **2** (30.4 $cm^{-1}$) previously,[34] and in line with a carbonyl group. The computed $^{18}O$ isotopic shift of 33 $cm^{-1}$ is in good agreement with the observation. The other signals assigned to **5** hardly undergo any shift upon $^{18}O$ substitution (see Figure 3 and Table S2). This is in agreement with harmonic vibrational computations that suggest that only the in-plane deformation mode of the three-membered ring (for $^{12}C(^{16}O)_2$, exp.: 1019 $cm^{-1}$ and calc.: 1008 $cm^{-1}$) should show a significant

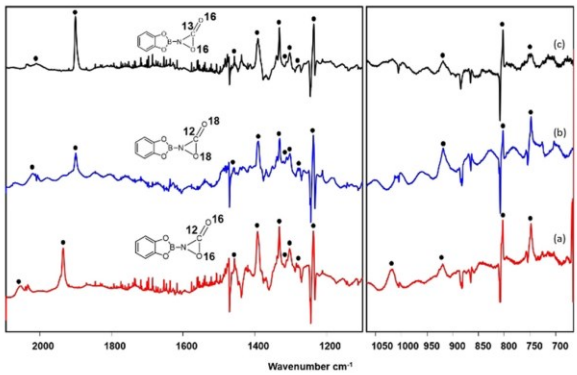


***Figure 3.*** Difference spectra obtained after irradiation of $N_2$ matrix with $\lambda > 550$ nm (following the irradiation with $\lambda = 254$ nm) in the presence of a) $^{12}C(^{16}O)_2$, after 100 min, b) $^{12}C(^{18}O)_2$, after 90 min, c) $^{13}C(^{16}O)_2$, after 60 min in solid $N_2$ at 10 K. ● correspond to the fundamental and overtone/combination bands in three of the isotopologues of **5**.

  

isotopic shift (15 $cm^{-1}$). The associated band could, however, not be detected in $^{13}C$ and $^{18}O$ isotopologues of **5**.

The $^{13}C$ isotopic shift is 34 $cm^{-1}$. This is very similar to the $^{18}O$ isotopic shift, and smaller than expected based on our harmonic vibrational computations at B3LYP/6–311++G(2d,p) (53.0 $cm^{-1}$) and comparison with **2** (53.1 $cm^{-1}$).[34] Note that Sander considered the $^{13}C$ isotopic shift of 53 $cm^{-1}$ to be larger than expected, but our computations for **2** at B3LYP/6–311++G(2d,p) arrive at isotopic shifts of 51 $cm^{-1}$ and 32 $cm^{-1}$ for $^{13}C$ and $^{18}O$, respectively, in a very good agreement with Sander's experimental data.[34] Similar to the $^{18}O$ isotopologue, no other signals assigned to **5** show a significant shift upon $^{13}C$ substitution, in agreement with the computed vibrational spectra (see Figure S2).

To shed light on the vibrational properties of the 3-oxaziridinone system, we computed the cubic force field for **5** (see Table S4). For a system like **5**, such computations are a formidable task as two second derivative calculations are required for each of the 45 normal modes of each of the three isotopologues. We chose the MP2/6–311++G(2d,p) level of theory as numerical noise resulting from DFT grids is then avoided. The analysis reveals that for all isotopologues, the C=O stretching frequency ($\nu_5$) is involved in Fermi resonances with the first overtone of $\nu_{19}$ ($2\nu_{19}$) in the case of $^{12}C(^{16}O)_2$ isotopologue and with the first overtone of $\nu_{20}$ ($2\nu_{20}$) in case of $^{13}C(^{16}O)_2$ and $^{12}C(^{18}O)_2$ isotopologues (see Table S4). For the $^{13}C(^{16}O)_2$ isotopologue, additional Fermi resonances of $\nu_5$ with the $\nu_{24}+\nu_{18}$ and $\nu_{24}+\nu_{20}$ combination bands can be identified while only the $\nu_{24}+\nu_{18}$ combination band was found to be in Fermi resonance with $\nu_5$ of $^{12}C(^{18}O)_2$. The vibrational deperturbation analysis (Table S5) places $\nu_5$ at 1951 $cm^{-1}$ and 1907 $cm^{-1}$ for the $^{12}C(^{16}O)_2$ and $^{12}C(^{18}O)_2$ isotopologues, respectively. The Fermi resonances then resulted in a shift of $\nu_5$ to 1906 and 1859 $cm^{-1}$, respectively. Compared to the experiment, the Fermi resonance seems to be too strong and the shift of $\nu_5$ thus too pronounced. The $^{18}O$ isotopic shift, 47 $cm^{-1}$, is higher than that of the experimental value (35 $cm^{-1}$). For the $^{13}C$ isotopologue, the deperturbation analysis arrived at a value of 1888 $cm^{-1}$ for $\nu_5$ which was shifted to 1863 $cm^{-1}$ after Fermi resonance. This explains the occurrence of $\nu_5$ at nearly the same position in the experimental IR spectra of $^{13}C$ and $^{18}O$ isotopologues (which are at 1900 $cm^{-1}$ and 1899 $cm^{-1}$ respectively). Hence, the Fermi resonances explain the unexpectedly small isotopic shift for $\nu_5$ of the $^{13}C$ isotopologue relative to $\nu_5$ of the $^{18}O$ isotopologue.

The reaction of **3** with $CO_2$ does not proceed thermally in accord with our previous experience that the reaction of **3** with closed-shell molecules ($N_2$, CO, $CH_4$, $H_2$, or $D_2$) requires photoexcitation.[38–40] The small kinetic isotope effect measured for the insertion of the closely related pinBN (pin = pinacolato) derivative into a CH bond of cyclohexane suggests that the singlet nitrene is undergoing the reaction.[35] The singlet nitrene $^1A_1$-**3** inserts into dihydrogen with a very low barrier according to previous computations,[38] while its cycloaddition to $CO_2$ is without potential energy barrier. A relaxed potential energy surface scan computed at B3LYP/6–311++G(2d,p) starting from a large distance between one of the oxygen atoms and the nitrogen atom of $^1A_1$-**3** results in barrierless potential energy curve that reaches species **5** as minimum (Figure S5). A TS can be located at the CASSCF-(14,14)/def2-SV(P) level, but its energy drops below that of reactants after considering dynamic correlation with NEVPT2//CASSCF and B3LYP//CASSCF single point evaluations, suggesting that the reaction between $^1A_1$-**3** and $CO_2$ can proceed without a potential energy barrier.

The oxaziridinone **5** (see Figure 2) has a pyramidal nitrogen atom (sum of bond angles: 292.0°) that is characteristic of aziridines, but contrasts the planar coordination in the aminoborane $CatBNH_2$ (**9**, sum of bond angles: 359.9° Figure 2). Compared to the nitrogen center in the latter, the pyramidal nitrogen atom is a poorer electron donor towards boron as evidenced by NBO[63] analysis (Figure S6a). This results in a longer BN bond with a smaller Wiberg bond index (WBI) than in **9** (Figure S6b). The nitrogen and oxygen lone pairs of the three-membered ring donate electron density into the $\pi^*$ orbital of the CO double bond according to second order perturbation analysis to a degree that is similar to carbamic acid (see Figure S6a). The NO distance in **5** is quite long (1.604 Å) compared to that in hydroxylamine (exp. 1.453 Å, calc. 1.446 Å).[58,64] The NBO analysis revealed that the NO natural bond orbital is comprised of natural atomic hybrids (NAH) on both nitrogen and oxygen atoms with p character of 96% each. The high percentage of p and a low percentage of s (4% on each NAHs) character of the NAH explains the unusually long NO bond in **5**. On the other hand, the NC and the endocyclic CO distances are quite short, 1.379 Å and 1.327 Å, respectively. Also, the exocyclic CO distance is quite short (1.177 Å) compared to typical CO double bonds of carboxylic acid derivatives (1.202–1.229 Å).[65–67] It appears that the inherently weak NO bond can "adjust" in length to minimize strain of the system and at the same time maximize the bonding to carbon (larger s character of N and O) by employing p orbitals for the N–O bond. Note that there exists a diradicaloid isomer of **5** with a significantly stretched NO bond (2.272 Å) and high spin density on the N and O atoms (see Figure S7). This is higher in energy than **5** by 3.6 kcal $mol^{-1}$ and collapses to **5** with a barrier of 2.8 kcal $mol^{-1}$. This suggests that the NO bond is quite weak and that its description as a dative bond is inappropriate. This is in agreement with the atoms in molecules analysis that found no N-O bond critical point for the parent oxaziridinone.[58] We could not observe any indication for formation of this higher energy isomer of **5** or for ring opening to the more stable isocyanatoxy borane **8**. The latter rearrangement is associated with a sizeable barrier (see Figure S8).

As the unusual three-membered heterocycle of **5** is unknown experimentally, we also estimate its strain energy. Using Liebman's method of combination with cyclopropane or similar three-member ring compounds (Figure S9),[68–71] we arrived at a strain energy of 36.7 kcal $mol^{-1}$ for **5** at the CBS-QB3[72] level of theory. The value is larger than that computed for aziridine (27.0 kcal $mol^{-1}$), but smaller than that of α-lactone (47.0 kcal $mol^{-1}$) and α-lactam (55.0 kcal $mol^{-1}$).[73,74] The reduced strain of oxaziridinone **5** is in agreement with the conclusions of Bach et al. that insertion of two hetero atoms decreases the strain of a three-membered ring.[73]

  

In summary, we here report the first example of the cycloaddition reaction between a nitrene and carbon dioxide. This cycloaddition reaction proceeds after photoexcitation of the triplet nitrene and its intersystem crossing to the singlet nitrene without barrier and produces the strained oxaziridinone system that has never been observed before. The three-membered heterocycle shows Fermi resonance between the CO stretching frequency and overtones of ring deformation modes causing unexpected isotope shifts for the $^{13}C$ and $^{18}O$ isotopologues of $CO_2$. The strain of this ring system amounts to almost 40 kcal mol$^{-1}$, which is smaller than that of α-lactones and α-lactames presumably due to the long N–O bond.

## Acknowledgements

This work was supported by Deutsche Forschungsgemeinschaft (BE 3183/11-1). We would like to express our sincere thanks to the state of Baden-Württemberg for bwHPC and to the German Research Foundation (DFG) through grant no INST 40/467-1 FUGG for the computation facilities. We would also like to thank Marie-Sophie Sättele for her help in the synthesis of boryl azide **4**. J.S. presently works at the Department of Chemistry, Cambridge University, U.K. Open access funding enabled and organized by Projekt DEAL.

## Conflict of Interest

The authors declare no conflict of interest.

**Keywords:** matrix isolation · nitrenes · strained heterocycles

[1] S. P., S. K. Mandal, *Chem. Sci.* **2020**, *11*, 10571 – 10593.
[2] Y. Wang, T. He, *J. Mater. Chem. A* **2021**, *9*, 87 – 110.
[3] Q. Tang, Y. Ma, J. Wang, *Sol. RRL* **2021**, *5*, 2000443.
[4] Z. Sun, J. Dong, C. Chen, S. Zhang, Y. Zhu, *J. Chem. Technol. Biotechnol.* **2021**, *96*, 1161 – 1175.
[5] M. Muringa Kandy, A. Rajeev K, M. Sankaralingam, *Sustainable Energy Fuels* **2021**, *5*, 12 – 33.
[6] T. Li, W. Zhang, H. Qin, L. Lu, S. Yan, Z. Zou, *ChemPhotoChem* **2021**, *5*, 495 – 501.
[7] J. Yuan, Y. Du, H. Zhang, *APL Mater.* **2020**, *8*, 060904.
[8] Z.-j. Wang, H. Song, H. Liu, J. Ye, *Angew. Chem. Int. Ed.* **2020**, *59*, 8016 – 8035; *Angew. Chem.* **2020**, *132*, 8092 – 8111.
[9] S. Samanta, R. Srivastava, *Mater. Adv.* **2020**, *1*, 1506 – 1545.
[10] B. Limburg, A. Cristofol, F. Della Monica, A. W. Kleij, *ChemSusChem* **2020**, *13*, 6056 – 6065.
[11] S. Remiro-Buenamanana, H. Garcia, *ChemCatChem* **2019**, *11*, 342 – 356.
[12] Y. Y. Birdja, E. Perez-Gallent, M. C. Figueiredo, A. J. Gottle, F. Calle-Vallejo, M. T. M. Koper, *Nat. Energy* **2019**, *4*, 732 – 745.
[13] A. Cherubini-Celli, J. Mateos, M. Bonchio, L. Dell'Amico, X. Companyo, *ChemSusChem* **2018**, *11*, 3056 – 3070.
[14] T. Sakakura, J.-C. Choi, H. Yasuda, *Chem. Rev.* **2007**, *107*, 2365 – 2387.
[15] F. J. Fernández-Alvarez, A. M. Aitani, L. A. Oro, *Catal. Sci. Technol.* **2014**, *4*, 611 – 624.
[16] S. Bontemps, L. Vendier, S. Sabo-Etienne, *J. Am. Chem. Soc.* **2014**, *136*, 4419 – 4425.
[17] S. Bontemps, L. Vendier, S. Sabo-Etienne, *Angew. Chem. Int. Ed.* **2012**, *51*, 1671 – 1674; *Angew. Chem.* **2012**, *124*, 1703 – 1706.
[18] C. A. Huff, M. S. Sanford, *J. Am. Chem. Soc.* **2011**, *133*, 18122 – 18125.
[19] C. Federsel, A. Boddien, R. Jackstell, R. Jennerjahn, P. J. Dyson, R. Scopelliti, G. Laurenczy, M. Beller, *Angew. Chem. Int. Ed.* **2010**, *49*, 9777 – 9780; *Angew. Chem.* **2010**, *122*, 9971 – 9974.
[20] W. Leitner, *Coord. Chem. Rev.* **1996**, *153*, 257 – 284.
[21] T. Yoshida, D. L. Thorn, T. Okano, J. A. Ibers, S. Otsuka, *J. Am. Chem. Soc.* **1979**, *101*, 4212 – 4221.
[22] M. Aresta, C. F. Nobile, V. G. Albano, E. Forni, M. Manassero, *J. Chem. Soc. Chem. Commun.* **1975**, 636 – 637.
[23] D. W. Stephan, *J. Am. Chem. Soc.* **2015**, *137*, 10018 – 10032.
[24] K. Edel, S. A. Brough, A. N. Lamm, S.-Y. Liu, H. F. Bettinger, *Angew. Chem. Int. Ed.* **2015**, *54*, 7819 – 7822; *Angew. Chem.* **2015**, *127*, 7930 – 7933.
[25] B. R. Barnett, C. E. Moore, A. L. Rheingold, J. S. Figueroa, *Chem. Commun.* **2015**, *51*, 541 – 544.
[26] F.-G. Fontaine, M.-A. Courtemanche, M.-A. Légaré, *Chem. Eur. J.* **2014**, *20*, 2990 – 2996.
[27] C. Das Neves Gomes, E. Blondiaux, P. Thuéry, T. Cantat, *Chem. Eur. J.* **2014**, *20*, 7098 – 7106.
[28] A. L. Travis, S. C. Binding, H. Zaher, T. A. Q. Arnold, J.-C. Buffet, D. O'Hare, *Dalton Trans.* **2013**, *42*, 2431 – 2437.
[29] G. Ménard, T. M. Gilbert, J. A. Hatnean, A. Kraft, I. Krossing, D. W. Stephan, *Organometallics* **2013**, *32*, 4416 – 4422.
[30] G. Ménard, D. W. Stephan, *J. Am. Chem. Soc.* **2010**, *132*, 1796 – 1797.
[31] S. N. Riduan, Y. Zhang, J. Y. Ying, *Angew. Chem. Int. Ed.* **2009**, *48*, 3322 – 3325; *Angew. Chem.* **2009**, *121*, 3372 – 3375.
[32] C. M. Mömming, E. Otten, G. Kehr, R. Fröhlich, S. Grimme, D. W. Stephan, G. Erker, *Angew. Chem. Int. Ed.* **2009**, *48*, 6643 – 6646; *Angew. Chem.* **2009**, *121*, 6770 – 6773.
[33] A. E. Ashley, A. L. Thompson, D. O'Hare, *Angew. Chem. Int. Ed.* **2009**, *48*, 9839 – 9843; *Angew. Chem.* **2009**, *121*, 10023 – 10027.
[34] W. W. Sander, *J. Org. Chem.* **1989**, *54*, 4265 – 4267.
[35] M. Filthaus, L. Schwertmann, P. Neuhaus, R. W. Seidel, I. M. Oppel, H. F. Bettinger, *Organometallics* **2012**, *31*, 3894 – 3903.
[36] H. F. Bettinger, H. Bornemann, *Z. Anorg. Allg. Chem.* **2011**, *637*, 2169 – 2174.
[37] H. F. Bettinger, M. Filthaus, *Org. Biomol. Chem.* **2010**, *8*, 5477 – 5482.
[38] H. F. Bettinger, M. Filthaus, P. Neuhaus, *Chem. Commun.* **2009**, 2186 – 2188.
[39] H. F. Bettinger, M. Filthaus, H. Bornemann, I. M. Oppel, *Angew. Chem. Int. Ed.* **2008**, *47*, 4744 – 4747; *Angew. Chem.* **2008**, *120*, 4822 – 4825.
[40] H. F. Bettinger, H. Bornemann, *J. Am. Chem. Soc.* **2006**, *128*, 11128 – 11134.
[41] V. Bhagat, J. Schumann, H. F. Bettinger, *Chem. Eur. J.* **2020**, *26*, 12654 – 12663.
[42] H. F. Bettinger, *Inorg. Chem.* **2007**, *46*, 5188 – 5195.
[43] W. Sander, C. Kötting, R. Hübert, *J. Phys. Org. Chem.* **2000**, *13*, 561 – 568.
[44] W. Sander, C. Kötting, *Chem. Eur. J.* **1999**, *5*, 24 – 28.
[45] C. Kötting, W. Sander, *J. Am. Chem. Soc.* **1999**, *121*, 8891 – 8897.
[46] C. Kötting, W. Sander, M. Senzlober, H. Bürger, *Chem. Eur. J.* **1998**, *4*, 1611 – 1615.
[47] C. Kötting, W. Sander, M. Senzlober, *Chem. Eur. J.* **1998**, *4*, 2360 – 2365.
[48] C. Kötting, W. Sander, J. Breidung, W. Thiel, M. Senzlober, H. Bürger, *J. Am. Chem. Soc.* **1998**, *120*, 219 – 220.
[49] J. Breidung, H. Bürger, C. Kötting, R. Kopitzky, W. Sander, M. Senzlober, W. Thiel, H. Willner, *Angew. Chem. Int. Ed. Engl.* **1997**, *36*, 1983 – 1985; *Angew. Chem.* **1997**, *109*, 2072 – 2075.

  

[50] For the reaction of a phosphinonitrene with $CO_2$ see: F. Dielmann, G. Bertrand, *Chem. Eur. J.* **2015**, *21*, 191 – 198.
[51] A. Herize, J. R. Mora, J. Lezama, E. Marquez, T. Córdova, G. Chuchani, *J. Phys. Org. Chem.* **2009**, *22*, 170 – 176.
[52] A. Rotinov, R. M. Domínguez, T. Córdova, G. Chuchani, *J. Phys. Org. Chem.* **2005**, *18*, 616 – 624.
[53] T. S. Dibble, Y. Zeng, *Chem. Phys. Lett.* **2010**, *495*, 170 – 174.
[54] A. Fontijn, S. M. Shamsuddin, D. Crammond, P. Marshall, W. R. Anderson, *Combust. Flame* **2006**, *145*, 543 – 551.
[55] J. C. Mackie, G. B. Bacskay, *J. Phys. Chem. A* **2005**, *109*, 11967 – 11974.
[56] D. E. Milligan, M. E. Jacox, S. W. Charles, G. C. Pimentel, *J. Chem. Phys.* **1962**, *37*, 2302 – 2310.
[57] Y.-G. Tao, Y.-H. Ding, J.-J. Liu, Z.-S. Li, X.-R. Huang, C.-C. Sun, *J. Comput. Chem.* **2001**, *22*, 1907 – 1919.
[58] D. J. R. Duarte, M. S. Miranda, J. C. G. Esteves da Silva, J. F. Liebman, *J. Struct. Chem.* **2016**, *27*, 663 – 670.
[59] M. S. Miranda, P. J. O. Ferreira, J. C. G. Esteves da Silva, J. F. Liebman, *Can. J. Chem.* **2015**, *93*, 406 – 413.
[60] M. S. Miranda, D. J. R. Duarte, J. C. G. Esteves da Silva, J. F. Liebman, *Can. J. Chem.* **2015**, *93*, 708 – 714.
[61] P. V. Sudhakar, J. Chandrasekhar, *J. Mol. Struct.* **1989**, *194*, 135 – 147.
[62] E. A. Pritchina, N. P. Gritsan, A. Maltsev, T. Bally, T. Autrey, Y. Liu, Y. Wang, J. P. Toscano, *Phys. Chem. Chem. Phys.* **2003**, *5*, 1010 – 1018.
[63] E. D. Glendening, A. E. Reed, J. E. Carpenter, F. Weinhold, NBO 6.0, Theoretical Chemistry Institute, University of Wisconsin, Madison, WI, **2013**.
[64] S. Tsunekawa, *J. Phys. Soc. Jpn.* **1972**, *33*, 167 – 174.
[65] F. H. Allen, O. Kennard, D. G. Watson, L. Brammer, A. G. Orpen, R. Taylor, *J. Chem. Soc. Perkin Trans. 2* **1987**, S1 – S19.
[66] K.-H. Hellwege, A. M. Hellwege, *Structure data of free polyatomic molecules*, Springer, Heidelberg, **1976**.
[67] G. Herzberg, *Molecular spectra and molecular structure. Vol. 3*, Springer, Heidelberg, **1966**.
[68] D. N. Zeiger, J. F. Liebman, *J. Mol. Struct.* **2000**, *556*, 83 – 94.
[69] A. Skancke, J. F. Liebman, *J. Org. Chem.* **1999**, *64*, 6361 – 6365.
[70] A. Skancke, D. Van Vechten, J. F. Liebman, P. N. Skancke, *J. Mol. Struct.* **1996**, *376*, 461 – 468.
[71] J. F. Liebman, P. N. Skancke, *Int. J. Quantum Chem.* **1996**, *58*, 707 – 715.
[72] J. A. Montgomery, Jr., M. J. Frisch, J. W. Ochterski, G. A. Petersson, *J. Chem. Phys.* **1999**, *110*, 2822 – 2827.
[73] R. D. Bach, O. Dmitrenko, *J. Am. Chem. Soc.* **2006**, *128*, 4598 – 4611.
[74] R. D. Bach, O. Dmitrenko, *J. Org. Chem.* **2002**, *67*, 3884 – 3896.

Manuscript received: April 15, 2021
Revised manuscript received: June 18, 2021
Accepted manuscript online: August 19, 2021
Version of record online: September 21, 2021

  

Angewandte Chemie
Eine Zeitschrift der Gesellschaft Deutscher Chemiker

Supporting Information

# The Reaction of $CO_2$ with a Borylnitrene: Formation of an 3-Oxaziridinone

*Virinder Bhagat, Julia Schumann, and Holger F. Bettinger**

ange_202105171_sm_miscellaneous_information.pdf

## Experimental and Computational Details

Experiments: The precursor for borylnitrene **3**, boryl azide **4**, was synthesized using the published procedure of Klapötke et al.[1] Matrix isolation experiments were performed by co-depositing the boryl azide **4** and nitrogen (Westfalen, 99.9999 %) doped with 3-5 % of $CO_2$ (Westfalen, 99.999 %), at the cold CsI window at 10 K. Also, the other isotopologues of carbon dioxide, $^{13}CO_2$ (Cambridge Isotope Laboratories, 99%) and $C^{18}O_2$ (Cambridge Isotope Laboratories, 95%), were used to perform similar experiments. Sumitomo SH-1 closed-cycle helium cryostat was used to obtain the temperature as low as 10 K.[2] The Infrared spectra in the range 400-4000 $cm^{-1}$ were obtained using Brucker's Vertex 70 FTIR spectrometer with a standard resolution of 0.5 $cm^{-1}$.

For inducing photochemistry in the deposited matrix, a low-pressure mercury lamp ($\lambda = 254$ nm, PenRay) and high-pressure mercury lamp (USHIO, USH-508S) were used. The combination of dichroic mirrors of required wavelength range along with Schott cutoff filter (550 OG) was used with high-pressure mercury to obtained $\lambda > 550$ nm.

Computations: All the geometries corresponding to the stationary points were optimized using the B3LYP[3-4] functional and 6-311++G(2d,p) basis set using Gaussian 16 software.[5] Natural bond orbital (NBO)[6-7] analyses were performed at B3LYP/6-311++G(2d,p) level of theory using the NBO 6.0[8] program. The confirmation of a stationary point as a minimum on the potential energy surface was done by computing harmonic vibrational frequencies at the same level of theory. The harmonic vibrations calculated at B3LYP/6-311++G(2d,p) were used to reproduce the simulated spectrum of the species **5** (three isotopologues**)** and species **6-8.** For identifying the combination bands and first overtones, which were seen in addition to the fundamental bands in the experimental spectrum, anharmonic calculations were performed at MP2/6-311++G(2d,p) using second-order vibrational perturbative approach of Barone et

al.[9-12] Complete Basis Set (CBS) method, CBS-QB3[13] of Petersson and coworkers were used in strain energy calculation of oxaziridinone **5.** Complete active space self-consistent field (CASSCF) theory in combination with def2-SV(P)[14] basis set was used to compute transition state that resulted in product **5** in the lowest energy singlet state as confirmed by intrinsic reaction coordinate calculation. The active space consisted of 14 orbitals and 14 electrons, see Figure S10. To include the effects of dynamic correlation for some points on the IRC, fully internally contracted N-electron valence state perturbation theory (FIC-NEVPT2) was used with the same basis set.[15] Also, the single point calculations at the IRC geometries were calculated with B3LYP functional in combination with def2-SV(P)[14] and def2-TZVP[14] basis sets. These CASSCF and FIC-NEVPT2 calculations were performed with the computational chemistry package ORCA.[16]

Table S1. Infrared Spectroscopic Data of $^{12}C^{16}(O_2)$ isotopologues of 3-Oxaziridinone **5** in Nitrogen matrix.

| Nitrogen matrix, 10 K | | | | B3LYP/6-311++G(2d,p) | | | |
|---|---|---|---|---|---|---|---|
| Vibrational Mode No.[a] | $\tilde{\upsilon}$, cm$^{-1}$ | I[b] | $\tilde{\upsilon}_i/\tilde{\upsilon}^c$ | $\tilde{\upsilon}$, cm$^{-1}$ | I[b] | $\tilde{\upsilon}_i/\tilde{\upsilon}^c$ | assignments |
| $\nu_5$ | 1934 | 100 | 1.000 | 2009 | 100[d] | 1.000 | carbonyl str |
| $\nu_9$ | 1457 | 67 | 1.000 | 1503 | 13 | 1.000 | skel. Ring, in pl. C-H |
| $\nu_{10}$ | 1393 | 96 | 0.978 | 1421 | 71 | 0.971 | B-N, ring str |
| $\nu_{11}$ | 1332 | 35 | 0.996 | 1360 | 35 | 0.996 | B-N, ring str |
| $\nu_{12}$ | 1312 | 2 | 0.993 | 1314 | 8 | 0.9781 | in plane C-H |
| $\nu_{13}$ | 1303 | 24 | 1.000 | 1300 | 8 | 0.995 | in plane C-H |
| $\nu_{14}$ | 1237 | 45 | 1.000 | 1250 | 29 | 1.000 | C-O (of the ring), ring str |
| $\nu_{20}$ | 1019 | 35 | 1.000 | 1008 | 13 | 1.000 | NCO ring str |
| $\nu_{22}$ | 919 | 21 | 1.000 | 933 | 1 | 1.000 | C-H wag |
| $\nu_{26}$ | 803 | 19 | 1.000 | 819 | 8 | 1.000 | ring breathing |
| $\nu_{28}$ | 748 | 37 | 1.000 | 754 | 12 | 0.997 | C-H wag |

[a] The numbering of the vibrational modes is according to calculated spectrum. [b] Intensity relative to the strongest band. [c] Ratio of frequencies of the natural $^{11}B$ vs $^{10}B$ isotopologues . [d] Computed absolute intensity: 850.0 km mol$^{-1}$

Table S2. Infrared Spectroscopic Data of $^{12}C^{18}(O_2)$ Isotopologues of 3-Oxaziridinone **5** in Nitrogen matrix.

| Nitrogen matrix, 10 K | | | | B3LPY/6-311++G(2d,p) | | | |
|---|---|---|---|---|---|---|---|
| Vibrational Mode No.[a] | $\tilde{\upsilon}$, $cm^{-1}$ | I[b] | $\tilde{\upsilon}_i/\tilde{\upsilon}^c$ | $\tilde{\upsilon}$, $cm^{-1}$ | I[b] | $\tilde{\upsilon}_i/\tilde{\upsilon}^c$ | assignments |
| $\nu_5$ | 1899 | 75 | 1.000 | 1976 | 100[d] | 1.000 | carbonyl str |
| $\nu_9$ | 1459 | 16 | 1.000 | 1503 | 13 | 1.000 | skel. Ring, in pl. C-H |
| $\nu_{10}$ | 1391 | 100 | 0.983 | 1420 | 71 | 0.971 | B-N, ring str |
| $\nu_{11}$ | 1331 | 47 | 0.994 | 1360 | 37 | 0.996 | B-N, ring str |
| $\nu_{12}$ | 1312 | 5 | 0.993 | 1314 | 8 | 0.978 | in plane C-H |
| $\nu_{13}$ | 1302 | 29 | 1.000 | 1300 | 8 | 0.995 | in plane C-H |
| $\nu_{14}$ | 1237 | 78 | 1.000 | 1250 | 29 | 1.000 | C-O (of the ring), ring str |
| $\nu_{20}$ | - | - | - | 993 | 15 | 1.000 | NCO ring str |
| $\nu_{22}$ | 919 | 51 | 1.000 | 933 | 1 | 1.000 | C-H wag |
| $\nu_{26}$ | 802 | 33 | 1.000 | 819 | 8 | 1.000 | ring breathing |
| $\nu_{28}$ | 748 | 38 | 1.000 | 754 | 12 | 0.997 | C-H wag |

[a] The numbering of the vibrational modes is according to calculated spectrum. [b] Intensity relative to the strongest band. [c] Ratio of frequencies of the natural $^{11}B$ vs $^{10}B$ isotopologues. [d] Computed absolute intensity: 840.0 km $mol^{-1}$

Table S3. Infrared Spectroscopic Data of $^{13}C^{16}(O_2)$ isotopologues of 3-Oxaziridinone **5** in Nitrogen matrix.

| Nitrogen matrix, 10 K | | | | B3LPY/6-311++G(2d,p) | | | |
|---|---|---|---|---|---|---|---|
| Vibrational Mode No.[a] | $\tilde{\upsilon}$, $cm^{-1}$ | I[b] | $\tilde{\upsilon}_i/\tilde{\upsilon}^c$ | $\tilde{\upsilon}$, $cm^{-1}$ | I[b] | $\tilde{\upsilon}_i/\tilde{\upsilon}^c$ | assignments |
| $\nu_5$ | 1900 | 100 | 1.000 | 1956 | 100[d] | 1.000 | carbonyl str |
| $\nu_9$ | 1457 | 17 | 1.000 | 1503 | 14 | 1.000 | skel. Ring, in pl. C-H |
| $\nu_{10}$ | 1392 | 92 | - | 1421 | 77 | 0.971 | B-N, ring str |
| $\nu_{11}$ | 1332 | 36 | 0.994 | 1360 | 37 | 0.996 | B-N, ring str |
| $\nu_{12}$ | 1312 | 2 | 0.993 | 1314 | 9 | 0.978 | in plane C-H |
| $\nu_{13}$ | 1303 | 21 | 1.000 | 1300 | 8 | 0.995 | in plane C-H |
| $\nu_{14}$ | 1236 | 63 | 1.000 | 1250 | 31 | 1.000 | C-O (of the ring), ring str |
| $\nu_{20}$ | - | - | - | 991 | 12 | 1.000 | NCO ring str |
| $\nu_{22}$ | 919 | 28 | 1.000 | 933 | 1 | 1.000 | C-H wag |
| $\nu_{26}$ | 802 | 17 | 1.000 | 818 | 9 | 1.000 | ring breathing |
| $\nu_{28}$ | 748 | 34 | 1.000 | 754 | 12 | 0.997 | C-H wag |

[a] The numbering of the vibrational modes is according to calculated spectrum. [b] Intensity relative to the strongest band. [c] Ratio of frequencies of the natural $^{11}B$ vs $^{10}B$ isotopologues. [d] Computed absolute intensity: 793.0 km $mol^{-1}$

| Table S4. Combination and overtone bands for the three isotopologues of **5** observed in experimental and computed spectra. | | |
|---|---|---|
| MP2/6-311++G(2d,p) | | Observed in Nitrogen matrix, 10 K |
| Combination/overtone | $\tilde{\nu}$, $cm^{-1}$ | $\tilde{\nu}$, $cm^{-1}$ |
| $^{12}C^{16}(O_2)$ isotopologues of 3-Oxaziridinone | | |
| $2^a\nu_{19}$ | 2036 | 2052 |
| $\nu_{30} + \nu_{32}$ | 1262 | 1284,1280 |
| $\nu_{24} + \nu_{38}$ | 1265 | |
| $\nu_{26} + \nu_{36}$ | 1285 | |
| $^{12}C^{18}(O_2)$ isotopologues of 3-Oxaziridinone | | |
| $2\nu_{20}$ | 1984 | 2018 |
| $\nu_{23} + \nu_{38}$ | 1281 | 1280,1276 |
| $\nu_{26} + \nu_{36}$ | 1273 | |
| $^{13}C^{16}(O_2)$ isotopologues of 3-Oxaziridinone | | |
| $2\nu_{20}$ | 1981 | 2010 |
| $\nu_{23} + \nu_{37}$ | 1288 | 1284 |
| $\nu_{26} + \nu_{36}$ | 1275 | |

[a] The $\nu_{19}$ vibration of $^{12}C^{16}(O_2)$ isotopologue of **5** is numbered as $\nu_{20}$ in $^{13}C$ and $^{18}O$ isotopologues of **5.**

Table S5. Analysis of the Fermi resonances involving the ν(C=O) stretching vibration ($\nu_5$) of the three isotopologues of **5** at the MP2/6-311++G(2d,p) level of theory.

| | $^{12}C(^{16}O)_2$ | | $^{13}C(^{16}O)_2$ | | $^{12}C(^{18}O)_2$ | |
|---|---|---|---|---|---|---|
| | anharm. | depert. | anharm. | depert. | anharm. | depert. |
| $\nu_5$ | 1906 | 1951 | 1863 | 1888 | 1859 | 1907 |
| $\nu_{19} + \nu_{19}$/ $\nu^a_{20} + \nu^a_{20}$ | 2036 | 1992 | 1982 | 1948 | 1984 | 1942 |
| $\nu_{18} + \nu_{24}$ | --- | --- | 1906 | 1905 | 1893 | 1887 |
| $\nu_{20} + \nu_{24}$ | --- | --- | 1806 | 1816 | --- | --- |

[a] The $\nu_{19}$ vibration of $^{12}C^{16}(O_2)$ isotopologue of **5** is numbered as $\nu_{20}$ in $^{13}C$ and $^{18}O$ isotopologues of **5.**

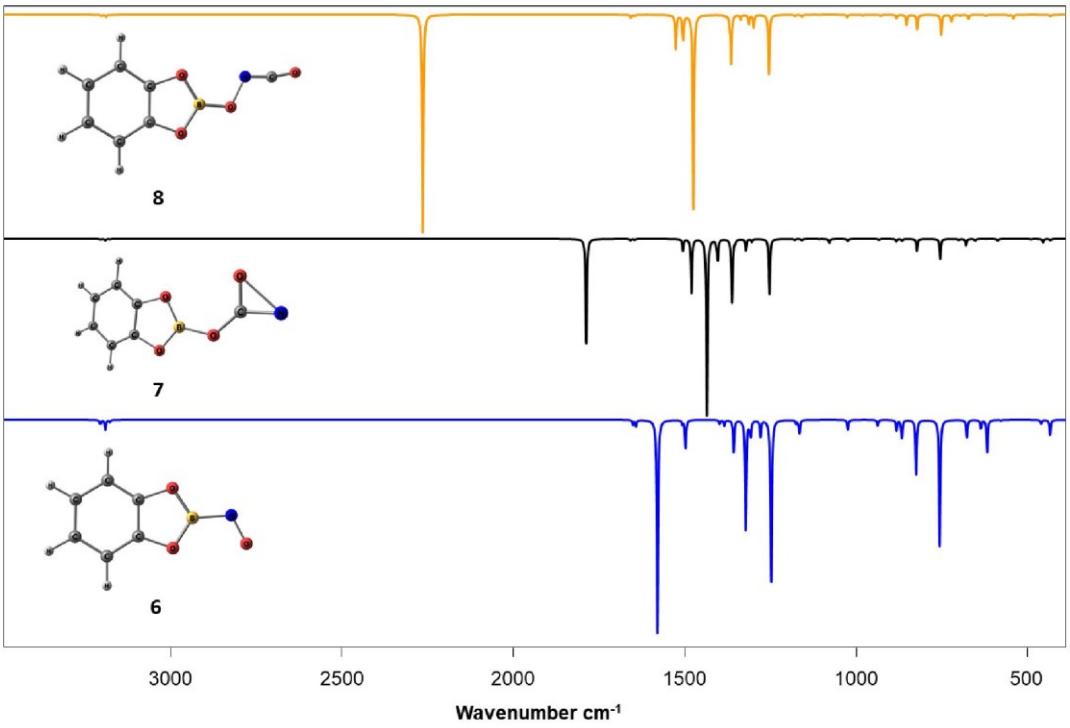


Figure S1. Comparison of the computed spectra of species **6**, **7** and **8** at B3LYP/6-311++G(2d,p) level of theory.

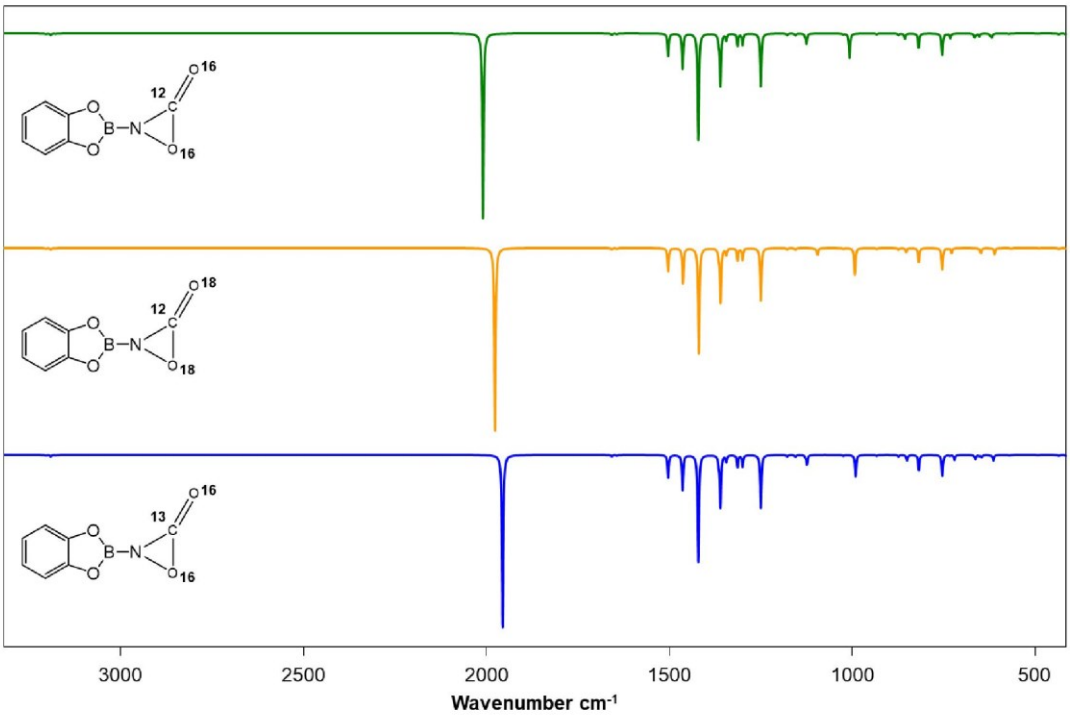


Figure S2. Comparison of computed Harmonic Infrared spectra of isotopologues of **5** formed as the result of reaction of $^{12}C(^{16}O)_2$, $^{13}C(^{16}O)_2$, and $^{12}C(^{18}O)_2$ with **3** at B3LYP/6-311++G(2d,p) level of theory.

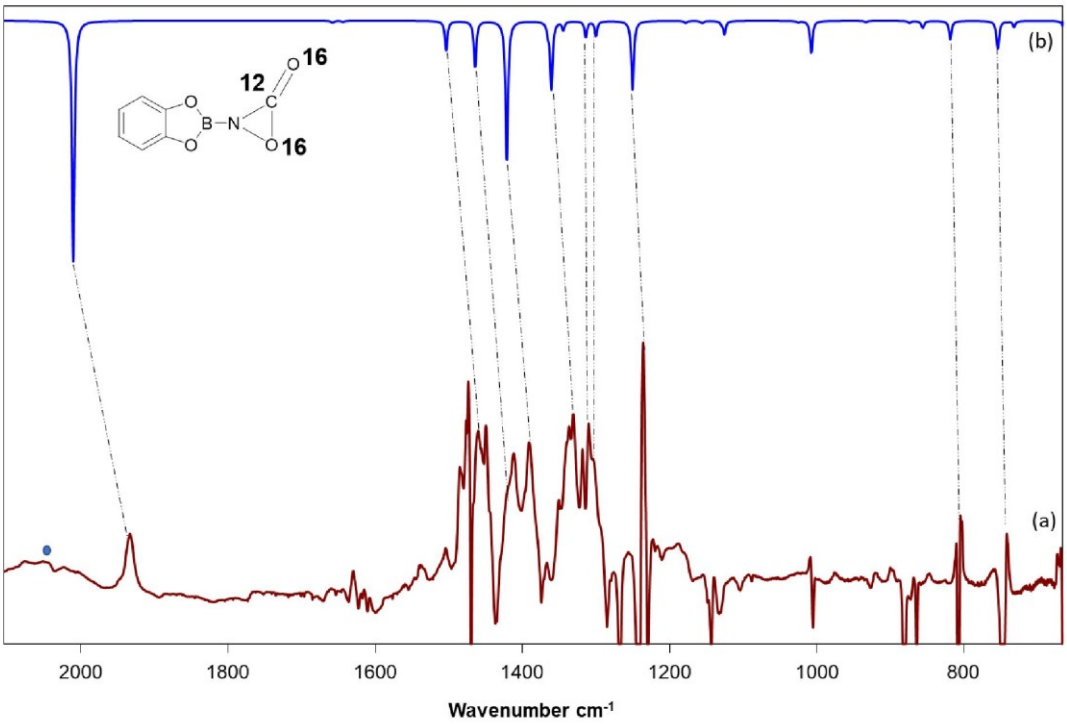


Figure S3. (a) Difference spectrum obtained after irradiation of Ar matrix with λ > 550 nm (following the irradiation with λ = 254 nm) in the presence of $CO_2$. (b) Calculated spectrum for $^{11}B$ and $^{10}B$ isotopologues (81:19) of 3-oxaziridinone **5** at the B3LYP/6-311++G(2d,p) level.

- Correspond to the signals for overtones/combination bands of the resulting product.

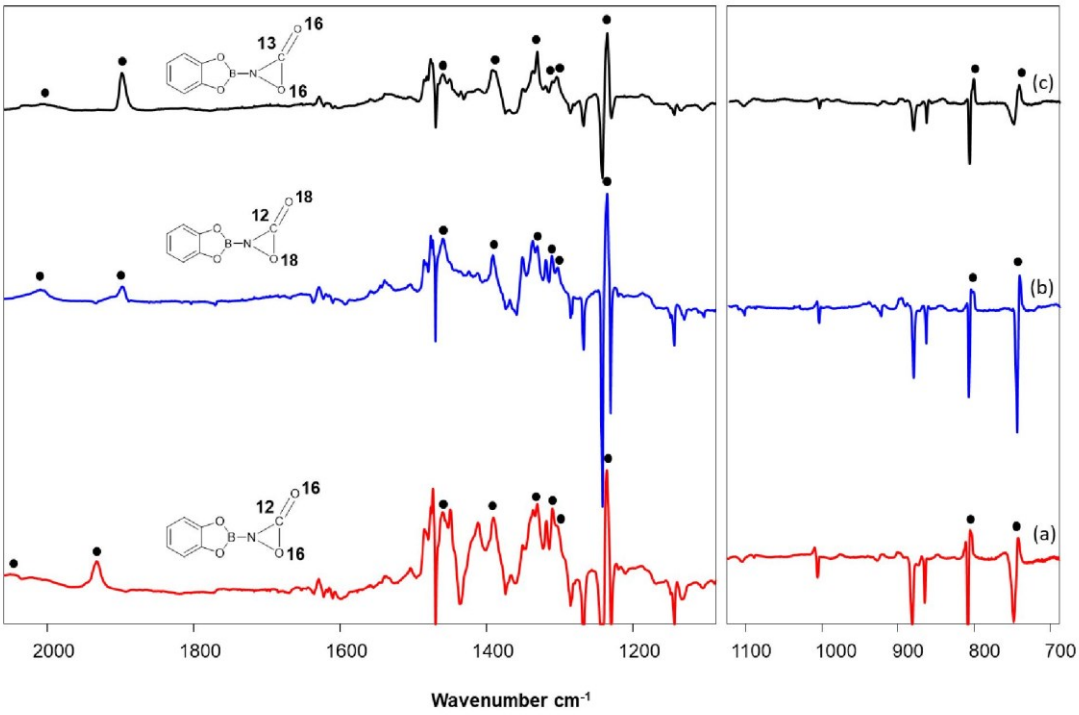


Figure S4. Difference spectra obtained after irradiation of Ar matrix with λ > 550 nm (following the irradiation with λ = 254 nm) in the presence of a) $^{12}C(^{16}O)_2$, after 100 min, b) $^{12}C(^{18}O)_2$, after 90 min, c) $^{13}C(^{16}O)_2$, after 60 min in solid Ar at 10 K. ● Correspond to the fundamental and overtone/combination bands in three of the isotopologues of **5**.

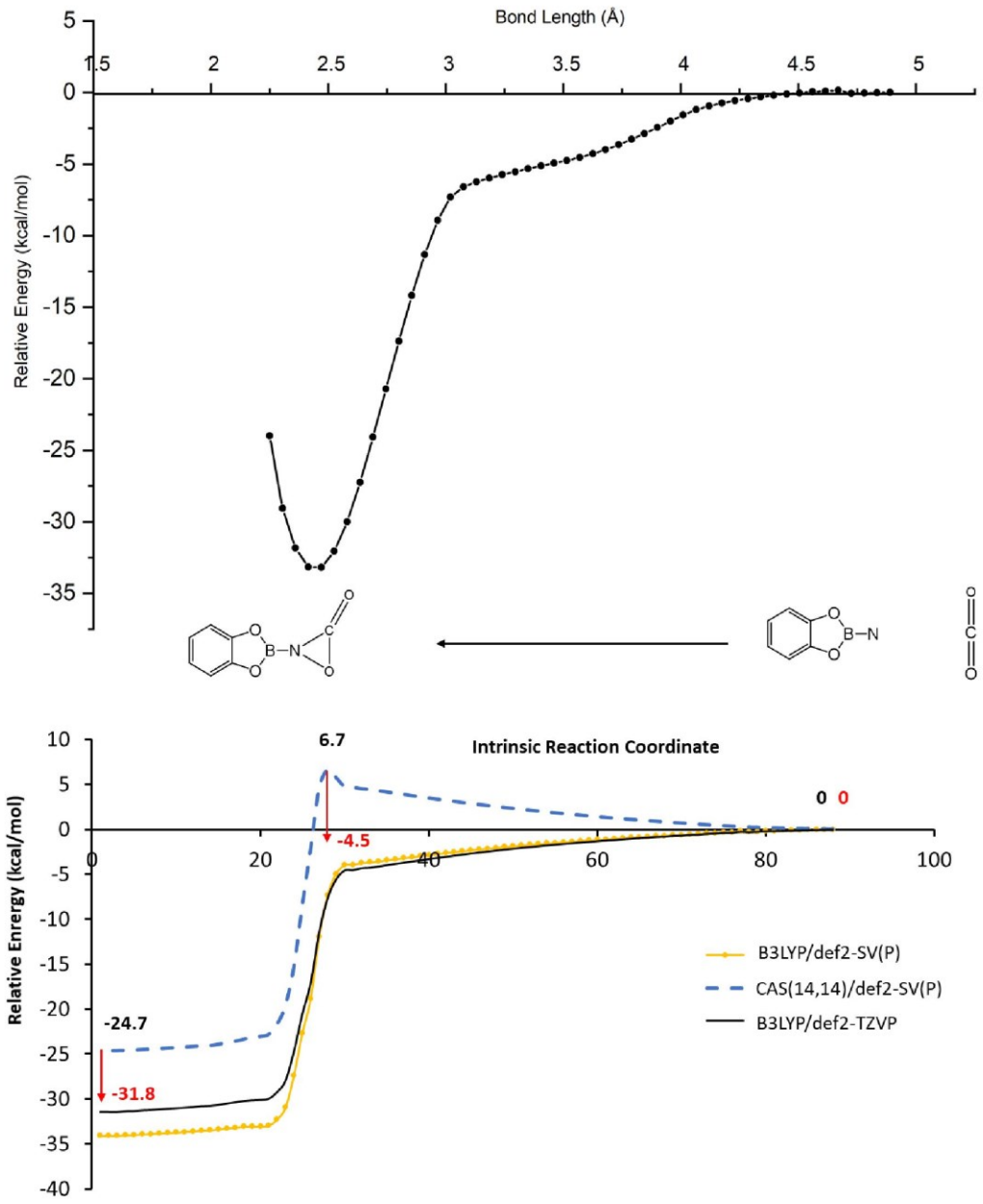


Figure S5. a) The relaxed potential energy scan between oxygen atom of $CO_2$ and nitrogen atom of borylnitrene **3** at B3LYP/6-311++G(2d,p). b) Intrinsic reaction coordinate calculation for TS connecting the reactants $^1A_1$-**3** + $CO_2$ and product **5** at CASSCF(14,14)/def2-SV(P) level of theory**.** The single point energies at the geometries obtained from above IRC calculation, computed at B3LYP with def2-SV(P) and def2-TZVP basis sets, are also inlcuded. Energies obtained after single point calculations at NEVPT2/def2-SV(P) level of theory at three geometries corresponding to first IRC point, TS, and last IRC point are shown in red font.

a)

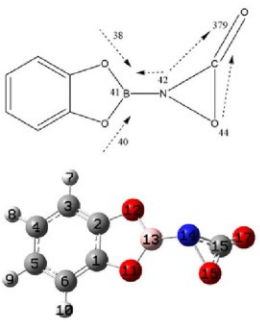

| Donor NBO (i) | Acceptor NBO (j) | E(2) E(j)-E(i) F(i,j) kcal/mol |
|---|---|---|
| 38. LP (2) O 11 | 41. LP*(1) B 13 | 60.34 |
| 40. LP (2) O 12 | 41. LP*(1) B13 | 59.11 |
| 42. LP (1) N 14 | 41. LP*(1) B13 | 27.29 |
| 42. LP (1) N 14 | 379. BD*(2) C15 - O17 | 7.95 |
| 44. LP (2) O 16 | 379. BD*(2) C15 - O17 | 27.60 |

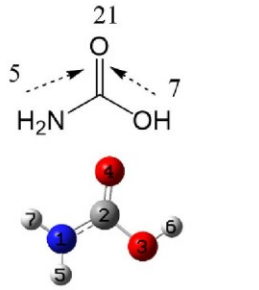

| Donor NBO (i) | Acceptor NBO (j) | E(2) E(j)-E(i) F(i,j) kcal/mol |
|---|---|---|
| 5. LP ( 1) N 1 | 21. BD*( 1) C 2- O 4 | 30.60 |
| 7. LP ( 2) O 3 | 21. BD*( 1) C 2- O 4 | 22.88 |

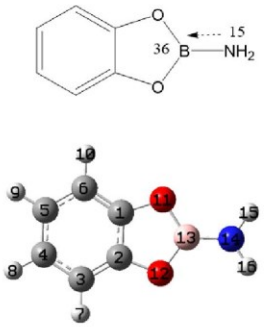

| Donor NBO (i) | Acceptor NBO (j) | E(2) E(j)-E(i) F(i,j) kcal/mol |
|---|---|---|
| 15. LP ( 1) N 14 | 36. LP* ( 1) B 13 | 77.92 |

b)

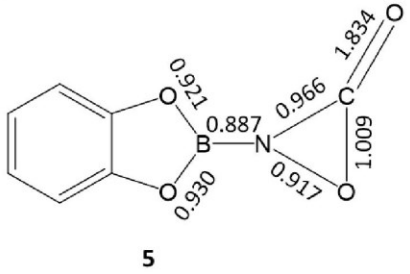


**5**

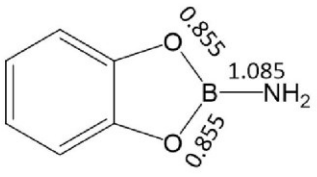


**9**

Figure S6. a) Second order perturbation interaction calculated at B3LYP/6-311++G(2d,p) between the π natural bond orbital and lone pairs on the three-membered ring in **5,** carbamic acid, and boryl amine **9**. b) Wiberg bond indices of **5** and **9** calculated using NBO calculations at B3LYP/6-311++G(2d,p).

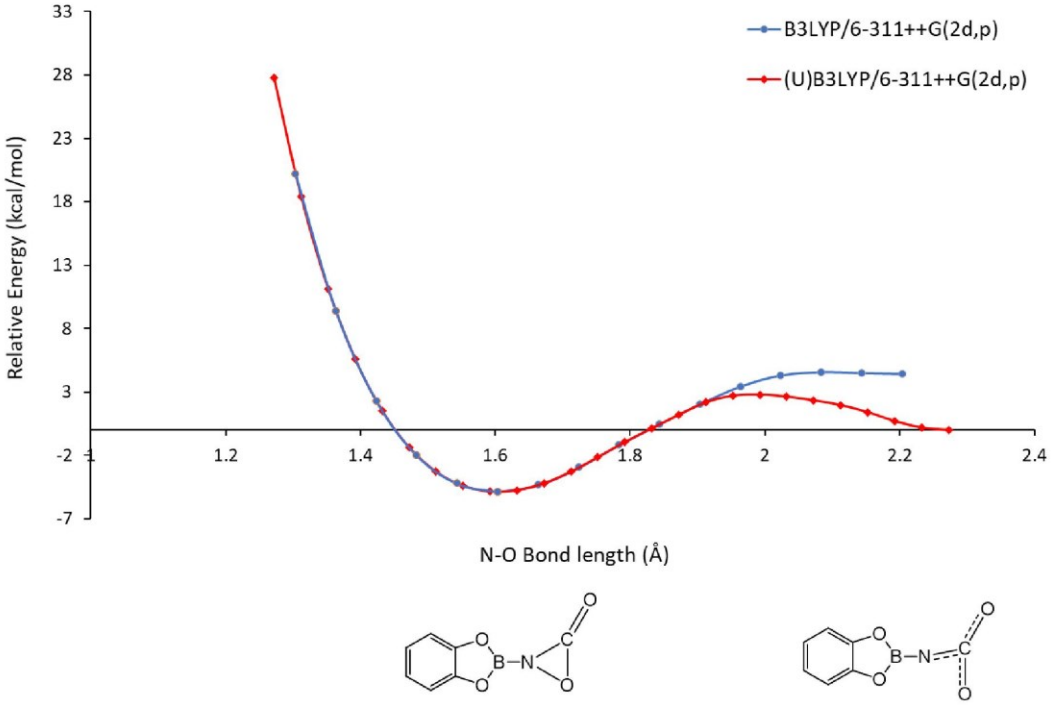


Figure S7. Relaxed potential energy surface calculated with the N-O bond length as the scan parameter at B3LYP/6-311++G(2d,p) and (U)B3LYP/6-311++G(2d,p) which resulted in two minima and one them corresponds to **5**.

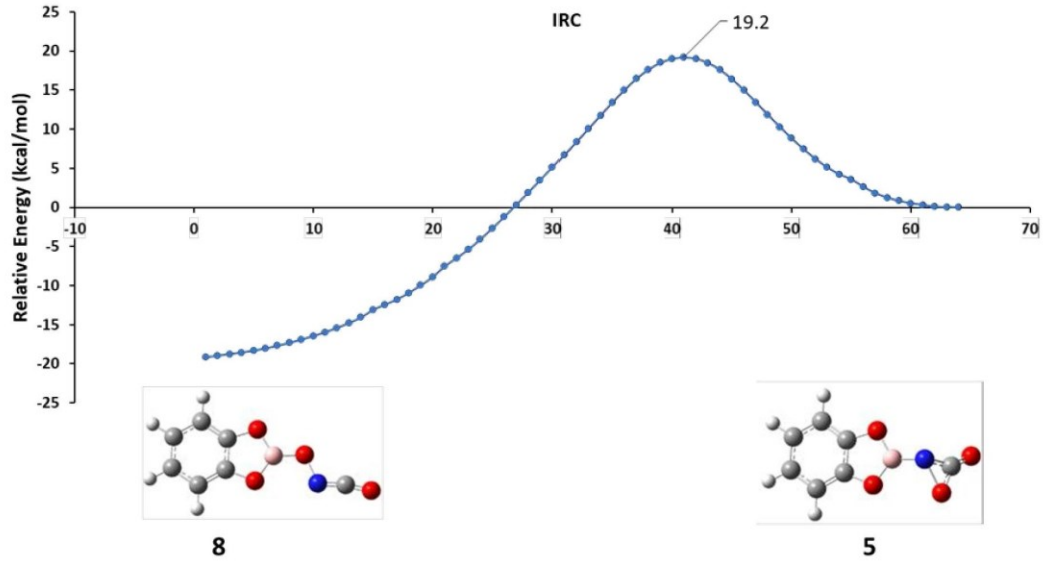


Figure S8. Intrinsic reaction coordinate calculation at B3LYP/6-311++G(2d,p) corresponding to the transition state connecting **5** and **8**.

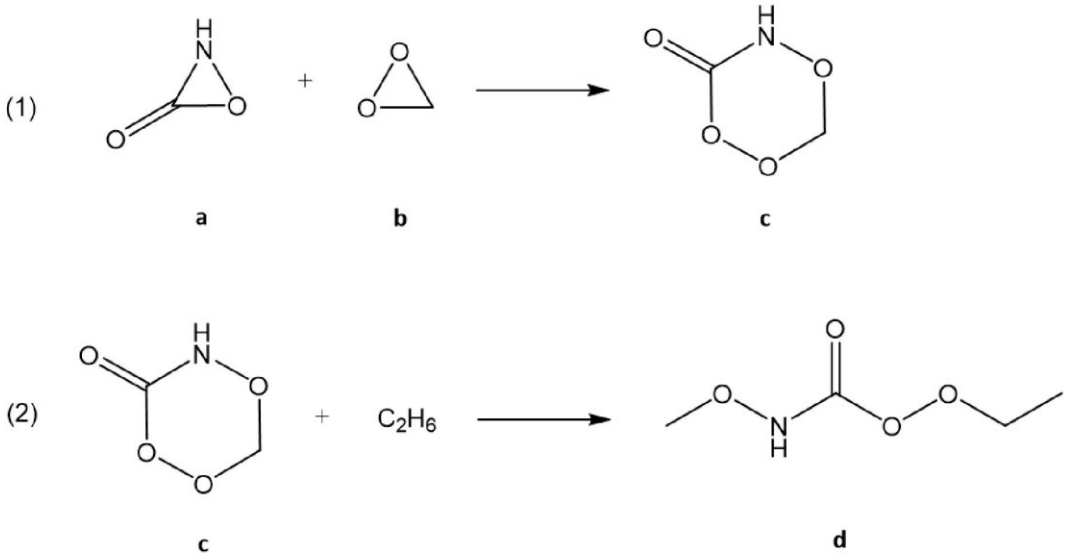


$$E_{strain,\,a} = [(E_a + E_b) - E_c] - E_{strain,\,b}$$

$$E'_{strain,\,a} = E_{strain,\,a} + E_{strain,\,c}$$

$$E_{strain,\,c} = -\Delta H_r(\text{of reaction 2})$$

Figure S9. Strain energy calculation for an oxaziridinone using combination with a three-member ring compounds dioxirane.

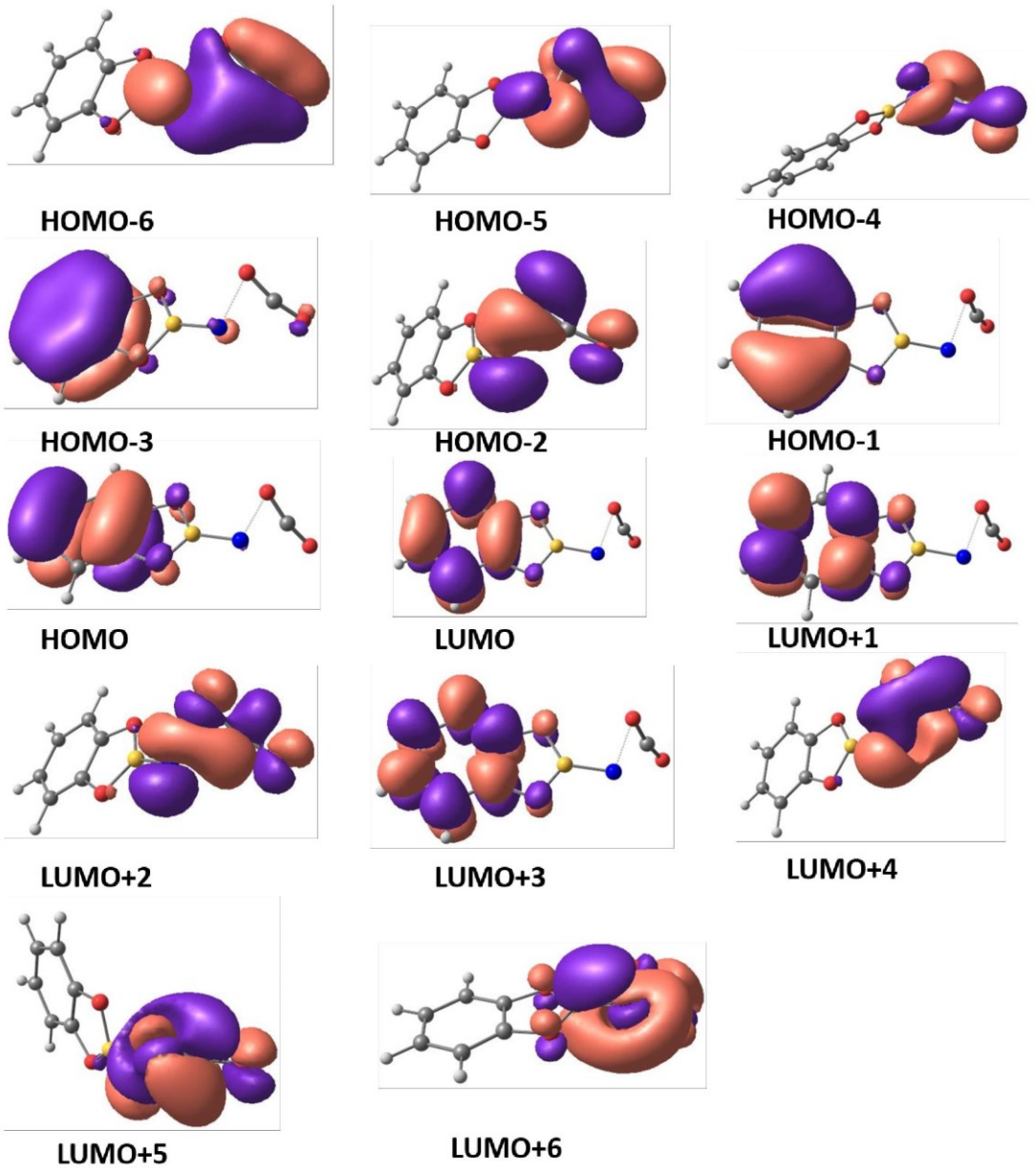


Figure S10. Active space orbitals used for the calculation of TS connecting the reactants $^1A_1$-**3** + $CO_2$ and product **5** at CASSCF(14,14)/def2-SV(P) level of theory.

Cartesian Coordinates and their corresponding energies (with zero point correction, in Hartree) of all the optimized species.

**$^1A_1$-3**

E = -461.07045

Spin = 0

Level of theory = B3LYP/6-311++G(2d,p)

| | | | |
|---|---|---|---|
| C | 0.06590600 | 0.69390800 | 0.00000000 |
| C | 0.06590600 | -0.69390800 | 0.00000000 |
| C | 1.23148200 | -1.42641200 | 0.00000000 |
| C | 2.42574900 | -0.69616500 | 0.00000000 |
| C | 2.42574900 | 0.69616500 | 0.00000000 |
| C | 1.23148200 | 1.42641200 | 0.00000000 |
| H | 1.21879400 | -2.50813200 | 0.00000000 |
| H | 3.36794400 | -1.22971100 | 0.00000100 |
| H | 3.36794400 | 1.22971100 | 0.00000000 |
| H | 1.21879400 | 2.50813200 | 0.00000000 |
| O | -1.24253100 | 1.16535700 | 0.00000000 |
| O | -1.24253100 | -1.16535700 | -0.00000100 |
| B | -2.00175500 | 0.00000000 | 0.00000000 |
| N | -3.42312100 | 0.00000000 | 0.00000100 |

**$^3A_2$-3**

E = -461.13261

Spin = 1

Level of theory = B3LYP/6-311++G(2d,p)

| | | | |
|---|---|---|---|
| C | 0.06726600 | 0.69717600 | 0.00000100 |
| C | 0.06726600 | -0.69717600 | 0.00000100 |
| C | 1.23805600 | -1.43002300 | 0.00000000 |

| | | | |
|---|---|---|---|
| C | 2.42584300 | -0.69955500 | -0.00000100 |
| C | 2.42584300 | 0.69955400 | -0.00000100 |
| C | 1.23805700 | 1.43002300 | 0.00000000 |
| H | 1.22673400 | -2.51180900 | 0.00000000 |
| H | 3.37060800 | -1.22840000 | -0.00000100 |
| H | 3.37060900 | 1.22839800 | -0.00000100 |
| H | 1.22673600 | 2.51181000 | 0.00000000 |
| O | -1.22821400 | 1.14867500 | 0.00000100 |
| O | -1.22821500 | -1.14867400 | 0.00000100 |
| B | -2.01539600 | 0.00000100 | 0.00000100 |
| N | -3.46289500 | -0.00000100 | -0.00000200 |

**5**

E = -649.76594

Spin = 0

Level of theory = B3LYP/6-311++G(2d,p)

| | | | |
|---|---|---|---|
| C | -1.16693500 | 0.66336900 | -0.02699900 |
| C | -1.22047700 | -0.71926000 | -0.14634100 |
| C | -2.40029400 | -1.42039300 | -0.03580400 |
| C | -3.55080600 | -0.66228200 | 0.20278800 |
| C | -3.49738600 | 0.72601600 | 0.32177600 |
| C | -2.29075400 | 1.42339300 | 0.20800200 |
| H | -2.43006800 | -2.49771800 | -0.12972000 |
| H | -4.50374500 | -1.16740900 | 0.29687900 |
| H | -4.40957800 | 1.27898900 | 0.50672300 |
| H | -2.23720700 | 2.50001900 | 0.29939900 |
| O | 0.14796200 | 1.08432300 | -0.17949900 |
| O | 0.05929900 | -1.20589700 | -0.37987700 |
| B | 0.84780600 | -0.07803700 | -0.38836600 |
| N | 2.26847100 | -0.16047400 | -0.69174200 |

| | | | |
|---|---|---|---|
| C | 3.30242300 | -0.11729100 | 0.21981200 |
| O | 3.10065000 | 1.12269300 | -0.20790600 |
| O | 3.99304500 | -0.74633000 | 0.93620100 |

**6**

E = -536.38685

Spin = 0

Level of theory = B3LYP/6-311++G(2d,p)

| | | | |
|---|---|---|---|
| C | -0.44331000 | 0.64461400 | -0.00000800 |
| C | -0.57322800 | -0.74062800 | 0.00000000 |
| C | -1.80385600 | -1.36370800 | 0.00001100 |
| C | -2.91977100 | -0.52539900 | 0.00001300 |
| C | -2.78958500 | 0.86590800 | 0.00000400 |
| C | -1.53789200 | 1.48386600 | -0.00000700 |
| H | -1.89261300 | -2.44188300 | 0.00001700 |
| H | -3.90927000 | -0.96471700 | 0.00002100 |
| H | -3.68065900 | 1.48087700 | 0.00000600 |
| H | -1.42616500 | 2.55987800 | -0.00001300 |
| O | 0.89831000 | 0.97092300 | -0.00001600 |
| O | 0.68530300 | -1.30770000 | -0.00000800 |
| B | 1.55006200 | -0.23892500 | -0.00001400 |
| N | 3.04369900 | -0.47878500 | -0.00003200 |
| O | 3.69868100 | 0.55228300 | 0.00004700 |

**7**

E = -649.75320

Spin = 0

Level of theory = B3LYP/6-311++G(2d,p)

| | | | |
|---|---|---|---|
| C | 1.06501700 | 0.58399900 | 0.00000200 |
| C | 1.34179400 | -0.77721400 | -0.00000100 |

| | | | |
|---|---|---|---|
| C | 2.63015000 | -1.26272100 | -0.00000300 |
| C | 3.65184500 | -0.30793600 | -0.00000200 |
| C | 3.37314300 | 1.05832400 | 0.00000100 |
| C | 2.05892600 | 1.53621000 | 0.00000300 |
| H | 2.83524400 | -2.32494900 | -0.00000500 |
| H | 4.68232700 | -0.63987600 | -0.00000300 |
| H | 4.19110000 | 1.76753300 | 0.00000200 |
| H | 1.83028600 | 2.59357000 | 0.00000500 |
| O | -0.31245900 | 0.76762500 | 0.00000300 |
| O | 0.14770200 | -1.48454800 | -0.00000100 |
| B | -0.81922500 | -0.50852500 | 0.00000100 |
| C | -3.16212100 | -0.02176500 | 0.00000000 |
| O | -2.15431500 | -0.86684900 | 0.00000300 |
| O | -3.21261900 | 1.25165000 | -0.00001000 |
| N | -4.42026100 | -0.15000700 | 0.00000500 |

**8**

E = -649.80019

Spin = 0

Level of theory = B3LYP/6-311++G(2d,p)

| | | | |
|---|---|---|---|
| C | -1.23949100 | -0.62481400 | 0.00000100 |
| C | -1.47195900 | 0.74601400 | 0.00000000 |
| C | -2.74459200 | 1.27155400 | -0.00000100 |
| C | -3.79893100 | 0.35179800 | -0.00000200 |
| C | -3.56558900 | -1.02212900 | -0.00000100 |
| C | -2.26641400 | -1.54158700 | 0.00000000 |
| H | -2.91461800 | 2.34009400 | -0.00000200 |
| H | -4.81771800 | 0.71840900 | -0.00000300 |
| H | -4.40604200 | -1.70471200 | -0.00000200 |
| H | -2.07330700 | -2.60618400 | 0.00000000 |

| | | | |
|---|---|---|---|
| O | 0.12751500 | -0.85710300 | 0.00000200 |
| O | -0.25974100 | 1.41555300 | 0.00000100 |
| B | 0.68301800 | 0.40436200 | 0.00000200 |
| O | 2.01362100 | 0.72724900 | 0.00000200 |
| O | 5.23209800 | -0.24651100 | -0.00000500 |
| N | 2.85550800 | -0.40447900 | 0.00000500 |
| C | 4.07032700 | -0.22276300 | -0.00000100 |

**9**

E = -462.46696

Spin = 0

Level of theory = B3LYP/6-311++G(2d,p)

| | | | |
|---|---|---|---|
| C | 0.17633200 | 0.69615400 | 0.00000000 |
| C | 0.17633200 | -0.69615400 | 0.00000000 |
| C | 1.34557600 | -1.42423600 | 0.00000000 |
| C | 2.54161300 | -0.69628900 | 0.00000000 |
| C | 2.54161300 | 0.69628900 | 0.00000000 |
| C | 1.34557600 | 1.42423600 | 0.00000000 |
| H | 1.33463900 | -2.50645000 | 0.00000000 |
| H | 3.48410400 | -1.22959200 | 0.00000000 |
| H | 3.48410500 | 1.22959100 | 0.00000000 |
| H | 1.33464000 | 2.50645000 | 0.00000000 |
| O | -1.12383900 | 1.15507300 | 0.00000000 |
| O | -1.12383900 | -1.15507300 | 0.00000000 |
| B | -1.91267800 | 0.00000000 | 0.00000000 |
| N | -3.30844600 | 0.00000000 | 0.00000000 |
| H | -3.84790300 | 0.84839500 | -0.00000100 |
| H | -3.84790000 | -0.84839600 | 0.00000100 |

**CO**

E = -113.34698

Spin = 0

Level of theory = B3LYP/6-311++G(2d,p)

| | | | |
|---|---|---|---|
| O | 0.00000000 | 0.00000000 | 0.48242700 |
| C | 0.00000000 | 0.00000000 | -0.64323600 |

**$CO_2$**

E = -188.63898

Spin = 0

Level of theory = B3LYP/6-311++G(2d,p)

| | | | |
|---|---|---|---|
| C | 0.00000000 | 0.00000000 | 0.00000000 |
| O | 0.00000000 | 0.00000000 | -1.16035800 |
| O | 0.00000000 | 0.00000000 | 1.1603580 |

**Carbamic acid**

E = -245.18192

Spin = 0

Level of theory = B3LYP/6-311++G(2d,p)

| | | | |
|---|---|---|---|
| N | -1.26785600 | -0.25331300 | -0.03772300 |
| C | 0.03602400 | 0.12442400 | -0.00157900 |
| O | 0.85540100 | -0.96410000 | 0.00214900 |
| O | 0.44197900 | 1.26350300 | 0.00463500 |
| H | -1.51878800 | -1.21518700 | 0.11539400 |
| H | 1.75795500 | -0.61635900 | 0.00356000 |
| H | -1.95935600 | 0.46297200 | 0.10030900 |

**Diradicaloid isomer of 5**

E = -649.76029

Spin = 0

Level of theory = B3LYP/6-311++G(2d,p)

| | | | |
|---|---|---|---|
| C | -2.65689800 | -1.26150600 | 0.00000100 |
| C | -3.66859100 | -0.31232000 | 0.00000400 |
| C | -3.39212300 | 1.07039400 | 0.00000300 |
| C | -2.09306100 | 1.55824300 | 0.00000000 |
| H | -2.85835500 | -2.32415800 | 0.00000200 |
| H | -4.70078700 | -0.63876900 | 0.00000700 |
| H | -4.21945700 | 1.76864300 | 0.00000500 |
| H | -1.87070900 | 2.61669800 | 0.00000000 |
| B | 0.83019500 | -0.49396100 | -0.00000600 |
| O | 0.25300200 | 0.79349400 | -0.00000400 |
| C | -1.08304400 | 0.60850100 | -0.00000200 |
| C | -1.35860400 | -0.77311600 | -0.00000200 |
| O | -0.19825600 | -1.45788100 | -0.00000500 |
| N | 2.17740900 | -0.82804600 | -0.00000700 |
| O | 3.75078600 | 0.41609000 | 1.06782300 |
| C | 3.21996500 | 0.02667400 | 0.00000000 |
| O | 3.75079400 | 0.41610900 | -1.06781000 |

TS connecting the $^1A_1$-**3** + $CO_2$ and **5**

E = -645.52169

Spin = 0

Level of theory = CASSCF(14,14)/def2-SV(P)

| | | | |
|---|---|---|---|
| C | -2.63255100 | -1.29191900 | -0.14719700 |
| C | -3.67231800 | -0.34306900 | -0.21546300 |
| C | -3.41933200 | 1.02470900 | -0.07343400 |
| C | -2.11378800 | 1.50911500 | 0.14364700 |
| H | -2.81496500 | -2.35162600 | -0.25425000 |
| H | -4.68675900 | -0.68178500 | -0.38070600 |
| H | -4.24101000 | 1.72660600 | -0.13075100 |
| H | -1.90462600 | 2.56338700 | 0.25604400 |

| | | | |
|---|---|---|---|
| B | 0.77616300 | -0.51265800 | 0.37973500 |
| O | 0.23129600 | 0.74735700 | 0.40259300 |
| C | -1.10756900 | 0.56491600 | 0.20651200 |
| C | -1.35938900 | -0.79943400 | 0.06523000 |
| O | -0.18260700 | -1.47819100 | 0.17569200 |
| N | 2.14942500 | -0.90449600 | 0.50736900 |
| O | 4.19725900 | 0.23852700 | -1.08837500 |
| C | 3.51829200 | 0.35767700 | -0.18987600 |
| O | 2.93931700 | 0.71248800 | 0.77756700 |

Cartesian Coordinates and their corresponding energies (with zero point correction, in Hartree) of all the optimized species used in strain energy calculation of **5**. The procedure shown in Figure S7 is followed in strain energy calculation of **5.**

**Dioxirane**

E = -189.64981

Spin = 0

Level of theory = B3LYP/6-311++G(2d,p)

| | | | |
|---|---|---|---|
| C | 0.00000000 | 0.73196800 | 0.00000000 |
| H | 0.00000000 | 1.30127500 | 0.92846500 |
| H | 0.00000000 | 1.30127500 | -0.92846500 |
| O | -0.75117900 | -0.43714700 | 0.00000000 |
| O | 0.75117900 | -0.43714700 | 0.00000000 |

E = -189.38367

Spin = 0

Level of theory = CBS-QB3

| | | | |
|---|---|---|---|
| C | 0.00000000 | 0.73196800 | 0.00000000 |
| H | 0.00000000 | 1.30127500 | 0.92846500 |
| H | 0.00000000 | 1.30127500 | -0.92846500 |
| O | -0.75117900 | -0.43714700 | 0.00000000 |
| O | 0.75117900 | -0.43714700 | 0.00000000 |

**5**

E = -649.76594

Spin = 0

Level of theory = B3LYP/6-311++G(2d,p)

| | | | |
|---|---|---|---|
| C | -1.16693500 | 0.66336900 | -0.02699900 |
| C | -1.22047700 | -0.71926000 | -0.14634100 |
| C | -2.40029400 | -1.42039300 | -0.03580400 |
| C | -3.55080600 | -0.66228200 | 0.20278800 |
| C | -3.49738600 | 0.72601600 | 0.32177600 |
| C | -2.29075400 | 1.42339300 | 0.20800200 |
| H | -2.43006800 | -2.49771800 | -0.12972000 |
| H | -4.50374500 | -1.16740900 | 0.29687900 |
| H | -4.40957800 | 1.27898900 | 0.50672300 |
| H | -2.23720700 | 2.50001900 | 0.29939900 |
| O | 0.14796200 | 1.08432300 | -0.17949900 |
| O | 0.05929900 | -1.20589700 | -0.37987700 |
| B | 0.84780600 | -0.07803700 | -0.38836600 |
| N | 2.26847100 | -0.16047400 | -0.69174200 |
| C | 3.30242300 | -0.11729100 | 0.21981200 |
| O | 3.10065000 | 1.12269300 | -0.20790600 |
| O | 3.99304500 | -0.74633000 | 0.93620100 |

E = -648.75045

Spin = 0

Level of theory = CBS-QB3

| | | | |
|---|---|---|---|
| C | -1.16836800 | 0.66570100 | -0.02708200 |
| C | -1.21826000 | -0.72033800 | -0.14575700 |
| C | -2.39925300 | -1.42489000 | -0.03528100 |
| C | -3.55357100 | -0.66851400 | 0.20275900 |
| C | -3.50374900 | 0.72206700 | 0.32114400 |
| C | -2.29711500 | 1.42362100 | 0.20715200 |

| | | | |
|---|---|---|---|
| H | -2.42415600 | -2.50266500 | -0.12917300 |
| H | -4.50569200 | -1.17651400 | 0.29672000 |
| H | -4.41791500 | 1.27325000 | 0.50528400 |
| H | -2.24432500 | 2.50072300 | 0.29719600 |
| O | 0.14485000 | 1.08889700 | -0.18105100 |
| O | 0.06232000 | -1.20259300 | -0.37884100 |
| B | 0.84939700 | -0.07204300 | -0.38955200 |
| N | 2.26853200 | -0.14995400 | -0.69033100 |
| C | 3.30683000 | -0.11828900 | 0.21898800 |
| O | 3.09873500 | 1.12362200 | -0.19302000 |
| O | 4.00238200 | -0.75505800 | 0.92272500 |

**Six membered ring addition product resulted from addition of 5 with dioxirane**

E = -839.49427

Spin = 0

Level of theory = B3LYP/6-311++G(2d,p)

| | | | |
|---|---|---|---|
| C | 2.04719500 | 0.65171000 | 0.01096800 |
| C | 2.03188600 | -0.73663000 | -0.02890100 |
| C | 3.18956400 | -1.48286600 | -0.02958300 |
| C | 4.39025500 | -0.76683400 | 0.01240800 |
| C | 4.40551700 | 0.62685800 | 0.05259700 |
| C | 3.22123800 | 1.37070100 | 0.05263700 |
| H | 3.16607600 | -2.56410600 | -0.06169200 |
| H | 5.32740200 | -1.30911300 | 0.01320800 |
| H | 5.35444700 | 1.14728700 | 0.08404900 |
| H | 3.22031100 | 2.45214800 | 0.08304900 |
| O | 0.74548800 | 1.12418800 | 0.00029700 |
| O | 0.71867200 | -1.17554900 | -0.06404100 |
| B | -0.02775100 | -0.01383400 | -0.04460200 |
| C | -2.30889900 | 1.04580400 | -0.03940600 |

| | | | |
|---|---|---|---|
| C | -3.25588300 | -1.41033800 | 0.40925700 |
| H | -3.65155700 | -2.40962900 | 0.23194200 |
| H | -3.17309400 | -1.17102000 | 1.47415700 |
| N | -1.46978600 | -0.05140600 | -0.06777000 |
| O | -4.13283200 | -0.53472700 | -0.23523000 |
| O | -3.66505500 | 0.83079400 | 0.03369800 |
| O | -2.00311100 | -1.36260500 | -0.22125500 |
| O | -1.93085600 | 2.17952600 | 0.01563500 |

E = -838.21402

Spin = 0

Level of theory = CBS-QB3

| | | | |
|---|---|---|---|
| C | 2.04644400 | 0.65279900 | 0.01030700 |
| C | 2.03192200 | -0.73875400 | -0.02667700 |
| C | 3.19297600 | -1.48468000 | -0.02698800 |
| C | 4.39484700 | -0.76641200 | 0.01268800 |
| C | 4.40914000 | 0.62939600 | 0.05021700 |
| C | 3.22252100 | 1.37351300 | 0.04969500 |
| H | 3.16821500 | -2.56627800 | -0.05704700 |
| H | 5.33289200 | -1.30838400 | 0.01378300 |
| H | 5.35814200 | 1.15107700 | 0.07991600 |
| H | 3.21861600 | 2.45534100 | 0.07782900 |
| O | 0.74413900 | 1.12264200 | -0.00066500 |
| O | 0.71932900 | -1.17760900 | -0.06008800 |
| B | -0.02899800 | -0.01660900 | -0.04323900 |
| C | -2.31027800 | 1.05146200 | -0.03937900 |
| C | -3.25673700 | -1.41427100 | 0.40457900 |
| H | -3.65194400 | -2.41266800 | 0.22013500 |
| H | -3.17588000 | -1.18036100 | 1.47201000 |
| N | -1.47152500 | -0.05196200 | -0.06407700 |
| O | -4.13361100 | -0.53532500 | -0.23860900 |

| | | | |
|---|---|---|---|
| O | -3.66747500 | 0.83061000 | 0.04264900 |
| O | -2.00331400 | -1.36320700 | -0.22581400 |
| O | -1.93274100 | 2.18410500 | 0.01396000 |

**Ethane**

E = -79.78408

Spin = 0

Level of theory = B3LYP/6-311++G(2d,p)

| | | | |
|---|---|---|---|
| C | 0.00000000 | 0.00000000 | 0.76438200 |
| H | 0.00000000 | 1.01767200 | 1.16224900 |
| H | -0.88133000 | -0.50883600 | 1.16224900 |
| H | 0.88133000 | -0.50883600 | 1.16224900 |
| C | 0.00000000 | 0.00000000 | -0.76438200 |
| H | 0.88133000 | 0.50883600 | -1.16224900 |
| H | 0.00000000 | -1.01767200 | -1.16224900 |
| H | -0.88133000 | 0.50883600 | -1.16224900 |

E = -79.63057

Spin = 0

Level of theory = CBS-QB3

| | | | |
|---|---|---|---|
| C | 0.00000000 | 0.00000000 | 0.76527200 |
| H | 0.00000000 | 1.01835400 | 1.16385600 |
| H | -0.88192100 | -0.50917700 | 1.16385600 |
| H | 0.88192100 | -0.50917700 | 1.16385600 |
| C | 0.00000000 | 0.00000000 | -0.76527200 |
| H | 0.88192100 | 0.50917700 | -1.16385600 |
| H | 0.00000000 | -1.01835400 | -1.16385600 |
| H | -0.88192100 | 0.50917700 | -1.16385600 |

**Ring opened product resulted after the addition of six membered ring species and ethene**

E = -919.28275

Spin = 0

Level of theory = B3LYP/6-311++G(2d,p)

| | | | |
|---|---|---|---|
| C | 2.01679900 | 4.01467400 | 0.06310000 |
| H | 2.91324800 | 3.97027700 | -0.55698800 |
| H | 1.19462700 | 4.40928800 | -0.53614900 |
| C | 1.67771800 | 2.64638500 | 0.61266200 |
| H | 0.77344000 | 2.67280300 | 1.22809000 |
| H | 2.50420900 | 2.23037400 | 1.19196700 |
| C | 2.24564300 | -0.32419500 | 0.01683900 |
| C | 3.49900200 | -3.05684100 | -0.57031600 |
| H | 3.97176600 | -2.30638900 | -1.20544600 |
| H | 4.25652200 | -3.72410700 | -0.15590300 |
| H | 2.75567500 | -3.63441200 | -1.12356900 |
| H | 2.20311300 | 4.70371000 | 0.88969700 |
| O | 3.37809500 | 0.05795700 | 0.02878700 |
| N | 1.12218400 | 0.48633600 | -0.14273800 |
| O | 1.82696800 | -1.62460400 | 0.14244700 |
| O | 2.91770800 | -2.45806400 | 0.58506900 |
| O | 1.43499500 | 1.79406800 | -0.53151700 |
| B | -0.27936000 | 0.18149800 | -0.10310700 |
| O | -1.23779400 | 1.16741000 | -0.28286000 |
| O | -0.84138200 | -1.06166400 | 0.12647800 |
| C | -2.44502000 | 0.50668400 | -0.15644600 |
| C | -2.20563100 | -0.83923900 | 0.09197200 |
| C | -3.72096600 | 1.01813700 | -0.24701300 |
| C | -3.22875600 | -1.74537600 | 0.26392300 |
| C | -4.77082900 | 0.10981300 | -0.07444900 |
| H | -3.89656000 | 2.06781700 | -0.44241200 |
| C | -4.53031300 | -1.24030800 | 0.17535800 |
| H | -3.03014400 | -2.79121900 | 0.45749500 |

| | | | |
|---|---|---|---|
| H | -5.79154400 | 0.46571200 | -0.13695700 |
| H | -5.36745000 | -1.91493000 | 0.30385400 |

E = -917.85560

Spin = 0

Level of theory = CBS-QB3

| | | | |
|---|---|---|---|
| C | 1.96370700 | 4.02798900 | 0.06158200 |
| H | 2.86004200 | 3.98848100 | -0.56035000 |
| H | 1.13524500 | 4.40473700 | -0.54179100 |
| C | 1.64277700 | 2.65569700 | 0.61726400 |
| H | 0.73391900 | 2.67120300 | 1.22801200 |
| H | 2.47373100 | 2.25549700 | 1.20290200 |
| C | 2.25035400 | -0.31270500 | 0.01385900 |
| C | 3.59944800 | -3.00847800 | -0.54090100 |
| H | 4.12111200 | -2.23291100 | -1.10529100 |
| H | 4.32332700 | -3.68594900 | -0.08304900 |
| H | 2.91511100 | -3.57258200 | -1.17987800 |
| H | 2.14189500 | 4.72709300 | 0.88239500 |
| O | 3.37704600 | 0.08207600 | 0.07189100 |
| N | 1.11811200 | 0.48792500 | -0.14524400 |
| O | 1.84571200 | -1.62231300 | 0.07166500 |
| O | 2.91166900 | -2.45441800 | 0.57875200 |
| O | 1.42166900 | 1.79986600 | -0.52907800 |
| B | -0.28218400 | 0.17285900 | -0.10976600 |
| O | -1.24516500 | 1.15626700 | -0.28653200 |
| O | -0.83956000 | -1.07214600 | 0.12140400 |
| C | -2.44992100 | 0.49268000 | -0.15703700 |
| C | -2.20467300 | -0.85560900 | 0.09069600 |
| C | -3.73069100 | 0.99955900 | -0.24438600 |
| C | -3.22641000 | -1.76667500 | 0.26482800 |
| C | -4.77828700 | 0.08590800 | -0.06918400 |

| | | | |
|---|---|---|---|
| H | -3.90855700 | 2.04936300 | -0.43887400 |
| C | -4.53194300 | -1.26543900 | 0.17969500 |
| H | -3.02117400 | -2.81182900 | 0.45702100 |
| H | -5.80096200 | 0.43855400 | -0.12894000 |
| H | -5.36668900 | -1.94365400 | 0.31008100 |

## References


[1] W. Fraenk, T. Habereder, T. Klapoetke, H. Nöth, K. Polborn, *J. Chem. Soc., Dalton Trans.* **1999**, 4283-4286.

[2] I. R. Dunkin, *Matrix-isolation techniques : a practical approach*, Oxford University Press, New York, **2002**.

[3] C. Lee, W. Yang, R. G. Parr, *Phys. Rev. B* **1988**, *37*, 785-789.

[4] A. D. Becke, *J. Chem. Phys* **1993**, *98*, 5648-5652.

[5] M. J. Frisch, G. W. Trucks, H. B. Schlegel, G. E. Scuseria, M. A. Robb, J. R. Cheeseman, G. Scalmani, V. Barone, G. A. Petersson, H. Nakatsuji, X. Li, M. Caricato, A. V. Marenich, J. Bloino, B. G. Janesko, R. Gomperts, B. Mennucci, H. P. Hratchian, J. V. Ortiz, A. F. Izmaylov, J. L. Sonnenberg, Williams, F. Ding, F. Lipparini, F. Egidi, J. Goings, B. Peng, A. Petrone, T. Henderson, D. Ranasinghe, V. G. Zakrzewski, J. Gao, N. Rega, G. Zheng, W. Liang, M. Hada, M. Ehara, K. Toyota, R. Fukuda, J. Hasegawa, M. Ishida, T. Nakajima, Y. Honda, O. Kitao, H. Nakai, T. Vreven, K. Throssell, J. A. Montgomery Jr., J. E. Peralta, F. Ogliaro, M. J. Bearpark, J. J. Heyd, E. N. Brothers, K. N. Kudin, V. N. Staroverov, T. A. Keith, R. Kobayashi, J. Normand, K. Raghavachari, A. P. Rendell, J. C. Burant, S. S. Iyengar, J. Tomasi, M. Cossi, J. M. Millam, M. Klene, C. Adamo, R. Cammi, J. W. Ochterski, R. L. Martin, K. Morokuma, O. Farkas, J. B. Foresman, D. J. Fox, Wallingford, CT, **2016**.

[6] J. P. Foster, F. Weinhold, *J. Am. Chem. Soc.* **1980**, *102*, 7211-7218.

[7] J. E. Carpenter, F. Weinhold, *J. Mol. Struct.* **1988**, *169*, 41-62.

[8] E. D. Glendening, A. E. Reed, J. E. Carpenter, F. Weinhold, **2013**, NBO 6.0, Theoretical Chemistry Institute, University of Wisconsin, Madison, WI.

[9] V. Barone, M. Biczysko, J. Bloino, *Phys. Chem. Chem. Phys.* **2014**, *16*, 1759-1787.

[10] J. Bloino, V. Barone, *J. Chem. Phys* **2012**, *136*, 124108.

[11] V. Barone, J. Bloino, C. A. Guido, F. Lipparini, *Chem. Phys. Lett* **2010**, *496*, 157-161.

[12] V. Barone, *J. Chem. Phys* **2005**, *122*, 014108.

[13] J. A. M. Jr., M. J. Frisch, J. W. Ochterski, G. A. Petersson, *J. Chem. Phys* **1999**, *110*, 2822-2827.

[14] F. Weigend, R. Ahlrichs, *Phys Chem Chem Phys* **2005**, *7*, 3297-3305.

[15] C. Angeli, R. Cimiraglia, J.-P. Malrieu, *J. Chem. Phys* **2002**, *117*, 9138-9153.

[16] F. Neese, *WIREs Computational Molecular Science* **2012**, *2*, 73-78.

THE JOURNAL OF PHYSICAL CHEMISTRY A
A JOURNAL OF THE AMERICAN CHEMICAL SOCIETY

pubs.acs.org/JPCA Article

# Computational Exploration of the Intersystem Crossing from the $\tilde{X}^3A_2$ to the $\tilde{a}^1A_1$ State in Boryl Nitrenes upon Photoexcitation

Virinder Bhagat and Holger F. Bettinger*

Cite This: J. Phys. Chem. A 2022, 126, 7660−7666 Read Online

ACCESS | Metrics & More | Article Recommendations | Supporting Information

**ABSTRACT:** The boryl nitrene CatBN (Cat = catecholato) turns highly reactive toward small inert molecules upon irradiation of its triplet ground state $\tilde{X}^3A_2$ with light of wavelength $\lambda$ > 550 nm. A computational study of a model boryl nitrene using complete active space self-consistent field (CASSCF) theory provides evidence for the population of the highly reactive electronic state $\tilde{a}^1A_1$ upon irradiation. Potential energy scans connecting different critical points (minima, minimum energy crossing points, and conical intersections) reveal two possible pathways that could relax photoexcited boryl nitrene from the Franck−Condon region of $\tilde{A}^3B_1$ to the $\tilde{a}^1A_1$ state minimum. Considering the energy barriers to relaxation from one electronic state to another and the magnitude of spin−orbit couplings, the energetically most favorable pathway involves photoexcitation to $\tilde{A}^3B_2$, followed by intersystem crossing to the open-shell singlet state ($\tilde{b}^1A_2$) and internal conversion to $\tilde{a}^1A_1$. The relevant minimum energy crossing point is about 7−8 kcal mol$^{-1}$ higher in energy than the Franck−Condon region.

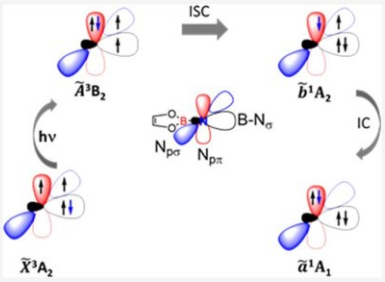


## INTRODUCTION

Nitrenes are reactive intermediates that consist of a monovalent nitrogen atom containing a sextet of electrons.[1−3] They have been extensively studied, under cryogenic conditions in combination with different spectroscopic methods, using trapping experiments at ambient conditions and computationally.[4,5] The reactivity of nitrenes depends both on the spin and the leading electronic configuration of the electronic state, and both intramolecular (e.g., 1,2-H shift, aromatic ring expansion, etc.)[5−10] and intermolecular reactions (e.g., intermolecular C−H insertion, dimerization reaction, etc.)[4,11−15] have been reported. The relative energies of the electronic states in a nitrene and consequently its reactivity can be altered by the substituents attached to the nitrogen atom. A case in point is the closed-shell singlet ground state of benzoyl nitrene that contrasts the triplet ground state of phenyl nitrene and indeed most other nitrenes.[16,17]

Electron donor-stabilized boryl nitrenes are a particular class of highly reactive nitrenes.[13] In matrix isolation experiments, 3-nitreno-1,3,2-benzodioxaborole **1** CatBN (Cat = catecholato) is formed in situ after photolyzing the corresponding azide precursor, 2-azido-1,3,2-benzodioxaborole **2**, which is co-deposited with different cryogenic matrix materials (Scheme 1a).[18] Boryl nitrene **1**, which has a triplet ground state ($\tilde{X}^3A_2$),[18] has shown high thermal reactivity toward $O_2$ and high photochemical reactivity toward $N_2$, CO, $CH_4$, $CO_2$, and $D_2$ when irradiated with light of wavelength $\lambda$ > 550 nm under matrix isolation conditions (Scheme 1a).[12,13,18−22] An electronic structure study of **1** revealed the energetic ordering of states of **1** as $\tilde{X}^3A_2$ < $\tilde{a}^1A_1$ < $\tilde{b}^1A_2$.[18] The closed-shell singlet state ($\tilde{a}^1A_1$ with leading configuration $\pi^2\sigma^0$, Scheme 1b) thus is the lowest singlet state, contrary to phenyl nitrene in which $\tilde{a}^1A_2$ is significantly below the $\tilde{b}^1A_1$ state.[17,18,23−28] The orbital occupancy in the $\tilde{a}^1A_1$ state is similar to that of the highly electrophilic vinylidenes, and their reactive centers are related by an isoelectronic substitution of the C═C by the B═N unit (Scheme 1b). The superelectrophilic difluorovinylidene inserts into highly stable species like methane and dihydrogen under matrix isolation conditions.[29−35]

In earlier studies on the photochemical reactivity of **1**, the $\tilde{a}^1A_1$ state, being similar to vinylidene, was presumed to be attained after irradiation with $\lambda$ > 550 nm and expected to react fast with $N_2$, CO, $CH_4$, $CO_2$, and $D_2$ as shown in Scheme 1a. Also, computational studies showed very low barriers for the reaction of the $\tilde{a}^1A_1$ state with $D_2$ and $CO_2$.[19,22] In addition, experiments have shown an efficient intermolecular C−H insertion for some boryl nitrenes in the solution phase.[12,14,15] The small measured kinetic isotope effect is indicative of an insertion reaction rather than a hydrogen abstraction, radical recombination mechanism.[14] This in turn suggests that a closed-shell singlet state is responsible for the high reactivity of boryl nitrenes toward closed-shell species.

The main objective of our study is to provide computational evidence in support of the assumption made in our previous

Received: August 2, 2022
Revised: September 26, 2022
Published: October 18, 2022





https://doi.org/10.1021/acs.jpca.2c05491
J. Phys. Chem. A 2022, 126, 7660−7666

**Scheme 1. Photochemical and Thermal Reactivity of Boryl Nitrene 1 with Different Highly Stable Molecules under Matrix Isolation Conditions**

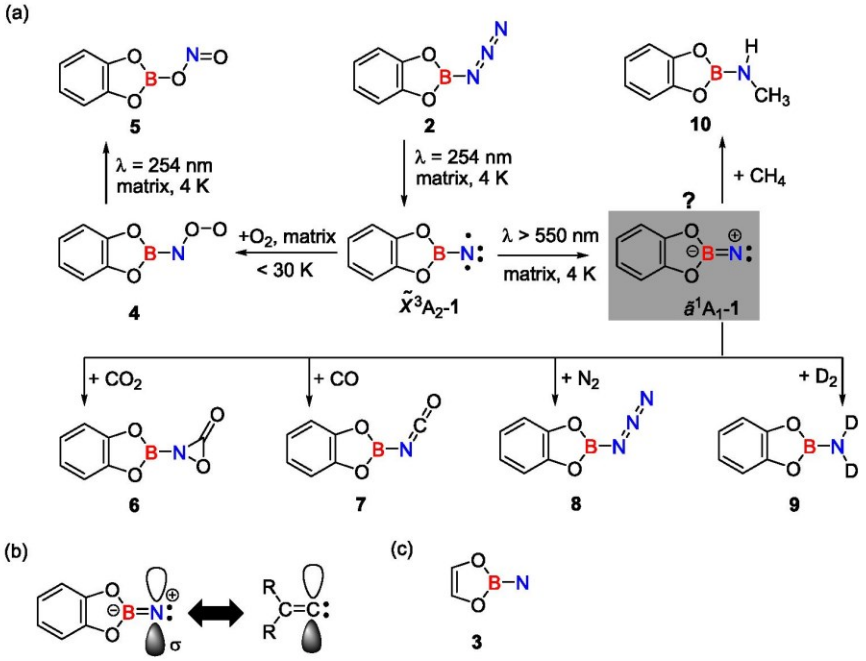


**Table 1. Calculated Vertical Transition Energies (in kcal mol$^{-1}$) for Boryl Nitrenes 1 and 3 from $\tilde{X}^3A_2$ State Minimum**

| | electronic transition | | | | |
|---|---|---|---|---|---|
| | CASSCF/cc-pVTZ[a] | | MRCI+Q/cc-pVDZ[a] | | |
| electronic state | 1[b] | 3[c] | 1[d] | 3[e] | leading electronic configuration |
| $\tilde{X}^3A_2$ | 0.0 | 0.0 | 0.0 | 0.0 | $\sigma_{B-N}^2$, $N_{p\pi}^1$, $N_{p\sigma}^1$ |
| $\tilde{a}^1A_1$ | 30.3 | 32.4 | 37.4 | 35.8 | $\sigma_{B-N}^2$, $N_{p\pi}^2$, $N_{p\sigma}^0$ |
| $\tilde{b}^1A_2$ | 39.8 | 39.4 | 38.8 | 36.8 | $\sigma_{B-N}^2$, $N_{p\pi}^1$, $N_{p\sigma}^1$ |
| $\tilde{A}^3B_2$ | 48.7 (0.0013)[f] | 50.8 (0.0014)[f] | 52.4 (0.0018)[f] | 53.5 (0.0018)[f] | $\sigma_{B-N}^1$, $N_{p\pi}^2$, $N_{p\sigma}^1$ |
| $\tilde{c}^1A_1$ | 65.0 | 63.0 | 65.3 | 61.5 | $\sigma_{B-N}^2$, $N_{p\pi}^0$, $N_{p\sigma}^2$ |

[a]Calculated at the geometries obtained at the CASSCF/cc-pVTZ level of theory. [b]Using CAS(12,12) active space. [c]Using CAS(12,10) active space. [d]Using CAS(12,12) as reference. [e]Using CAS(12,10) as reference. [f]Corresponding oscillator strengths.

experimental studies about the involvement of the $\tilde{a}^1A_1$ state in the photoreaction of **1** once its triplet ground state is irradiated with light of $\lambda > 550$ nm under matrix isolation conditions. Considering a large computational cost for studying the mechanism of intersystem crossing in **1** that finally leads to $\tilde{a}^1A_1$ using multiconfigurational self-consistent field theory, we have chosen a smaller model boryl nitrene **3** as shown in Scheme 1c. Our study mainly consists of exploring (1) the similarity between boryl nitrenes **1** and **3** in terms of the nature of low-lying electronic states that are relevant in the experimental studies; (2) two different pathways, Pathway 1 and Pathway 2, that could lead to the $\tilde{a}^1A_1$ state of **3** from the lowest $\tilde{X}^3A_2$ state upon photoirradiation.

## ■ COMPUTATIONAL DETAILS

All of the calculations were performed using ORCA 5.0.1[36] and Molpro 2021.3[37] computational chemistry packages. Geometry optimizations of the minima were done using state-specific complete active space self-consistent field (SS-CASSCF)[38,39] theory combined with Dunning's triple-$\zeta$ basis set cc-pVTZ.[40] The state-average formalism of CASSCF (SA-CASSCF)[32,33] with equal weight of all considered states in conjunction with the cc-pVTZ basis set was used for the optimization of critical points [minimum energy crossing points (MECPs) and conical intersections (CIs)] analytically using the algorithm implemented[41,42] in Molpro 2021.3. Multireference configuration interaction with single and double excitations along with Davidson correction for unlinked quadruples (MRCI+Q),[43,44] using CAS(12,10) for **3** and CAS(12,12) for **1** as the reference, along with Dunning's cc-pVDZ[45] basis set was used to calculate the vertical excitation energy at the ground state minimum geometries obtained at the CASSCF/cc-pVTZ level of theory. The calculations of spin−orbit coupling interactions were carried out at the SA-CASSCF/cc-pVTZ level of theory. Linear least motion paths (LLMP) connecting two critical points were constructed using SA-CASSCF/cc-pVTZ with equal weights over the number of states involved (two singlets and two triplets for Pathway 1 and three singlets and three triplets for Pathway 2). The MacMolplt program was used to obtain the geometries that connect two critical points on a LLMP (minima, MECPs, and CIs).[46]



https://doi.org/10.1021/acs.jpca.2c05491
J. Phys. Chem. A 2022, 126, 7660−7666

## RESULTS AND DISCUSSION

**Comparison of Vertical Excitation Energy in Boryl Nitrenes 1 and 3.** The choice of active space is very important in the multiconfigurational treatment of a chemical system using the CASSCF method. In our case, for boryl nitrene **3**, the active space was constructed using 12 electrons and 10 orbitals as shown in Figure S1. The orbitals in the active space are as follows: three orbitals mainly concentrated on the nitrogen atom ($N_{p\pi}$, $N_{p\sigma}$, and $N_{LP}$), two sigma orbitals corresponding to the B−N bond ($\sigma_{BN}$ and $\sigma^*_{BN}$), two out-of-plane lone pairs one each on the two oxygen atoms ($O3_{LP-\pi}$ and $O4_{LP-\pi}$), $\pi_{C1-C2}$ and $\pi^*_{C1-C2}$, and a vacant p orbital on boron $B_{p\pi}$. The comparison of CASSCF and MRCI+Q vertical excitation energies from the ground state $\tilde{X}^3A_2$ shows very similar values for **1** and **3** (Table 1). This suggests that **3** is a suitable model for the simulation of **1**. Furthermore, the comparison shows that the excited state energies obtained for **3** at the CASSCF level only differ slightly from the more sophisticated MRCI+Q method (Table 1). This implies that the CASSCF method can reliably describe the relevant excited state manifold of **3**.

Considering the wavelength of light used in experimental studies to induce photochemistry in boryl nitrene **1**, which is $\lambda$ > 550 nm ($E$ < 52 kcal mol$^{-1}$), and the calculated vertical transition energy between the $\tilde{X}^3A_2$ and $\tilde{A}^3B_2$ states as shown in Table 1, we expect the ground state to be excited to the $\tilde{A}^3B_2$ state. The oscillator strength for excitation to the $\tilde{A}^3B_2$ state of **1** and **3** is non-negligible (0.0018 at the MRCI+Q/cc-pvDZ level of theory), which indicates that irradiation with $\lambda$ > 550 nm results in $\tilde{X}^3A_2$ to $\tilde{A}^3B_2$ excitation.

Consequently, the geometric structures of the MECPs and CIs that could lead to the relaxation of $\tilde{A}^3B_2$ to the $\tilde{a}^1A_1$ state of boryl nitrene **3** were optimized (Figure 1). The considerable variation in BN bond lengths in the minima of different electronic states from 1.499 to 1.431 Å (see Figure 1) is indicative of the difference in the electron occupancy of the orbitals ($\sigma_{B-N}$, $N_{p\pi}$, and $N_{p\sigma}$) concentrated on the nitrogen and boron atoms. Comparatively, short distances were obtained for the states with the $N_{p\pi}^2$ leading configuration, namely, $\tilde{A}^3B_2$ and $\tilde{a}^1A_1$. The leading configuration has a higher proportion in the overall wavefunction for the $\tilde{A}^3B_2$ state as compared to the $\tilde{a}^1A_1$ state, and hence, the former state has the shortest BN distance. In addition to this, we obtained two MECPs that are relevant for intersystem crossing: $\tilde{A}^3A''/\tilde{b}^1A''$ (MECP1) and $\tilde{A}^3B_2/\tilde{c}^1A_1$ (MECP2) and two CIs that lead to internal conversion: $\tilde{b}^1A_2/\tilde{a}^1A_1$ (CI1) and $\tilde{c}^1A'/\tilde{b}^1A''$ (CI2). The calculations of the crossing points provide us with the branching space: gradient difference (GD) and derivative coupling (DC) vectors for CIs and gradient difference vectors for MECPs (Figure 2). The geometries of the minima and critical points are planar except for MECP1 and CI2 in which the BN bond is out of the plane defined by two oxygen atoms and two carbon atoms (OCCO plane). Accordingly, the irreducible representations of the $C_s$ point group are used for their description.

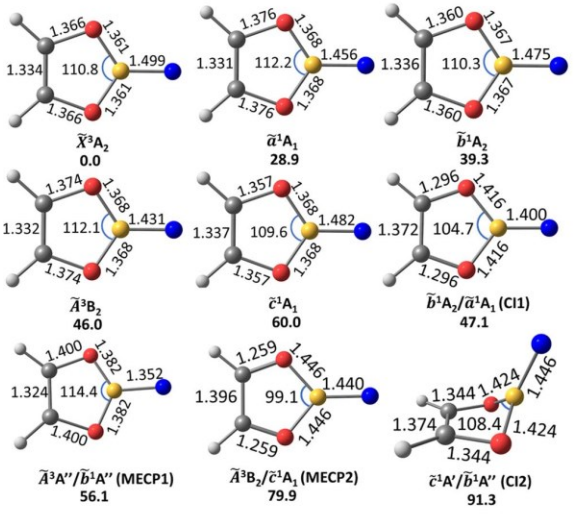


**Figure 1.** Calculated (CASSCF/cc-pVTZ) geometrical parameters and the relative energies (in kcal mol$^{-1}$) corresponding to the minima of different electronic states of **3**, minimum energy crossing points (MECPs), and conical intersections (CIs).

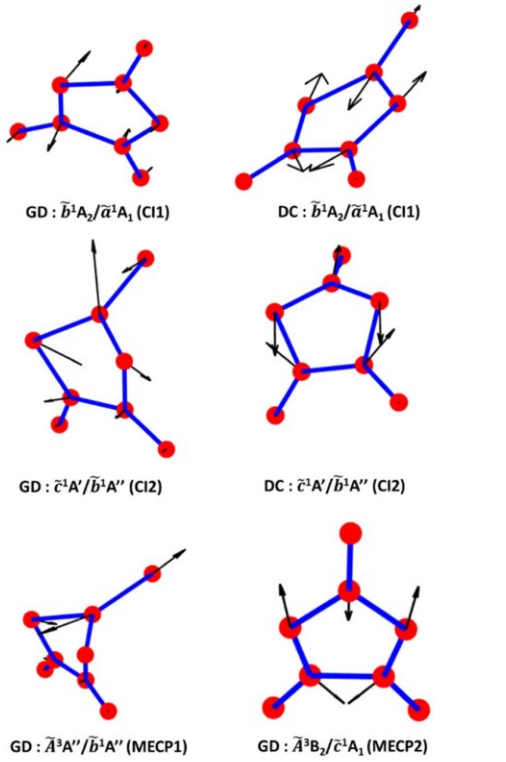


**Figure 2.** Gradient difference (GD) and derivative coupling (DC) vectors correspond to the different critical points calculated at the SA-CASSCF/cc-pVTZ level of theory.

**Pathway 1.** Based on the optimized critical points, the first pathway for population of $\tilde{a}^1A_1$ is photoexcitation in the Franck−Condon (FC) region to the $\tilde{A}^3B_2$ state, followed by MECP1−$\tilde{b}^1A_2$−CI1−$\tilde{a}^1A_1$ minimum relaxation. Figure 3 shows the potential energy profiles connecting two critical points. According to the energy profile connecting $\tilde{A}^3B_2$ to $\tilde{b}^1A_2$ (Figure 3a), this step involves a barrier of 7−8 kcal mol$^{-1}$. Hence, the energy required to approach the region of MECP1 is quite small.



https://doi.org/10.1021/acs.jpca.2c05491
J. Phys. Chem. A 2022, 126, 7660−7666

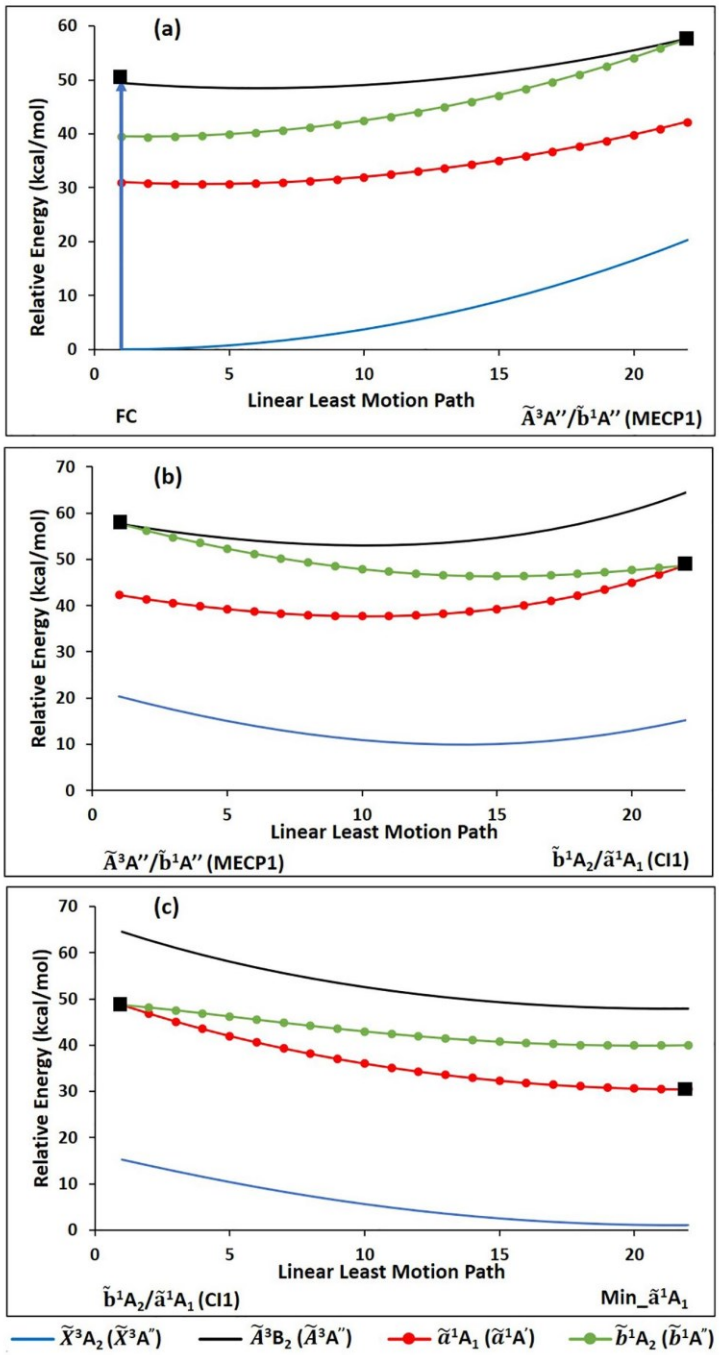


**Figure 3.** Linear least motion paths corresponding to Pathway 1 between different stationary points and critical points of **3**, constructed using the SA-(2S,2T)-CASSCF/cc-pVTZ level of theory.

Further, the major electronic configurations of $\tilde{A}^3B_2$ and $\tilde{b}^1A_2$ are such that intersystem crossing at MECP1 is allowed by El-Sayed's rules.[47,48] This is also supported by the spin–orbit coupling of 34.9 $cm^{-1}$ between these two states calculated at the MECP1 geometry at the CASSCF(12,10)/cc-pVTZ level of theory. The visualization of the energy profile in Figure 3a reflects the sloped topology of MECP1, which is another indication of effective population transfer from $\tilde{A}^3B_2$ to $\tilde{b}^1A_2$ state at MECP1.[49] The $\tilde{b}^1A_2$ state is then expected to be relaxed to the $\tilde{a}^1A_1$ state via conical intersection CI1, which leads to $\tilde{a}^1A_1$ minimum as shown in Figure 3b,c. Both relaxation steps do not involve a potential energy barrier.

**Pathway 2.** MECP2, which is the optimized crossing point between the $\tilde{A}^3B_2$ and $\tilde{c}^1A_1$ states, provides an additional



https://doi.org/10.1021/acs.jpca.2c05491
J. Phys. Chem. A 2022, 126, 7660−7666

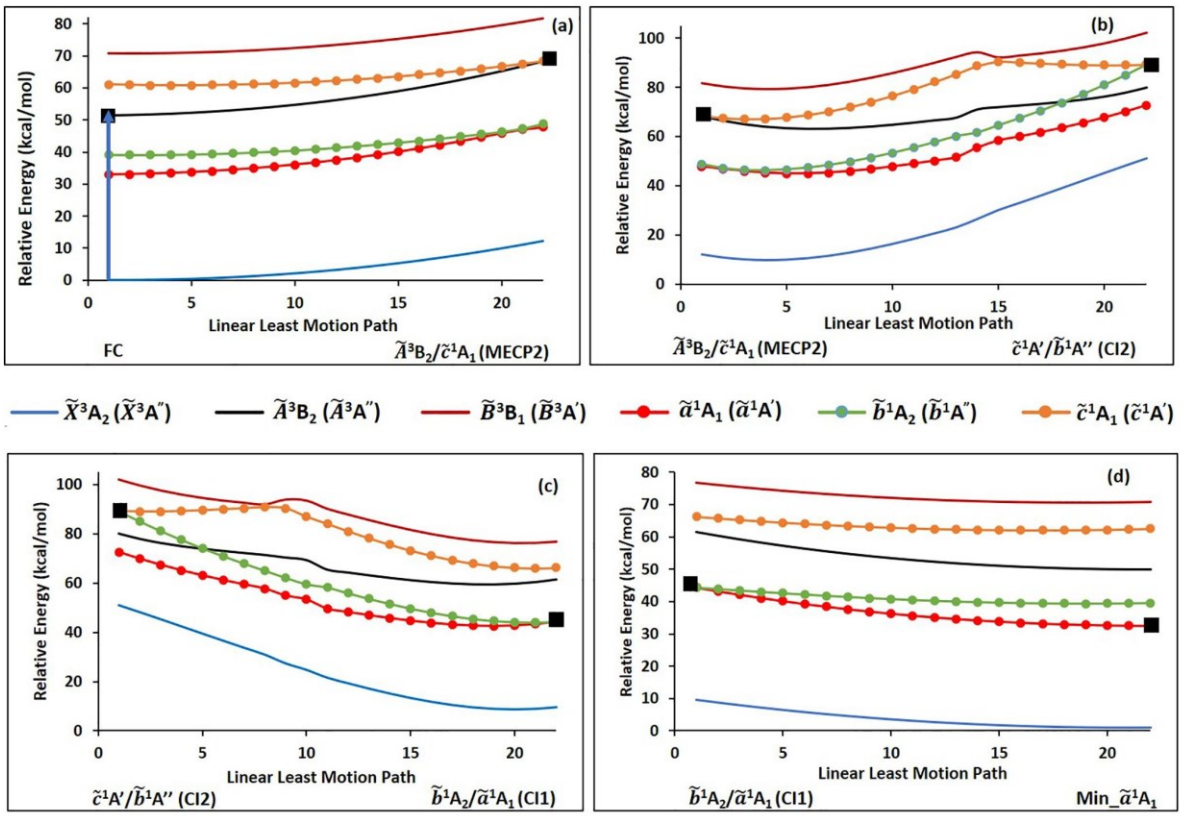


**Figure 4.** Linear least motion paths corresponding to Pathway 2 between different stationary points and critical points of **3**, constructed using the SA-(3S,3T)-CASSCF/cc-pVTZ level of theory.

channel for relaxation of the $\tilde{A}^3B_2$ state to the $\tilde{a}^1A_1$ state. Based on optimized CI2 and CI1, the possible pathway can be $\tilde{X}^3A_2$ excited to $\tilde{A}^3B_2$ at FC−MECP2−CI2−CI1−$\tilde{a}^1A_1$ minimum. Computed potential energy profiles in Figure 4 show the stepwise relaxation of boryl nitrene **3** to the $\tilde{a}^1A_1$ state after its photoexcitation to $\tilde{A}^3B_2$. According to Figure 4a, there is an energy barrier of 17 kcal mol$^{-1}$ to reach MECP2 from the FC region. In addition, there is a non-negligible spin−orbit coupling of 21.5 cm$^{-1}$ between the $\tilde{A}^3B_2$ and $\tilde{c}^1A_1$ states at the MECP2 geometry.

Figure 4b presents the potential energy profile for the transformation of the $\tilde{c}^1A_1$ state to the $\tilde{b}^1A_2$ state via CI2 with an energy barrier of around 20 kcal mol$^{-1}$. Once $\tilde{b}^1A_2$ is attained, the further relaxation to the $\tilde{a}^1A_1$ state via CI1 and finally to its minimum takes place without a barrier as shown in Figure 4c,d.

The above discussion on possible pathways indicates the higher feasibility of Pathway 1 over Pathway 2 to populate the $\tilde{a}^1A_1$ state. In Pathway 1 (Figure 5), the first step seems to be the bottleneck as it is the only step that involves a potential energy barrier to reach MECP1. At this point, spin−orbit coupling is high and the topology of the surfaces is sloped.[49] These are also the important features for efficient population transfer in an intersystem crossing. In contrast, in Pathway 2, the first two steps must surpass sizeable energy barriers of 17 and 20 kcal mol$^{-1}$, respectively, which will impede the population transfer from higher to lower energy states.

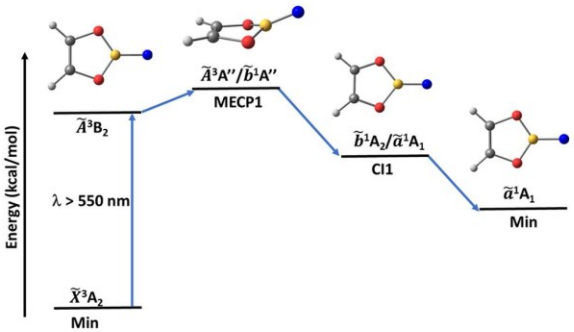


**Figure 5.** Overview of the plausible mechanism for the formation of the $\tilde{a}^1A_1$ state of **3** after its photoirradiation in the ground state $\tilde{X}^3A_2$.

## CONCLUSIONS

We have found evidence through the computational study of model triplet boryl nitrene **3** for an energetically favorable pathway from the photoexcited triplet state to the lowest energy closed-shell singlet state. According to our computations, irradiation ($\lambda$ > 550 nm) of **3** results in excitation to the $\tilde{A}^3B_2$ state, which then undergoes intersystem crossing through MECP1 to the $\tilde{b}^1A_2$ state. The favorability of this process is reflected by the computed spin−orbit coupling (34.9 cm$^{-1}$) between the two states at the geometry corresponding to MECP1 and the topological features (sloped) near the



https://doi.org/10.1021/acs.jpca.2c05491
J. Phys. Chem. A 2022, 126, 7660−7666

intersection (MECP1). Subsequently, the system relaxes to the $\tilde{a}^1A_1$ minimum via CI1 without additional barriers. We conclude that the computational evidence for efficient intersystem crossing supports the involvement of the vinylidene-like singlet state in the reactions of **1** with small inert closed-shell molecules.

## ■ ASSOCIATED CONTENT

### Supporting Information

The Supporting Information is available free of charge at https://pubs.acs.org/doi/10.1021/acs.jpca.2c05491.

Graphics of the active space orbitals used in the CASSCF calculations for boryl nitrenes **1** and **3** and Cartesian coordinates along with the corresponding energies of all the optimized minima and critical points (PDF)

## ■ AUTHOR INFORMATION


### Corresponding Author

**Holger F. Bettinger** − *Institut für Organische Chemie, Universität Tübingen, 72076 Tübingen, Germany;* orcid.org/0000-0001-5223-662X; Email: holger.bettinger@uni-tuebingen.de

### Author

**Virinder Bhagat** − *Institut für Organische Chemie, Universität Tübingen, 72076 Tübingen, Germany*

Complete contact information is available at: https://pubs.acs.org/10.1021/acs.jpca.2c05491


### Notes

The authors declare no competing financial interest.

## ■ ACKNOWLEDGMENTS

This work was supported by the Deutsche Forschungsgemeinschaft (DFG) through grant BE 3183/11-1. The authors are sincerely thankful for support by the state of Baden-Württemberg for bwHPC and DFG through grant no INST 40/467-1 FUGG (Justus 2 cluster).

## ■ REFERENCES


(1) Shainyan, B. A.; Kuzmin, A. V.; Moskalik, M. Y. Carbenes and nitrenes. An overview. *Comput. Theor. Chem.* **2013**, *1006*, 52−61.

(2) Dequirez, G.; Pons, V.; Dauban, P. Nitrene Chemistry in Organic Synthesis: Still in Its Infancy? *Angew. Chem., Int. Ed.* **2012**, *51*, 7384−7395.

(3) Bräse, S.; Gil, C.; Knepper, K.; Zimmermann, V. Organic Azides: An Exploding Diversity of a Unique Class of Compounds. *Angew. Chem., Int. Ed.* **2005**, *44*, 5188−5240.

(4) Gritsan, N. P.; Platz, M. S.Kinetics and Spectroscopy of Substituted Phenylnitrenes. In *Advances in Physical Organic Chemistry*; Academic Press, 2001; Vol. *36*, pp 255−304.

(5) Wentrup, C. Flash Vacuum Pyrolysis of Azides, Triazoles, and Tetrazoles. *Chem. Rev.* **2017**, *117*, 4562−4623.

(6) Bock, H.; Dammel, R. Gas-phase reactions. 66. Gas-phase pyrolyses of alkyl azides: experimental evidence for chemical activation. *J. Am. Chem. Soc.* **1988**, *110*, 5261−5269.

(7) Jing, W.; Zheng, S.; Xinjiang, Z.; Xiaojun, Y.; Maofa, G.; Dianxun, W. The CH3N Diradical: Experimental and Theoretical Determinations of the Ionization Energies. *Angew. Chem.* **2001**, *113*, 3145−3147.

(8) Chapman, O. L.; Le Roux, J. P. 1-Aza-1,2,4,6-cycloheptatetraene. *J. Am. Chem. Soc.* **1978**, *100*, 282−285.

(9) Chapman, O. L.; Sheridan, R. S.; LeRoux, J. P. Photochemical interconversion of phenylnitrene and the isomeric pyridylmethylenes. *J. Am. Chem. Soc.* **1978**, *100*, 6245−6247.

(10) Bednarek, P.; Wentrup, C. 3-Pyridylcarbene and 3-Pyridylnitrene: Ring Opening to Nitrile Ylides. *J. Am. Chem. Soc.* **2003**, *125*, 9083−9089.

(11) Shields, C. J.; Chrisope, D. R.; Schuster, G. B.; Dixon, A. J.; Poliakoff, M.; Turner, J. J. Photochemistry of aryl azides: detection and characterization of a dehydroazepine by time-resolved infrared spectroscopy and flash photolysis at room temperature. *J. Am. Chem. Soc.* **1987**, *109*, 4723−4726.

(12) Bettinger, H. F.; Filthaus, M.; Bornemann, H.; Oppel, I. M. Metal-Free Conversion of Methane and Cycloalkanes to Amines and Amides by Employing a Borylnitrene. *Angew. Chem., Int. Ed.* **2008**, *47*, 4744−4747.

(13) Bettinger, H. F.; Filthaus, M. Borylnitrenes: electrophilic reactive intermediates with high reactivity towards C−H bonds. *Org. Biomol. Chem.* **2010**, *8*, 5477−5482.

(14) Filthaus, M.; Schwertmann, L.; Neuhaus, P.; Seidel, R. W.; Oppel, I. M.; Bettinger, H. F. C−H Bond Amination by Photochemically Generated Transient Borylnitrenes at Room Temperature: A Combined Experimental and Theoretical Investigation of the Insertion Mechanism and Influence of Substituents. *Organometallics* **2012**, *31*, 3894−3903.

(15) Müller, M.; Maichle-Mössmer, C.; Bettinger, H. F. C−H functionalization of tetramethylsilane employing a borylnitrene. *Chem. Commun.* **2013**, *49*, 11773−11775.

(16) Pritchina, E. A.; Gritsan, N. P.; Maltsev, A.; Bally, T.; Autrey, T.; Liu, Y.; Wang, Y.; Toscano, J. P. Matrix isolation, time-resolved IR, and computational study of the photochemistry of benzoyl azide. *Phys. Chem. Chem. Phys.* **2003**, *5*, 1010−1018.

(17) Borden, W. T.; Gritsan, N. P.; Hadad, C. M.; Karney, W. L.; Kemnitz, C. R.; Platz, M. S. The Interplay of Theory and Experiment in the Study of Phenylnitrene. *Acc. Chem. Res.* **2000**, *33*, 765−771.

(18) Bettinger, H. F.; Bornemann, H. Donor Stabilized Borylnitrene: A Highly Reactive BN Analogue of Vinylidene. *J. Am. Chem. Soc.* **2006**, *128*, 11128−11134.

(19) Bettinger, H. F.; Filthaus, M.; Neuhaus, P. Insertion into dihydrogen employing the nitrogen centre of a borylnitrene. *Chem. Commun.* **2009**, 2186−2188.

(20) Bettinger, H. F.; Bornemann, H. Noble Gas Atoms as Electron Donors: Is the Stabilization of Strongly Electrophilic Borylnitrenes Feasible? *Z. Anorg. Allg. Chem.* **2011**, *637*, 2169−2174.

(21) Bhagat, V.; Schumann, J.; Bettinger, H. F. Unusual Nitrene Oxidation Product Formation by Metathesis Involving the Dioxygen O−O and Borylnitrene B−N Bonds. *Chem. - Eur. J.* **2020**, *26*, 12654−12663.

(22) Bhagat, V.; Schumann, J.; Bettinger, H. F. The Reaction of CO2 with a Borylnitrene: Formation of an 3-Oxaziridinone. *Angew. Chem., Int. Ed.* **2021**, *60*, 23112−23116.

(23) Bettinger, H. F.; Sander, W. Dehydrophenylnitrenes: Quartet versus Doublet States. *J. Am. Chem. Soc.* **2003**, *125*, 9726−9733.

(24) Hrovat, D. A.; Waali, E. E.; Borden, W. T. Ab initio calculations of the singlet-triplet energy difference in phenylnitrene. *J. Am. Chem. Soc.* **1992**, *114*, 8698−8699.

(25) Kim, S. J.; Hamilton, T. P.; Schaefer, H. F. Phenylnitrene: energetics, vibrational frequencies, and molecular structures. *J. Am. Chem. Soc.* **1992**, *114*, 5349−5355.

(26) Sugisaki, K.; Toyota, K.; Sato, K.; Shiomi, D.; Kitagawa, M.; Takui, T. Ab initio and DFT studies of the spin−orbit and spin−spin contributions to the zero-field splitting tensors of triplet nitrenes with aryl scaffolds. *Phys. Chem. Chem. Phys.* **2011**, *13*, 6970−6980.

(27) Winkler, M. Singlet−Triplet Energy Splitting and Excited States of Phenylnitrene. *J. Phys. Chem. A* **2008**, *112*, 8649−8653.

(28) Johnson, W. T. G.; Sullivan, M. B.; Cramer, C. J. *meta* and *para* substitution effects on the electronic state energies and ring-expansion reactivities of phenylnitrenes. *Int. J. Quantum Chem.* **2001**, *85*, 492−508.




https://doi.org/10.1021/acs.jpca.2c05491
J. Phys. Chem. A 2022, 126, 7660−7666

(29) Breidung, J.; Bürger, H.; Kötting, C.; Kopitzky, R.; Sander, W.; Senzlober, M.; Thiel, W.; Willner, H. Difluorovinylidene, F2C=C. *Angew. Chem., Int. Ed.* **1997**, *36*, 1983−1985.
(30) Kötting, C.; Sander, W. Insertion of Difluorovinylidene into Hydrogen and Methane. *J. Am. Chem. Soc.* **1999**, *121*, 8891−8897.
(31) Kötting, C.; Sander, W.; Breidung, J.; Thiel, W.; Senzlober, M.; Bürger, H. A Charge-Transfer Complex of Xenon and Difluorovinylidene. *J. Am. Chem. Soc.* **1998**, *120*, 219−220.
(32) Kötting, C.; Sander, W.; Senzlober, M. Evidence for the Non-Concerted Addition of Difluorovinylidene to Acetylenes. *Chem. - Eur. J.* **1998**, *4*, 2360−2365.
(33) Kötting, C.; Sander, W.; Senzlober, M.; Bürger, H. Oxidation of Difluorovinylidene. *Chem. - Eur. J.* **1998**, *4*, 1611−1615.
(34) Sander, W.; Kötting, C. Reactions of Difluorovinylidene—A Super-Electrophilic Carbene. *Chem. - Eur. J.* **1999**, *5*, 24−28.
(35) Sander, W.; Kötting, C.; Hübert, R. Super-electrophilic carbenes and the concept of Philicity. *J. Phys. Org. Chem.* **2000**, *13*, 561−568.
(36) Neese, F. Software update: The ORCA program system—Version 5.0. *Wiley Interdiscip. Rev.: Comput. Mol. Sci.* **2022**, *12*, No. e1606.
(37) Werner, H.-J.; Knowles, P. J.; Knizia, G.; Manby, F. R.; Schütz, M. Molpro: a general-purpose quantum chemistry program package. *Wiley Interdiscip. Rev.: Comput. Mol. Sci.* **2012**, *2*, 242−253.
(38) Knowles, P. J.; Werner, H.-J. An efficient second-order MC SCF method for long configuration expansions. *Chem. Phys. Lett.* **1985**, *115*, 259−267.
(39) Werner, H.-J.; Knowles, P. J. A second order multiconfiguration SCF procedure with optimum convergence. *J. Chem. Phys.* **1985**, *82*, 5053−5063.
(40) Dunning, T. H., Jr. Gaussian basis sets for use in correlated molecular calculations. I. The atoms boron through neon and hydrogen. *J. Chem. Phys.* **1989**, *90*, 1007−1023.
(41) Lindh, R. The reduced multiplication scheme of the Rys-Gauss quadrature for 1st order integral derivatives. *Theor. Chim. Acta* **1993**, *85*, 423−440.
(42) Eckert, F.; Pulay, P.; Werner, H.-J. Ab initio geometry optimization for large molecules. *J. Comput. Chem.* **1997**, *18*, 1473−1483.
(43) Langhoff, S. R.; Davidson, E. R. Configuration interaction calculations on the nitrogen molecule. *Int. J. Quantum Chem.* **1974**, *8*, 61−72.
(44) Duch, W. o. a.; Diercksen, G. H. F. Size-extensivity corrections in configuration interaction methods. *J. Chem. Phys.* **1994**, *101*, 3018−3030.
(45) Woon, D. E.; D, T. H., Jr. Gaussian basis sets for use in correlated molecular calculations. III. The atoms aluminum through argon. *J. Chem. Phys.* **1993**, *98*, 1358−1371.
(46) Bode, B. M.; Gordon, M. S. Macmolplt: a graphical user interface for GAMESS. *J. Mol. Graphics Modell.* **1998**, *16*, 133−138.
(47) El-Sayed, M. A. Spin—Orbit Coupling and the Radiationless Processes in Nitrogen Heterocyclics. *J. Chem. Phys.* **1963**, *38*, 2834−2838.
(48) El-Sayed, M. A. Triplet state. Its radiative and nonradiative properties. *Acc. Chem. Res.* **1968**, *1*, 8−16.
(49) Atchity, G. J.; Xantheas, S. S.; Ruedenberg, K. Potential energy surfaces near intersections. *J. Chem. Phys.* **1991**, *95*, 1862−1876.





https://doi.org/10.1021/acs.jpca.2c05491
*J. Phys. Chem. A* 2022, 126, 7660−7666

**Supporting Information**

# Computational Exploration of the Intersystem Crossing from the $\widetilde{X}^3A_2$ to the $\widetilde{a}^1A_1$ State in Boryl Nitrenes upon Photoexcitation

Virinder Bhagat, Holger F. Bettinger*

Institut für Organische Chemie, Universität Tübingen, Auf der Morgenstelle 18, 72076 Tübingen, Germany

holger.bettinger@uni-tuebingen.de

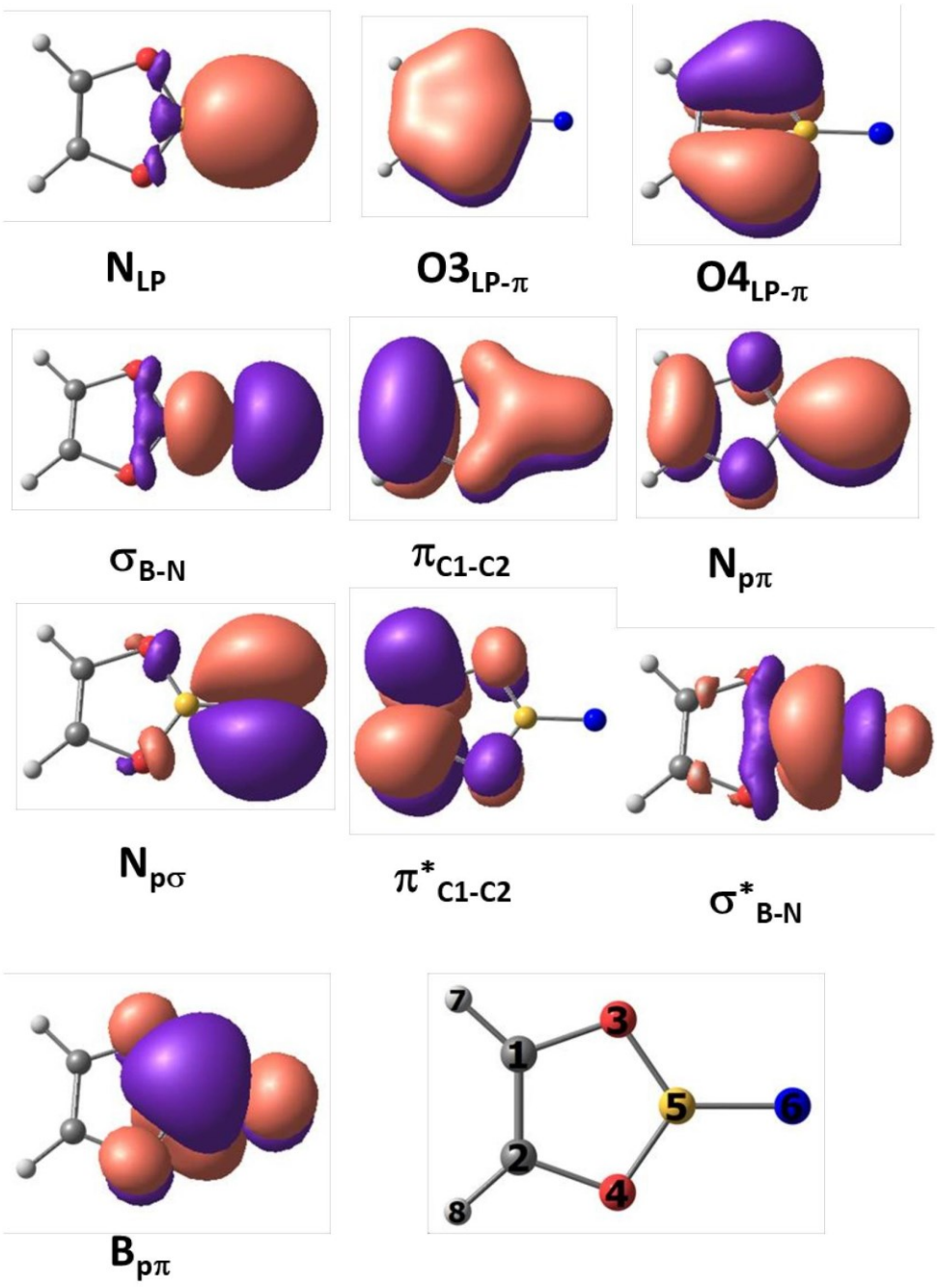


Figure S1. CASSCF(12,10) state-averaged (2 singlets, 2 triplets) natural orbitals calculated at cc-pVTZ basis set at $\tilde{X}^3A_2$ minimum of **3**.

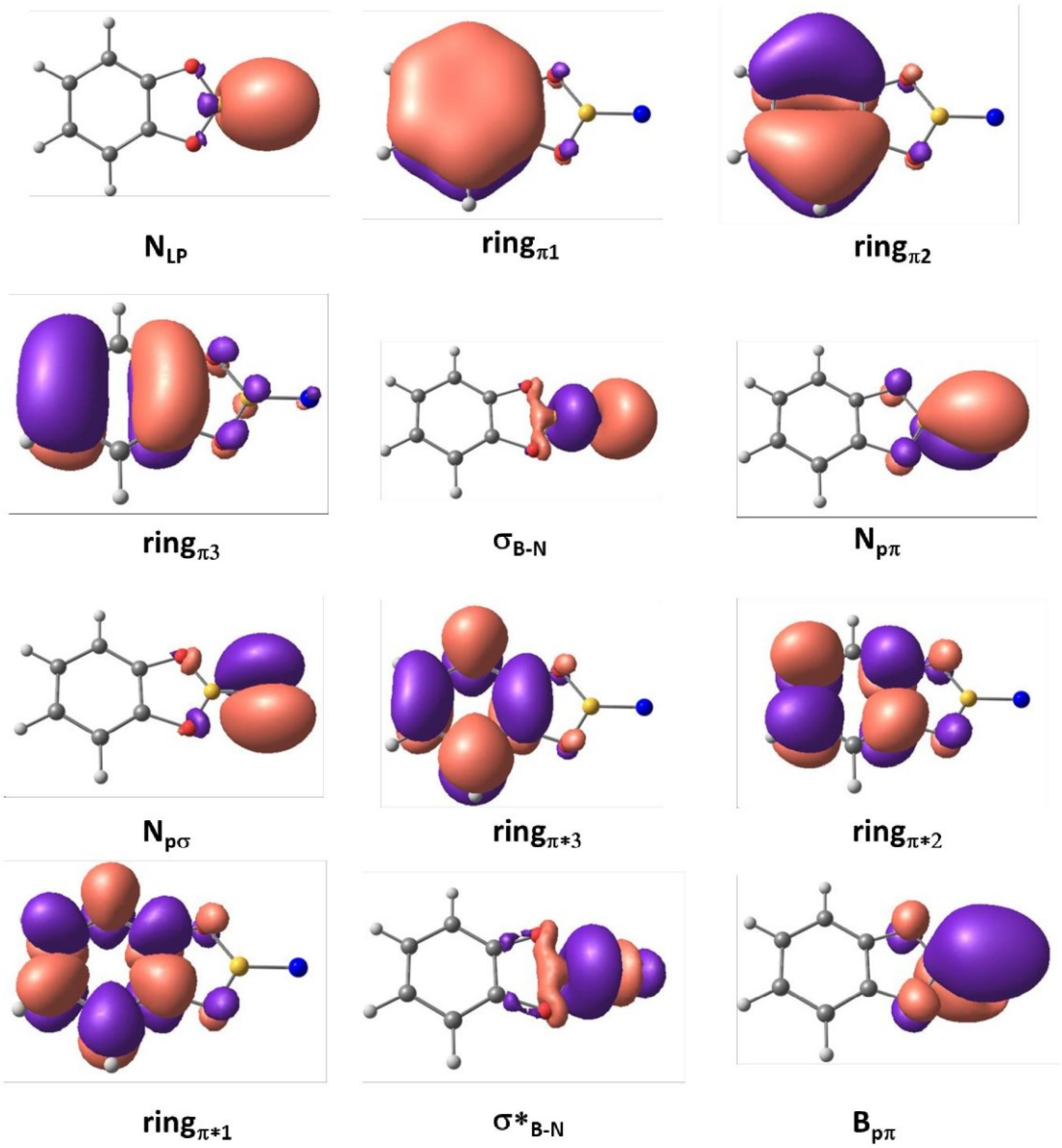


Figure S2. CASSCF(12,12) state-averaged (2 singlets, 2 triplets) natural orbitals calculated at cc-pVTZ basis set at $\tilde{X}^3A_2$ minimum of **1**.

Cartesian Coordinates and their corresponding energies (in Hartree) of all the optimized critical points at CASSCF/cc-pVTZ.

| Boryl nitrene **3** | $\widetilde{X}^3A_2$ minimum | E = -305.95198 |
|---|---|---|
| C 0.085830000000 | 0.698984000000 | -1.213982000000 |
| C 0.101125000000 | -0.634413000000 | -1.184892000000 |
| O 0.266098000000 | 1.182257000000 | 0.050730000000 |
| O 0.291853000000 | -1.057817000000 | 0.099581000000 |
| B 0.390198000000 | 0.080170000000 | 0.839485000000 |
| N 0.606041000000 | 0.114909000000 | 2.322749000000 |
| H -0.036388000000 | 1.391566000000 | -2.013612000000 |
| H -0.004886000000 | -1.363808000000 | -1.953502000000 |

| Boryl nitrene **3** | $\widetilde{a}^1A_1$ minimum | E = -305.90598 |
|---|---|---|
| C 0.086699000000 | 0.697587000000 | -1.208012000000 |
| C 0.101949000000 | -0.632730000000 | -1.179037000000 |
| O 0.267480000000 | 1.197196000000 | 0.061191000000 |
| O 0.293586000000 | -1.072340000000 | 0.110609000000 |
| B 0.390395000000 | 0.080134000000 | 0.840906000000 |
| N 0.599941000000 | 0.114007000000 | 2.280977000000 |
| H -0.035779000000 | 1.387464000000 | -2.009950000000 |
| H -0.004399000000 | -1.359468000000 | -1.950126000000 |

| Boryl nitrene **3** | | $\widetilde{b}^1A_2$ minimum | E = -305.88935 |
|---|---|---|---|
| C | 0.000000000000 | -0.668233000000 | -1.342750000000 |
| C | 0.000000000000 | 0.668233000000 | -1.342750000000 |
| O | 0.000000000000 | -1.122377000000 | -0.060714000000 |
| O | 0.000000000000 | 1.122377000000 | -0.060714000000 |
| B | 0.000000000000 | 0.000000000000 | 0.719307000000 |
| N | 0.000000000000 | 0.000000000000 | 2.194173000000 |
| H | 0.000000000000 | -1.376681000000 | -2.138128000000 |
| H | 0.000000000000 | 1.376681000000 | -2.138128000000 |

| Boryl nitrene **3** | | $\widetilde{A}^3B_2$ minimum | E = -305.87867 |
|---|---|---|---|
| C | 0.087260000000 | 0.698088000000 | -1.204121000000 |
| C | 0.102572000000 | -0.633043000000 | -1.175100000000 |
| O | 0.267829000000 | 1.196736000000 | 0.063155000000 |
| O | 0.293829000000 | -1.071724000000 | 0.112597000000 |
| B | 0.390853000000 | 0.080263000000 | 0.844058000000 |
| N | 0.596797000000 | 0.113395000000 | 2.259696000000 |
| H | -0.035355000000 | 1.387189000000 | -2.006786000000 |
| H | -0.003913000000 | -1.359055000000 | -1.946941000000 |

| Boryl nitrene **3** | | $\tilde{c}^1A_1$ minimum | E = -305.85637 |
|---|---|---|---|
| C | 0.086244000000 | 0.700855000000 | -1.211263000000 |
| C | 0.101557000000 | -0.636152000000 | -1.182092000000 |
| O | 0.265371000000 | 1.179350000000 | 0.045517000000 |
| O | 0.291035000000 | -1.055173000000 | 0.094237000000 |
| B | 0.391752000000 | 0.080415000000 | 0.850199000000 |
| N | 0.605097000000 | 0.114777000000 | 2.316360000000 |
| H | -0.036354000000 | 1.391209000000 | -2.013243000000 |
| H | -0.004830000000 | -1.363431000000 | -1.953158000000 |

| Boryl nitrene **3** | | CI1($\widetilde{b}^1A_2/\widetilde{a}^1A_1$) | E = -305.87692 |
|---|---|---|---|
| C | 0.094367641300 | 0.718063642000 | -1.186906566100 |
| C | 0.100746506900 | -0.653690473600 | -1.154284284900 |
| O | 0.269637115700 | 1.182926595400 | 0.010127537000 |
| O | 0.277366837200 | -1.059484148900 | 0.063843362400 |
| B | 0.398174104400 | 0.082666288100 | 0.892893343600 |
| N | 0.599826318000 | 0.116504716700 | 2.277590879900 |
| H | -0.027279343400 | 1.385635478000 | -2.010895290800 |
| H | -0.012967979200 | -1.360772705200 | -1.945811325800 |

| Boryl nitrene **3** | MECP1($\widetilde{\boldsymbol{A}}^3$A''/$\widetilde{\boldsymbol{b}}^1$A'') | E = -305.86255 |
|---|---|---|
| C 0.092593713000 | 0.694497771800 | -1.188380195600 |
| C 0.109218577600 | -0.628776738300 | -1.159622546000 |
| O 0.091260151800 | 1.222529749800 | 0.107713776500 |
| O 0.120420227800 | -1.099877906000 | 0.158186705700 |
| B 0.340424367100 | 0.079720610500 | 0.843706767900 |
| N 0.748924454000 | 0.112859042500 | 2.132545848700 |
| H 0.081351336500 | 1.380016256000 | -2.003452169900 |
| H 0.115678373100 | -1.349119393500 | -1.944140532200 |

| Boryl nitrene **3** | MECP2($\widetilde{\boldsymbol{A}}^3B_2$/$\tilde{\boldsymbol{c}}^1A_1$) | E =-305.82462 |
|---|---|---|
| C 0.088206048200 | 0.730895811600 | -1.194320965000 |
| C 0.101493152300 | -0.665156723400 | -1.163683369400 |
| O 0.258046892300 | 1.161141895200 | -0.022965547800 |
| O 0.279048403300 | -1.040275940400 | 0.025359851000 |
| B 0.405060471300 | 0.082070316300 | 0.928860968000 |
| N 0.616602324700 | 0.115306558600 | 2.352723541600 |
| H -0.037514808200 | 1.397969539500 | -2.020084772300 |
| H -0.011071283100 | -1.370102064800 | -1.959332050900 |

| Boryl nitrene **3** | | CI2($\tilde{\boldsymbol{c}}^1$A′/$\widetilde{\boldsymbol{b}}^1$A′′) | E = -305.80645 |
|---|---|---|---|
| C | 0.072498487400 | 0.719656788400 | -1.091573009900 |
| C | 0.088093079100 | -0.653366906800 | -1.058145774000 |
| O | -0.344823595700 | 1.211652030700 | 0.087166064100 |
| O | -0.318817848600 | -1.096789976800 | 0.143273636900 |
| B | 0.158116261000 | 0.079325365500 | 0.788518921900 |
| N | 1.232992575900 | 0.114895463400 | 1.754539347500 |
| H | 0.390706142700 | 1.376709224200 | -1.871594549100 |
| H | 0.421106099000 | -1.340232596000 | -1.805626982100 |

| Boryl nitrene **1** | | $\widetilde{\boldsymbol{X}}^3A_2$ minimum | E = -458.70825 |
|---|---|---|---|
| C | 0.000000000000 | 0.692956000000 | 0.148923000000 |
| C | 0.000000000000 | -0.692956000000 | 0.148923000000 |
| C | 0.000000000000 | -1.426890000000 | 1.311185000000 |
| C | 0.000000000000 | -0.696060000000 | 2.506637000000 |
| C | 0.000000000000 | 0.696060000000 | 2.506637000000 |
| C | 0.000000000000 | 1.426890000000 | 1.311185000000 |
| H | 0.000000000000 | -2.498158000000 | 1.299935000000 |
| H | 0.000000000000 | -1.222028000000 | 3.441248000000 |
| H | 0.000000000000 | 1.222028000000 | 3.441248000000 |
| H | 0.000000000000 | 2.498158000000 | 1.299935000000 |
| O | 0.000000000000 | 1.133154000000 | -1.145768000000 |
| O | 0.000000000000 | -1.133154000000 | -1.145768000000 |
| B | 0.000000000000 | 0.000000000000 | -1.906703000000 |
| N | 0.000000000000 | 0.000000000000 | -3.407499000000 |

# Acknowledgments

I am deeply grateful to many people who supported me throughout my PhD journey at the Institute of Organic Chemistry, University of Tübingen.

I owe a debt of gratitude to my PhD supervisor, Prof. Dr. Holger F. Bettinger, for entrusting me with the opportunity to conduct my doctoral research under his guidance. I would like to mention his invaluable support and insightful guidance during my PhD. I am particularly grateful for the academic flexibility and freedom he extends to every PhD student, including me, in the lab. I would also like to thank my second supervisor, Prof. Dr. Reinhold Fink, and other committee members, Prof. Dr. Stephanie Grond and Prof. Dr. Florian Beuerle, for their interest in my work.

Thereafter, a heartfelt thanks to my current and former lab mates, including Ankit, Christina, Ralf, Marvin, Abdollah, André, Janis, Laura, Maren, Mario, Rita, Sonja, Johannes, Constanze, Florian, and John, for creating and sustaining a friendly and joyful atmosphere in the lab. Special appreciation to Serhii, Csaba, and John for introducing me to engaging card games and board games.

I feel obliged to mention the lab's technical staff, Florian and Veronika, for addressing various lab-related miscellaneous problems during my PhD. I also must thank the staff of NMR department, Dr. Markus Kramer and Dominik, for their assistance in conducting EPR measurements.

A special mention goes to Divanshu for being a supportive and encouraging friend and for all the help he offered me, inside and outside of the lab, throughout my PhD tenure. Also,

I would like to acknowledge Phillip for all our healthy scientific discussions and for lightening the mood in the lab during our extended coffee breaks. I am thankful to Marie for all her assistance during my early days in Germany and for being a good friend throughout my stay in Tuebingen.

I am grateful to my friend Keshav for being a constant source of support and for all the meaningful and seemingly meaningless discussions since our college days in Mohali. Moreover, I extend my thanks to my cousin and friend Vishal for entertaining me throughout my stay in Germany on our long phone calls and while I was in India during vacation. I would also like to acknowledge my friends from IISER Mohali, including Mayank, Jaskaran, Jagmeet, and Gurdeep, as well as my school friends, namely Amit, Rohit, Dheeraj, Sahil, Sourav, Shubham, Vishav, and Abhay. Their constant efforts to revive all the good old memories during our virtual and in-person meetings have been truly cherished.

Finally, I would like to express my most profound appreciation to my family members for being the unwavering pillars of strength in my life. The hardships and sacrifices my father and mother made are worth mentioning here, which enabled me to study at the highest levels of academic studies. Their constant financial and emotional support has helped me to navigate through the rough and tough moments of life, which could have been impossible to deal with otherwise. Also, I would like to mention my loving brother and sister-in-law; their loving and caring nature has added an extra layer of support for me during this journey. Their extraordinary cooking skills made my stay in India during my vacation even more wonderful and enjoyable.